An Analysis of the Effect of Process Parameters on the Formability of Sheet Metal

An Analysis of the Effect of Process Parameters on the Formability of Sheet Metal

A thesis presented for the degree of

Doctor of Philosophy

of the

University of Aston in Birmingham

by

Peter Kai-Sun Lee

April, 1972

Contents:

Acknowledgements

The author gratefully acknowledges the supervision by Professor T.C. Hsü, the encouragement of Professor T.B. Worth, the former Head of Department, the advice of Dr. C.Y. Choi and the help of all laboratory staff in the Production Engineering Department.

Synopsis

This investigation is in two parts, theory and experimental verification.

(1) Theoretical Study

In this study it is, for obvious reasons, necessary to analyse the concept of formability first. For the purpose of the present investigation it is sufficient to define the four aspects of formability as follows:

(a) the formability of the material at a critical section,

(b) the formability of the material in general,

(c) process efficiency,

(d) proportional increase in surface area.

A method of quantitative assessment is proposed for each of the four aspects of formability.

The theoretical study also includes the distinction between coaxial and non-coaxial strains which occur, respectively, in axisymmetrical and unsymmetrical forming processes and the inadequacy of the circular grid system for the assessment of formability is explained in the light of this distinction.

(2) Experimental Study

As one of the bases of the experimental work, the determination of the end point of a forming process, which sets the limit to the formability of the work material, is discussed. The effects of three process parameters on draw-in are shown graphically. Then the delay of fracture in sheet metal forming resulting from draw-in

is analysed in kinematical terms, namely, through the radial displacements, the radial and the circumferential strains, and the projected thickness of the workpiece. Through the equilibrium equation of the membrane stresses, the effect on the shape of the unsupported region of the workpiece, and hence the position of the critical section is explained. Then, the effect of draw-in on the four aspects of formability is discussed throughout this investigation.

The triangular coordinate system is used to present and analyse the triaxial strains involved. This coordinate system has the advantage of showing all the three principal strains in a material simultaneously, as well as representing clearly the many types of strains involved in sheet metal work.

Notation:

ε = logarithmic (natural) strain

$\vec{\varepsilon}$ = total strain (vector)

ε_θ = circumferential strain

ε_s = meridional-tangential strain

ε_h = through-thickness strain

$\varepsilon_{\bar{h}}$ = projected thickness strain

$\bar{\bar{\varepsilon}}_h$ = average thickness strain of the product

ε^*_h = numerically maximum through-thickness strain at the critical section

ε_r = radial strain

σ = true or effective stress

σ_θ = circumferential stress

σ_r = radial stress

r_o = initial radial distance

r = current radial distance

s = length of the meridional section

D_o = initial diameter of the concentric circles on the work

D_c = current diameter of the concentric circles on the work

h_o = original thickness of the product

h = current thickness of the product

$\bar{h}$ = projected thickness

$\bar{\bar{h}}$ = average through-thickness of the deformed shell

A_o = area of the initially unsupported region

A = area of the formed shell

A_r = area of the part of the blank formed into the shell

t = time

a = radius of the initially unsupported region

d = distance between the initial and the final edge of the unsupported region, measured in the blank

τ = frictional force per unit area

E = energy

r_p = punch profile radius

D = blank diameter

F = load on the pressure plate

n = work hardening index

w_o = initial arc length in the coupon specimen

w = current arc length in the coupon specimen after deformation

ρ = radius of curvature

P = punch penetration

P_o = punch penetration at which the action of draw-in starts

ψ = draw-in

H = gross process efficiency

$\overline{H}$ = net process efficiency

η = characteristic index for strain or type of deformation at the critical section

k = constant

K = constant

C = constant

θ = angle

θ_o = angle

ϕ = angle

Ω = angle

α = angle

Chapter 1. - INTRODUCTION

The success of sheet metal forming processes is generally attributed to a quality of the material called formability. The assessment of the formability of sheet metal is of fundamental significance to the improvement and selection of sheet materials as well as the design and costing of forming processes. In spite of its importance to sheet metal engineers, there has not been an agreed single method for assessing formability. The problems associated with the assessment of the formability of sheet metal are, by nature, complex and difficult to solve, because of the number of variables involved.

Sheet metal can be formed into practically an infinite variety of shapes under different forming conditions. There is a correspondingly large number of possible sheet metal tests to rate the formability of materials. One of the problems a sheet metal engineer has to solve is the choice of an existing sheet metal test to suit his particular purpose so that the test results are perfectly reliable. The test results are reliable only when the test conditions are the same as the actual forming operations. The more the forming conditions deviate from those in the test, the less reliable the test results are for predicting the performance in the forming process.

With regard to sheet metal tests, it is after thought that formability can be defined as what the test measures. Such definitions have certain theoretical limitations. For example, in the Erichsen test, the maximum penetration is used as the formability index and the limiting drawing ratio (L.D.R.) is used in the Swift's deep drawing test. One may ask several questions regarding these tests and the

definitions of formability:

(1) Which definition of the formability is more acceptable than the other?

(2) Can the formability be represented only by one parameter or one sheet metal test?

(3) Is the parameter chosen, like the punch penetration in the Erichsen test or L.D.R. in the Swift's test, the right one to represent the formability?

(4) Are the test conditions in each test sufficiently and correctly specified?

Several parameters can be chosen in a single test to represent formability or ductility. In the tension test, the parameter sometimes used is the strain (or the stress) at the beginning of instability. It means that the material can sustain to that degree of straining without necking or failure in that particular type of forming. In the majority of sheet metal forming processes, the strain distribution is not uniform as in the tension test, and it is impracticable to measure all the strains in the product. For this reason, strains have hitherto not been generally used as the basis for the assessment of ductility in sheet metal. Other parameters, like the punch penetration or L.D.R. are thus chosen to represent formability. Although they are all related to the limit of stretching or deformation at which the formed product will not fail, they represent entirely different forming characteristics. As far as the strains in the product are concerned, it does not necessarily mean that the deeper the punch penetration, the greater the maximum strains. In

order to assess the L.D.R. in the Swift's deep drawing test, the diameter of the blank has to be changed. Obviously, the mode of deformation (or the state of strain) will vary with the blank diameter. Therefore, it is easier and quicker to measure the punch penetration or other conventional parameter. However, as will be shown later, punch penetration represents formability only partially.

In addition to the problems mentioned above, the success of the deformation of a given material depends also on many other factors, such as the mechanical properties of the work and the forming conditions. Therefore, formability has hitherto appeared to be an elusive quality to measure.

In view of this, a more generalized theoretical approach is carried out in this project so that the formability of sheet metal can be defined precisely and quantitatively. This theoretical approach is based on the detailed kinematical analysis of sheet metal forming processes.

For simplicity, the formability investigated in this project is confined to the type of strain paths occuring in axisymmetrical sheet metal forming processes, in other words, to coaxial strain paths in which the direction of the principal strains remained fixed with respect to the material during deformation. The effect of non-coaxiality at the necking region is ignored. It is assumed that the material is homogeneous and the elastic strains are negligibly small. Unsymmetrical strains due to anisotropy, which are small and occur in the flange only even when the punch penetration is large, are ignored because necking and fracture do not occur in the flange in this project. Initiation of wrinkling, deterioration of

surface finish and the threshold of plastic instability are the three main types of failure in sheet metal products. Only fracture is discussed in this project. The theoretical analysis of the instability at the necking region after the local thinning is outside the scope of this project.

In sheet metal industries, sheet materials like steel and aluminium are widely used. Steel sheets are chosen for this investigation. It will be clear in the Conclusions (Chapter 14) that they are valid for other sheet metals too. Also, only the radial line making 0^{o} from the direction of rolling is considered. In some sheet metal forming processes, the formability of the material is sensitive to strain rates - such as explosive forming and forming of superplastic materials - and in the study of these processes, the assessment of the strain rates is obviously important. A great many sheet metal processes, however, are in effect quasi-static, in which the effects of strain rate may be neglected. In this project, the forming speed was therefore set to as slow a value as possible, so that the strain history can be traced and the end point can be more easily observed.

The concept of sheet metal formability is generalized from that of the ductility as determined in the tension test. Thus, if a strip is cut from sheet metal with its width about the same as the thickness and tested in tension, a ductility index can be determined, on the basis either of the maximum uniform strain, or of the strain at fracture. Such a ductility index corresponds to a strain path involving one tensile strain along the surface of the sheet and two equal compressive strains in the other two directions. Similarly, in the bulge test, where the stresses are biaxial tension, the material

fails under one type of strain only. Sheet metal, however, can be, and usually is, deformed in other ways than those in the tension or bulge test, and fails over a whole range of strain conditions. The formability of sheet metal is, therefore, defined as a spectrum of ductility index, or the variation of ductility with states of strains. This definition can then be interpreted as the properties (or abilities) of the material to resist local thinning and fracture. The first part of the project is, therefore, to investigate whether a formability curve for a given material can be obtained or not.

A material can, however, be formed into different shapes and frequently to different extent in two or more different forming processes. A scale is obviously needed to measure the extent of forming if the formability is to be expressed quantitatively. Punch penetration, which has often been used to represent the extent of forming, is not very useful, because for the same material, it depends on the particular conditions under which it is measured. The penetration, for instance, of a flat-ended small punch is hardly comparable with that of a hemispherical one. Some other parameter has, therefore, to be chosen.

The majority of the sheet metal forming processes consists of changing a flat sheet into a shell of non-developable surface through tensile surface strains. Surface strain may be defined as numerically equal to the thickness strain (ε_h) because: Volume of a sheet metal

= Original surface area (A_o) x Original thickness (h_o) of the material

= Current surface area (A) x Current (average) thickness (h) of the product

owing to the incompressibility of the material.

Hence, the surface strain $= \log_e \left(\frac{A}{A_o}\right)$

$= -\log_e \left(\frac{h}{h_o}\right)$

$= -\varepsilon_h$ ——————— Eq. 1.1.

Most sheet metal products have a larger surface area and a smaller average thickness than the blank. Since sheet metal usually fails through excessive thinning, it is reasonable to choose the maximum surface strains as a measure of the extent of forming.

The practical sheet metal engineer is more interested in the maximum attainable average surface strain or the possible overall extent of forming. Therefore, formability can also be expressed in terms of the proportional increase in surface area.

The maximum overall extent of forming depends not only on the material properties which resist excessive thinning or fracture, but also on how effectively the material is utilized in a process. In all sheet metal products, the thickness is non-uniform, and obviously, the more uneven the thickness is, the less the general increase in area for the same maximum possible thinning at the critical section. Therefore, the surface area (or average surface strain) can show not only the overall increase in surface area, but also the effectiveness with which the material is being utilized in a process. An ideal process, in which the ductility of every part of the material is exhausted at the same time, is defined in this project as one of perfect efficiency. In practice, a product only fails at a certain section while the other parts of the product have only been partially thinned. Therefore, the process efficiency for all processes will be less than 100%. The more evenly thinned the product is, the greater is the process efficiency; and the greater the process efficiency, the greater is

the overall increase in surface area for the same maximum possible thinning at the critical section. Another new aspect of formability is thus introduced, namely, the process efficiency for the characteristic of the forming process. The formula for the process efficiency is derived in a latter chapter.

By distinguishing between these different aspects of formability, it is possible to compare quantitatively not only the performance of two different materials in any single forming process as is done in most sheet metal tests, but also the performance of the same material in two different forming processes. Thus, it is possible to explain why the relative performance of two materials in one process (for example, material A is better than material B) may be reversed, as it sometimes is, in a second process (material B better than material A). In other words, distinction can now be made in quantitative terms between the performance of a material of high formability in an unfavourable process (such as one with a pointed punch) and that of a material of low formability in a relatively safe process (such as one with a round punch).

In the typical sheet metal forming process, the flange is usually used as a means of controlling the metal flow. The action whereby the material in the flange is drawn into the curved portion is called draw-in. In some cases, like in the Erichsen test, draw-in causes the scattering in the results because the British Standard No. 3855, 1965, does not specify the exact amount of draw-in. It merely specifies "the test piece shall be clamped between the die and the blank-holder with a load of 1000$\pm$100 kgf". Thus, the problem of eliminating draw-in completely has to be solved before consistent

results can be obtained. If the clamping force is too high, the material at the flange tends to be squeezed out by the compressive stress. If the surface of the serrated die or pressure plate is too rough, the strength of the material will be reduced because the work is partially cut and the material will be more easily drawn in. In fact, the problem of eliminating draw-in is very difficult to solve.

Since draw-in has an important effect on formability, it is desirable to find, in quantitative terms, the exact manner in which it improves formability, as it is the object of part of this project to do.

Chapter 2. - REVIEW OF PAST LITERATURE

Sheet metal tests are procedures for rating the formability of materials. There are nineteen different sheet metal tests in current use, according to Shawki[1], but from the theoretical point of view, many sheet metal tests may be said, in general, to comprise three elements, namely, the process, a measure for the extent of forming and a formability index.

1. The process

Most sheet metal tests are themselves sheet metal forming processes. It is implied that the forming process in a sheet metal test is the representative process to which all sheet metal forming resembles, hence the formability rating determined in it is, by implication, the 'true' formability of the material or something very near to it. One sheet metal forming process can differ from another in the geometry of the supported part, the geometry of the punch, the solidity of the punch (elastic, solid or fluid), and the amount of draw-in. Strictly speaking, the formability measured in one particular process is an adequate index only for the performance of the material in the same or very similar processes.

2. A measure for the extent of forming

To measure formability, it is obviously necessary to have some means or quantity which measures the extent of forming. The simplest way to measure this extent of forming is the height of the work, measured from the plane of the flange. The height by itself is too particular and it is limited in its significance. Actually, it is better to use a non-dimensional height. There are, of course, other ways of

measuring the extent of forming, such as the maximum through-thickness strain, the increase in surface area, or in deep drawing, the amount of draw-in.

3. A formability index

It is natural, once the extent of forming is defined, to use the maximum attainable extent as a formability index. This index should preferrably be non-dimensional, but is not so in many sheet metal tests. In practice, the determination of this index is closely related to the determination of the end point - the point at which the work is considered to have failed. Many such end points had been chosen: maximum load, maximum load per unit contact area, visible crack, etc.

The following table and Fig. 2.1. show how these aspects vary among existing tests.

	Process *	Extent of Forming	Formability Index (end point)	Ref.
Simple Tension Test	4,8 or 12 depending on the direction of test	ultimate uniform strain	maximum load or initiation of local necking	2,3
Swift's Test	5	limiting drawing ratio (L.D.R.)	maximum amount of draw-in	4,5
Fukui Test	5	ratio of two diameters before and after deformation	maximum amount of draw-in	6,
Erichsen Test	5-6	height of the work	a crack just letting light through	BS3855, 1965
Bulge Test	6	height of the work	maximum pressure	7,8,9
K.W.I. Expanding Test	8	depth of penetration or ratio of diameters of expanded and original holes.	cracks around hole's periphery	10

* Numbers in this column represent type of deformation at the critical section (see Chapter 4).

There is already a vast body of literature dealing with the existing tests, discussing their development, mechanisms during the forming operation and applications, etc. Only those significantly related to this project are reviewed in the following:

A. The Uniaxial Tensile Test

This is the most familiar and the simplest test for metals. The dimensions of standard test pieces and the standard methods of testing are specified in the British Standard No. 18, 1962. During the test, the specimen is pulled axially in a tensile-testing machine until it breaks, the load and elongation being usually recorded continuously. A lot of information, such as the yield points, Young's modulus, ultimate tensile strength, etc., are then determined. In relation to the present investigation, the most significant feature of the tension test is that necking starts (or the uniform strain ceases) when the maximum load is reached[2],[3].

The results derived from the tensile test cannot be applied directly to sheet metal pressings because the deformation of the material differs from that in sheet metal forming in the following ways:

(1) biaxial stretching of the sheet, instead of uniaxial tension,

(2) presence of friction on the sheet at the neck,

(3) radial drawing, bending and unbending in sheet metal forming.

B. Stretch Forming Tests

In these tests the material is subjected to biaxial tension by means

of either a solid punch (e.g. the Erichsen test) or fluid pressure (e.g. hydrostatic bulge test).

(1) The Erichsen test

The general configuration of the test and its principal dimensions are specified in the British Standard No. 3855, 1965. During the test, the blank, acted upon by a cylindrical punch with spherical nose (or a steel ball) of 20 mm of standard diameter, is held against a holder (with a standard round region of 27 mm diameter initially unsupported) to prevent, to a certain extent, inward flow thereunder. The clamping load is set to 1000 ($\pm$ 100) kgf. The maximum punch penetration attained at fracture is taken as the Erichsen value. It will be shown in this thesis that the Erichsen test cannot, in its present form, be considered suitable for the general assessment of the forming quality of sheet metal.

(2) The hydrostatic bulge test

This test is somewhat similar to the Erichsen test except that the solid punch is replaced by oil pressure. Therefore, the reasons that the Erichsen test cannot be acceptable to represent the formability of sheet metal generally are also applicable to this test. It is interesting to note that the stresses and strains in the formed blank in this test can be more easily found because no friction is involved between the punch and material[7],[8],[9]. The polar height at the maximum pressure (instability pressure, a feature very similar to the tension test) is used for the comparison of different materials. In this test, there do not seem to have standard dimensions and methods of testing. Generally, 0.036 in. thick blanks and a bulge diameter of 10 in. are used with special clamping methods[7],[11] to prevent draw-in.

C. Drawing Tests

(1) Wedge drawing test

In this test, a wedge-shaped piece of metal is pulled through a tapered die. The object of this test is to determine the maximum length of the tapered part which can be successfully drawn. The forming process in this test simulates only the mode of deformation in the flange during deep drawing. Even for this aspect of deep drawing, the test conditions do not represent those in cup drawing for the following reasons:

(i) It disregards the bending and unbending of the material in the forming operation.

(ii) The friction occurs between the edge of the test-piece and the die, instead of on the surfaces of the sheet as in real forming processes.

As far as the formability is concerned, this test cannot be said to provide a measure at all because the material rarely fails in the flange in sheet metal forming.

(2) Deep drawing test

There are several proposals for the deep drawing test[12],[13],[14] of which the best known is the Swift's test[4,5]. In the early standard Swift's test, a flat nosed punch of 2 in. diameter with a profile radius of 0.125 in. was usually used. Recently, the International Deep Drawing Research Group on Swift's Cup-Drawing Test[15] proposed a standard test procedure. Details of the test conditions are as follows:

Punch diameter	50 mm
Punch radius	4.5 mm
Die opening diameter	53.65 mm
Die radius	13.0 mm
Surface roughness	CLA 0.04-0.15 μm
Punch speed	1.7 mm/sec

In the test, the clamping load is set so that it is just sufficient to prevent wrinkling of the specimen. The die and the pressure plate are lubricated with polythene film or grease. The punch is left essentially unlubricated.

During the test, a circular specimen is drawn through a circular die by a flat nosed punch. The maximum possible diameter of blank that can be successfully drawn with a punch of specified size defines the limiting drawing ratio (L.D.R.) of the material

$$\text{L.D.R.} = \frac{\text{Limiting Blank Diameter}}{\text{Punch Diameter}}$$

To understand the contribution of this widely used test to the research on sheet metal, it is essential to distinguish between two totally different types of sheet metal forming processes. In most sheet metal forming processes, the work is stretched biaxially so that a plane sheet is changed into a shell of non-developable surface. Any improvement on this process consists in making the work stretch further without failure. In deep drawing, or cup drawing, on the other hand, the plane sheet is transformed to a cylindrical or prismatic surface with a bottom, and improvement in the process consists of producing a deeper cup than it is hitherto possible to do. In other words, in sheet metal forming in general, formability is a matter of maximum extent of biaxial stretching, but in cup drawing, drawability is a matter of the maximum possible draw-in. The former is a matter of ductility in stretching a sheet, and the latter is a matter either of the strength of the cup to withstand the drawing load, or of the success in preventing wrinkling in the flange, depending on the prevailing mode of failure.

There are reasons to believe that Swift's test has its limitations. It has been found that there is sometimes no correlation between press-shop performance and the test results.[21] Also, there is often some doubt on whether the L.D.R. should be represented in terms of blank diameter. The blank-holding pressure plays a significant role in determining the L.D.R. and this leads to the idea that "a more sensitive method of material assessment can be based on varying press-plate loading rather than by varying the blank diameter".[16]

It should be also noted that in the Swift's test the end point is difficult to determine. Even with a large number of specimens, it is difficult to determine the L.D.R. accurately because at the largest drawing ratio apparently identical specimens do not always behave in a consistent manner. This point has been discussed before[17] and will not be discussed further here.

(3) Fukui Test[6]

It has been mentioned in connection with the Swift's test that the clamping load has a significant effect on determining the L.D.R. The Fukui test is the one in which no clamping is required, hence, the influence of the clamping load does not enter into the test.

In the test, a circular specimen of given diameter (for a particular thickness range) is drawn through a conical die (with cone angle of about 60^{o}) by a flat nosed punch. The test value is given by the following:

$$\text{Fukui value} = \frac{\text{Average diameter of test piece after fracture}}{\text{Blank diameter}}$$

Due to earing the periphery of the test piece is non-circular. The diameters across the ears and in the hollows are measured and the average diameter calculated.

While some research workers thought that the sheet metal test might not be refined enough and, therefore, devoted much of their time to finding a means to improve or to simplify the test conditions,[17,18,19] others were looking for other radically different ways to represent the formability of sheet metal. Swift expressed his doubt that no single test is sufficient to assess completely the formability of sheet metal[5]. Campbell[20] was the first person who tried to re-examine the definition of formability rather than to find a single sheet metal test. Apparently, Campbell measured the strains at fracture (i.e. ultimate ductility). Formability was thus represented in terms of fracture strains as a line in a coordinate system with the transverse principal strain (or circumferential strain ε_θ) as the abscissa and the longitudinal principal strain (or meridional-tangential strain ε_s) as the ordinate, by using the tensile and bulge tests. Later, Keeler[21,22,23] using a different criterion of the end point, completed the diagram with more data from laboratory punch-stretching experiments and production motor-pressings, and the concept of formability limit of sheet metal was thus proposed. The different properties of a particular material under different forming processes were then represented graphically. Goodwin[24] extended the formability limit to negative values of the circumferential strains by using elliptical blanks with a hemispherical punch. Nakazima[25] obtained some results in the same region by using rectangular coupon specimens of various widths. The latter type of specimens is, of course, simplier in its preparation. Yoshida[26] not only obtained three

separate curves representing the limits of diffused neck, local neck and fracture, respectively, but also completed the diagram with the strain history (or strain path).

To measure the surface strains, the non-directional circular grid pattern was used by most of the writers mentioned above. The inadequacy of this system and its effect on the final results on formability will be discussed in Chapter 7.

In order to analyse the strains involved in the formed product, in the past, three principal strains and strain distribution were often plotted in three separate graphs.[4] After the locus for the limiting strains (or the formability curve) is well known, it had been plotted in a bewildering variety of coordinate system. In the Cartesian coordinate system used by Keeler and others, the two axes in Fig.2.2. represent the major surface strain (vertical axis) and the minor surface strain (horizontal axis) respectively. In Campbell's or most Japanese scientists' results, however, the Cartesian axes are the minor surface strain (vertical axis) and the major surface strain (horizontal axis) respectively as shown in Fig. 2.3. This requires an awkward visual and mental exercise if their results are to be compared with each other. In addition, there are several handicaps when either Cartesian coordinate system is used.

(1) The lines representing pure shear and uniaxial tension and compression are not evenly distributed, as can be seen in Fig. 2.3. As Yoshida[27] has shown when applied to axisymmetrical forming processes, the strains and strain paths in the product cover the area to the right of the

lines marked O(2) and O(8) in Fig. 2.3. Strain rates are, of course, obtained by differentiation along a strain path, and the direction of the strain rate in a coordinate system like Fig. 2.3. represents the type of incremental strain occuring at that particular instant. The uneven distribution of typical strains in Figs. 2.2. and 2.3. makes it difficult to interpret the instantaneous directions of the strain paths.

(2) Lines inclined at 45^{o} with the axes do not represent the same type of strain and of the lines inclined at $\tan^{-1}(\frac{1}{2})$ with the axes, some are significant but some are not.

(3) It is difficult to represent the non-coaxial strain path in which the axes of the principal strains rotate with respect to the material.

(4) Finally, the most useful and important limiting through-thickness strain, a quantity of obvious interest to the sheet metal engineer, is not shown.

It will be shown in Chapter 4 that by using a better coordinate system much that has been obscured can be easily revealed. The adoption of this new coordinate system is therefore an important aspect of this investigation.

The determination of the formability limit is closely related to the criterion of the end point which is usually related to the problems of the plastic instability. Many theories[28,29,30,31] about the plastic instability of a sheet metal have been proposed, but are based upon conditions so idealized that none of them can as yet be

used to predict the exact necking behaviour in real situations in sheet metal under various forming conditions. On the practical side, up to the present, there is still no consensus on the definition of the end point and many criteria of the end point have been proposed and remain in current use. For example, in the tensile test, the onset of necking is sometimes chosen as the end point. This criterion is well acceptable in this type of deformation. In the Erichsen test, according to the British Standard No. 3855, 1965, page 5, is defined as "either (i) the point at which a crack occurs through the full thickness of the test piece sufficient to allow the passage of light through part of its length, or, (ii) at which there is a decrease in the force sustained by the test piece". Campbell[20] measured the failure strains after fracture, but Keeler[22] took those just before the onset of visible necking. Goodwin[24] defined the failure strains as those which existed in the neck itself. Pearce[32] chose the strains at the corresponding circle opposite to the fractured one in a round specimen as the limiting strain. Veerman, et al[33] proposed to measure the circle either below or above the crack one with some special treatment. Yoshida[26] regarded the change-over point from 'diffused necking' to 'localized necking' as the end point. Unfortunately, up to the present time, there is still no general acceptance of a satisfactory criterion of the end point. Unless the end point can be determined on a sound theoretical basis and accurately determined with relatively simple experimental technique, the research on sheet metal will lack a sound basis and the results by different workers cannot be expected to agree. The end point is so important that the neck-development in sheet metal during forming will be closely examined in Chapter 6.

There is another feature, namely, draw-in, which is inevitable in most forming operations. Draw-in is very important in the assessment of formability because it has a pronounced effect on the formability, however defined, e.g. as the maximum height of the product. Moreover, the amount of draw-in itself depends on such process parameters as lubrication, load on the pressure plate and blank size. Therefore, the effect of draw-in once studied embraces many process parameters. In the past, the effect of draw-in was ignored because either the amount of draw-in is maximum as in the cup drawing test; or there is little or no draw-in, as in the Erichsen or bulge tests. Kaftanoglu and Alexander[18] discovered that the Erichsen number was seriously modified by the action of draw-in through the inward flow of material from the flange. Yokai and Alexander[19] defined the draw-in as the circumferential strain at the inner edge of the die hole, which is taken to be equivalent to the inner diameter of the blankholder in the Erichsen test. In this investigation, draw-in is defined differently and is related more thoroughly and precisely to the behaviour of the work material and the assessment of formability.

Chapter 3. - DEFINITIONS

Since an important portion of this investigation is concerned with the analysis in depth of the concept of formability, it is necessary, for the clarity of later discussions, to devote this chapter to discussing the definitions of the basic terms.

3.1. Strains and strain paths

Strain is the quantitative measurement of the displacement of points in a material relative to one another when the material is deformed. Depending on the severity of deformation, the strains in metals can be classified into elastic and plastic strains respectively. In the elastic region of the stress-strain relationship, the material will revert to its original state when the applied load is released. Beyond the elastic region, the material undergoes plastic deformation causing permanent change in shape. In most manufacturing processes, the plastic strains are usually over a thousand times greater than the elastic strains; therefore, only the plastic strains are considered in this research and the elastic strains are neglected. The logarithmic (natural) strains are used because:

(a) they are additive, whereas engineering strains are not. Thus, consider a simple example of a bar of material with gauge length ℓ_o, and suppose it is strained under an uniaxial stress to a length ℓ_1. The strain $\varepsilon_1 = \ell n(\frac{\ell_1}{\ell_o})$. If the bar is further extended from ℓ_1 to ℓ_2, the further strain will be $\varepsilon_2 = \ell n(\frac{\ell_2}{\ell_1})$ and the total strain will be $\varepsilon = \ell n(\frac{\ell_1}{\ell_o}) + \ell n(\frac{\ell_2}{\ell_1}) = \ell n(\frac{\ell_2}{\ell_o})$

(b) For large plastic strains, the condition of volume constancy is expressed in terms of principal logarithmic strains simply

as $\varepsilon_1+\varepsilon_2+\varepsilon_3= 0$, if the material is considered to be incompressible.

Consider a unit cube of side ℓ_o, being deformed into a rectangular parallelpiped with sides ℓ_1, ℓ_2 and ℓ_3. If the condition of incompressibility is assumed, the volume of the cube will remain constant, i.e.

$$\text{Volume} = \ell_o \times \ell_o \times \ell_o = \ell_1 \times \ell_2 \times \ell_3$$

$$\frac{\ell_1}{\ell_o} \times \frac{\ell_2}{\ell_o} \times \frac{\ell_3}{\ell_o} = 1$$

$$\ell n\left(\frac{\ell_1}{\ell_o}\right) + \ell n\left(\frac{\ell_2}{\ell_o}\right) + \ell n\left(\frac{\ell_3}{\ell_o}\right) = 0$$

$$\text{i.e. } \varepsilon_1 + \varepsilon_2 + \varepsilon_3 = 0$$

3.2 Three principal strains in axisymmetrical forming

The formability investigated in this research is confined to the type of coaxial strain paths which generally occur in axisymmetrical sheet metal forming processes. Some reflection will show that in forming a material from an isotropic blank, the direction of the principal stresses and principal strains remain fixed with respect to the material so long as the strain near the surface due to friction and the strains involved in ear-ing are neglected. If a material is formed from an anisotropic blank which produces four ears due to the directionality of its mechanical properties, the deformation lacks axial symmetry and the strains are non—coaxial. In such a case, it is nevertheless possible to represent the deformation by the strain paths of the material on two radial lines in the blank, one along the direction of rolling (or perpendicular to it), and one making 45^o angle with the first line. It can be easily shown that, by symmetry, the strains along these lines are always coaxial. In this investigation, only the radial line making 0^o from the direction of rolling is considered. Unsymmetrical strains due to anisotropy, which are small in the present project even when the punch penetration

is large, are ignored. Thus in an axisymmetrical sheet metal forming workpiece, the principal strains are, by symmetry, the meridional-tangential, the circumferential and the through-thickness strains, and remain so throughout the forming process. Strictly speaking, it is necessary to consider the geometrical surface which lies midway between the two surfaces of the work as the reference surface. Three orthogonal coordinate axes are chosen (Fig. 3.2.) and defined as:

a) the tangential or s-axis, which coincides with the meridional tangent to the reference surface;
b) the through-thickness or h-axis, which is normal to the reference surface;
c) the circumferential or θ-axis, which is perpendicular to both the s- and h- axis.

The coordinate h is thus defined as the distance from the reference surface measured along the normal, the coordinate θ as the distance along the normal section of the reference surface (a circle), and the coordinate s as the length of the meridional section of the reference surface measured from its intersection with the axis of symmetry. It is assumed that the simple shear stress in the sh-plane, due to friction, is small and may be neglected. Under such an assumption, the principal stress $\bar{\sigma}_s$ in the axisymmetrical forming process are, by symmetry, in the directions of the s-, h-, and θ- axis. Consequently, the principal strains are always in the direction of these coordinate axes. By definition, the three principal (natural) strains are:

$$\varepsilon_\theta = \log_e \left(\frac{D_c}{D_o}\right)$$

$$\varepsilon_s = \log_e \left(\frac{ds}{dr_o}\right)$$

$$\varepsilon_h = \log_e \left(\frac{h}{h_o}\right)$$

where D_c is the current and D_o is the initial diameter of the concentric circles on the work; s is the current and r_o is the initial distance from the centre of the blank measured along the meridional contour; and h is the current and h_o is the initial thickness of the work. By the incompressibility of metals in the plastic range under hydrostatic stresses under normal forming conditions, the sum of the three principal strains is zero. Thus

$$\varepsilon_\theta + \varepsilon_s + \varepsilon_h = 0 \qquad \text{Eq. 3.1.}$$

The history describing various states of deformation of a point in the material is called the strain path of that point. When a material is deformed plastically, its properties depend not only on the intensity of the strain to which it has been subjected, but also on its strain history. In research on processes involving plastic deformation, it is often necessary to determine the strain path of the material.

There are two kinds of strain paths, coaxial and non-coaxial. A coaxial strain path is one in which the directions of the principal strains remain fixed with respect to the material. For the sake of clarity, two simple examples in Fig. 3.1. are used to illustrate them.

In Fig. 3.1. a, a square with an inscribed circle is stretched in a certain direction. The square will then be gradually deformed into a rectangular and the circle will become an ellipse. The major axes of the ellipse will always remain fixed along the fixed directions shown in Fig. 3.1. a. In a non-coaxial strain path, the directions of the principal strains rotate with respect to the material. In Fig. 3.1. b., in simple shear, a square is deformed eventually to a parallelogram and a circle will become an ellipse but with its major axis rotated.

In the research on sheet metal forming, it is important to distinguish between coaxial and non-coaxial strain paths because for the same final strain, the former requires less strain energy of deformation than the latter. Owing to the widespread use of circles printed on the blank for strain measurement, it is necessary to discuss these two types of strain path further in a separate Chapter, Chapter 7.

In research of metal forming, it is only necessary to determine two principal strains because the third, if required, can be calculated by using equation 3.1. The two principal strains determined experimentally in this investigation are ε_θ and ε_h.

In this investigation, some coupon specimens with parallel sides are used in order to obtain the negative values of the circumferential strains (ε_θ). There are two axes of symmetry in the coupon specimens and the strains along them are, for obvious reasons, always coaxial. Fortunately, when these coupon specimens are stretched by solid punch, they start to fail at some point along the longitudinal axis (shown vertical in Fig. 3.3.). It is, therefore, possible to plot the strain path of the critical section (or failure point) in the same way as for the circular specimens. The thicknesses, from which the through-thickness strains are determined, are measured in the same way as in the circular specimens, and it will be explained later. Strictly speaking, there is no circumferential strain in the coupon specimens, because the concentric circular arcs printed on them do not remain circular after deformation. It is, of course, possible to measure the strain along the curve into which a concentric circular arc is deformed(Fig. 3.3.); thus, if w is the length of the curve in the deformed state and w_o is the length of the circular arc before it is

deformed into the curve, then,

$$\varepsilon_\theta = \log_e \frac{dw}{dw_o} \qquad \text{Eq. 3.2.}$$

Indeed, in both the circular and the coupon specimens, the strain bears the same relation to the axis of symmetry. The method of determining the quantity dw/dw_o in equation 3.2. (for point N in Fig. 3.3.) is as follows:

Suppose a point P in the undeformed specimen on the circular arc passing through N, making an angle θ_o with the longitudinal axis, moves to P' after deformation, and suppose point N moves to N'. The curve N'P' into which the circular arc NP is deformed is, in general, a space curve, of which we see in Fig. 3.3. the projection on the plane of the flange. Let x be the distance of P' from the longitudinal plane of symmetry (passing through the vertical axis in Fig. 3.3.). Measurements are made of the distance x along curve N'P' for the intersections between the initial radial and circular lines, and from these measurements values for $dx/d\theta_o$ are obtained by graphical differentiation. Let Ω be the angle between a tangent to N'P' and the plane of the flange and $(90^o - \phi)$ be that between the projection of that tangent on the plane of the flange and the longitudinal plane of symmetry. Then,

$$\frac{dw}{dw_o} = \frac{1}{r_o} \frac{dw}{d\theta_o}$$

$$= \frac{1}{r_o \cos\phi \cos\Omega} \frac{dx}{d\theta_o} \qquad \text{Eq. 3.3.}$$

where r_o is the original radial distance of P (or length of $\overline{OP}$). By symmetry, the angles ϕ and Ω at N' are equal to zero, hence, at that point,

$$\frac{dw}{dw_o} = \frac{1}{r_o} \frac{dx}{d\theta_o} \qquad \text{Eq. 3.4.}$$

3.3 Necking and the Critical Section

When a material is deformed plastically, it can be either under uniform or non-uniform straining. In the tension test, the reduction in the cross-section area of a tensile bar before necking is the same everywhere throughout the specimen. This is called uniform straining. If the bar is stretched further, a neck will be formed as soon as the maximum applied load is reached. Once a neck is formed, most of the straining takes place in the neck, which leads to fracture, while the part outside the neck ceases to deform further. This is called necking. There is another type of necking in which, once a neck is formed, other parts of the product is still undergoing deformation but with various amount of straining. In the Erichsen test, bulge test, or ordinary sheet metal forming operation, there is always a thinnest section in the product almost as soon as the blank begins to be formed. This thinnest section moves continuously outward in the Erichsen test but stays stationary at the pole of the bulge in the bulge test. This type of necking due to local thinning is called diffused necking.

A section or point in the specimen where failure eventually occurs during forming is called the critical section. If the states of strain at the critical section from the beginning to the end of the process are recorded, they form a strain path which represents the complete strain history of the material at that section. The strain path of the material at that section is of particular interest to the engineer because its end point represents the maximum amount of deformation which the material can sustain along that strain path in a forming process. The position of the critical section in the product will vary with the forming conditions.

3.4. End Point

In order to assess formability of sheet metal quantitatively, it is necessary to determine the end point of the strain path at the critical section of a material.

When the severity of deformation is beyond what the material can withstand, the material will become unstable and will fail in several ways. A common type of failure in sheet metal forming is fracture due to excessive thinning at the critical section even though sheet metal may also fail in the forming process by puckering, which is a problem of plastic instability; or by developing excessive surface roughness, which is a problem of metallurgical structure. In this investigation, the ultimate failure is taken to be fracture. Although fracture is the eventual catastrophic failure in sheet metal, the threshold condition for necking formation is chosen as the end point of successful forming, because, even if the process can be continued after the neck has formed but before the material cracks, the groove thus produced in the workpiece is usually considered to have made it unacceptable. Besides, there is really no practical advantage in forming sheet metal so nearly to fracture because the range of punch penetration between necking and fracture is usually very small.

The difficulty of determining the beginning of neck forming in sheet metal accurately in experiments is well known to research workers in this field. For the purpose of elucidating this phenomenon, a microscopic strain study by using fine grids (0.01125 in. pitch) was carried out in this project and the discussion on the point is made in Chapter 6.

3.5. Draw-in (ψ)

In the majority of sheet metal forming processes, a flat specimen is clamped at the edge and the unsupported part is pressed into the die with a solid or liquid punch. The material outside the edge of unsupported area tends to be drawn into the die throat during the forming operation. The size of the flange, the load applied on the flange and the lubrication condition at the flange, have all an influence on the results. Thus, the flange is mainly used to control the flow of the material in forming processes.

In order to measure and compare how much material is being drawn inwards, it is necessary to choose a proper point or edge as a reference. If draw-in is measured anywhere, some inconsistencies will result. Theoretically, the reference edge for draw-in measurements can be fixed in any closed curve in the flange, including the final position of the outer edge of the blank (but no further). When different sizes of blanks are tested, the value of the draw-in will not be constant if the outer edge of the flange is chosen as a basis of a quantitative definition of draw-in. The velocity contour throughout the flange will vary with the materials being tested and the testing conditions. For example, a mild steel flange may move differently from an aluminium flange. Therefore, the measurements of draw-in based on a curve inside the flange will not provide a reasonable basis of comparison.

Since the flange is either cropped off or further formed later, it is reasonable not to count the flange as part of the formed product, and to use the initial edge of the unsupported region as the reference. Then, it does not really matter what the velocity contour of the flange is.

It is necessary to specify the initial, as against the current, edge of the unsupported region because the clamp has rarely, if ever, a sharp edge, but is round, and, as the forming process progresses, the edge of the unsupported portion moves slightly along the round edge of the clamp. For convenience, the initial edge of unsupported region is chosen as the reference because when there is no draw-in, the flange remains fixed and only the part of the blank within the initial edge of unsupported region is formed into a curve shell.

It is convenient to define the amount of draw-in in a manner analogous to the surface strain, namely,

$$\text{Draw-in,} \quad \psi = \log_e \frac{A_r}{A_o} \qquad \text{Eq. 3.5.}$$

where A_r is the area inside the circle A'A' in Fig. 3.4. and A_o is the area inside A A in the same figure. AA is the initial boundary of the unsupported part of the blank. The region of the blank inside the circle AA is called the active region. When there is draw-in, the contour A'A' in the blank occupies the position of curve AA at a certain stage of forming.

3.6. Formability

The successful performance of sheet metal in forming processes is generally called formability. As such, formability is a rather complex idea. In order to define formability logically and quantitatively, it is necessary to introduce four aspects of formability. They are:

a) the formability of the material at a critical section,

b) the formability of the material in general,

c) process efficiency,

d) proportional increase in surface area.

a) The formability of the material at a critical section

In forming processes, sheet metal generally fails locally. The position in the workpiece where necking and fracture eventually occurs is called the critical section. The behaviour of the material at the critical section, where the material necks and fractures eventually, decides how far or how thin a material can be stretched. The possible overall extent of forming thus depends solely on the maximum strain at the critical section of a material. The end point of the strain path of the material at the critical section represents the formability of the material at the critical section. The surface strain is used as the measure of the extent of forming because sheet metal is usually deformed by biaxial stretching or tensile surface strain. The formability of the material at the critical section is, therefore, the maximum attainable surface strain at that section. In other words, the formability at the critical section is a limiting strain which is the negative of the thickness strain (Eq. 1.1.) at the critical section, according to the definition of the extent of forming herein adopted.

b) Formability of a material

A material can be deformed under various forming conditions. For each set of forming conditions, there is a strain path and a terminal strain ratio at its critical section. Each strain path of the material at the critical section has its own end point, and a curve drawn through a number of these end points represents the limit of formability of a material. Thus, formability of sheet metal is not a simple material property, which can be represented by a number or an index, but is a spectrum

of properties, which can only be represented by a curve. Here, the concept of formability of a material is first generalized from that of the ductility as determined in the tension test. Thus, formability of the material at the critical section is, in fact, a ductility index under a particular set of strain conditions. Formability of a material, on the other hand, means a spectrum of ductility indices covering a range of forming conditions. For example, it is well known that by using the same material, the thinnest portion of the specimen in a bulge test is thinner than that in the Erichsen test. An example of the formability curve (for mild steel sheets) is shown in Fig. 8.4.

c) Process efficiency (H)

Mechanical engineers are interested in the overall extent of forming. The maximum overall extent of forming measured by the increase in surface area from the blank to the shell, depends not only on the formability of the material, as defined in the last two paragraphs, but also on how effectively the formability is utilized in a process. In a hypothetical ideal process in which the thickness of the shell is everywhere uniform so that when the material at the critical section begins to neck, the material everywhere else starts to neck also, the utilization of the formability of the material may be said to be the best possible. However, in all sheet metal products the thickness is non-uniform, and obviously, the more uneven the thickness, the less the general increase in area for the same possible thinning at the critical section. In this case, the process efficiency is defined as the ratio of the (numerical) average through-thickness strain of the product, $\bar{\bar{\varepsilon}}_h$, to the (numerical) maximum through-thickness strain (i.e. at the critical section), ε_h^*.

$$\text{Process efficiency, } \% = \frac{\bar{\bar{\varepsilon}}_h}{\varepsilon_h^*} \times 100\% \qquad \text{Eq. 3.6.}$$

In the hypothetical process, the thickness of the shell is everywhere uniform so that $\bar{\bar{\varepsilon}}_h = \varepsilon_h^*$. The process efficiency is then said to be 100%. The average through-thickness strain of the product can be more easily expressed in terms of surface strains of the product because the total volume of the work material in the shell is equal to $A \times \bar{\bar{h}} = A_o \times h_o$ where

h_o is the original through-thickness of the blank.

A_o is the original surface area of the unsupported part of the blank.

A is the surface area of the deformed shell.

$\bar{\bar{h}}$ is the average through-thickness of the deformed shell.

$$\therefore \frac{\bar{\bar{h}}}{h_o} = \frac{A_o}{A}$$

The average through-thickness strain of the product is $\log_e (\frac{\bar{\bar{h}}}{h_o})$, and is always negative. The numerical average through-thickness strain of the product, $\bar{\bar{\varepsilon}}_h$, is

$$\bar{\bar{\varepsilon}}_h = \log_e (\frac{h_o}{\bar{\bar{h}}})$$

$$= \log_e (\frac{A}{A_o})$$

$$= \log_e A - \log_e A_o \qquad \text{Eq. 3.7.}$$

Equation 3.6. becomes

$$\text{Process efficiency, } \% = \frac{\log_e A - \log_e A_o}{\varepsilon_h^*} \times 100\%$$

In most sheet metal forming processes, part of the flange is drawn in. To take account of the effect of draw-in on the value of process efficiency, distinction should be made between the gross and the net process efficiencies.

The gross process efficiency (with draw-in)

$$H, \% = \frac{\log_e A - \log_e A_o}{\varepsilon_h^*} \times 100\% \qquad \text{Eq. 3.8.}$$

The net process efficiency (without draw-in)

$$\bar{H}, \% = \frac{\log_e A - \log_e A_r}{\varepsilon_h^*} \times 100\% \qquad \text{Eq. 3.9.}$$

where A_r is the area inside the circle A'A' in Fig. 3.4. Figs. 3.5., 3.6., and 3.7. show how these process efficiencies vary with process parameters.

d) Proportional increase in surface area

Process efficiency, which depends on the uniformity of the thickness, is of particular significance to research workers. The practical sheet metal engineer is more likely to be interested in the maximum attainable average surface strain, or the possible overall extent of forming.

The surface area of the shell formed is determined by evaluating an integral involving the current thickness or through-thickness strain. Thus by Pappus' Theorem,

$$dA = 2\pi r\, ds$$

$$A = 2\pi \int r\, ds$$

$$= 2\pi \int \frac{ds}{dr_o} r\, dr_o \qquad \text{Eq. 3.10.}$$

where A is the surface area of the shell, and ds is the infinitesimal length of the meridional section(Fig. 3.4.). However, by the definition of the meridional-tangential strain,

$$\varepsilon_s = \log_e \left(\frac{ds}{dr_o}\right)$$

hence,

$$A = 2\pi \int e^{\varepsilon_s} e^{\varepsilon_\theta} r_o \, dr_o$$

$$= 2\pi \int e^{-\varepsilon_h} r_o \, dr_o \qquad \text{Eq. 3.11.}$$

To illustrate this method, Fig. 3.8. is shown here and in it $r_o \exp(-\varepsilon_h)$ is plotted against r_o, and the quantity $\frac{A}{2\pi}$ is found by measuring the area under the appropriate curve with a planimeter. The limits of the integration are chosen to cover whatever part of the shell is being measured. The upper limits of integration for the two curves are different (with draw-in, P=0.954" without draw-in, P=0.6943"), owing to different amount of draw-in.

By measuring the maximum attainable increase in surface area for different amounts of draw-in, the effect of draw-in on a certain process can be investigated.

Chapter 4. - THE APPLICATION OF THE TRIANGULAR COORDINATE SYSTEM IN AXISYMMETRICAL FORMING

In the Cartesian coordinate system, mentioned previously in Chapter 2, the lines representing pure shear and uniaxial tension and compression are not evenly distributed, as shown in Fig. 2.3. and the through-thickness strain is not shown. It seems that another more versatile system is required. In this project, it is proposed to use the triangular system first proposed by Professor Hsu [34] [35] [36] [40] for which both the strain history and the strain distribution can be easily observed. Also, the lines representing pure shear and uniaxial tension and compression are evenly distributed.

4.1. Strain Representation

Owing to equation 3.1., the three principal strains which specify the deformation at a point - ε_h , ε_s and ε_θ - are not independent variables and have, between them, only two degrees of freedom. It is possible, therefore, to represent them graphically in a two dimensional coordinate system. A system of triangular coordinates with three axes at 120^o to each other (Fig. 4.1.) is adopted. By virtue of equation 3.1., the three principal strains may be plotted in the system, and the three strains can be read from such a diagram simultaneously. The origin represents the undeformed state of the blank, and the coordinate line for each of the strains are shown in the Fig. 4.1., with indication of the positive and negative regions in each case.

A point P in Fig. 4.1. represents, a state of coaxial strain with a set of three principal strains whose sum is zero,

$$\varepsilon_h = \varepsilon \cos \theta$$

$$\varepsilon_s = \varepsilon \cos (\theta - 120^\circ)$$

$$\varepsilon_\theta = \varepsilon \cos (\theta - 240^\circ)$$

where ε, the intensity of the strain, is represented by the length of OP; and $\left[\cos \theta + \cos(\theta - 120^\circ) + \cos(\theta - 240^\circ)\right]$ vanishes identically. Thus, equation 3.1. is satisfied.

A locus of successive states of strains for a particular material then represents the strain history (or strain path) of that particle. In general, a strain path extends outwards from the origin. A straight radial strain path represents proportional deformation in which the ratios between the three principal strains ($\varepsilon_h : \varepsilon_\theta : \varepsilon_s$) remain constant.

In Fig. 4.1., the angle θ represents the ratios between the principal strains. It is desirable to represent the ratios $\varepsilon_h : \varepsilon_\theta : \varepsilon_s$ by a single number, and, instead of a number from 0 to 2π, or 0° to 360°, it is convenient to use a number from 0 to 12, as in Fig. 4.2., because it is easy to visualize the direction of the lines by analogy to the clock face. This number is to be called the characteristic index for strain because it represents the characteristic or type of deformation of the different strain paths and to be represented by η so that,

$$\eta = \frac{6}{\pi} \theta$$

This kind of diagram may be called the "Clock Diagram".

To facilitate the interpretation of strain path, a number of radial paths representing familiar modes of deformation, may be discussed. In the strain path along the ε_h-axis ($\eta = 12$), ε_h is tensile (positive) and ε_θ and ε_s are both compressive (negative) and numerically equal to $\varepsilon_h/2$, as can be seen by referring to Fig. 4.2. Therefore, the deformation is the same as that in a specimen in the tension test, stretched along the h-axis. This type of deformation may be called pure tension.

In the strain path along the negative branch of the ε_h-axis ($\eta = 6$), the deformation is the reverse of pure tension, namely pure compression (negative) and ε_s and ε_θ are tensile and both numerically equal to $\varepsilon_h/2$. Along the strain path marked $\eta = 3$, the strains have no vertical component on the ε_h-axis, hence ε_h is zero and ε_s and ε_θ are equal in magnitude but opposite in sign; in other words, the deformation is pure shear or plane strain in the $s\theta$ -plane. Obviously, the strain path along $\eta = 9$ is also one of plane strain in the $s\theta$ -plane and differs from that along $\eta = 3$ only in the signs of ε_s and ε_θ being reversed. Radial strain paths may also be drawn along the ε_s- and ε_θ- axis in their opposite direction and perpendicular to them, and their significance can be easily found by analogy to the four strain paths discussed earlier. In Fig. 4.2, it is shown that all odd numbers of η represent pure shear or plane strain (i.e. one of the principal strains remains unchanged); the paths for $\eta = 12, 4, 8$, represent pure tension, and those for $\eta = 2, 6, 10$, represent pure compression. Fig. 4.3. shows the deformations of a cube corresponding to a point at a distance ($\ell n\ 3$) from the origin and having various values of η from 0 to 12. A radial strain path may, of course, fall between those represented by whole numbers in η , such as OB in Fig. 4.2. Such a strain path may be considered to be the resultant of two components, one along $\eta = 2$(OA) and along $\eta = 1$(AB), and the relative proportion of OA and AB may be found by the usual method of vectorial resolution. In other words, the law of vector addition or subtraction applied to coaxial strain paths may be applied here.

In the analysis of a strain path, it is important to distinguish between finite and incremental strains. For example, a strain path OCD is shown in Fig. 4.4. At C, the finite strains are represented by the vector $\overrightarrow{OC}$ whose magnitude represents the intensity and whose direction, or value

of η, represents the characteristic of the deformation. The characteristic index for the finite strain at C isabout 2. The incremental strain at C is represented by a vanishingly small segment of the strain path in the vicinity of point C. The characteristic index of such an incremental strain is that of the tangent at C, which is about 4. In other words, at C, the resultant deformation up till then is the same as that produced along the radial strain path drawn from O to C, but the instantaneous process of deformation is similar to one along $\eta = 4$.

The punch penetration (P), whose value varies along path OCD, represents the progress of the forming process. If the current finite deformation is represented by a vector $\vec{\varepsilon}$, the strain path is represented by the vector function

$$\vec{\varepsilon} = \vec{\varepsilon}(P)$$

and the strain rate, a vector also, by the differential coefficient $\frac{d\vec{\varepsilon}}{dt}$ where t is time, and the direction of $\frac{d\vec{\varepsilon}}{dt}$ is along the tangent of the strain path.

The triangular coordinate system has been applied to cup drawing[36] and compression[35]. It may be interesting to mention that Mizuno[37] has independently used the same system for the study of cup drawing. This system may be applied to many sheet metal forming processes, especially axisymmetrically drawn sheets and pressed plates. In the case of the axes of the principal strains rotating with respect to the material during deformation, an additional axis (direction of principal axes) can be included so that the triangular coordinate becomes a cylindrical one. This enables us to show clearly the variables in four parameters (ie. three principal strains and the direction of principal axes) in a single space graph. The triangular coordinate system is used

throughout this investigation. The interpretation of this system in axisymmetrical forming will be discussed in the next section with an example.

4.2 The Clock Diagram and its interpretation

Fig. 4.5. shows a typical example of the strain paths represented in the triangular coordinates system to be called the "Clock Diagram". The strains for the material along the radial line 0^{o} from the direction of rolling are represented by the solid lines (Fig. 4.5.) from the origin of the graph. All the points on the strain paths at the stage or penetration are joined by a curve (dotted line) for constant penetration. This curve shows the strain distribution along a certain radial line at a particular stage. Concentric circles equally spaced at 0.0789" (average reading over 33 steps) are printed on the workpieces and are numbered from the centre (as number 0)outwards. The test conditions are shown in the inset.

The fan-shaped strain paths should, strictly speaking, fall within the range $2 \leq \eta \leq 6$. The deformation comprises two pure compressions, two plane strains and one pure tension. A few points near the punch end are shifted to the range $7 > \eta > 6$, and this is due to the circumferential strains being measured from the outside surface of the product while the through-thickness strains are effectively measured from the reference surface which lies mid-way between the two (outside and inner) surfaces of the work. Strictly speaking, it is necessary to modify the circumferential strains by taking the thickness and the direction of the current normal to the reference surface into consideration. In this research, these complicated adjustments are not considered to be necessary, because they do not have much effect on the general conclusions deduced from the present results. Fig. 4.6. shows the difference between uncorrected and corrected circumferential strains in the clock diagram.

The deformed product can usually be divided into four major zones (shown in Fig. 4.5.) namely,

a) Flat bottom and punch radius profile - the section that the material is in contact with the punch, (coloured red)

b) Wall - the unsupported section of the material, (coloured yellow)

c) Die radius profile - the section that the material is in contact with the die radius profile, (coloured green)

d) Flange - flat section (coloured blue).

These four zones are shown clearly in the clock diagram in Fig. 4.5.

a) Flat bottom and punch radius profile

Fig. 4.5. shows that the punch comes in contact with the material from the circle number 0 to number 13 eventually. At the flat bottom of the punch the material for the circles numbered 1 to 5 is stretched in balanced biaxial tension in the $s\theta$-plane throughout the forming process, producing uniform thinning, hence the deformation is along 6 o'clock. In the region of the punch radius profile (the circles number 5 to 13), the deformation is represented by the strain distribution curve as a downward bulge, which represents local thinning, (or diffused neck) and eventually aggravates itself towards fracture. It is well known that the failure of the circular specimen will generally occur within this region in forming process. As can be seen in Fig. 4.5., the bulge develops at a very early stage of the forming process. The tip of the bulge keeps shifting from the circle number 5 (ε_h = 0.003), through 6, 8, 10, to 11.7 (ε_h = 35.3). It shows that the thinning is a continuous process and it starts long before the maximum load is reached. The local thinning is, in fact, due to localized high tensile stress in the direction of the meridional tangent. At the critical section of the material, (the circle number 11.7) the circumferential strain is inhibited by the cylindrical part of the punch surface. The deformation thus consists of meridional-tangential stretching accompanied by thinning

without much circumferential strain (i.e. along 5 o'clock).

b) Wall

The unsupported section of the material is getting smaller as the forming process is going on (circumferential compression). There is finally a narrow band which escapes plastic bending throughout the process. At this tiny section (between the circles number 13 and 15), the meridional-tangential stress σ_s is tensile, σ_h is small because the inner surface is a free surface, and the circumferential stress σ_θ is zero because it changes from compressive at the die radius to tensile in the wall portion of the material. Here, the stress system and the resultant deformation are pure tension with stretching in the direction of the s-axis and equal contractions in the circumferential and through-thickness directions. (i.e. along 4 o'clock).

c) Die radius profile

There is another small bulge in this zone shown in Fig. 4.5. Here the secondary thinning occurs. On the other hand, the plastic bending on the die radius profile causes also a thinning of the material between the circles number 15 to 22, although this bulge does not represent local thinning, but locally intense radial drawing without change of thickness.

d) Flange

In this zone, the amount of thickening which is caused mainly by the circumferential compression due to radial drawing is very small. There is a particular section (the circle number 23) whose thickness is unchanged. At the early stage, the material on this strain path is thickening due to the circumferential compression but eventually it is subjected to the radial drawing with constant thickness.

In general, when there is no draw-in, most of the material is subjected to thinning, the fan-shaped strain distribution will be confined to cover the range between 3 and 6 o'clock and the zone for the flange of the product in Fig. 4.5. will disappear because no or very little deformation occurs in this section. With greater amount of draw-in in the process, thickening of the flange will be greater and so the fan-shaped strain paths will be more widely spread out (covering the range between 2 and 6 o'clock).

In Fig. 4.5., any line joining a point with the origin O is a vector $\vec{\varepsilon}$, whose magnitude represents the intensity of the strain (or the effective strain) and whose direction (or the value for η), represents the characteristic of the deformation. Also, there are two types of strain gradient i) a vector $\frac{d\vec{\varepsilon}}{ds}$ and ii) three scalar components $\frac{d\varepsilon_\theta}{ds}$, $\frac{d\varepsilon_s}{ds}$, and $\frac{d\varepsilon_h}{ds}$.

i) The vector $\frac{d\vec{\varepsilon}}{ds}$

The direction of the $\frac{d\vec{\varepsilon}}{ds}$ is the tangent to the strains distribution curve (dotted lines) and its magnitude is solved by

$$\frac{d|\vec{\varepsilon}|}{ds} = \frac{d|\vec{\varepsilon}|}{d\,r_o} \cdot \frac{dr_o}{ds}$$

$$= \frac{d\,\vec{\varepsilon}}{d\,r_o} \cdot e^{-\varepsilon_s}$$

ii) The three scalar components $\frac{d\varepsilon_\theta}{ds}$, $\frac{d\varepsilon_s}{ds}$ and $\frac{d\varepsilon_h}{ds}$.

$$\frac{d\varepsilon_\theta}{ds} = \frac{d\varepsilon_\theta}{dr_o}\,\frac{dr_o}{ds} = \frac{d\varepsilon_\theta}{dr_o} \cdot e^{-\varepsilon_s}$$

Similarly,

$$\frac{d\varepsilon_s}{ds} = e^{-\varepsilon_s}\,\frac{d\varepsilon_s}{dr_o}$$

$$\frac{d\varepsilon_h}{ds} = e^{-\varepsilon_s}\,\frac{d\varepsilon_h}{dr_o}$$

If $|\vec{\varepsilon}|$, ε_θ, ε_s and ε_h are plotted against r_o, $\frac{d|\vec{\varepsilon}|}{dr_o}$, $\frac{d\varepsilon_\theta}{dr_o}$, $\frac{d\varepsilon_s}{dr_o}$ and $\frac{d\varepsilon_h}{dr_o}$ can be obtained.

There are two points where $\frac{d\varepsilon_\theta}{dr_o} = 0$ or $\frac{d\varepsilon_\theta}{ds} = 0$. These two values of ε_θ are the highest and lowest at the material. It happens at the circles number 8 and 18 in Fig. 4.5.

Chapter 5. - EXPERIMENTAL EQUIPMENT, MATERIAL, TECHNIQUE AND PROCEDURE

5.1 Experimental Equipment

A. Test Machine

The Hille 20/40 ton Universal Sheet Metal testing machine was used. The machine, which was designed for research work, was a hydraulic press incorporated with an electronic X-Y recorder enabling the punch load and punch travel (by penetration) in a pressing operation to be measured. The primary clamping was used to prevent the formation of wrinkles. Circular specimens were centred by means of three centering fingers.

Performance data:

Maximum depth of draw:	5 in.
Maximum blank diameter:	6.5 in.
Maximum drawing load:	20/40 ton
Low pressure primary clamping	800-5000 lb.
High pressure primary clamping	2000-25000 lb.

Drawing speed: infinitely variable up to 15.7 in./min.

B. Punch Tools

The general configuration of the test and the principal dimensions are indicated in Fig.5.1.

i)	Punches: Punch diameter	1.968 in. (50mm)
	Choice of punch profile radius	0.197 in. (5mm)
		0.394 in. (10mm)
		0.591 in. (15mm)
		0.787 in. (20mm)

0.984 in. (25mm)

ii) Die: For the thickness of specimens between 0.036-0.051 in.

Die hole diameter 2.111 in. (53.64mm)

Die shoulder radius 0.511 in. (13mm)

iii) Serrated die and pressureplate

They were used to prevent draw-in during the forming process, and they were made to the same size as the standard ones. The serrations on the surfaces that sandwiched the sheet metal were produced on a lathe giving a groove similar to that on a gramophone record. The dimensions are shown in Fig. 5.1.

C. Hordern, Mason & Edward O.P. 55. Geared Single Action, Open Front Inclinable Power Press

This was used for the production of blanks using a pillar die set.

D. Measuring Machine

(a) Societe Genevoise Universal Measuring Machine. Photo 5.1.

Model: MU 214 B

Calibration: inches

Smallest unit of measuring: 0.00001 inch

All linear measurements (circumferential strains) were made in this machine. The maximum accuracy of measurement required was 0.0001" but this machine was used because

i) It could be easily operated.

ii) Precise (and stable) vertical movement of the eye-piece provided easy measurement in tracing the profile of the deformed shell.

iii) The two concentric circles and the double cross-wires as seen from the eye-piece of the microscope, Fig. 5.2., provided the means of locating the centre of the grid width so that the distance between the centres of the printed circles could be measured,

independent on the width of the grid which might be expanded or contracted in forming process.

(b) The thicknesses were measured by a dial gauge, reading to 0.0001 inch. Tapered anvils were attached to the dial gauge. The holes in the arms were bored in the jig-boring machine. The set up is shown in Fig. 5.3. and Photo 5.2.

The errors in measuring the thickness strains were due to

(i) the anvil being located offset from the centre of the grid width,

(ii) the measurements not being normal to the measuring surface.

A magnifying lens was used to improve locating the anvil. The errors could be controlled within (0.0002"/0.046") x 100% or 4.4% A graph of through-thickness strain distribution (h vs. r_o) was plotted to smooth out the scatter.

E. Printing Equipment and Chemicals

(a) Rig for photographic printings Fig. 5.4. and Photo 5.3.

For the measurement of strains, a circular grid pattern was printed on one side of the blank by using photographic technique. The rig was specially designed to obtain the best printing results.

The photo-negative glass plate with concentric circles, 0.0789" apart (average reading over 33 steps), was derived from a standard master (0.0789" $\pm$ 0.0005") belonging to a gear projector. In order to have the grids printed sharply on to the blanks, the photo-emulsion face of the glass plate was so placed that it was directly in contact with the blanks. With due care, the risk of scratching the negative by the edges of the blank was reasonably small.

Four micrometer heads were mounted on the rig. The alignment of the centres of the negative and the blank was done by adjusting the four micrometer heads. The discrimination of the micrometer heads was 0.01 mm.

The advantages of using this rig in the photographic method were as follows:

(i) Being a quicker method than the scribed one.

(ii) No damage to the blank surface because too many scribed lines on the surface of the blank might affect the experimental results.

(iii) High repeatability of producing the grids.

(iv) Different sizes of circular blanks (varied from $4\frac{1}{2}$" to $6\frac{1}{2}$" diameter) could be centred by adjusting the micrometer heads.

(v) After aligning the centre of the grids with that of the blank, the micrometer heads could (and should) be turned back a little to allow for thermal expansion owing to the heat generated by the ultra-violet lamp during the exposure period.

(vi) The increment of the radius of successive circles on the blank had only a maximum deviation 0.0002 in. from its average value of 0.0789".

(vii) The centre of the glass plate and that of the blank could be aligned to within 0.0004" (0.01 mm).

For the determination of the end point or for more accurate results a special checker-board pattern of 0.01125" pitch (the average reading over 100 squares) was used.

(b) Centrifuge

This is used to enable a thin and even coating of resist to be

applied on to blanks. An old record player with rotating speed at 120 r.p.m. was used.

(c) Ultra-violet lamp

(125 W) connected to A.C. mains through a choke. This was used for exposure of treated blanks.

(d) Photographic chemicaLs

(i) Kodak Printed Circuit Resist (KPCR): a solution of resin in an organic solvent which becomes light sensitive when it is dry.

(ii) Kodak Printed Circuit Resist Thinner: a solution to be mixed with the KPCR to give a thin and even coating.

(iii) Kodak Printed Circuit Dye Developer: for dissolving the unexposed area of the above resist.

5.2 Data on Materials

The material used for the investigation was "Extra Deep Drawing Quality" Steel 0.0460" thick of the following chemical composition:

Carbon	0.080% max
Silicon	0.035%
Manganese	0.450%
Phosphorus	0.030%

A batch of 12 metal sheets (6' x 3') were supplied with clear markings on one side of the metal sheet. These markings were used

(i) to indicate the direction of rolling,

(ii) to distinguish top face from the bottom one,

(iii) to enable the alignment of specimens for subsequent operations,

(iv) to ensure that all specimens were in the same relative position (0^{o} to the direction of rolling had been chosen) in tests.

All specimens were tested in the as-received condition.

5.3 Experimental Technique

A. Preparation of Circular Specimens

(a) The metal sheets were sheared into strips. Each of them had markings, a lightscribed straight line with several arrowheads spaced at appropriate distance to represent the direction of rolling shown in Fig. 5.5.

(b) A slightly larger size in outer diameter than the required blanks were produced on the Hordern, Mason & Edward power press. Each blank had a diameter scribed line with an arrow-head shown in Fig. 5.5.

(c) The blanks were turned in a lathe, with very low turning speed and plenty of lubrication supplied, to the required size in order to remove the work-hardened material and the irregularities at the rim.

(d) Uniformity of thickness within each specimen was checked so that only those with less than 0.0002"difference in thickness between the thickest and the thinnest parts were accepted.

(e) The blanks were placed on the surface plate and weights were put on them to ensure that the test blanks remained flat when not in use.

B. Printing of Grids

To enable the measurement of strains, a pattern of concentric circles spaced equally at 0.0789" was printed on the unmarked face of the blank.

The procedure of photographic printing is as follows:

(a) All blanks were degreased with turpentine and cleaned with pumic powder.

(b) A mixture of Kodak Printed Circuit Resist and Kodak Thinner at the ratio of 2:1 in volume was coated on to that surface of the blank which had not been marked.

(c) A thin and even coating could be obtained if the blank was spun in the centrifuge.

(d) The residual coating at the rim of the blank was removed by using a perspex wedge.

(e) The coated blank was placed on the specially designed rig shown in Fig. 5.4. and Photo 5.3.

(f) Four micrometer heads mounted on the rig were adjusted to align the centre of the blank with that of the circular grids of the photo-negative. The readings on each micrometer head for a given size of the blank were noted so that no further alignment was necessary if the same size of the blank was to be printed.

(g) The blank was so adjusted that the rolling direction was in line with the North-West direction of the photo-negative.

(h) A "Tico" circular pad, 0.5" thick, was put on top of the blank to give a uniform loading when a light weight was applied. This was to ensure that the coated face of the blank and the photo-emulsion face of the glass plate would be in contact firmly to give sharper and clearer printed lines.

(i) The four micrometer heads were turned back a little to allow for the thermal expansion of the blank owing to the heat generated by ultra-violet lamp.

(j) Each blank was exposed to the ultra-violet light for about $6\frac{1}{2}$ minutes.

(k) The exposed blank was placed in a bath of dye-developer for 2 minutes $\pm$ 2 seconds.

(l) The blank was then carefully rinsed with water.

(m) The blank was dried under a fanblower for 2 minutes after which the grid pattern was fairly permanent.

5.4 Experimental Procedure

Before beginning the programme proper, a number of preliminary tests were made to give a rough guide of the realistic range for the various parameters, e.g. the geometries of the specimens and tools, the load on the pressure plate, lubrication conditions, punch travelling speed and the temperature of testing, etc.

A. Formability limiting curve for mild steel sheet

The preliminary tests indicated that for finding the whole picture of the formability limiting curve of the material in practice, i.e. within the range of 4 and 6 o'clock in the clock diagram, certain parameters should be varied:-

(a) Hemispherical punch and circular specimens

With various lubrication conditions and loads on the pressure plate, the formability limiting curve of the material would lie within the 5 and 6 o'clock range.

(b) Flat-bottom punch or 15 mm punch profile radius and circular specimens

With various lubrication conditions and loads on the pressure plate, the formability limiting curve of the material would exist between $4\frac{1}{2}$ and $5\frac{1}{2}$ o'clock.

(c) Specially designed coupons specimens with parallel sides were needed in order to shift the formability limiting curve of the material to the region between 4 and 5 o'clock.

The test proper was then based on the above information for guidance.

B. Effect of process parameters on formability of mild steel sheet

To find the effect of process parameters on the formability of mild steel sheet, three major parameters, ie. load on the pressure plate,

blank size and punch profile radius were chosen and the range of conditions used may be summed up as follows:

Blank Dia. in. \ Punch Profile Radius, mm.	5	10	15	20	25
5.250	8500	8500	3500 8500 20000 Serrated Die	8500	8500
5.625			8500		
6.400			8500		

Load on the pressure plate, lbf.

(a) Constant punch travelling speed = 0.360 in/min.

(b) P.T.F.E. sheets 0.003" thick were used as lubricant on the photoprinted side of the blank.

C. Tracing the profile of the deformed product

After the measurements of all strains, the shells were filled with the mixture of plaster of paris powder and water. After the mixture had solidified, the shells were then cut into quarters. In this way, the distortion caused by cutting was reduced. The profile could be traced out easily with the cut portion of the shell.

D. Test procedure

The forming operations were performed in the Hille Universal Sheet Metal Tester.

(a) The blank was placed with the grid pattern side on the die so that the lines would appear on the outside of the deformed product.

(b) The blank was centred by means of the three centring fingers with its 0^{o} radial line always pointing to a certain direction (say, south).

(c) P.T.F.E. sheets of 0.003" thick were used as lubricants, with one sheet on the photo-printing side of the blank throughout the experiment. Additional P.T.F.E. sheet of 0.001" thick would be put between the blank and the punch if required.

(d) The desired clamping load on the pressure plate was then applied to the blank.

(e) The X-Y recorder was adjusted to record the punch load with respect to the punch travel.

(f) A very low punch travelling speed, 0.360 in/min, was set throughout the experiment in order to facilitiate the recognition of the end point.

(g) For exploring the strain histories (or strain paths) in the work, the forming process was stopped at six different punch penetration, with one specimen for each, including

(i) a shell with onset of visible necking,

(ii) a fractured shell

Rectangular coupon specimens of widths, 1", 2" and $2\frac{1}{2}$" and 5" long were milled. They were centred by means of a microscope tube mounted on to the Hille machine.

In order to obtain a complete picture of the formability curve between $\eta = 5$ and $\eta = 6$ range, additional test conditions were set to deform the circular specimens. The were shown in the inset of Fig. 8.4.

Chapter 6. - DETERMINATION OF THE END POINT

Many research workers have experienced the difficulties of determining the onset of plastic instability in sheet metal forming. The problem of deciding the onset of plastic instability in this case is quite different from that in the tension test. The end point can be decided by the initiation of local necking in the tension test but in sheet metal forming it is as difficult to locate or detect the initiation of local necking as to tell when a hunchhack started hunching physically or structually. Before trying to solve the problem of determining the end point, it is necessary to investigate the development of necking in sheet metal during forming.

In sheet metal forming, there is always a thinnest section (shown as a downwards bulge in the clock diagram) in the work almost as soon as the blank begins to be formed. This is because the meridional-tangential stress generally increases towards the centre owing to the smaller cross-sectional area ($2\pi rh$) there, where r is the radial distance from the axis of the punch and h is the current thickness of the blank. Over the punch, however, the tangential force increases towards the edge of the contact area, owing to friction. Thus, near the edge of the contact area over the punch, the tangential stress is maximum and the section tends to be thinnest. This thinnest section moves continuously outward because the edge of the contact area moves continuously outward. Therefore, the local thinning occurs under both a stress and a strain gradient.

Theoretically, it is possible that the material is work-hardened in such a non-uniform manner and subjected to such a stress distribution that necking does not occur at all, and fracture occurs over a wide area. Such a set of particular conditions do not actually occur, so that there is a local neck. The onset of this local neck is, however,

difficult to locate precisely because the necking process in sheet metal differs from that in the tension test specimen in at least three fundamental aspects. Firstly, in the tension test necking occurs in homogeneous strain, but in sheet metal it occurs in the region of diffused thinning which is due to the non-uniform stress distributions in the specimen at all stages in the forming process. Secondly, necking in sheet metal occurs in the region in contact with the punch, hence there is a complex frictional constraint on the material being deformed into a neck. Thirdly, there is an interaction between two principal strains, the circumferential and the meridional-tangential, because they both depend on changes in the radial positions. For these reasons, the neck is formed in sheet metal in such a way that it is difficult to tell when the diffused thinning ends and when the local neck starts. So long as the material outside the neck does not stop deformation, any method of locating the end point must be essentially arbitrary.

Many theories [28] [29] [30] [31] about the plastic instability of a sheet metal have been proposed, but some of them are based upon so idealized conditions that they are insufficient or inadequate to express accurately the necking behaviour of sheet metal under various forming conditions. If the well known equation $\sigma = k\,\varepsilon^{n}$ (where σ is the true or effective stress, ε the true or effective strain, k is a constant and n the work hardening index) itself only inaccurately expresses the relationship between the stress and strain over the whole range of deformation, any attempt to extend the conditions of instability by using the above equation will be in vain. Several empirical methods to determine the end point have thus been suggested and they are reviewed as follows.

(1) The occurence of a crack through the full thickness of the test piece, sufficiently open to transmit daylight through at least a portion of its length [19] [38].

However, as soon as a crack happens, the through-thickness strain at the fracture point is very large. Even before fracture, generally, a groove due to local thinning is formed and the work-piece is usually considered to be unacceptable.

(2) Sometimes, there is also a perceptible noise and, in general, the commencement of rupture is accompanied by a drop in the punch force which may also be regarded as the end point [38] [45].

In the tension test, the maximum load indicates the initiation of instability, while the local necking begins and deformation stops elsewhere in the specimen. Therefore, the strain at the end point can be determined very accurately. In balanced biaxial stretching, as in the bulge test, the maximum load may still coincide with the beginning of instability [7] [8] but there is now no other guide, such as maximum uniform deformation to locate exactly the onset of local necking. A general shape of a curve for the load (or oil pressure) against the punch penetration (polar height) is usually of the shape shown in Fig 6.1. As can be readily seen, there is a wide range of the polar height in which it is not so easy to locate precisely where the maximum load is. If an automatical cut-off mechanism is used, the results will then depend on the sensitivity of the device and the repeatability of its action. A curve of the through-thickness strain at the critical section, ε_h^*, plotted against the punch penetration, P, is shown in Fig. 6.2. It is easy to realize here that the variation in ε_h^* will be very large if the end point is not accurately located on the scale of the punch penetration.

In most sheet metal forming processes, the X-Y recorder shows that the load is still increasing at the onset of the neck because, owing to the increasing area of contact, less and less load is transmitted to the critical section. It is, therefore, necessary to find other ways to locate the end point. Nevertheless, it suggests that the end point is somewhere near the maximum load rather than that at the very end of the process, i.e. fracture.

(3) Strain at a point opposite to that of fracture [32].

As the strain at fracture is difficult to determine, a proposal for determining the end point has been made in which the strain at a point opposite to the fracture in an axisymmetrical product is taken as the limiting strain. Thus, it is proposed to form the product (inset of Fig. 6.3.) till it fractures, say, at A. As soon as fracture occurs, the process is stopped and the strain at B is measured and taken to be the limiting strain or the end point in the forming process.

It is difficult to find a reasonable ground to justify such a definition of the end point. The arbitrary value of this definition and the inconsistencies it can introduce into sheet metal research can be explained as follows. In Fig. 6.3., the through-thickness strains of points A and B are plotted against penetration. At penetration, P_n, a neck, localized with regard to the circumference, develops at A. As forming progresses beyond this penetration, the deformation in the product becomes increasingly unsymmetrical with respect to the axis of symmetry, and the strains at A and B become increasingly different, as shown in NF and NG. At F, fracture occurs at A and the process is stopped, and the strain at B , namely ε_g, is measured and taken as the end point. As can

be readily seen in Fig. 6.3., strictly speaking, the strain chosen as the end point should be ε_n, corresponding to the beginning of the local neck. If the measured strain at B is to be ε_n, the strain at B must remain constant after a neck has developed at A and the curve for the strain at B must be ONH. Obviously, the strain at B can never follow such a path, and indeed, some reflection will shown that such a strain history for B is geometrically impossible. Thus, all that can be said of the measured ε_g is that it lies somewhere between the fracture strain ε_f and the strain at the beginning of the local neck, ε_n.

If the distance between F and G, namely, $(\varepsilon_f - \varepsilon_g)$, is constant of all specimens of the same material in a particular test, this method can yield consistent, even though arbitrary, results on the end point. Of course, this distance does not remain constant from one specimen to the next. Under identical test conditions, some specimens develop a neck very much localized in the circumferential direction whereas others neck nearly simultaneously at all points of the same latitude. Such difference in the behaviour of sheet metal products is well known to all research workers in this field and is, in fact, due to slight differences in the distribution of draw-in around the circumference. Now, in one specimen the strain at a point opposite to the fracture may follow the curve ONG, whereas in another specimen the strain at the corresponding may follow the curve ONG'. Therefore, this method yields inconsistent results, which show themselves in the scatter in the results in the reference (32).

It may be interesting to note in passing that the limiting strains obtained from the results by this method is higher than that measured by Keeler who used the beginning of necking as the cri-

terion. It is because even after the neck is formed, the material at A and B are still further strained until one of them reaches fracture.

(4) Beginning of necking to be judged visually

Keeler[31] tried to distinguish between diffused and local necking. He found that "when sheets were securely clamped and stretched over rigid punches, localized necking could not occur and plastic instability appeared as diffused necking which was located by the point of discontinuity in the curve of the meridional-tangential strains at the critical section (ε_s^*) plotted against the punch penetration (P) as shown in Fig. 6.5. A."
In the present investigation, diffused necking is found to occur as early as the blank begins to deform (Fig. 6.4.).

The meridional-tangential strain at the critical section in the specimen on which Figs. 6.4. and 6.6. are based is plotted in Fig. 6.5. B. in the same way as Keeler did his results, and it can be seen that the curve is hyperbolic. Even if diffused necking can be located as Keeler defined and did, it is found no practical use because the material after diffused necking can still be stretched further without failure.

Keeler also stated that fracture was identified with a trough of local shear on the surface at about the time an arrest (or maximum load) appeared in the load record. Therefore, on this basis, the onset of a trough of local shear was used to be the end point. Here, he apparently tried to apply the phenomenon of instability in the simple test or bulge test in which there is no friction between the punch and the blank to where friction is present. In the present investigation, it is found that the necking does not always occur when the maximum load is reached,

as has been explained earlier.

In order to investigate the formation of necking in sheet metal forming, a special checker-board pattern of 0.01125" apart (the average reading over 100 squares) was used. The pattern was printed on $5\frac{1}{4}$" diameter blank of 0.080% carbon steel, 0.0460" thick formed in a punch-and-die assembly sketched in the inset of Fig. 6.4.

When the through-thickness strain of the material at the critical section, ε_h^*, is plotted against the punch penetration P, as shown in Fig. 6.2., it can be seen that the through-thickness strain at fracture (point F) of the material at the critical section is considerably higher numerically than that corresponding to the first appearance of a groove (point G).

In Fig. 6.4., the thickness of the material is plotted against the original radial distance, r_o. It shows that there is diffused necking throughout a sheet metal operation and necking becomes progressively more localized towards the end of the process. The problem of determining the end point in sheet metal forming hinges, therefore, on the separation of the local from the diffused necking. In the tension test, the beginning of local necking can be readily seen if the variation of the diameter or longitudinal strain is plotted against the original length at various stages near the start of neck forming[(2)]. In sheet metal forming, however, such curves show no clear-cut transition from the diffused to the local necking. In Fig. 6.4., curve C corresponds to a specimen in which no groove is detactable and curve D to one in which it is conspicuous. Between curve C and curve D it is hardly possible to decide, on the basis of Fig. 6.4. alone, which of them represents diffused and which local

necking. It is true that from curve C to D, the thickness to the left of the thinnest section remains the same, but this feature cannot be used to define local thinning because in that part of the specimen the thickness has remained constant even before curve C is reached (see curve B/C).

Since local thinning in sheet metal is not a clear-cut process, any definition of the start of neck formation must necessarily be partially arbitrary. A definition of the beginning of neck formation must satisfy two conditions: it must make it easy to locate the beginning of a neck, so defined, and it must coincide with or be slightly before the appearance of a groove on the workpiece. Such a satisfactory definition can, in fact, be found in the variation of the circumferential strain, as shown in Fig. 6.6. in which the curves correspond to those similarly labelled in Fig. 6.4. The difference between curves C and D is now conspicuous, because whereas the former is a smooth curve, the latter contains a bulge. Some more observations may be made in connection with necking. The groove starts from the outside surface and progresses towards the inside. This is because near the crown the strains and stresses on the outside surface are greater than those on the inside. Ths inside surface is burnished due to friction and relative movement between the sheet metal and the punch. There may be no or just a little necking on the inside surface while the groove appears outside first. The product thus can be judged by its outside surface alone to determine the end point. The neck usually develops from one point or an arc to a circular groove around the punch, followed by fracturing and tearing. In Fig. 6.6., it shows that the beginning of necking lies at the stage between curve C and curve D. It is tedious to find the beginning of bulge in the circumferential strains in every

forming process. Simpler methods were tried.

By examining the profile and measuring the gap between the material and a copper wire which is pressed on the surface, the beginning of the groove can be detected. However, the results will depend on the thickness of the wire and the pressure. Also, the product sometimes neck without a pronounced groove appearing on the outside surface, especially when the critical section is near to 6 o'clock in the clock diagram.

In practice, it is easier and quicker to judge visually whether the product is acceptable or not. Since the punch speed was set to 0.006" per second, it is possible to pick up some specimens around the onset of necking with 0.006" difference in penetration among them. In Fig. 6.7, it is shown that three regions can be distinguished on the penetration scale with regard to the detection of necking, namely, visible necking, uncertainty region and no visible necking at all. If the strain is chosen from the half way in the uncertainty physical necking region, the error may be within $\pm$ 0.02 of the through-thickness strain at the critical section of the product.

Some metal sheets may show no visible necking, especially in the bulge test (i.e. strain path along 6 o'clock). In that case, it is necessary to examine the strain variation by using fine grids rather than judging its surface appearance.

The method in this investigation is arbitrary because the onset of the local neck depends on visual judgement. It is, however, consistent with practical application because it is mostly by visual examination that a sheet metal product is rejected.

Chapter 7. - THE EFFECT OF USING THE CIRCULAR GRID SYSTEM

Owing to the widespread use of small circles printed on the blank for strain measurements, it is particularly important to discuss its effect on the assessment material formability.

As far as strain measurements are concerned, this method has been claimed to be the most convenient way because:

1) the circular grid pattern can easily and quickly be photoprinted on the blank without alignment operation as has to be done for concentric circles used in this investigation;

2) the circle is non-directional;

3) when the material is deformed, the circles elongate into ellipses. The major axes of the ellipses are parallel to the direction of maximum elongation;

and

4) the principal strains can be readily measured from the major and minor axes of an ellipse.

The convenience of this circular grid system is, however, more apparent than real. If the state of strain at a point rather than a surface is required, it is very doubtful whether or not the accuracy by using this method can still be obtained. The reasons are as follows:

1) it is difficult to locate the directions of the two principal axes of an ellipse accurately, and inaccurate location of their directions has an effect on their measured magnitude;

2) when the blank is deformed, the ellipses generally appear not on a plane but on the curved surface. The measured lengths of two principal axes are likely to be smaller than they should be.

Measured strains from the ellipse are therefore dependent on the gauge length. The bigger the circles, the lower the actual value of the strains at a point is obtained; and the smaller the circles, the greater the scatter in the results due to the difficulties mentioned above. In this investigation, a pattern of concentric circles is used for strain measurements with the gauge length effectively zero.

Apart from the gauge length problem, the critical section rarely coincides with the two principal axes of the ellipse. The multiple circles technique was thus proposed[39] to correct, to some extent, the error of the measured strains at the critical section due to non-alingment of the critical section with the principal axes of the ellipse.

Even if the inaccuracy involved in taking an average strain as the state of strain at a point is ignored, one should still realize that there is a more fundamental defect in this method, namely, non-coaxiality between successive strains is invisible owing to the non-directionality of the circles. This method, at its best, can only be applied to axisymmetrical forming processes and is inadequate for general forming processes such as car body forming, which involves non-coaxial strains. The distinction between the two types of strain paths were explained in Chapter 3.

To explain the limitation and its effect on the assessment of material formability by using small circles for strain measurements, it is preferrable to demonstrate the reason graphically.

If a complicated deformation occurs, it can usually be simplified into several steps. The deformation shown in Fig. 7.1.D. is a resultant of that shown in Fig. 7.1.B. and 7.1.C. The first step represented by Fig. 7.1.B. is pure shear with horizontal stretching till the strain is ε,

accompanied by vertical contraction till the strain is $-\varepsilon$. The undeformed state 7.1.A, is represented by the unit square and the circle, and the first deformed state is then represented by the solid rectangle and ellipse. It is obvious that the area of the body remains the same after the deformation. The second step is represented by Fig. 7.1.C, which is shown as a deformation of the virgin material, for the sake of clarity, and it is also pure shear and in it the material is stretched along OX' which makes an angle θ with the horizontal, till the strain ε and compressed along OY' till that strain is $-\varepsilon$. The final shape of the ellipse of the overall deformation consisting of the first step followed by the second depends on the magnitude of θ. For two extreme values of θ, the shape of the final ellipse can, in fact, by ascertained. Thus, when θ is $\pi/2$, the two steps cancel each other and the ellipse in Fig. 7.1.C, is restored to a circle; and when θ is zero, the effect of the second step is to double that of the first, so that the final ellipse is twice as long and half as high as that in Fig. 7.1.B. Between zero and $\pi/2$, there must be a certain value of θ , say α , for which the proportions of the ellipse after the second step are the same as those before it (i.e. the first step shown in Fig. 7.1.B.). In other words, when θ is equal to α , the second step of the deformation produces no change in shape. Since, in all the deformations discussed here, the area of the figures remains constant, the final ellipse in Fig. 7.1.D. is of the same size as those in Fig. 7.1.B. and 7.1.C., where θ is equal to α.

It is thus demonstrated that deformation does not necessary produce change of shape when the circles and ellipses are used, and that this happens when strains are <u>non-coaxial</u>. Two conclusions may be drawn from this fact. Firstly, when an ellipse on the surface of a sheet metal workpiece does not change its shape in a part of the forming

process, it may or may not have been deformed, and whether or not it has been deformed can in no way be experimentally determined from the deformed circular grid.

This conclusion is not of great importance, because deformation without change of shape occurs only under the rare coincidence of a certain set of matching conditions. The second conclusion is more general and important, namely, that from the measurements, taken at various stages of a forming process, of the proportions of an ellipse into which a circle in the blank is deformed, we cannot, in general, deduce the amount of deformation occurring between one stage and another.

Not only the circles and the ellipses have their weakness for the quantitative determination of strains, but they also cannot be used to distinguish the two types of strain paths. Thus, Fig 7.1. shows deformations which are non-coaxial. The same shape of the ellipse shown in Fig. 7.1. D can be reproduced from the coaxial strains. In Fig. 7.2.B, the first step is the same as in Fig. 7.1. B. The second step Fig. 7.2. C. is a rigid body-rotation so that the major axis of the ellipse is in the same direction as that in Fig. 7.1. D. Comparing Fig. 7.2.D. with Fig. 7.1. D., the final ellipse is the same in shape. The difference between the coaxial and the non-coaxial can only be detected from the rectangle and the parallelogram. Therefore, by judging the circles and the ellipses alone one cannot tell whether the strains are the coaxial or the non-coaxial.

The importance of the distinction between coaxiality and non-coaxiality can also be domonstrated in connection with energy of plastic deformation as follows:

A. Non-coaxial strain path

In Fig. 7.1., let the energy absorbed by the material in the first step of deformation by E_1 per unit volume and in the second step by E_2 per unit volume so that the total energy absorbed in Fig. 7.1.D. is $(E_1 + E_2)$.

B. Coaxial strain path

In Fig. 7.2., let the energy absorbed in the first step be the same as in Fig. 7.1.B. i.e. E_1. No energy is consumed in the rigid body rotation. Therefore, there is no energy absorbed in the second step. The total amount of energy absorbed in Fig. 7.2.D. is E_1 only.

It can be readily seen that the energy of plastic deformation in the coaxial and the non-coaxial strains is different even though the final shape of the ellipse is the same. This difference is of vital importance in assessing the formability of material because the formability of material is a matter of reserve ductility. In forming processes, the limit of formability of the material is reached when the ductility in the material is exhausted. The ductility of metal can be exhausted not only by straining it further and further - as in the tension test - but also by working it, or making it absorb energy of plastic deformation - as in low cycle fatigue. Therefore, the energy absorbed by a material is a measure of the degree to which its ductility is used up. Suppose, a material is used in an unsymmetrical industrial process and is deformed in the way similar to that described in Fig. 7.1. Suppose also that the material fails in the second step of the deformation after absorbing energy equal to $(E_1 + E_2)$. The strain at fracture can be determined from the final ellipse. If the material is then tested in one of the current sheet metal tests, which are generally axisymmetrical processes (i.e.

coaxial strains), it will be found that at the same strain as in Fig. 7.2.D, the material is far from failing, having only absorbed energy E_1. Therefore, when sheet metal is tested axisymmetrically and is used in processes involving non-coaxial strains, the formability will appear to be over-estimated, especially if the deviation from coaxiality is large. Thus, if a material is used in processes involving non-coaxial strains, it should only be tested under similar non-coaxial strains so that its formability, so assessed, can be applied to the forming processes in a significant way. This, sometimes, may explain why the formability curve of sheet metal obtained by Keeler is a band rather than a line when the circular grid system is used in testing a process involving non-coaxial strains. Hitherto, results on the limit of formability show sizable scatter both in the American[21] and in the Japanese results[27] and one distinctive feature of this investigation is that here the limit of formability is graphically represented by a single curve. Although the problem of non-coaxility does not enter the results in the present investigation, it does explain the essential differences in quality between the experimental results in this thesis and the corresponding ones in most of the existing literature on this topic.

Chapter 8. - RESULTS AND CONCLUSIONS ON FORMABILITY OF SHEET METAL IN GENERAL

A. General Shape of the Formability Curve

In this investigation, the formability of the steel sheet is shown as two branches of curves (curve A in Fig. 8.1). The general shape of the formability curve, as a whole is here discussed first.

In the forming tests, the scatter in the results can be due to many causes, such as inhomogeneity of the work material, inaccuracy in locating the blanks, variable draw-in, and errors arising out using the circular grid system of too large a diameter. All these errors, sometimes, cause the curve for the limit of formability to be shown in the past as a broad band instead of a line[22] [24]. If coaxiality is taken into consideration in using the circular grid system as discussed in Chapter 7, the scatter can be improved to some extent. Testing a sheet steel in axisymmetrical pressings, (i.e. coaxial strains), Woodthorpe and Pearce[32] showed that the results were so good that the formability curve could be drawn as a line.

There are several standard sheet metal tests in current use. Three well known tests are chosen in order to show the general shape of the formability curve.

In the bulge test, the strain path at the critical section of a material is along 6 o'clock radial line (balanced biaxial stretching) in the clock diagram while the flat-bottom cup test is approximately along 5 o'clock radial line (pure shear), and in the tension test, it is approximately along 4 o'clock (pure tension). It is also known that the magnitude of the through-thickness strain of the product measured at the critical section in the flat-bottom cup test is relatively smaller

as compared with that in the bulge test or the tension test. This is because the more nearly equal the two strains, ε_s and ε_θ are, the thinner the material can be stretched. This suggests that the formability curve is neither a circle with the origin of the triangular coordinate as the centre, nor a straight line perpendicular to any clock radial line. There must be two inclined lines or curves so that three points can be joined between 4 and 6 o'clock region (Fig. 8.1.).

A formability curve obtained by Yoshida[41] for mild steel sheets is replotted in the triangular coordinates system as shown curve B in Fig. 8.1. Yoshida's curve is more or less like a horseshoe with the η= 4 and 6 lines being asymtotic to the both ends of the curve. Therefore, two values, one along 4 o'clock radial line and another along 6, may be difficult to determine accurately. Also, if the formability curve is shifted due to some other parameters, it is likely that this curve would have no intersection with either or both of 4 and 6 o'clock radial lines, - which is unlikely.

Some curves for the limit of formability are compared in Fig. 8.1. In it, curve C[40] is for an aluminium alloy and it shows that the formability is inferior to that represented in curve A as can be expected; and curve D is reproduced form the results obtained by Keeler[22] and Goodwin[24].

Incidently, the empirical results of the formability curve of sheet steel (between 4 and 6 o'clock) obtained in this research show that the curve is approximately symmetrical along 5 o'clock radial line. If this were true for all isotropic materials, such as fully annealed mild steel, we may extend the formability curve further so that it may cover the whole range of values of η. Theoretically, the curve

would finish up like a flower, symmetrical with respect to all the 12 radial lines, shown in Fig. 8.2. The flower-shaped formability curve may be distorted due to many factors such as anistropy, Bauschinger effects and the strain history of the sheet.

Each material, of course, has its own shape of formability curve. With different mechanical properties or chemical compositions, the curve will be shifted or changed in shape. For example, in the experiments it was found that necking usually appeared earlier along the rolling direction than perpendicular to it when anistropic circular specimens were tested. This shows that two separate formability curves can be plotted for failure along and perpendicular to the rolling direction. Shang and Hsü[46] illustrated this and their results are replotted as shown in Fig. 8.3. in which the formability curve for aluminium sheet along the rolling direction is represented as the solid curve and along the one perpendicular to the direction of rolling as the dotted curve. There fore, in a certain forming process, the strain path at the critical section for the one along the rolling direction crosses its formability curve sooner than the one perpendicular to its rolling direction. For the same reason, the formability curve for other mechanical properties, e.g. work hardening, can be plotted in the same way and their effects can be investigated.

The formability curve also depends on the criterion of the end point adopted. The "equivalent point" criterion as an end point used by Woodthorpe and Pearce[32] gives a higher value than the one by Keeler[22].

Metallurgists will no doubt be interested in the effects of the chemical compositions in the material on the formability curve and such effects can constitute significant problems for their investigation.

The formability curve for the sheet steel in the range $4 < \eta < 6$ (failure in the direction of rolling) is shown in Fig. 8.4., together with the

strain paths leading to it. The insets show the testing conditions under which the various strain paths are obtained.

Two observations are made on the results on formability. First, the limiting through-thickness strain is numerically the smallest when the material is deformed without circumferential strain ($\eta = 5$). If there is circumferential strain in the deformation, no matter whether it is tensile or compressive, the material can reach numerically greater through-thickness strain without failure. Secondly, the general discontinuity of the two branches of the curve strongly suggests that two different mechanism of failure are operative, one in the range of $4 < \eta < 5$ and another in that $5 < \eta < 6$. No visible difference in the shape of the local neck has been observed in this investigation. From theoretical considerations, it is reasonable to suppose that any observable difference is most easily detectable for strain paths slightly to the left and to the right of $\eta = 5$. However, it is precisely in this small range that the difference in the deformation is likely to be small.

Strain paths A to J in Fig. 8.4. correspond to axisymmetrical forming processes by using a rigid punch. The range of the ratio $\varepsilon_\theta/\varepsilon_s$ is somewhat smaller than from zero to one. Strain path A is that of a critical section near the crown of a hemisphere punch lubricated with teflon sheet between the punch and the work, hence ε_θ and ε_s are nearly equal; and strain path F, is that of a critical section near the end of a flat ended punch where the circumferential strain is severely inhibited, hence the strains along path F has only small components on the ε_θ-axis.

The complexity of sheet metal formability arises from the fact that ductility is path dependent, that is, it depends not only on the final strains at the threshold of plastic instability, but on the previous strains, or strain path as well. A strain path in sheet metal can

differ from another in two distinct ways, in strain ratios and in the rotation of the principal strains, the former alone occurring in coaxial strain paths and both the former and the latter occurring in non-coaxial ones. Since only axisymmetrical forming processes are considered in this research, so a strain path can differ from another in strain ratios only. All strain paths of critical sections in Fig. 8.4. must therefore be similar in shape, namely, roughly radial and slightly curved to the right in the region between 5 and 6 o'clock as will be explained presently. The strain path would be radial if the geometry of the product remained constant so that the stresses increased proportionally as in paths F and A. However, in practice the geometry of the forming process varies, the critical section moves from the unsupported region towards the part of the blank in contact with the punch, and as it does so, the circumferential strain suffers greater and greater restraint, hence the curving to the right. This can be shown in Fig. 11.1. in which the fine solid lines represent the movement of the critical section and the dotted lines show the limits of the contact regions between the work and the punch. Fig. 8.4. also shows that to change the characteristic index at the critical section from $\eta = 6$ towards $\eta = 5$ and beyond, it is necessary to make the material fail further and further away from the crown. Three process parameters can be controlled in order to vary the characteristic index(η) of the strain at the critical section, namely, the frictional force on the pressure plate (which changes the amount of draw-in), the lubrication of the punch, and the punch profile radius. If these three process parameters are suitably controlled to finish with 6 o'clock, a product with its numerically maximum through-thickness strain can be obtained.

B. Zig-zag Strain Path

It is well known that a blank can be deformed into a deeper cup without fracture by redrawing in one or more stages. The strain path of the critical section in the redrawing operation will be shown as zig-zag in shape because the straining system is varied from one stage to another. Recently, drawability can be determined by a single blank test[17] in which the clamping load changes in the half way or near to the end of the process so that the zig-zag strain path in the test is expected. It is interesting and important to investigate the zig-zag strain path because as mentioned in Section 8.A., the complexity of sheet metal formability arises from the fact that ductility is path dependent.

Fig. 8.4. shows how the strain paths can be swung from $\eta = 5$ to $\eta = 6$ as the testing conditions are varied. An experiment was carried out to obtain a zig-zag strain path at the critical section as shown in Fig. 8.5. when the testing conditions were reset half way through the axisymmetrical forming process. A circular specimen of $5\frac{1}{4}$" diameter was first deformed by using a hemispherical solid punch with teflon sheet between the punch and the work. The serrated die and pressure plate was used and the load 21,000 lbf. on the pressure plate was set to prevent any draw-in. On forming the specimen through half way, the teflon sheet between the punch and the work was removed and the serrated die and pressure plate were changed into the ordinary smooth set with teflon sheet of 0.005" thick between the die and the work. The clamping load 2000 lbf. was set on the pressure plate to allow more draw-in.

Strain paths shown in Fig. 8.4. are all nearly radial and curved a little to the right. They, sooner or later, are bound to meet the formability curve as the forming operation progresses. The zig-zag strain path at the critical section in Fig. 8.5. does not change its direction as much

as expected. It is because the range of the characteristic indices of the incremental strains which are tangents to the strain paths are only limited to the region between 4 and 6. The product fails when the zig-zag strain path at the critical section reached the formability curve.

In Chapter 4, Fig. 4.5. shows that under a certain fixed set of test conditions throughout the experiment, a downward bulge due to the local thinning will occur. When the test conditions are varied from one stage to another, an additional second downward bulge will occur due to the change in the straining system. Two bulges represent two local thinnings occurring during forming. Therefore, the number of bulges in the clock diagram depends generally on the number of stages of test conditions varied. In the zig-zag strain path test, the clamping load is varied once in the half way of the experiment, and therefore two downward bulges are expected as shown in Fig. 8.5. The position of the critical section will depend on which of them will reach the formability curve first.

Incidentally, two fractures happened at different sections along different rolling direction, (photograph 8.1.) in the preliminary test. It suggests that there are two formability curves, one for specimen along the rolling direction and another for along the one perpendicular to the rolling direction. When the strain paths of two sections along two different directions simultaneously reach their formability curves, two fractures (or two critical sections) can be expected.

Photograph 8.1. also shows that two fractures occur not only at different directions but also at different radial position in the work. This is because in the clock diagram, there are two downward bulges, say, A and

B along the rolling direction and A' and B' along the one perpendicular to the rolling direction as shown in Fig. 8.6. At the maximum attainable penetration, along the rolling direction, the bulge A reaches its formability curve sooner than B but along the one perpendicular to the rolling direction, the bulge B' reaches its formability curve earlier than A'. Therefore, two fractures occur at different radial position.

The conclusions reached in this Chapter are of such fundamental importance that they bear re-sta-ting here.

1) Although ductility, among other mechanical properties of metals, is path dependent, and hence, strictly speaking, no unique curve of limiting formability can be drawn, yet, in practice, the strain paths in axisymmetrical sheet metal forming processes are so similar in shape that, for all intents and purposes, there is a unique formability curve.

2) Strictly speaking, ductility depends also on the history of the hydrostatic stress during the forming process. In most sheet metal forming process, however, the hydrostatic stress is too small, and too nearly constant, to have any effect on the ductility.

3) Even with drastic changes in the forming conditions, the strain path of the critical section in a forming process changes only slightly. However, when it is changed, there is a possibiiity of multiple failures.

Chapter 9. - EFFECT OF PROCESS PARAMETERS ON DRAW-IN

In sheet metal forming, the material in the flange is continuously fed into the formed product. This phenomenon is called draw-in. The amount of draw-in is measured with reference to the initial edge of the unsupported region (AA in Fig. 3.4.) and is defined (in Chapter 3) in a manner analogous to the surface strain, thus,

$$\text{Draw-in, } \psi = \log_e \left(\frac{Ar}{Ao}\right)$$

Owing to the relatively large number of process parameters that can be varied in a sheet metal forming process, it is often thought that sheet metal forming is so complex as to make it difficult to draw clear conclusions about it. It is helpful to realize that several process parameters influence the behaviour of the workpiece through one single quantity, namely, draw-in. Since draw-in itself is a fairly complicated phenomenon, it is necessary to vary only one of the test parameters while the others are kept fixed, in order to isolate the effect on draw-in of a single parameter at a time. The following parameters are varied for draw-in in this investigation and those fixed parameters are specified as in previous section on the experimental technique in this thesis:

1) punch profile radius (r_p)

2) size of blank (D)

3) load on the pressure plate (F)

When draw-in (ψ) is plotted against the punch penetration (P), the results are shown in Figs. 9.1., 9.2. and 9.3., which show that there are two bases on which the different amount of draw-in can be compared:

1) amount of draw-in for the same penetration,

and

2) maximum amounts of draw-in at failure.

The former basis of comparison is the more logical and it may be said to correspond to a scientist's point of view. Engineers, however, are likely to be more interested in the maximum attainable amount of draw-in to make the deepest possible product, hence the latter criterion, which may be said to correspond to a technologist's point of view.

Fig. 9.1. shows that the punch profile radius (r_p) has no significant effect on the total amount of maximum attainable draw-in, but it has an effect on the rate of draw-in with respect to punch penetration. Obviously, for the same penetration, but with different punch profile radius, the amount of material in contact with the punch head is different. For instance, when the profile radius is small, the work material at the punch end is relatively inactive, The unsupported region is stretched to a greater extent and hence there is greater draw-in. This also shows why it is inadequate to use the penetration for rating the formability, regardless of punch profile. Figs. 9.2. and 9.3. show that both the rate of draw-in and the total amount of maximum attainable draw-in are affected by the blank size, D, and the load on the pressure plate F. It indicates that draw-in is controlled largely by friction and blank resistance (size) while the punch profile has little influence on its total amount. Therefore, it is reasonable to say that the lubrication condition between the sheet metal and the pressureplate and die must have an effect on draw-in as well; that is, the better the lubrication, the more is the draw-in, other parameters being equal.

Fig. 9.3. also shows that there is always some draw-in in the process even though a very large load is applied on the pressure plate. For instance, even when 20,000 lbf. is applied on the pressure plate, draw-

in of 0.05 in magnitude is obtained. Therefore, the serrated die and pressure plate has sometimes to be used to reduce the amount of draw-in to a minimum.

From those three sets of results, the variation of the amount of draw-in, ψ , with respect to the punch penetration, P, can be expressed in a relatively simple manner. The empirical equation

$$\psi = K P^2 - C \qquad \text{Eq. 9.1.}$$

where P is the penetration in inch and K and C are constants, fits well the curves in Figs. 9.1., 9.2. and 9.3. There is a penetration, P_o, at which the action of draw-in starts, and

$$P_o = \sqrt{\frac{C}{K}} \qquad \text{Eq. 9.2.}$$

This value of penetration represents the minimum radial tension in the workpiece necessary to overcome the static friction on the flange. In the case of the curve for 15 mm punch profile radius in Fig. 9.1., $P_o = 0.246$ in., $K = 0.231/in^2$ and $C = 0.014$. The values of the constants K and C depend on the punch profile, the size of blank, load on the pressure plate and the units used for penetration. Of the two constants in equation 9.1., K is the more important, because, the amount of draw-in at small penetration is of little interest, and the amount of draw-in at large penetration depends largely on K. It is therefore reasonable to choose the constant K for the basis of comparison.

In Fig. 9.4., the constant K is plotted with respect to i) the punch profile radius, r_p, ii) the load on the pressure plate, F, and iii) the blank diameter, D. It shows that three parameters can have the same value of K within a certain range. It can be seen from the following table that either changing punch profile radius from 15 mm to 18 mm with the holding load (8500 lbf.) and the blank diameter (5.25") kept

constant or changing the holding load from 8500 lbf. to 12750 lbf. with the punch profile radius (15 mm) and the blank diameter (5.25") kept constant is equivalent to changing the blank diameter from 5.25" to 5.95" with the punch profile radius (15 mm) and the holding load (8500 lbf.) kept constant. It is because they have the same value of K, 0.200.

Test parameters / K, per $in.^2$	r_p mm	F lbf.	D in.
0.231	15	8,500	5.25
0.200	18	8,500	5.25
0.200	15	12,750	5.25
0.200	15	8,500	5.95

In other words, the curve of draw-in against penetration remain unchanged in spite of the aforesaid changes in the process parameters producing the same amount of draw-in for the same penetration.

Careful examination of Figs. 9.1. to 9.3. will show that the constant C in equation 9.1. is practically constant for the range of the test condition covered. The amount of draw-in, ψ, may therefore be expressed as a function of

i) punch penetration, P,

ii) punch profile radius, r_p

iii) load on the pressure plate, F,

and

iv) size of blank, D,

Thus,

$$\psi = K(r_p, F, D).\ P^2 - C \qquad \text{Eq. 9.3.}$$

where K is expressed as a function of r_p, F and D. A partial view of this function is shown in Fig. 9.4. showing that the function $K(r_p, F, D)$ is not linear.

The variation of K with respect to the three parameters r_p, F, D, can be more easily illustrated by ignoring the variation with D. Then, the variation of K with the other two parameters may be shown graphically as in Fig. 9.5. where the relation $K(r_p, F)$ is shown as a surface. In practice, a two-dimensional chart shown in Fig. 9.5. with coordinates for r_p and F, showing contours of constant K will be readily serviceable. Such a chart may be useful for choosing the set of forming conditions to yield a particular amount of draw-in.

Needless to say, the addition of the blank diameter D as an independent variable in Equation 9.3. does not change the principle involved in expressing K as a function of r_p and F. In practical terms, the effect of D may be accommodated in a coefficient or correcting factor or equivalent load on the pressure plate, according to which is the most convenient device in any particular case.

Chapter 10. - EFFECT OF DRAW-IN AND PUNCH SHAPE ON THE STRAIN DISTRIBUTION

In this investigation, concerned with the study of formability and its tests, one important task is to simplify the many factors affecting the strains and strain histories in the product, such as the shape and size of the punch, the load on the pressure plate, the blank diameter, and so on. It has been shown in Chapter 9 that, in a particular set of punch and die, all the process parameters produce their effects on the forming process in a simple manner, namely, in the growth of draw-in with respect to punch penetration. It is important to realize that the relationship between draw-in and penetration determines completely the forming process in a set of punch and die. In other words, if the draw-in versus penetration curve in two processes is the same, the behaviours of the workpiece are identical at every stage throughout the two processes no matter how different the lubrication, the load on the pressure plate and the blank diameter may be between the two processes. Conversely, the only way to change the behaviour of the workpiece in a forming process is to change the variation of draw-in with respect to penetration, by changing the blank diameter, or the lubrication, or the load on the pressure plate, or combination of these process parameters.

Since the behaviour of draw-in with penetration, or the history of draw-in, determines the behaviour of the workpiece, it is highly desirable, for the purpose of research, to be able to represent graphically the behaviour of the workpiece clearly and completely. The behaviour of the workpiece consists of the history of the strain distribution which can be conveniently represented by curves in the triangular coordinate, as has been explained in Chapter 4. In this Chapter, the histories of the strain distribution are shown in the clock diagrams for two variations in draw-in (one due to different blank diameters and another due

to different load on the pressure plate) and one variation in the radius of the punch profile. The range of process parameters covered are shown in the following table.

Punch Profile Radius, mm \ Blank diameter, in.	5.25	5.625	6.40
5 (0.197 in.)	8,500		
10 (0.394 in.)	8,500		
15 (0.591 in.)	3,500 8,500 20,000 Serrated die	8,500	8,500
20 (0.787 in.)	8,500		
25 (0.984 in.)	8,500		

Figures denote the loads on the pressure plate, in lbf.

In discussing the results in this Chapter, it is helpful to make a general observation of all the clock diagrams first before discussing the variations in the histories of the strain distribution due to specific process parameters.

10.1. General Observations on the Histories of Strain Distribution

Since the observations in this section apply to all or most of the clock diagrams in this Chapter, it is helpful to make a cursory perusal of all clock diagrams which have common features among them.

In all the clock diagrams in this Chapter, the two ends of all the strain distribution curves must lie on the lines corresponding to 2 and 6 o'clock, that for the rim of the workpiece along the former, and for the centre along the latter, because at the rim the stress is uniaxial circumferential compression (2 o'clock) and at the centre it is balanced biaxial stretching (6 o'clock). Of course, if there is no draw-in, the strain path at 2 o'clock has no length (the rim undeformed); and, similarly, if the punch profile radius is small, the strain path at 6 o'clock is short (the bottom of the workpiece being little stretched). The relative mode of deformation (between 2 and 6 o'clock) and the Mohr circles for principal stresses in axisymmetrical forming processes are shown in Fig. 10.1.

A few points lie between 6 and 7 o'clock owing to the circumferential strains being measured on the outer surface of the work, instead of at the midpoint of the surface (or the reference surface). In this research, these complicated adjustments are not considered to be necessary, because they do not have much effect on the general conclusions deduced from the present results.

Between 2 and 6 o'clock, the clock diagrams for workpieces formed by solid punches consist of two bulges, the horizontal one around 3 o'clock, corresponding to radial drawing of the flange, and the downward one around 5 o'clock, corresponding to local necking at the edge of the punch end. In the downward bulge, the circumferential strain is nearly zero, and the material is thinned by tangential stretching along the meridian. This downward bulge is usually thin and long, corresponding to large strain gradients on the two sides of the local neck. In the horizontal bulge around 3 o'clock, on the other hand, the thickness remains nearly constant and circumferential compression is accompanied by tangential

stretching in the meridional direction. The horizontal bulge is usually fat and broad, representing less strain gradient than in the other bulge. The local neck is easier to visualize because local thinning, corresponding to a downward bulge, is easy to see in the specimen; but localized circumferential compression, represented by a horizontal bulge to the right, can only be visualized in localized large inward radial movements, as shown in Fig. 10.2.

In a clock diagram, the distribution of the energy of deformation can also be generally observed. At any particular point in the clock diagram, the energy of deformation increases with the distance from the origin (or the effective strain) and is proportional to the original radial distance from the centre of the specimen (represented by the circled numbers on the strain paths). Obviously, most of the energy of deformation is represented by the horizontal bulge around 3 o'clock, in other words, in the radial drawing. Therefore, for the same shape of the product, much less energy is consumed and the product, including the flange, is less work hardened in a process without draw-in than in one with draw-in.

In most clock diagrams representing processes with solid punches, there are three radial strain paths, along 2, 4 and 6 o'clock. The strain paths between 4 and 6 o'clock tend to curve slightly to the right because as the forming process progresses, more and more of this part of the work comes into contact with the punch and the circumferential tensile strain is more and more inhibited by friction. The strain paths between 2 and 4 o'clock tend to curve slightly downwards as a particle enters the throat of the die, the circumferential compression becomes less rapid than when it is in the flat flange and there is more tangential stretching in the meridional direction. These general tendancies in the curvatures of the strain paths are of vital theoretical importance in the definition of formability, because it is owing entirely to the similarity of the strain paths in all axisymmetrical forming processes that the formability curve

can be defined at all (see Chapter 3).

The ranges of three principal strains in the product can be easily determined in the clock diagram. The largest range is in the through-thickness strain (ε_h), represented by the vertical distance between the highest and the lowest point in a strain distribution curve. It can also be easily seen that the thinning strain ($-\varepsilon_h$) is always numerically larger than the thickening strain ($+\varepsilon_h$), and that, as a whole, the product is thinner than the blank (only a small part of the strain distribution is above the origin). The second largest range is usually in the meridional-tangential strain (ε_s), and it is always tensile (positive). The smallest range is in the circumferential strain (ε_θ), partly tensile (near the centre of the blank) and partly compressive (near the rim).

10.2. Effect of Blank Diameter on the History of Strain Distribution

Blank diameter in. / Punch Profile Radius mm	Fig. 10.3.	Fig. 10.4.	Fig. 10.5.
15 (0.591 in.)	8,500 lbf	8,500 lbf	8,500 lbf
	5.25	5.625	6.40

Figures denote the loads on the pressure plate.

The ranges of process parameters covered are shown in the above table, i.e. only the blank diameter varies from 5.25 to 6.40 in. while all the other process parameters are kept constant.

To understand the effect of the blank diameter on the behaviour of the workpiece, it is easier to consider the (circular) line which forms the inner edge of the flat flange, in other words, the boundary of the initial unsupported region (shown as AA in Fig 3.4.). As has been explained before, the behaviour of the workpiece inside this boundary is determined completely by the flow of material crossing this boundary (draw-in) at any particular

stage of the forming process. The behaviour of the flat flange depends, of course, not only on this flow, but also on the movements of the outer edge or rim. The clock diagrams, it may be noted, represent the strain histories of the whole work, including the flange.

By considering the radial tensile stress at the inner edge of the flat flange, it is readily understood that this stress is needed to deform the flat flange and increases with the size of the blank. Thus, large blanks tend to inhibit draw-in owing to the larger resistance to radial movement. The details of this effect can be seen in Figs. 10.3. to 10.5. Careful examination of these figures will show that, as the blank diameter increases, the downward bulge around 5 o'clock, representing local thinning, becomes longer for the same penetration, and that the horizontal bulge becomes relatively smaller. By superimposing one clock diagram on another, it can also be seen that the directions of the strain paths remain very much the same from one diagram to the next. It means that at any particular point in the blank the material particle is subjected to nearly the same type of deformation regardless of the blank diameter, but the severity of that deformation is changed by the blank size.

It is also interesting to notice that there is a relatively small difference between Figs. 10.3. and 10.4., as compared with that between Figs. 10.4. and 10.5., especially with regard to the amount of radial movements in the flange, as represented by the horizontal bulge. A quantitative explanation can be given for this apparent discrepancy as follows. By considering the equilibrium of an elementary area in the flange as shown in Fig. 10.6., it can be easily shown that

$$\frac{d\,\sigma_r}{d\,r} = \frac{\sigma_\theta - \sigma_r}{r} - 2\frac{\tau}{h} \qquad \text{Eq. 10.1.}$$

where τ is the frictional force per unit area and h the thickness of the

element. Since the circumferential stress, σ_θ, is always compressive (negative) in this part of the work, the tensile radial stress, σ_r, decreases with radius r, till it becomes zero at the rim. On the right hand side of the equation 10.1., the first term shows that the rate of decrease of σ_r becomes less as r increases— $(\sigma_\theta - \sigma_r)$ being roughly proportional to the effective flow stress of the material. The second term on the right hand side of equation 10.1. is constant with respect to the radius, r. Thus, a small increase in the blank diameter does not materially change the distribution of the radial stress, because in the additional area only small stresses are involved. The stress distribution and hence the strain distribution will be conspicuously affected as between Figs. 10.4. and 10.5. The effect of friction depends, of course, on the area rather than the diameter. As can be shown, the increase in the blank area between Figs. 10.3. and 10.4. is $\{[\pi (5.625)^2/\pi (5.25)^2] - 1\}$ %, i.e. 15 percent, whereas that between Figs. 10.3. and 10.5. is $\{[\pi (6.40)^2/\pi (5.25)^2] - 1\}$ %, i.e. 49 percent.

10.3. Effect of Holding Pressure on the History of Strain Distribution

	Fig. 10.7.	Fig. 10.8.	Fig. 10.9.	Fig. 10.10.
Load on the Pressure Plate, lbf. / Punch Profile radius, mm	3,500	8,500	20,000	Serrated die
15	5.25 in.	5.25 in.	5.25 in.	5.25 in.

Figures denote the blank diameter.

The ranges of process parameters covered are shown in the above table. In Figs. 10.7. to 10.10. are presented clock diagrams for four identical forming processes except for the holding pressure which varies from 3500lbf.

to infinity (corresponding to the serrated die), with Fig. 10.3 repeated in Fig. 10.8 for the sake of convenient reading.

By the arguments presented in Chapter 9, it is evident that the effect of higher holding pressure is equivalent to that of larger blank diameter , except for the strains in the flange, because both the holding pressure and the blank diameter produce their effects through the amount of draw-in. Perusal of Figs. 10.7 to 10.10, in this order, and a parallel examination of Figs. 10.3 to 10.5, also in the right order, will show convincingly that the effect of increasing the holding pressure can be very accurately reproduced by keeping the holding pressure constant but increasing appropriately the blank diameter instead. In particular, a careful comparison between Figs. 10.9 and 10.5 will reveal that there is hardly any detactable difference between them except for the size of the last strain distribution curve, which is due to the larger maximum penetration in Fig. 10.5. Indeed, in certain parts of these two clock diagrams, the experimental curves are so nearly the same that the similarity between them is greater than that between those in two specimens in an identical forming process.

From Figs. 10.7 to 10.10, the two prominent tendencies may be observed in the clock diagrams, the progressive suppression of the horizontal bulge and the sharpening of the downward bulge. At one extreme (Fig. 10.10), the horizontal bulge (or radial drawing) is totally suppressed by the serrated die so that the whole clock diagram lies between 5 o'clock (i.e. zero circumferential strain at the edge of the clamped area) and 6 o'clock (balanced biaxial stretching at the centre of the bottom of the work). Obviously, the possible extent of forming is limited because necking starts at the critical section at a relatively low penetration. The punch load is also relatively small (shown as 4.8 tonf. in X Y - recorder) because little energy of deformation is involved. At the opposite extreme (Fig. 10.7), the major part of the

energy of deformation is consumed in the flange where large radial drawing occurs (large horizontal bulge). The punch load, in this case, is shown as 7.9 tonf. in X Y - recorder. Under certain conditions, even though local thinning occurs (shown as the downward bulge in the clock diagram), a shell may be successfully formed if the process is continued long enough as long as, in the largest strain distribution curve, the tip of the downward bulge does not reach the limiting strain at which serious necking leads to fracture.

10.4. Effect of Punch Profile on the History of Strain Distribution

	Fig. 10.11.	Fig. 10.12.	Fig. 10.13.	Fig. 10.14.	Fig. 10.15.
Punch Profile Radius, mm. / Blank diameter, in.	5	10	15	20	25
5.25	8,500 lbf	8,500 lbf	8,500 lbf	8,500 lbf	8,500 lbf

Figures denote the loads on the pressure plate.

The ranges of process parameters covered in this section are shown in the above table. In Figs. 10.11. to 10.15., clock diagrams are shown for the same process parameters except in the punch profile radius varying from 5 mm (0.197 in.) to 25 mm (0.984 in.). Fig 10.13. is, again, the same as Fig. 10.8. or 10.3. repeated here for convenience.

In studying the effect of the punch profile on the behaviour of the workpiece, it is important to mention that once the punch profile is changed, there is no longer geometrical similarity between the forming processes investigated. It is, therfore, necessary to use another basis

of comparison instead of comparing the draw-in with respect to penetration, as in Sections 10.2. and 10.3. Perusal of Figs. 10.11. to 10.15. will show that the upper part of the horizontal bulges (representing the work in the flange and at the die throat) are identical. Fig. 10.16. also shows that the maximum punch load at the maximum penetration for these five different punch profile radii is approximately the same. It may be concluded that an identical punch load will produce the same magnitude of radial drawing in the flange and the die throat, regardless of the punch profile, so that the deformation in that part of the work is the same.

The main difference between Figs. 10.11. to 10.15. lies in the bulge at 5 o'clock, which becomes progressively larger as the punch becomes more rounded. As has been shown in Fig. 10.16., between Figs. 10.11. to 10.15., the punch load remains nearly unchanged. The different downward bulges in these figures represent, therefore, the different deformations of the work inside the throat of the die between rounded and more nearly flat-ended punches for the same punch load. As can be expected, the more rounded the punch end is, the more material is involved in the uneven thinning (fatter downward bulge). The edge of a flat-ended punch end, in other words, makes the neck more localised. What is perhaps less expected is the effect of the punch profile on the maximum thinning. Figs. 10.11. to 10.15. show that, for the same punch load, the maximum thinning is greater on a rounded punch than on a flat-ended one. There is a prevalent idea that sharp edges at the punch end "cut" into the work producing local thinning. The results shown in this section are independent of indentation and bending and are for stretching of the sheet metal only. Apart from indentation and bending effects, a relatively sharp edge at the punch end tends to inhibit outward movements of the material at the punch end, a "draw-out", so to speak. It can be easily seen that thinning in this part of the work depends solely on

"draw-out", with which both the (tensile) circumferential strain and the (tensile) meridional-tangential strain are associated. Also, other things being equal, the energy involved in an incremental punch travel is greater for rounded than for flat-ended punches because of the more deformation and greater volume of material involved in the incremental punch movement near to the end of the process. It is also interesting to note that the critical section moves nearer to the centre of the work as the punch end becomes more rounded.

10.5. Concluding Remarks

The clock diagram , showing the complete history of the strain distribution, represents all the strains and strain paths in a workpiece. Therefore, theoretically, all information related to axisymmetrical forming processes can be derived from it, for example, the amount of draw-in with respect to penetration, the surface area of the sheet metal product etc. There are also many interesting results, of little practical significance, which can be derived from the clock diagrams presented in this Chapter, especially those related to the strain rates, obtainable by differentiating the strain paths, and the strain gradients, obtainable by differentiating the strain distribution curves. These results, which may be significant and useful in relation to some problems of sheet metal forming which lie outside this investigation, are not included in this thesis.

The object of this Chapter is to demonstrate the usefulness and completeness with which a clock diagram represents the strains and strain histories in a sheet metal product and to show the effects of some of the process parameters on the behaviour of the workpiece. In the following Chapters, various significant data will be presented in the most convenient way in order to advance the theory on formability which is the purpose of this thesis to verify.

Chapter 11. - EFFECT OF DRAW-IN ON THE DISPLACEMENTS AND THE STRAINS IN THE WORK

11.1. Effect of Draw-in on the Displacements in the Work

Since draw-in is inevitable in ordinary forming processes, its effect on the fundamental aspect of sheet metal forming, i.e. displacements in the workpiece, is investigated first.

In a typical axisymmetrical process, a point P in the blank (Fig. 11.1.), at an initial distance r_o, from the axis of symmetry, moves to Q, of coordinates (r, ℓ,). The displacements are determined by the following functions:

$$\ell = \ell\ (r_o) \qquad \text{Eq. 11.1.}$$

$$r = r\ (r_o) \qquad \text{Eq. 11.2.}$$

It is easier to show the displacements by tracing out the profile of the product at successive stages than to express the above two equations analytically. The loci of the movements of particles in the work can be shown pictorially as was done by Mizuno[37].

The effect of draw-in on the displacements can thus be visualized if two identical processes, except one is with and the other is without draw-in, are compared. The difference is not conspicuous; hence the need for other means of comparisons so that any differences in these effects of draw-in can be detected easily. A method such as that shown in Fig. 11.2. may be used to this end.

So far as the effect of draw-in on the displacements inside the edge of the unsupported region (AA in Fig. 11.1.) is concerned, the movement

perpendicular to the flange is ignored, namely, in the L direction. When there is no draw-in, the function represented in equation 11.2. satisfies two boundary conditions, thus

$$(r)_{r_o} = 0 \qquad = \quad 0 \qquad \text{Eq. 11.3.}$$

$$(r)_{r_o} = a \qquad = \quad a \qquad \text{Eq. 11.4.}$$

where a is the initial radial distance of the edge of the unsupported region (AA in Fig. 11.1.). When there is draw-in, the dotted circle A'A' in Fig. 11.1. coincides with the edge AA at a particular stage of the forming process, so that the boundary condition represented in equation 11.4. becomes

$$(r)_{r_o} = a + d \qquad = \quad a \qquad \text{Eq. 11.5.}$$

where d is the origin radial distance between A and A' in Fig. 11.1. The current radial positions (r) at the end of four processes, one without and three with various amount of draw-in, are illustrated in Fig. 11.2. The 45-degree line (dashed) represents the hypothetical case in which the radial positions throughout the workpiece remain unchanged in the forming process. The distance d in equation 11.5. is shown for curve D in Fig. 11.2. The effect of draw-in on the displacements can be readily seen from Fig. 11.2. Thus, a vertical line drawn from the 45-degree line to a curve represents radial displacement, upward for outward movement (or draw-out) and downward for inward movement.

Two observations from Fig. 11.2. can be made as follows:

A. When there is no draw-in (curve A), all the displacements are outward because the punch is pushed into a rigidly clamped blank and all material inside the edge of active region must be undergoing thinning. (Actually, in the upper curve A, there is a slight inward movement near the edge of the initially unsupported region-r_o equals 1.566 in. - but is is hardly distinguishable without using fine lines in a large drawing). Whenever there is draw-in (curve B), there is a point which makes no movement at all. The position of this point depends on the amount of draw-in. The larger the amount of draw-in is, the nearer the position of this point to the axis of the punch will be, so that a larger part of the blank will move inward. It has to be noted that the area of material being drawn inward is proportional to the square of the radius, Therefore, though the range of diameter involving inward movement may seem small in Fig. 11.1., the area involved is larger than it may appear to be. The thinning effect will be counteracted by the action inward movement.

B. The larger the amount of draw-in, the smaller the part of the blank that moves outward. The draw-out generally takes place over the punch end, and this is because the tangential stress is maximum (Chapter 6) near the edge of the contact area over the punch end. The amount of draw-out is relatively more severe for the one without than the one with draw-in although the penetration in the former (curve A, penetration 0.6943 in.) is less than the latter (curve D, penetration 1.1995 in.).

To sum up, draw-in has pronounced effects on the radial displacements in the outer third of the initial radial distance of the unsupported part of the blank, but has relatively small effects on the inner two-thirds.

11.2. Effect of Draw-in on the Strains on the Work

More conclusions can be drawn from Fig. 11.2. if the strains, which are related to the displacements, are considered. For example, the circumferential strain (ε_θ) was defined earlier as follows:

$$\left(\frac{r}{r_o}\right) = \exp\ (\varepsilon_\theta) \qquad \text{Eq. 11.6.}$$

Hence, in Fig. 11.2. the slope of a line drawn from the origin to a point on a curve represents the circumferential strain at that point, with a slope greater than unity for expansion and that smaller for contraction. Without draw-in, all the circumferential strains are tensile, but, with even a small draw-in, they become compressive for a large part of the work.

Suppose the radial strain (ε_r) is introduced and it is defined as

$$\left(\frac{dr}{dr_o}\right) = \exp\ (\varepsilon_r) \qquad \text{Eq. 11.7.}$$

The exponential of the radial strain can be found from the slope of the curves in Fig. 11.2. Thus, Fig. 11.2. shows that without draw-in the average slope (the average over the original radius) is unity, that is, the exponential of the radial strain is equal to unity; and with draw-in, the average slope is less than unity, that is, the average radial strain is compressive.

The effect of draw-in on the thickness strain can be shown by using equations 11.6 and 11.7. Let the draw-in be imagined to occur while the blank is <u>flat</u>, the equation 3.1., i.e. $\varepsilon_\theta + \varepsilon_s + \varepsilon_h = 0$ will become

$$\varepsilon_\theta + \varepsilon_s + \varepsilon_{\bar{h}} = 0 \qquad \text{Eq. 11.8.}$$

where $\varepsilon_{\bar{h}} = \log_e \left(\frac{\bar{h}}{h_o}\right)$ Eq. 11.9.

The projected thickness of the formed product, $\bar{h}$, is understood to be measured in the direction perpendicular to the plane of the flange and h_o is the original thickness of the blank.

In Fig. 11.3, when there is no draw-in, the average projected thickness is the thickness of the blank, but when there is draw-in, the average projected thickness is greater than that of the blank. Fig. 11.3 shows that draw-in amounts to the feeding action during forming to make the work thicker, thereby delaying fracture. This is why the greater the amount of draw-in is, the deeper a shell can generally be formed.

It should be noted that, although draw-in feeds the material into the curved portion of the product, it is not equivalent to using a thicker blank. A thicker blank of the same material begins to neck at the same strain as the thin one, hence, in the forming processes of two sheets of the same material, one thicker than the other, the maximum penetration is identical.

The effect of draw-in on the strains in the workpiece can be shown more clearly in the strain distribution diagram. In Fig. 11.4 both strain distribution curves are for identical specimens in the identical process, except one is with draw-in (dotted line) and the other without draw-in (solid line). These curves represent terminal conditions i.e. the specimens are formed till the material at their critical sections begins to neck. For clarity, the strain distribution for lesser penetrations are omitted. The numbers on the curves indicate the number of concentric rings printed on the blank, counting from the centre, each ring being 0.0789" from the next.

Four main features of the curves are discussed.

a) Without draw-in, the strain distribution curve consists only of a finger between 5 and 6 o'clock, which represents local thinning;

and with draw-in, apart from the finger for local thinning, there is also a bulge between 3 and 4 o'clock which represents radial drawing in the flange and a local thinning over the die radius profile.

b) At the maximum penetration, the tip of the finger for the one without draw-in is near 6 o'clock while with draw-in, the tip of the finger tends to shift to 5 o'clock. The distance between the origin of the triangular coordinates and the tip of the finger (i.e. the effective strain) is larger for the one without than the one with draw-in.

As far as the thickness strain is concerned, without draw-in, the thickness for the point on the tip of the finger is numerically larger than the corresponding one with draw-in, that is, the material can be stretched thinner at the critical section for the one without than the one with draw-in.

c) Although the two penetrations are unequal - 0.6943 in. for the solid curve and 0.954 in. for the dotted curve - it can be easily imagined that the discrepancy between the two curves with respect to general and maximum thinning would be greater than in Fig. 11. 4. if curves for equal penetrations were plotted.

d) As the distance below the origin in Fig. 11.4. indicates thinning, more numbered points near the tip of the finger represent more wide-spread thinning in a formed product.

So far as the whole forming process is concerned, the effect of draw-in on the strain distribution has to be shown in terms of process efficiency.

Chapter 12. - EFFECT OF DRAW-IN ON THE SHAPE OF THE PRODUCT, THE POSITION OF THE CRITICAL SECTION AND ITS STRAIN PATH

The shapes of two products formed from a given set of tools with the same penetration but different test conditions, such as lubrication or load on the pressure plate, can be generally differentiated through the unsupported region only, because portions elsewhere usually will have the same shape (or profile) as the punch head and the die. In the experiments in this investigation, the unsupported region of the workpiece is relatively small so that the difference in shape will not be easily traced. Therefore, the effect of draw-in on the shape of the products will have to be demonstrated in ways other than direct comparison. That such a difference must exist can be readily explained through the equilibrium equation of the membrane stresses in the unsupported part of the work. It can be shown that at the unsupported region,[9]

$$\frac{\sigma_\theta}{\rho_\theta} + \frac{\sigma_s}{\rho_s} = 0 \qquad \text{Eq. 12.1.}$$

where σ is the stress, ρ is the radius of curvature and the subscripts have the same meaning as before.

In Fig. 11.2., it has been shown that when there is no draw-in, the circumferential strain (ε_θ) is always positive, hence the circumferential stress (σ_θ) is also tensile (or positive) throughout the workpiece. The meridional-tangential stress (σ_s) is always tensile and positive as well. Equation 12.1. indicates that the two curvatures must be of opposite signs. The product without draw-in is, therefore, of the shape of a round tent. When there is draw-in, the circumferential

strain in part or whole of the unsupported region is negative, and the circumferential stress can either be compressive (negative) or tensile (positive) depending on the numerical magnitude of the circumferential strain. Some reflection will show that the shape of the product varies from a tent to an ellipsoid of revolution. It is thus demonstrated that the shape of the formed product is different with and without draw-in. It may be concluded that the effect of draw-in on the shape of the product is significant if the amount of draw-in and the unsupported region of the workpiece are large.

In Fig. 11.4. for two processes one with and one without draw-in, different numbered points at or near the tip of the finger are observed. Since the number, indicating the radial distance from the centre of the circular blank, at the tip of the finger at the maximum attainable penetration represents the position of the critical section where necking and fracture eventually occur, it is shown that draw-in has an important effect on the position of the critical section in the product with respect to the original radial distance from the centre. This effect can be seen more clearly in Fig. 12.1. which shows the meridional section of two specimens formed in the same die and punch to the maximum attainable penetration with and without draw-in (right- and left-hand side, respectively). The dotted lines show the limits of the cont-act regions between the punch and the work and the fine solid lines crossing the sections of the work represent the movements (or the strain paths) of the critical sections during the forming process. First of all, it can be seen that, with draw-in, a deeper shell can be formed successfully. Draw-in thus delays fracture by the feeding action as described earlier. Obviously, the higher the punch penetration, the more the part of the blank eventually comes into contact with the punch head. Therefore, with draw-in, the limit of

the contact region between the punch and the work at the maximum attainable penetration is farther from the axis of symmetry. Careful examination will show that the two dotted lines are not exactly symmetrical with respect to the vertical axis, because draw-in not only delays fracture but also introduces compressive circumferential stresses which alter the contour of the unsupported region; hence the difference in the extent of the contact zone between the work and the punch.

In Chapter 6, it was explained that near the edge of the contact area over the punch the tangential stress is maximum and the section is thinnest. Therefore, at the maximum attainable penetration, the critical section must fall near (usually within) the edge of the contact region between the work and the punch, if no special treatment (such as lubrication) is being provided between the punch and the work. This is shown in Fig. 12.1. in which the solid lines eventually fall within (and very near to) the dotted lines in both cases. Therefore, with draw-in, the position of the criticalsection, as with the edge of the contact region between the work and the punch, is farther from the axis of symmetry. It may be concluded that the more the amount of draw-in, the farther the edge of the eventual contact region between the work and the punch from the axis of symmetry and so does the initial radial position of the critical section.

As far as the movement of the critical section is concerned, the curvatures of the two fine solid lines are different as shown in Fig. 12.1. Without draw-in, the curvature of the fine solid line is greater. This is because, as explained in Chapter 11 and Fig. 11.2., the larger the amount of draw-in is, the less the part of the blank moving outward (or draw-out) over the punch head. With no draw-in, the draw-out is larger and more severe than that with draw-in. This also explains why

the change in circumferential strain at the critical section (change in r) on the right-hand side of Fig. 12.1. is less than that on the left-hand side. This further leads to the conclusion that, the less the change in circumferential strain at the critical section, the nearer to 5 o'clock the strain path of this section; and, similarly, the greater the change in the circumferential strain, the nearer to 6 o'clock the strain path; and indeed it is shown to be so in Fig. 12.2. Draw-in has exactly the same effect of the punch profile radius on the strain path of the critical section because a smaller punch profile radius also inhibits draw-out.

In general, the strain path of the material nearer to the centre of the blank is nearer to balanced stretching (along 6 o'clock), hence the more the amount of draw-in is, the nearer the strain path of the critical section to 5 o'clock.

It may be concluded that the strain path of the critical section is effected by draw-in in two ways: the initial radial position of the critical section, and the curvature of the strain path.

The improvement on the formability of the sheet metal owing to draw-in will be discussed in the next chapter.

Chapter 13. - THE EFFECT OF DRAW-IN ON FORMABILITY

The effect of draw-in on the overall performance of a specimen is a complicated matter, hence it is desirable to discuss it by analysing it into its various aspects as follows:-

A. The Effect of Draw-in on the Maximum Through-thickness Strain at the Critical Section (ε_h^*)

The effect of draw-in on shifting the strain path of the critical section was described in Chapter 12. In Fig. 12.2., the vertical distance between the origin and a point on the formability curve is numerically the maximum through-thickness strain at the critical section (ε_h^*). A significant feature of Fig. 12.2. is that, near to 6 o'clock, ε_h^* is much larger than to at 5 o'clock. This means that it is generally advantageous to control the process parameters so that the strain path at the critical section moves towards 6 o'clock (balanced biaxial stretching) and that the material may be formed to the maximum possible thinnest value (i.e. maximum utility of the material). However, Fig. 12.2. also shows that as draw-in increases, the (numerically) maximum attainable through-thickness strain (ε_h^*) actually decreases, owing to the unfavourable change of the strain path away from 6 o'clock towards 5 o'clock.

B. Effect of Draw-in on the Proportional Increase in Surface Area

The practical sheet metal engineer is interested in the maximum attainable average surface strain, or the possible overall extent of forming. The quantity which he would wish to measure most of all is likely to be the maximum attainable increase in the surface area of the product. The effect of draw-in on the maximum attainable increase in the surface area is shown in Fig. 13.1. which is obtained from the process by varying the load on the pressure

plate, as well as by using the serrated die and holding plate. The dashed line making 45 degrees with the axes represents a hypothetical process in which the blank, including the extra material drawn into the active region, suffers no change in average thickness. As can be seen, when A_r/A_o-(real area)/ (original area) - is greater than unity, some material from the flange is drawn into the active region. Therefore, the (A_r/A_o) - axis in Fig. 13.1. represents the proportion of draw-in. The dashed line indicates

$$\frac{A}{A_o} = \frac{A_r}{A_o}$$

$$\text{i.e. } A = A_r$$

It means that there is no change in area, hence no change in the thickness, when draw-in occurs.

The solid curve in Fig. 13.1 is almost a straight line. The straight line can be represented by the empirical equation,

$$\frac{A}{A_o} = 1.12 + 1.0125 \left(\frac{A_r - A_o}{A_o}\right) \qquad \text{Eq. 13.1.}$$

The left-hand side of this equation is the exponential of the nominal average surface strain, and the second term on the right-hand side represents the effect of draw-in. In other words, if there is no draw-in (i.e. $A_r = A_o$), the average increase in surface area is 12 percent; but if there is draw-in, then of the extra blank area fed into the workpiece by the draw-in, only 1.25 percent increase in area can be materialised. In other words, the extra material drawn into the active region is almost unstretched at all. Of course, so long as the coefficient of $(A_r - A_o)/ A_o$ in equation 13.1. is positive, draw-in is beneficial to the overall performance of sheet metal.

Examination of Fig. 13.1. will show that the real proportional increase in area, A/A_r, actually decreases slightly with draw-in as can be shown more clearly in Fig. 13.2. In other words, the overall thickness of the shell formed to the limit in this process increases with draw-in, but that effect is less than is necesaary to cancel the beneficial effect of draw-in to produce a deeper shell.

C. Effect of Draw-in on the Process Efficiency

Process efficiency as defined in Chapter 3 is used to assess the degree of uniformity of the thickness in the workpiece. Obviously, the more even the thickness distribution, the larger the general increase in area for the same maximum possible thinning at the critical section, and the better the utilization of the formability of the material. Therefore, process efficiency measures the extent to which the maximum attainable surface strain at the critical section ($-\varepsilon_h^*$) is exploited in the process.

In Fig. 13.3. it is shown that the variation of the gross and the net process efficiencies in a process with various amount of draw-in, obtained by varying the load on the pressure plate, and by using the serrated die and holding plate. It shows that the net process efficiency, which represents the degree of uniformity of the thickness in the workpiece, remains virtually constant (Fig. 13.3.). In other words, with greater draw-in, the product becomes literally thicker as compared with the one without draw-in (Fig. 11.3.) but actually with little change in the distribution of thickness. This implies that there is no improvement on the thickness uniformity if the drawn portion of the flange is taken into account.

The real advantage of draw-in can be shown by the gross efficiency, which increases considerably with draw-in as shown in Fig. 13.3.

The increase in the gross process efficiency is due to the use of a nominal area, A_o, rather than the real area, A_r, in the calculation. Therefore, the gross process efficiency represents the nominal uniformity in the thickness of sheet metal products. Indeed, the gross process efficiency can be, sometimes, greater than 100% (i.e. the ideal uniform thickness distribution) if the amount of draw-in is large. The gross process efficiency can be re-written in terms of the net process efficiency and draw-in as follows:

Gross process efficiency, %

$$= \frac{\log_e A - \log_e A_o}{\varepsilon_h^*} \times 100\%$$

$$= \frac{\log_e A - \log_e A_r + \log_e A_r - \log_e A_o}{\varepsilon_h^*} \times 100\%$$

$$= \left(\frac{\log_e A - \log_e A_r}{\varepsilon_h^*}\right) + \left(\frac{\log_e A_r - \log_e A_o}{\varepsilon_h^*}\right) \times 100\%$$

$$= (\text{Net process efficiency}) + \left(\frac{\text{draw-in}}{\varepsilon_h^*}\right) \times 100\% \qquad \text{Eq. 13.2.}$$

In equation 13.2., the net process efficiency remains virtually constant irrespective of draw-in. Therefore, the gross process efficiency varies with the second term in the brackets in equation 13.2. As can be seen, the draw-in increases while the corresponding ε_h^* decreases, the gross process efficiency thus increases considerably. Obviously, the gap between the gross and the net process efficiencies in Fig. 13.3. is the difference between them and is equal to $((\text{draw-in})/\varepsilon_h^*)$.

Fig. 13.3. also shows that to some extent (draw-in, 0.25 - 0.35), as the draw-in increases, the (numerically) maximum through-

thickness strain at the critical section (ε_h^*) varies slightly. This causes the slope of the gross process efficiency curve falling slightly within this range.

The ratio of the gross process efficiency to the net process efficiency is given by:-

$$\frac{\text{Gross process efficiency}}{\text{Net process efficiency}}$$

$$= \frac{(\log_e A - \log_e A_o)/\varepsilon_h^*}{(\log_e A - \log_e A_r)/\varepsilon_h^*}$$

$$= \frac{\log_e A - \log_e A_o}{\log_e A - \log_e A_r}$$

$$= \frac{\log_e (\frac{A}{A_o})}{\log_e (\frac{A}{A_o})}$$

where $\log_e (\frac{A}{A_o})$ = nominal average surface strain

= nominal overall average thickness strain

$\log_e (\frac{A}{A_r})$ = real average surface strain

= real overall average thickness strain

D. The Utilization of the Material With Reference to its Thickness Strain

When the numerical value of thickness strain is plotted against draw-in as shown in Fig. 13.4. which is obtained by varying the load on the pressure plate, the utilisation of the material in forming process can be easily interpreted.

In Fig. 13.4. the higher the numerical value of the thickness strain means the thinner a material can be formed without failure. Four different thickness strain curves are drawn. Curves A and B

represent the thickness strains at the critical section of a material and curves C and D are the overall average thickness strains of a deformed product.

Curve A in Fig. 12.4. shows the maximum attainable thinning at the critical section of a product in the bulge test, that can be stretched in balanced biaxial tension extrapolated from the formability curve in Fig. 8.4. In other words, it is the maximum formability or the best utilization of the material in the forming processes. For test conditions other than the balanced biaxial stretching ($\eta = 6$), failure at the critical section occurs at a numerically lower value of the thickness strain and is shown as curve B in which the thickness strain decreases numerically with the amount of draw-in. This was explained in detail in section A, Chapter 13, and is due to the unfavourable change of the strain ratio at the critical section as draw-in increases. If, instead of the thickness strain at the critical section (the thinnest section in the product), the overall average thickness strain of the whole product is considered, numerically smaller values will be expected and shown as curves C and D. It means that most of the material other than that at the critical section is not fully utilized. Curves C and D are based, respectively, on the surface strains represented the nominal ($\ell n \frac{A}{A_o}$) and the real ($\ell n \frac{A}{A_r}$) overall average thickness strains. The nominal overall average thickness strain, curve C, is shown to increase with the amount of draw-in but the real overall average thickness strain, curve D, remains nearly constant. The reasons for these variations have been explained in Section B, Chapter 13.

The difference among the four curves may be interpreted in terms of a threefold loss of the utility of a material in forming processes.

The difference between curves A and B represents the first loss of utility owing to unfavourable strain ratio (at the critical section). The second loss of utility (difference between curves B and C) is due to uneven distribution of strain but there is some gain when the amount of draw-in is greater than 0.26 as shown in Fig. 13.4. This gain is due to the benefit of draw-in.

The third loss of utility between curves C and D, is due really to a realistic but unfavourable way of accounting.

How efficient the thickness of a material is utilized can be also shown by the ratios among the curves. The ratio between curves B and A may be said to correspond to a theoretical efficiency, which means the degree of unfavourable strain ratios. Obviously, the ratio between curves C and B is the gross process efficiency and that between D and B is the net process efficiency. They were discussed in Section C, Chapter 13, and will not be repeated here.

Chapter 14. - CONCLUSION AND SUGGESTIONS FOR FUTURE WORK

A. Conclusion

In this investigation, an attempt is made to analyse the effect of process parameters on the formability of sheet metal because such efforts may be considered to be both of scientific and of technological interest. The results obtained so far in this thesis do not, in fact, cover more than one familiar material, nor are the results repeated for extensive ranges of test conditions. Indeed, such repetitions and coverage are never contemplated. The interesting and significant part of this research, in the view of the investigator, lies rather in the clarification and enrichment of the basic ideas of sheet metal engineering, ideas which are indispensable for the assessment and improvement of sheet metal performance, either from the metallurgical (or suppliers') point of view, or from the mechanical (or die designers') point of view. In other words, they are the fundamental ideas of formability and the tests to assess it.

As has been discussed in the foregoing chapters, in the course of trying to find the effects of the process parameters on the formability of sheet metal, it is found necessary to define "formability" first. The complex concept of formability has to be analysed as far as possible into clear-cut components or aspects, if progress is to be made in even representing the effects of the process parameters on it, which is the object of this project to discover. Thus, in the theoretical study of this investigation, the analysis of formability, as distinguished from drawability, is based on the generalization that, in sheet metal forming, a plane sheet is transformed into a thin shell by biaxial stretching. Formability is shown and clarified by representing it quantitatively

in four aspects, namely,

1) the formability of the material at the critical section,

2) the formability of the material in general,

3) the process efficiency,

4) the proportional increase in surface area.

Hence, the material formability (aspects 1 and 2) is distinguished from the extent to which the formability (or ductility) is exploited in particular processes (aspects 3 and 4). It cannot be unreasonable to expect that such an analytical approach to the problem will benefit industry in the end. Inadequacy in material formability should hence-forth be set apart from poor process efficency, and the effects of poor die design or inherently difficult shape of the product should no longer be thought to be due to poor work material, and vice versa.

Once a clear analysis of the concept of formability is made, other familiar problems in sheet metal research become automatically easier to solve. It is often thought that there are so many ways in which sheet metal can be deformed that it is generally desirable to search for a sheet metal test which can represent them all and from which the test result will be universally applicable. This is found impossible because formability itself is a spectrum of a ductility index and cannot be adequately represented by a single ductility index, as is done in current sheet metal tests. Also, many sheet metal engineers try to modify Swift's or Erichsen test or some other test in a never ending search for empirically chosen test conditions which will yield results consistent, to one degree or another, with the known performance of a particular sheet metal in a particular set of forming processes. Such methods of trial-and-error should now no longer be necessary because once the curve that represents completely the material formability of

any particular work material, is found, it can be interpreted to predict the material performance in any particular forming process. The unifying principles that make such general results on formability possible are few and simple:

1) A meticulous and precise method determining the end point of the forming process.

2) The limit of formability, though path dependent, is nevertheless, unique, because the strain paths of the critical section in most practical forming processes are very similar to each other.

and

3) The hydrostatic stress in all ordinary sheet metal forming processes is too small to show its effects on the ductility of the material.

Thus apart from the problem of non-coaxiality of the successive strains, all the numerous process parameters, such as punch profile radius, load on the pressure plate, blank size, surface finish and lubrication, are seen to produce only one effect, namely, the direction of the strain path of the critical section in the clock diagram, or, in more familiar terms, the strain ratios at the critical section of the workpiece. Such effects on the strain ratios at the critical section become particularly easy to see by using the triangular coordinate system (which, if widely adopted, will make literature on sheet metal research much easier to assimilate and compare in the future), and by uncovering the various but similar, effects on draw-in.

To find the strains involved in the formed products, the non-directional circular grid system, which fails to distinguish between the coaxial and non-coaxial strains, has been shown to be at best inaccurate and at its worst inadequate for assessing the formability, hence another system of markings has been used. Every strain path of the critical section in

the axisymmetrical processes plotted in the triangular coordinate system is nearly a straight radial one. It indicates proportional deformation in which the ratios among the three principal strains ($\varepsilon_h : \varepsilon_\theta : \varepsilon_s$) remain nearly constant.

The determination of the formability curve is closely related to the criterion of the end point used but the limit of strain path of the critical section is difficult to determine because no clear-cut transition from the diffused to the local necking is shown in the forming processes. An arbitrary method (from the practical point of view, initiation of necking rather than fracture) is chosen as the end point, and this method is based on the study of the circumferential and the through-thickness strain distributions.

For deformation with three different process parameters (punch profile radius, blank size and load on the pressure plate) the relationship between draw-in (ψ) and penetration (P) is $\psi = K P^2 - C$, where K and C are constants. Draw-in has been found to be inevitable during forming. The effects of draw-in are first analysed in kinematical terms. For the same penetration, the (numerically) maximum through-thickness strain at the critical section decreases with the amount of draw-in owing to the unfavourable change of the strain path away from 6 o'clock towards 5 o'clock. Fortunately, the action of draw-in generally favours the forming processes. In a given process, the overall thickness of a formed product with draw-in is greater than the one without it. The material at the flange is drawn to form part of the product to enable further deformation by this feeding action which tends to delay fracture. This improves substantially the attainable surface area of the product and the gross process efficiency. Draw-in has also a pronounced effect on the radial displacements in the outer third of the initial radial

distance of the unsupported part of the blank. By varying the amount of draw-in, the strain distribution changes. This leads to the change of the general shape of the formed product, especially in the unsupported region, from an ellipsoid of revolution (with draw-in) to that of a round tent (without draw-in). The position of the critical section shifts outward from the axis of symmetry, as the amount of draw-in increases. Draw-in affects the curvature of the strain path of the critical section as well.

B. Suggestions for Future Work

The results obtained so far have led to definite conclusions in sheet metal engineering, but they have also suggested further investigations along certain lines like the following:

i) The development of the neck

The difficulty of determining the end point is due to the fact that no clear-cut transition from the diffused to the local necking is shown in the forming processes. An arbitrary method is thus used in this investigation. As the determination of the end point of formability is a crucial matter in the study of sheet metal, the development of the neck (or the plastic instability) may be further investigated so that a more precise criterion of end point may be devised.

ii) Unsymmetrical forming processes

There are two kinds of strain paths, coaxial and non-coaxial respectively. In this investigation, it is confined to the coaxial one (axisymmetrical forming processes). It is desirable to extend the investigation to the case of non-coaxial one because most industrial forming products are usually unsymmetrical especially in regions where the amount of draw-in varies along the edge of the unclamped portion of the work. Also, in axisymmetrical forming, the slope of the zig-zag strain path (which is especially connected with re-drawing) do not normally cover a wide range of characteristic indices. Therefore, there is no significant effect observed (Chapter 8). In non-coaxial strain paths, however, the combined effect of the curvature of zig-zag strain paths and that of the non-coaxiality may be more severe

so that their effects can be explored. In any case, it is important to establish how great the effect of non-coaxiality is on the formability of the material.

iii) Stresses

An attempt may be useful to represent the "stress path" in the triangular coordinate system so as to obtain a whole picture of the stress-strain relationship during forming. This has indeed been done before,[42] [43] most of them were dealt with in the bulge test,[44] [9] [11] but it is desirable to correlate results on stress with those of strain in the work both in axisymmetrical and unsymmetrical forming processes with solid punch. Hence, the work-hardening index (n) can be obtained accurately, if possible, and its effects on the formability.

iv) Comparison of formability based on material properties and process efficiency

A very fundamental concept of formability is laid down in this investigation. Different materials such as aluminium, titanium or other sheet metal may be tested as well. Material formability based on the formability curve, is a complex characteristic, such that it is theoretically impossible to say that one material is more formable than another under all conditions, because the ductility is path dependent and two formability curves may, for all we know, cross each other.

v) Anisotropy (the r-value)

Sheet metal, even after annealing, tends to have directionality during deformation owing to the development of preferred orientation of the grains of the material. This effect is known as the anisotropy of sheet metal. It is obvious that the r-value has

effects on the formability of the material because the r-value itself is one of the material property. It is expected that, by varying the r-value, a family or system of formability curves can be obtained for any given anisotropic material.

vi) Metallurgical Studies

Changes in the formability curve due to metallurgical changes in the material - leading to improved materials, either generally or in narrow ranges of η-value.

BIBLIOGRAPHY

1. G.S.A. SHAWKI, Assessing deep-drawing qualities of sheet, Sheet Metal Industries, 42, 1965, 363-368; 417-424; 524-532.

2. T.C. HSU AND A.S. WILLIAMSON, Plastic deformation of an aluminium alloy in the tension test, Proc. Am. Soc. Testing Mats., 65, 1965, 575-595.

3. W. JOHNSON AND P.B. MELLOR, Plasticity for mechanical engineers, 1962, Van Nostrand Reinhold press.

4. S.Y. CHUNG AND H.W. SWIFT, Cup-drawing from a flat blank, Proc. I. Mech. E., 165, 1951, 199-228.

5. H.W. SWIFT, The mechanism of a simple deep-drawing operation, Sheet Metal Industries, 31, 1954, 817-828.

6. S. FUKUI, Sci. Pap. I.P.C.R., Tokyo, 34, 1938, 1422-1527; 35, 1939, 377-385.

7. P.B. MELLOR, Stretch forming under fluid pressure, J. Mech. Phys. Solids, 5 (1), 1956, 41-56.

8. N.M. WANG AND M.R. SHAMMAMY, On the plastic bulging of a circular diaphram by hydrostatic pressure, Research Publication, G.M.R., 837, 1968.

9. R. HILL, A theory of the plastic bulging of a metal diaphram by lateral pressure, Phil. Mag. 41 (Ser. 7), 1950, 1133-1142.

10. E. SIEBEL AND A. POMP, Ein neues prüfverfahren für feinblech, Mitt. K.W. Inst. für Eisenforschung, 11 (136), 1929, 287-291.

11. W.F. BROWN, JR. AND G. SACHS, "Strength and failure characteristics of thin circular membranes", Trans. A.S.M.E., 70, 1948, 241-249.

12. I. BLUME, Ermittlung der ziefähigkeit von tiefstanzblechen, Metallborse, 12, 1922, 1945-1946.

13. G.R. FISCHER, A.E.G.-tiefziehprüfverfahren, A.E.G. Mitteilungen. 7, 1929, 483-486.

14. M SCHMIDT, Die prüfung von tiefzeiehblech, Arch. Eissenhuttenwesen, 3, 1929, 213-222.

15. I.D.D.R.G. WG. III - Recommended procedure for carrying out the Swift - I.D.D.R.G. cup forming test - I.D.D.R.G./ WG. III (14A), 67.

16. J. WALLIS, Deep drawing: A review of the practical aspects of Prof. H.W. Swift's researches, Butterworths Scientific Publications, London, 1954, 122-124.

17. R.D. BUTLER, B.B. MORETON AND D.V. WILSON, The importance of drawing and fracture loads in the Swift cup drawing test, Sheet Metal Industries, 40, 1963, 620-632.

18. B. KAFTANOGLU, AND J.M. ALEXANDER, An investigation of the Erichsen test, Journal of the Institute of Metals, 90, 1961-62. 457-470.

19. M. YOKAI AND J.M. ALEXANDER, A further investigation of the Erichsen test, Sheet Metal Industries, 44. 1967, 466-475.

20. M. GENSAMER, Strength and ductility,(Campbell's lecture)Trans. Am. Soc. Metals, 36, 1946, 30-60.

21. S.P. KEELER, Determination of forming limits in automotive stampings, Sheet Metal Industries, 42, 1965, 683-691.

22. S.P. KEELER, Circular grid system - A valuable aid for evaluating sheet metal formability, 45, 1968, 633-641.

23. S.P. KEELER, Understanding sheet metal formability, Sheet Metal Industries, 48, 1971, 357-364; 440-449; 511-517; 589-618; 687-699; 739-745.

24. G.M. GOODWIN, Application of strain analysis to sheet metal forming problem in the press shop, La Metallurgia Italiana, 60 (8), 1968. 767-774.

25. H. NAKAJIMA, Effect of strain path on fracture strain, Proc. Conference on the Technology of Sheet Metal Forming 1969, 85-97. (In Japanese).

26. K. YOSHIDA, K. ABE, K. MIHAUCHI, AND T. NAKAGAWA, Instability and fracture behaviours in sheet metal forming; La Metallurgia Italiana, 60 (8), 1968, 685-699.

27. K. YOSHIDA, A study of deformation constitutional diagram and its application, Reports of the Institute of Physical and Chemical Research, 44 (4), July, 1968, 169-185.

28. H.W. SWIFT, Plastic instability under plane stress, J. Mech. Phys. Solids, 1, 1952, 1-18.

29. O. HOFFMAN AND G. SACHS, Introduction to the theory of plasticity for engineers, N.Y. McGraw-Hill Press, 1953.

30. R. HILL, On discontinuous plastic states with special reference to localized necking in thin sheets, J. Mech. Phys. Solids. 1, 1952, 19-30.

31. S.P. KEELER AND W.A. BACKOFEN, Plastic instability and failure in sheets stretched over rigid punches, Tran. Am. Soc. Metals, 56, 1963, 35-48.

32. J. WOODTHORPE AND R. PEARCE, The effect of r and n upon the forming limit diagrams of sheet steel, Sheet Metal Industries, 46, 1969, 1061-1067.

33. C. CHR. VEERMAN, L.HARTMAN, J.J. PEELS AND P.F. NEVE, Determination of appearing and admissible strains in cold-reduced sheets, Sheet Metal Industries, 48, 1971, 678-680; 692-694.

34. T.C. HSU, The characteristics of coaxial and non-coaxial strain paths, Journal of Strain Analysis, 1 (3), 1966, 216-222.

35. T.C. HSU AND A.J. YOUNG, Plastic deformation in the compression test of pure copper, Journal of Strain Analysis, 2 (2), 1967, 159-170.

36. T.C. HSU, W.R. DOWLE, C.Y. CHOI, AND P.K. LEE, Strain histories and strain distributions in a cup drawing operation, Trans, A.S.M.E. 93 B(2), 1971, 461-466.

37. T. MIZUNO AND K. KADEDA, A study of cup drawing, Paper presented at the 21st Joint Meeting of Japan Society of Technology of Plasticity, Japan Society of Mechanical Engineers and other seven societies, Osaka, 19-21st Nov., 1971. (Original in Japanese, Translated by the authors into English for Prof. T.C. Hsu.).

38. L.R. HAWTIN, D.R. MEAR AND R.H.C. JOHNSON, An appraisal of current information on the Erichsen test, Sheet Metal Industries, 40, 1963, 495-499.

39. K. TAKASHINA, T. HERAI, H. KOMORIDA AND T. HORITA, Relation between the manufacturing conditions and the average strain according to the scribed circle tests in steel sheets, La Metallurgia Italiana, 60(8), 1968, 757-765.

40. T.C. HSU, The kinematics of axisymmetrical sheet metal forming processes and the definition of drawability, Proc. International Conference on the Science and Techno logy of Iron and Steel, Tokyo, Part II, 1971, 903-907.

41. K. YOSHIDA, Recent research on press forming limit of sheet steel, Iron and Steel, 56 (3), 1970, 402-419 (In Japanese).

42. H. FORD, Researches into the deformation of metals by cold rolling, Proc. I. Mech. E., 159, 1948, 115-143.

43. R. HILL, The mathematical theory of plasticity, Oxford press, 1950.

44. B. KAFTANOGLU AND J.M. ALEXANDER, On quasistatic axisymmetrical stretch forming, Int. J. Mech. Sci., 12, 1970, 1065-1084.

45. British Standard No 3855, 1965. P. 5.

46. H.M. SHANG AND T.C. HSU, Test for sheet metal formability with coupon and circular specimens (in press).

List of figures:

Photographs:

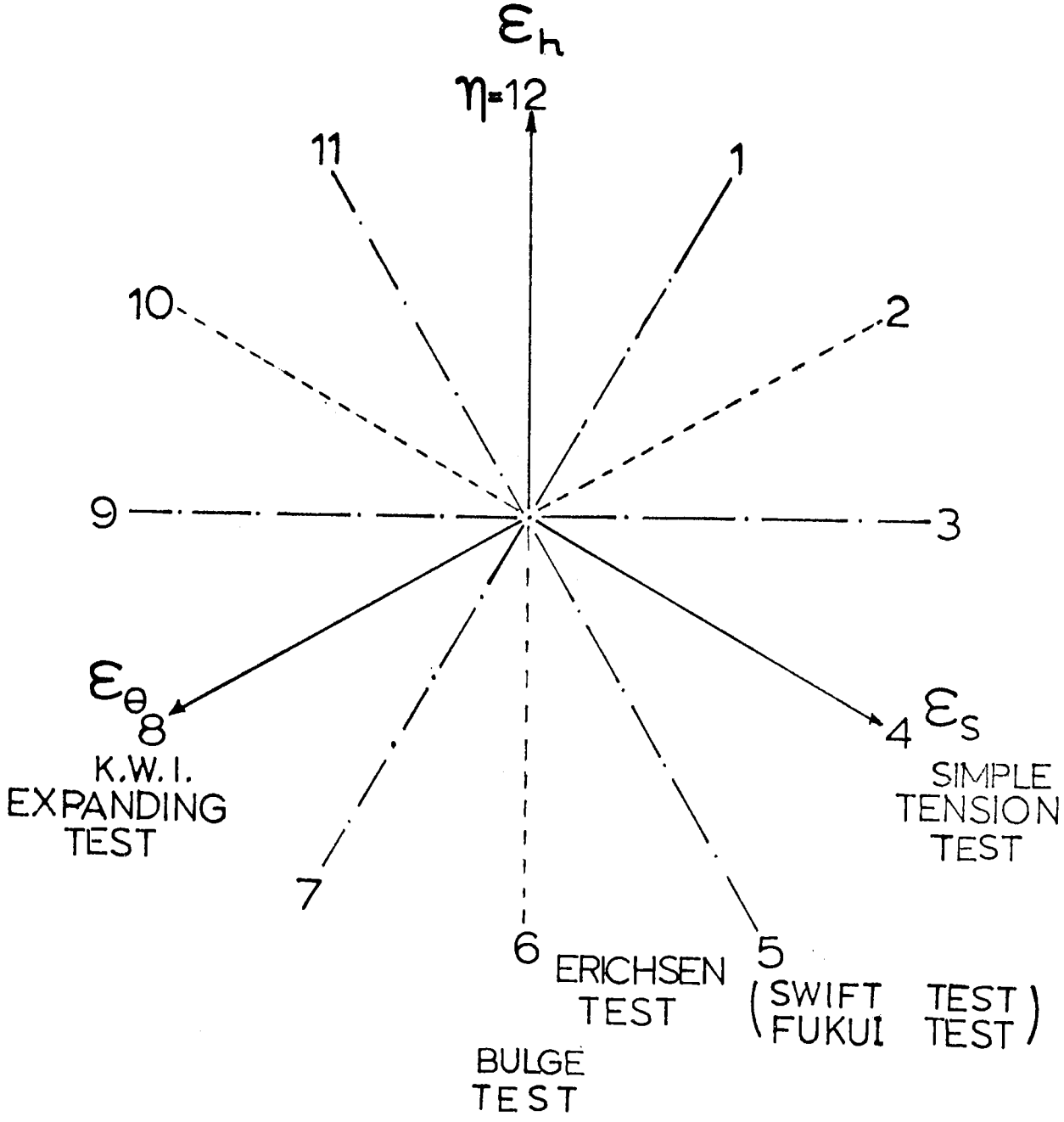
ε_h
η=12
11
1
10
2
9
3
ε_θ
8
K.W.I.
EXPANDING
TEST
4
ε_s
SIMPLE
TENSION
TEST
7
6
ERICHSEN
TEST
5
(SWIFT TEST
FUKUI TEST)
BULGE
TEST

FIG. 2.1.

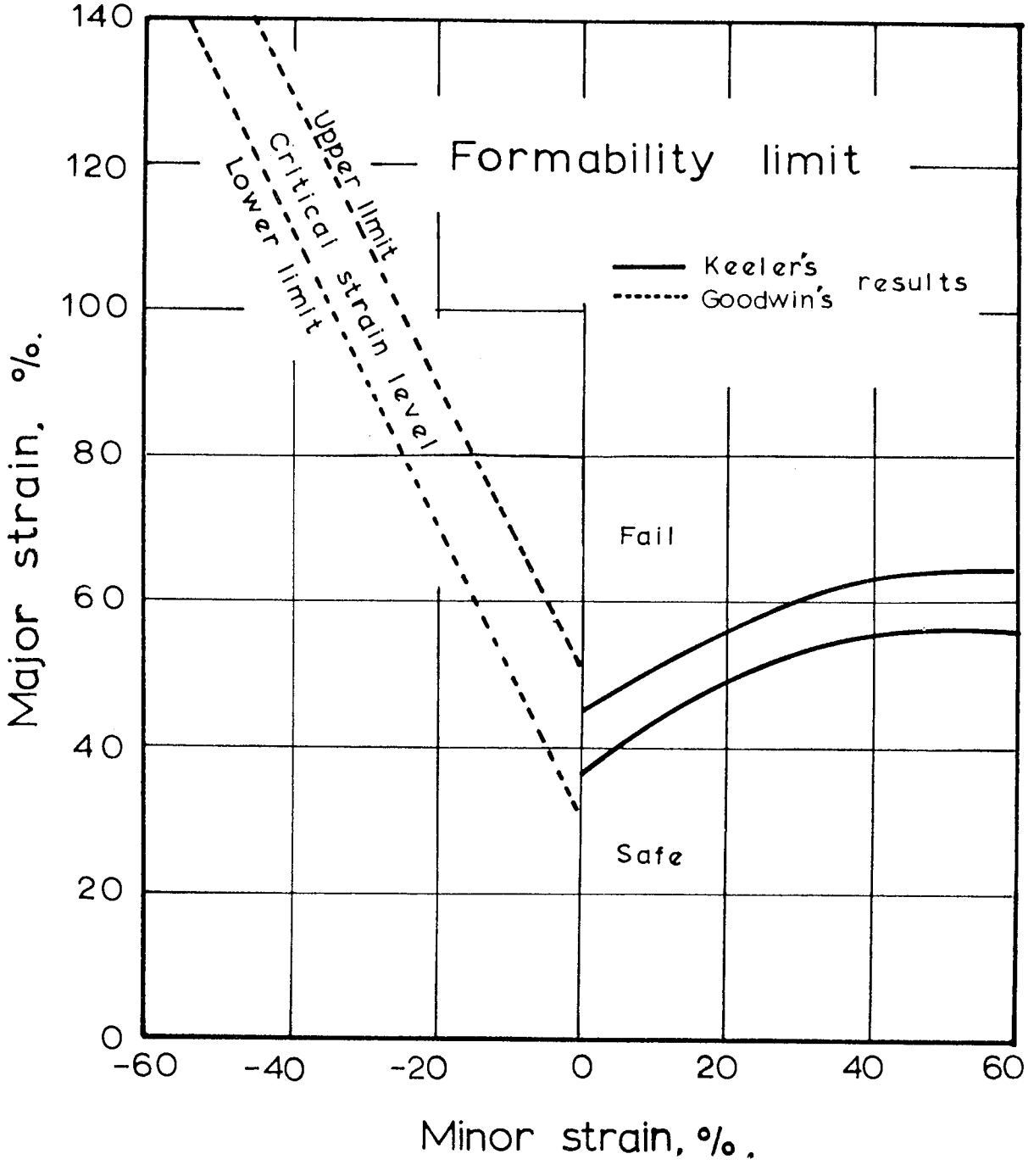

FIG. 2.2. after ref.(24)

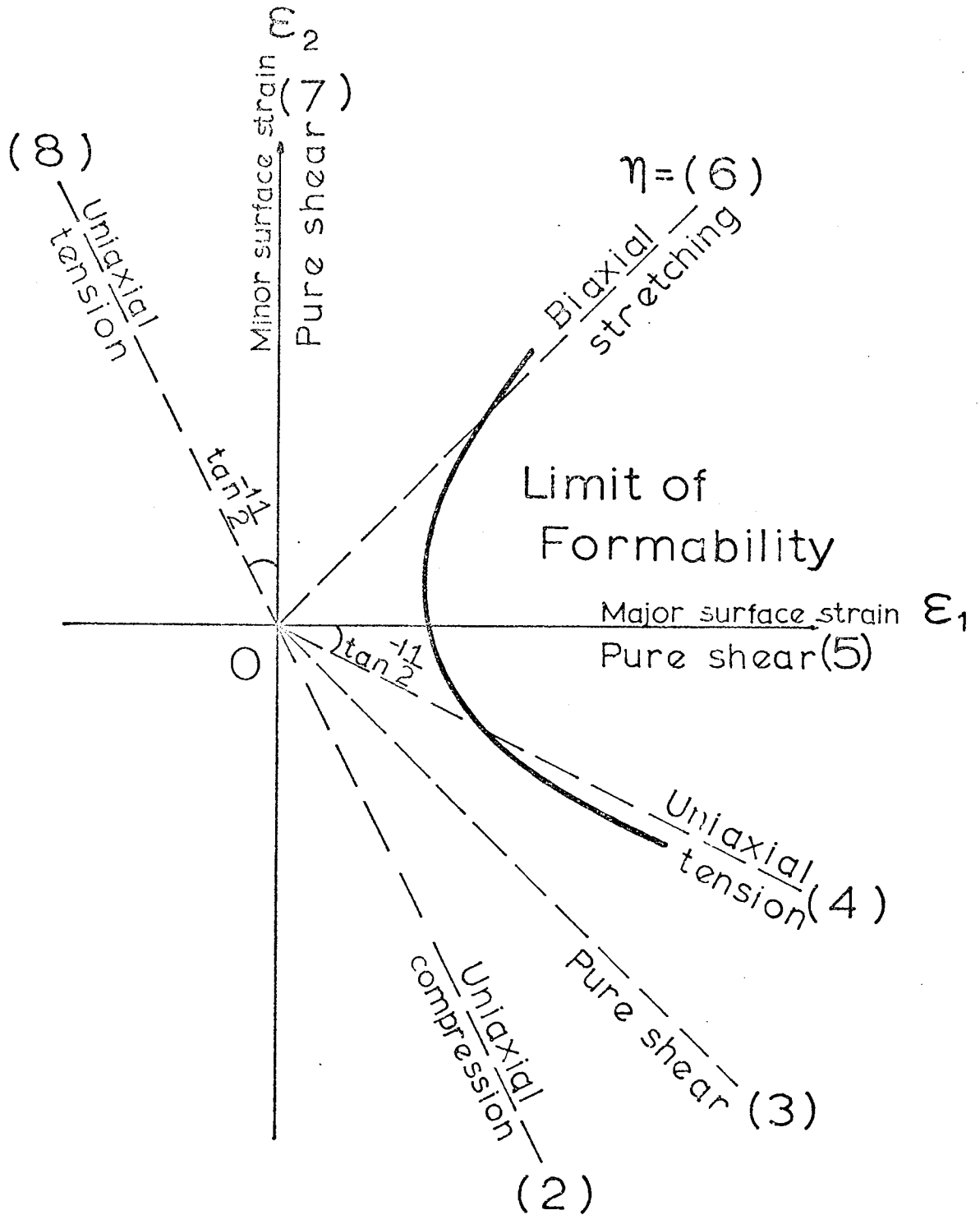
Minor surface strain ε_2
Pure shear (7)
(8)
Uniaxial tension
$\tan^{-1}\frac{1}{2}$
$\eta = (6)$
Biaxial stretching
Limit of Formability
Major surface strain ε_1
Pure shear (5)
O
$\tan^{-1}\frac{1}{2}$
Uniaxial tension (4)
Pure shear (3)
Uniaxial compression
(2)

FIG. 2.3.

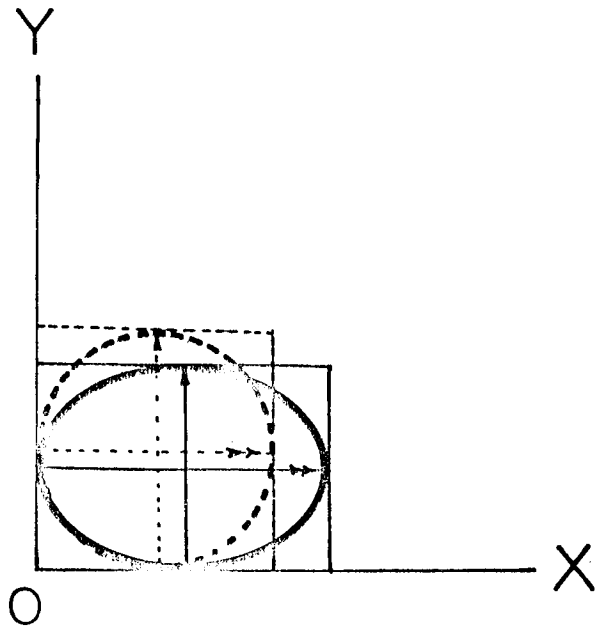

Coaxial strain

FIG. 3.1.a.

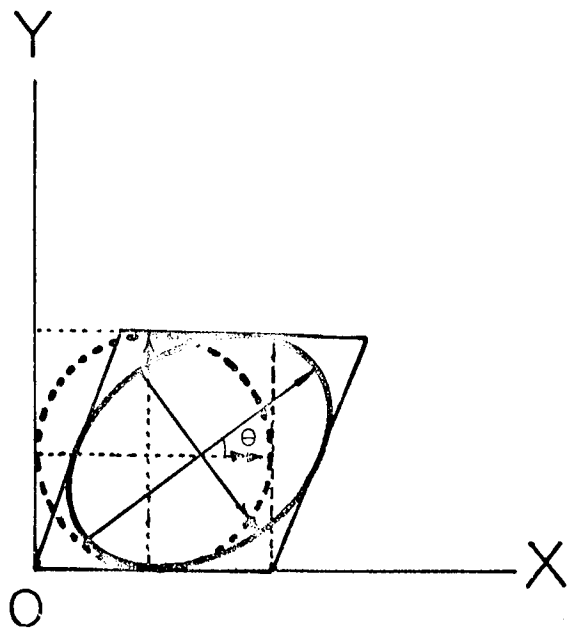

Non-coaxial strain

FIG. 3.1. b.

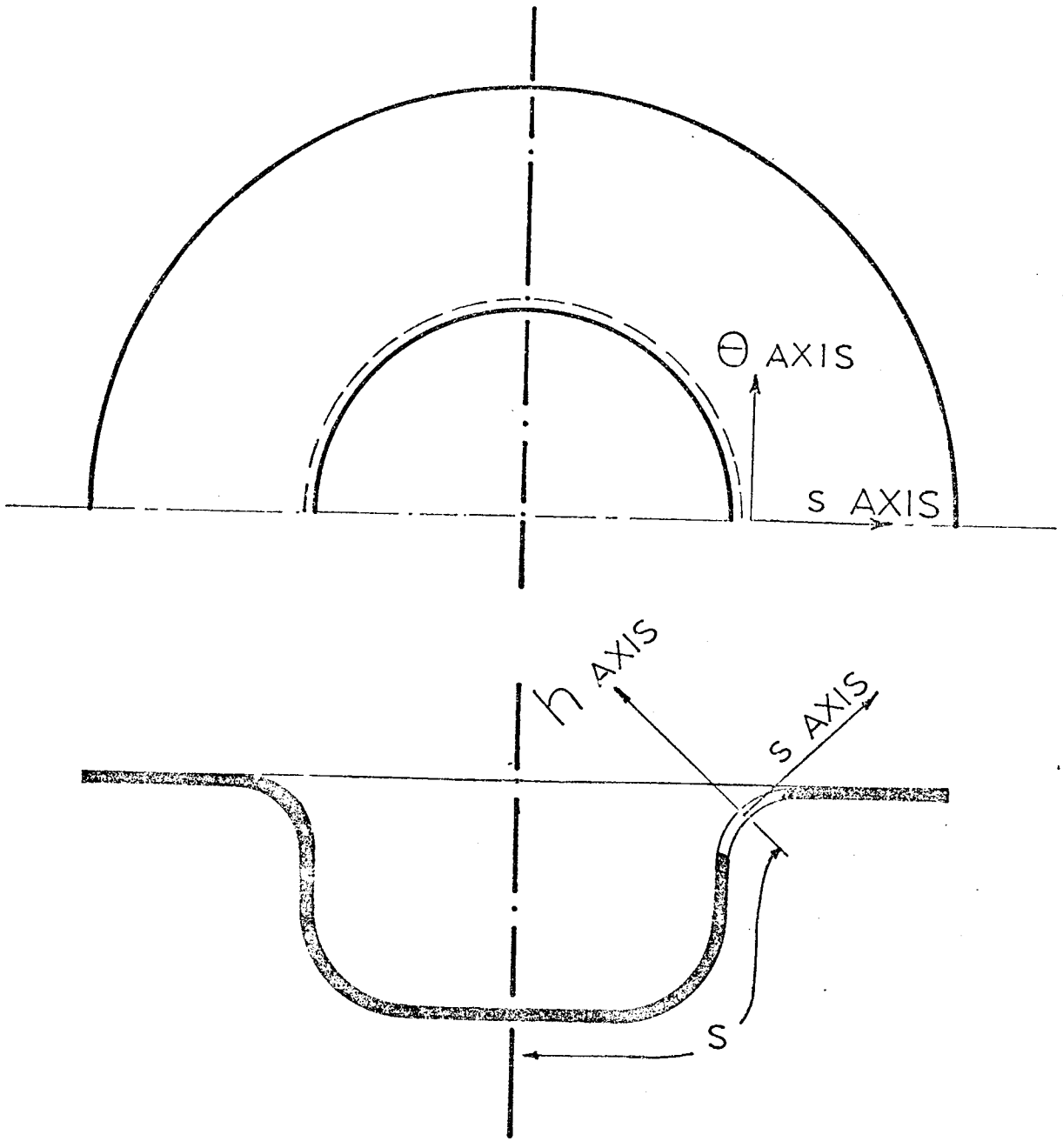

FIG. 3.2.

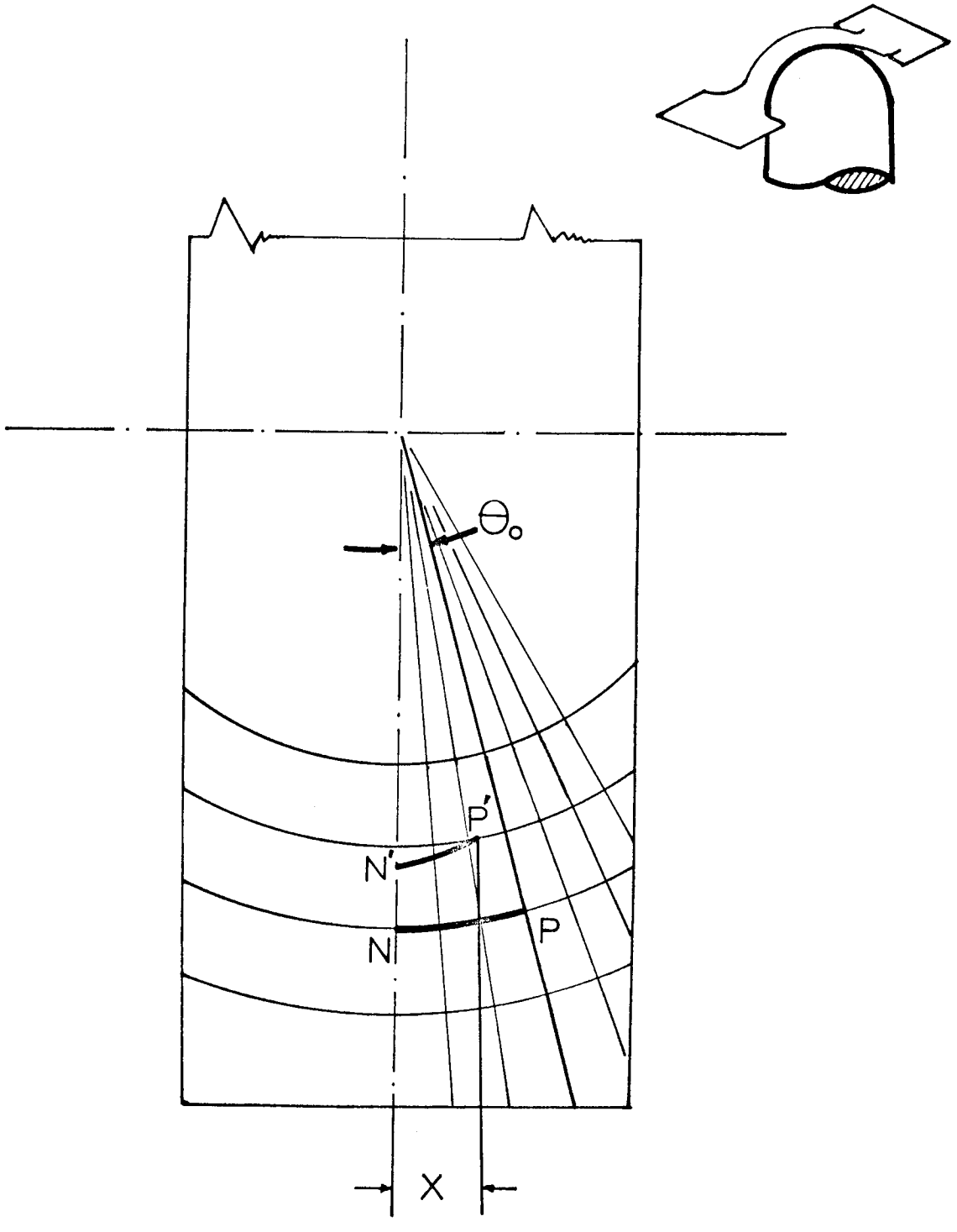

FIG. 3.3.

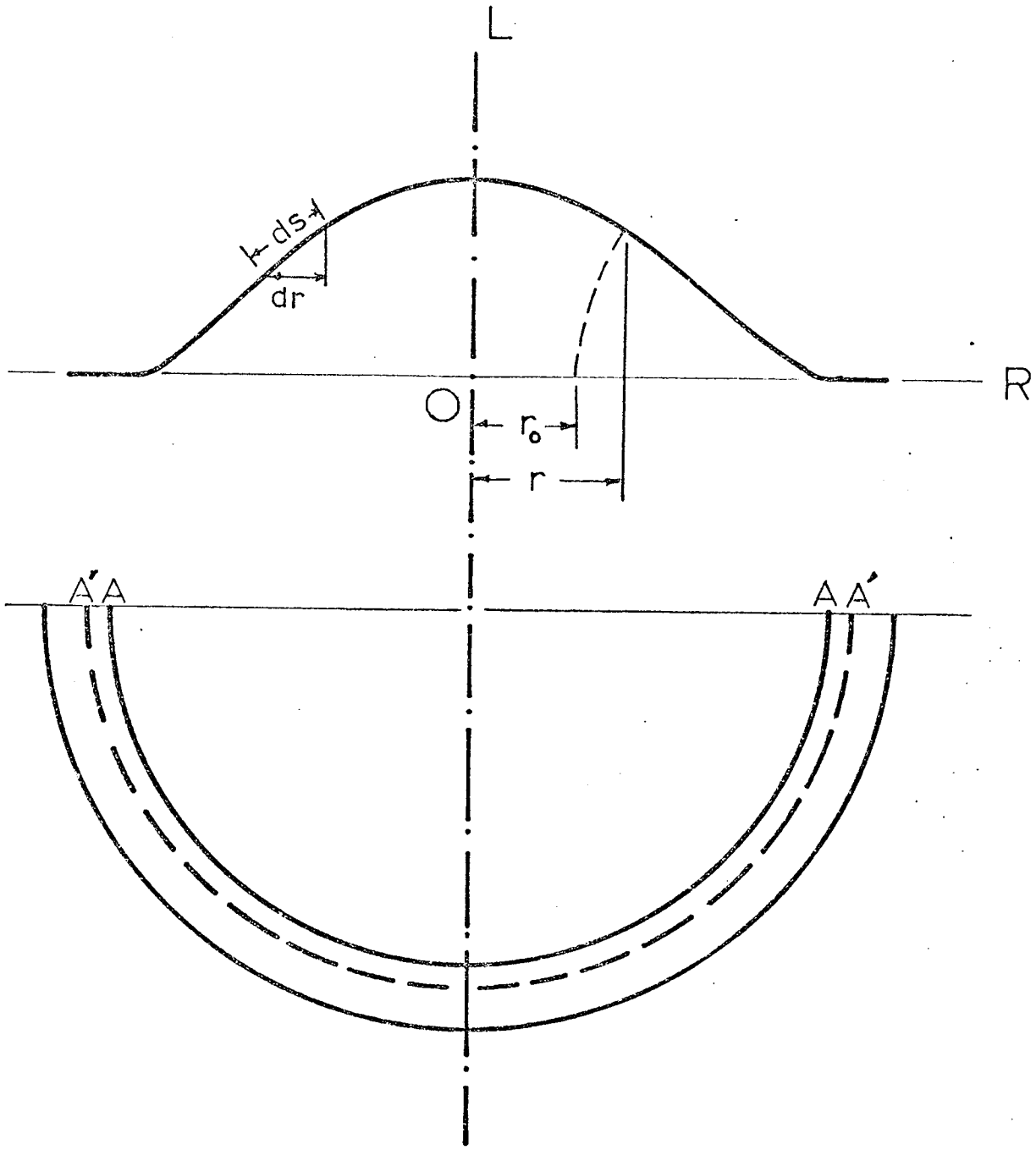

FIG. 3.4.

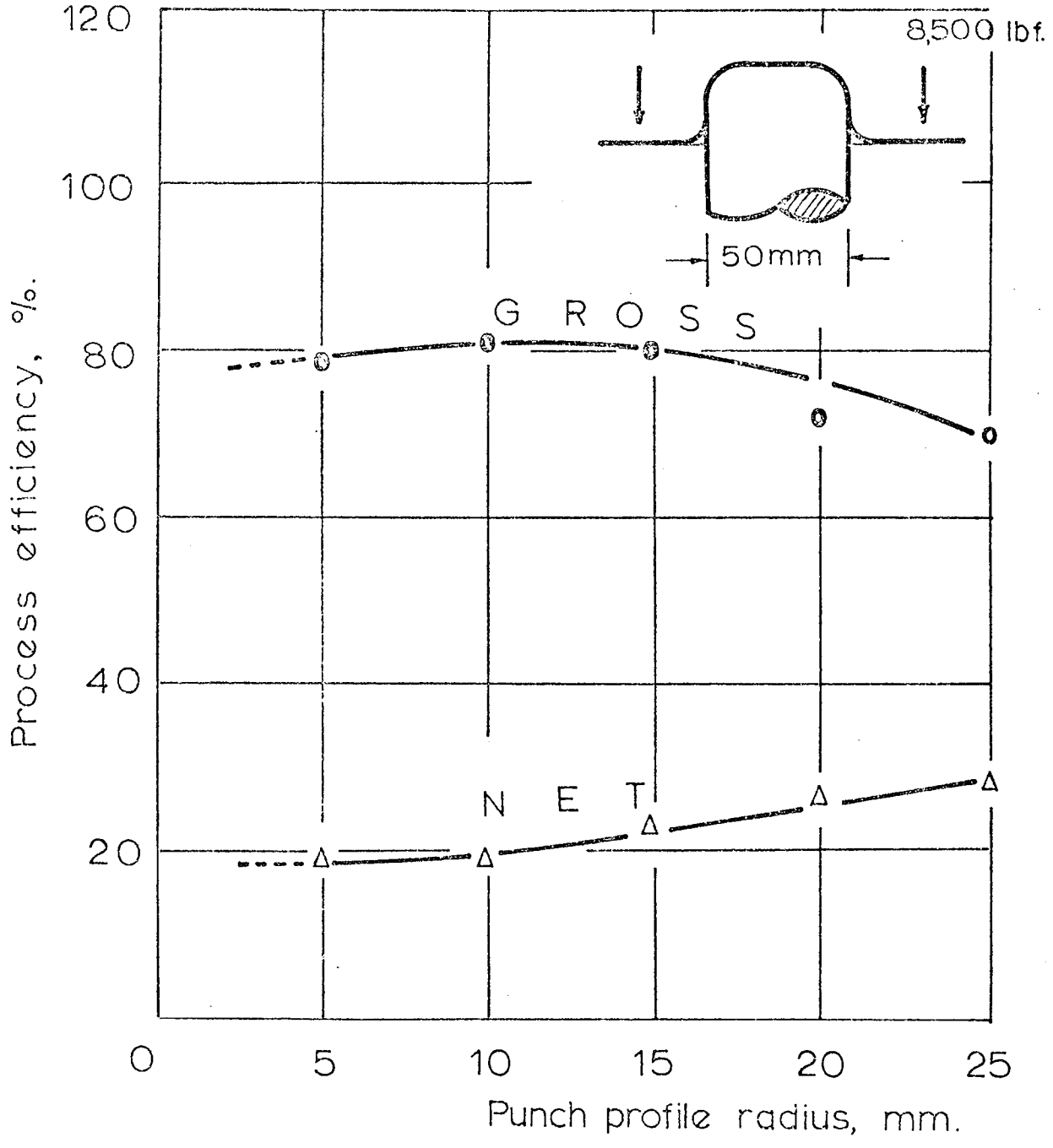
120
100
80
60
40
20
0
5
10
15
20
25
Process efficiency, %.
Punch profile radius, mm.
8,500 lbf.
50mm
G R O S S
N E T

FIG. 3.5.

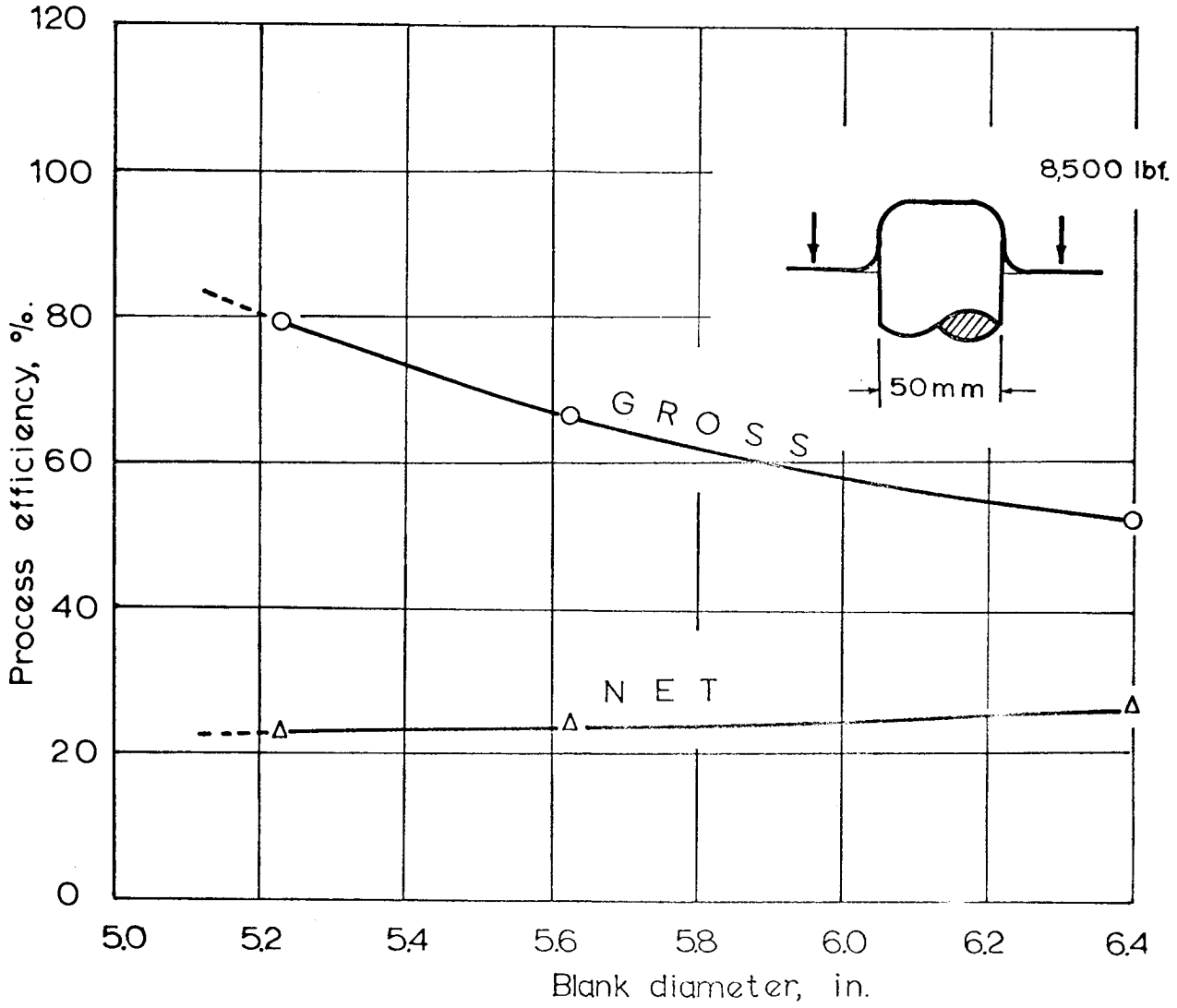
120
100
80
60
40
20
0
Process efficiency, %.
8,500 lbf.
50mm
GROSS
NET
5.0
5.2
5.4
5.6
5.8
6.0
6.2
6.4
Blank diameter, in.

FIG. 3.6.

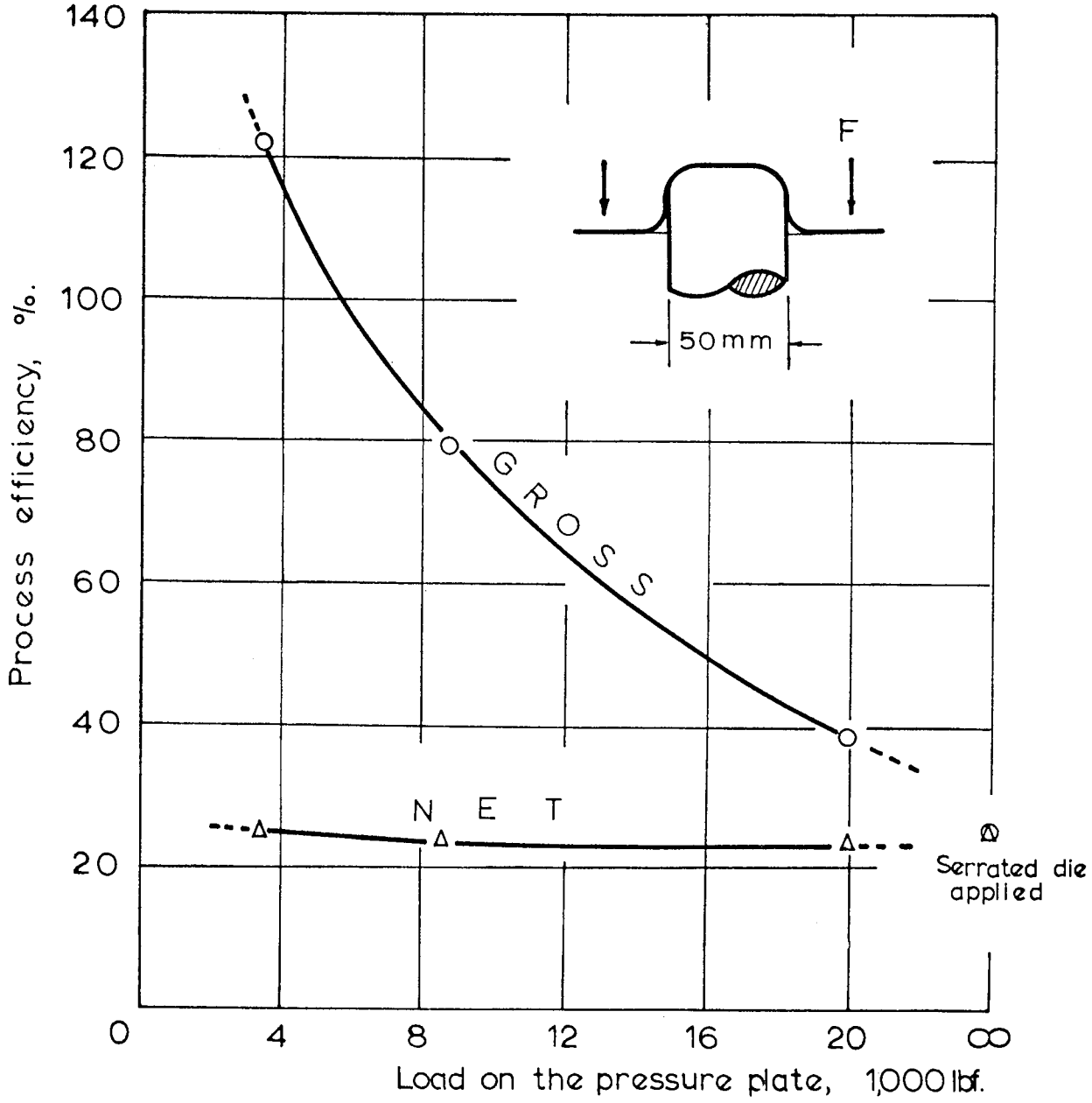
140
120
100
80
60
40
20
0
Process efficiency, %.
F
50 mm
GROSS
NET
Serrated die applied
4
8
12
16
20
∞
Load on the pressure plate, 1,000 lbf.

FIG. 3.7.

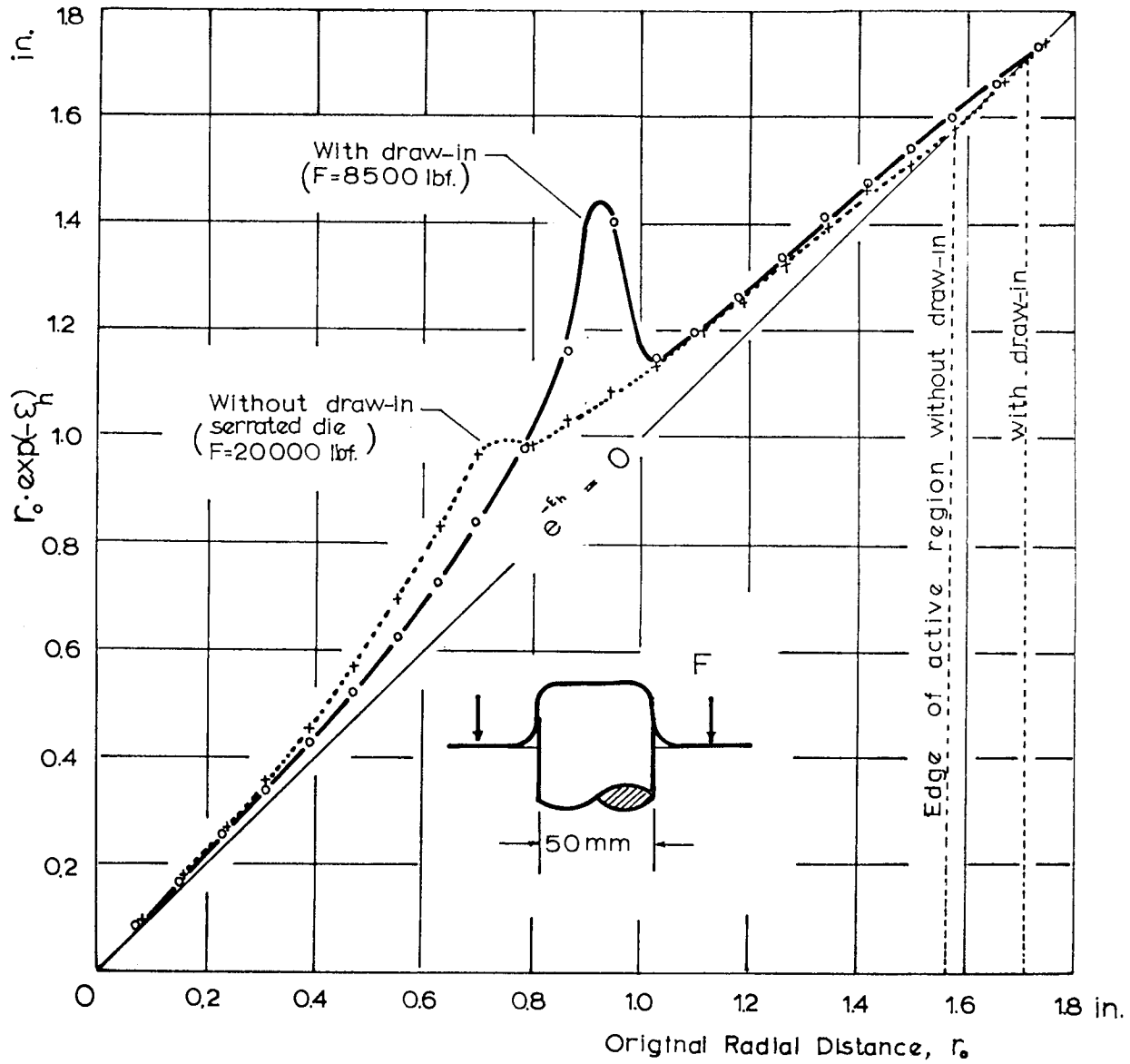
in.
1.8
1.6
1.4
1.2
1.0
0.8
0.6
0.4
0.2
0
$r_o \cdot \exp(-\varepsilon_h)$
With draw-in
(F=8500 lbf.)
Without draw-in
(serrated die
F=20000 lbf.)
$e^{-\varepsilon_h} = 0$
F
50mm
Edge of active region without draw-in
with draw-in
0.2
0.4
0.6
0.8
1.0
1.2
1.4
1.6
1.8 in.
Original Radial Distance, r_o

FIG. 3.8.

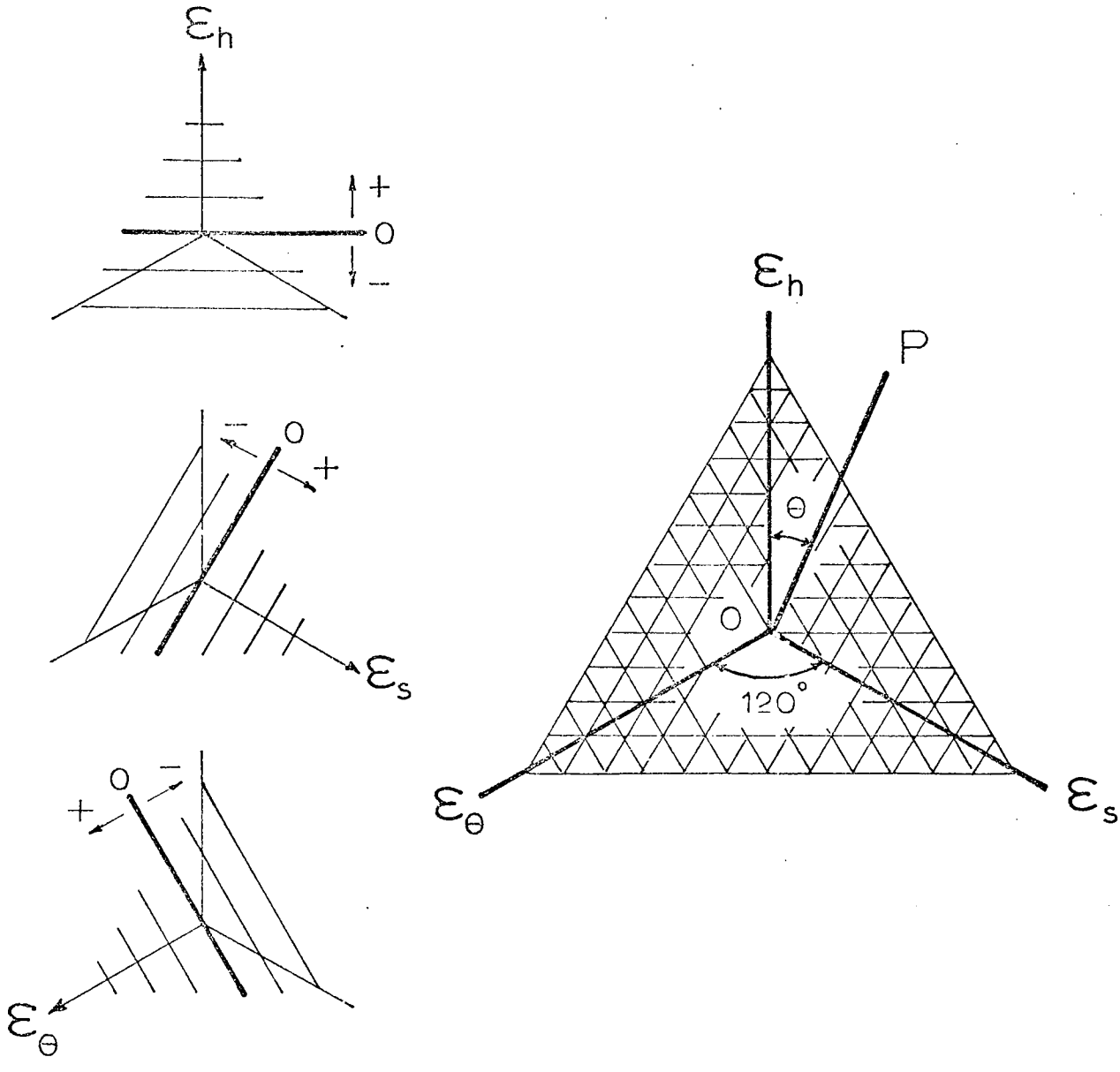
ε_h
+
0
−
−
0
+
ε_s
0
−
+
ε_θ
ε_h
P
θ
0
120°
ε_θ
ε_s

FIG. 4.1.

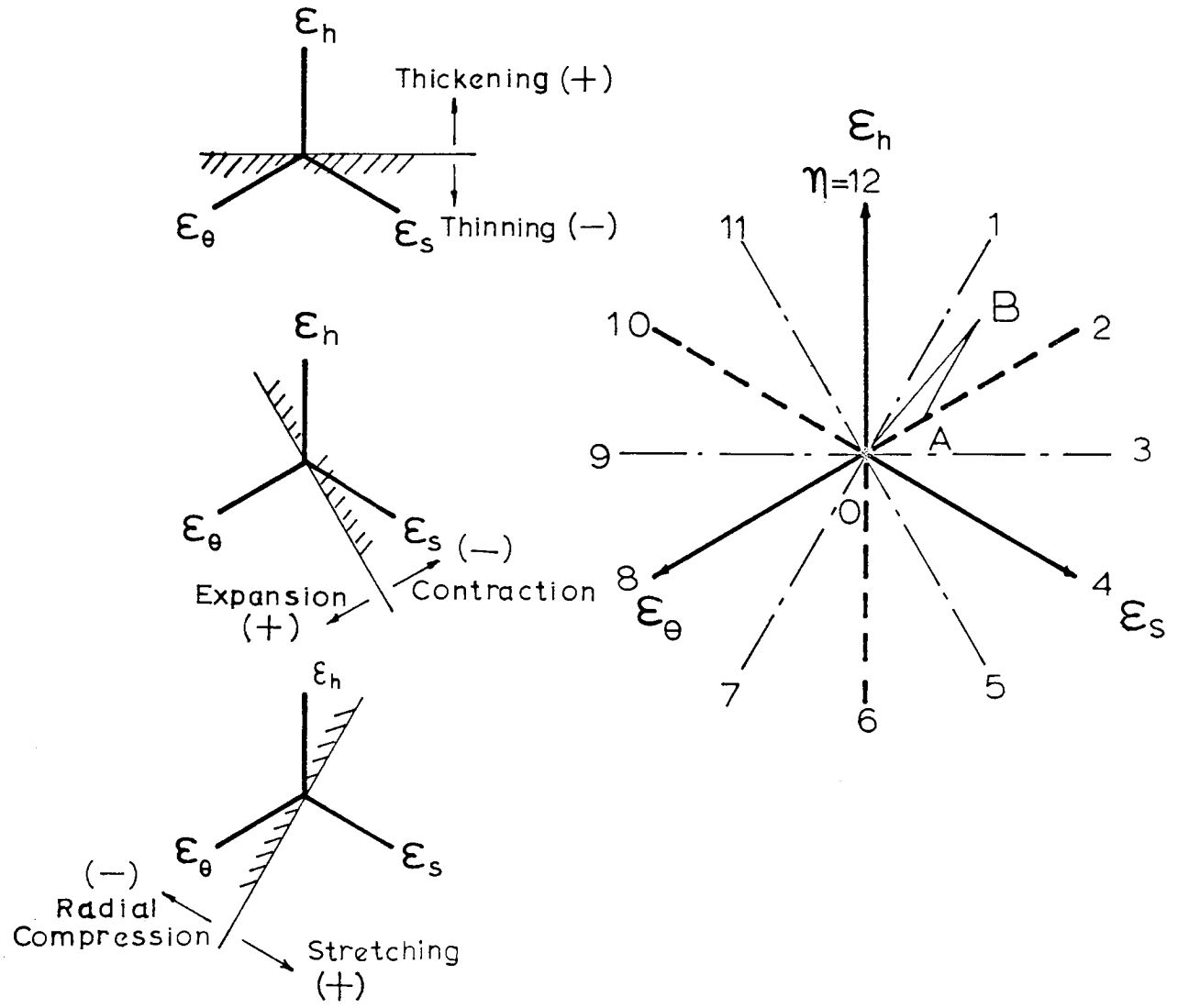
ε_h
Thickening (+)
ε_θ
ε_s
Thinning (−)
ε_h
ε_θ
ε_s (−)
Expansion (+)
Contraction
ε_h
ε_θ
ε_s
(−) Radial Compression
Stretching (+)
ε_h
η=12
11
1
10
B
2
9
A
3
O
8
ε_θ
4
ε_s
7
5
6

FIG. 4.2.

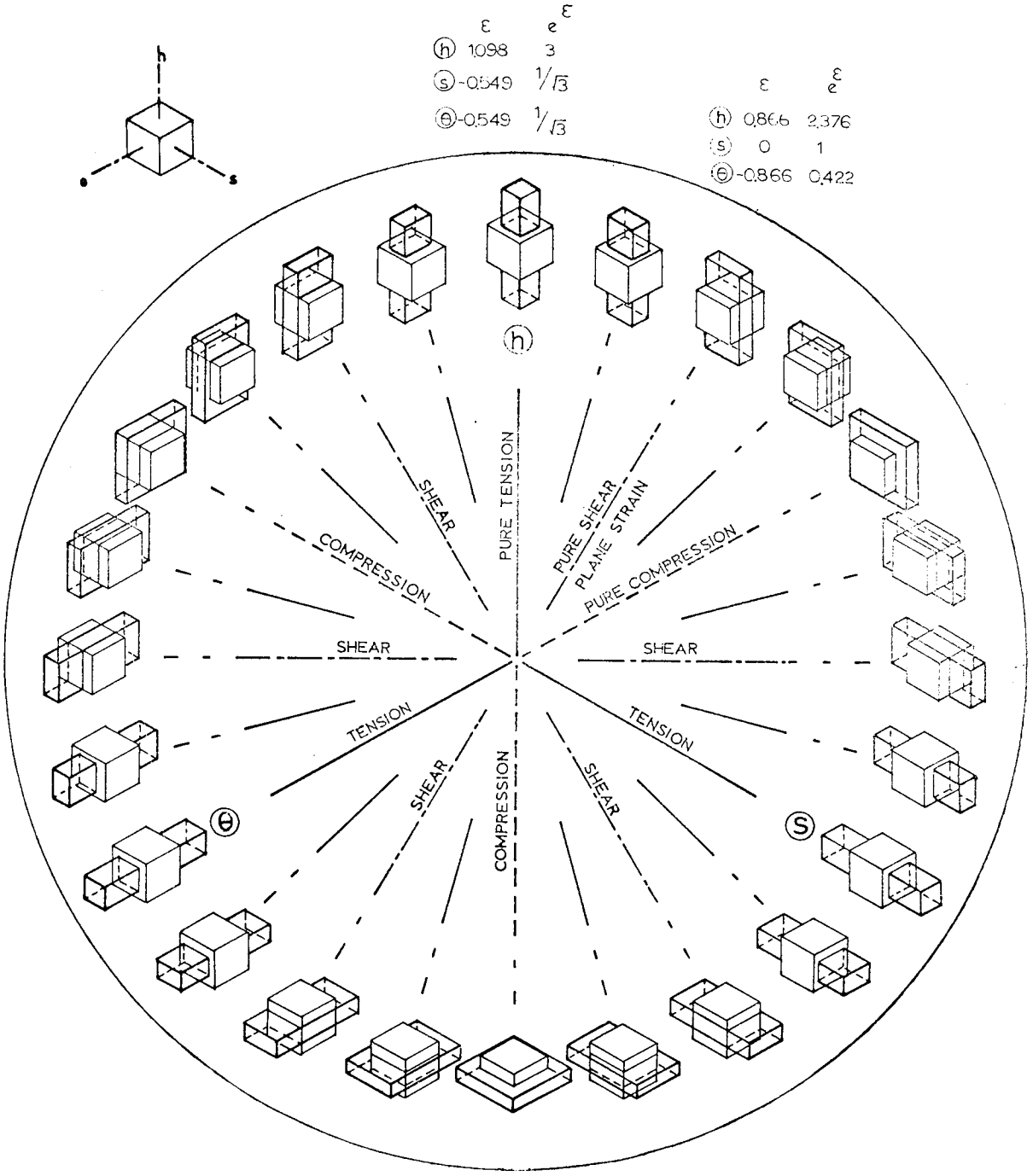
ε e^ε
(h) 1.098 3
(s) -0.549 1/√3
(θ) -0.549 1/√3
ε e^ε
(h) 0.866 2.376
(s) 0 1
(θ) -0.866 0.422
h
s
θ
PURE TENSION
PURE SHEAR
PLANE STRAIN
PURE COMPRESSION
SHEAR
COMPRESSION
TENSION

FIG. 4. 3.

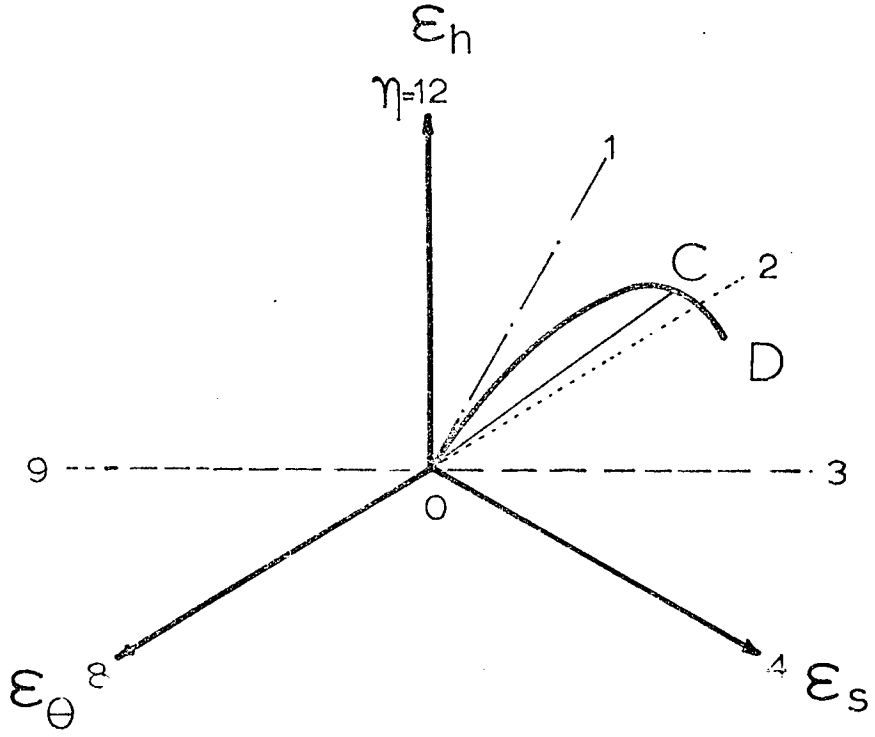
ε_h
η=12
1
C
2
D
9
3
0
ε_θ
8
4
ε_s

FIG. 4.4.

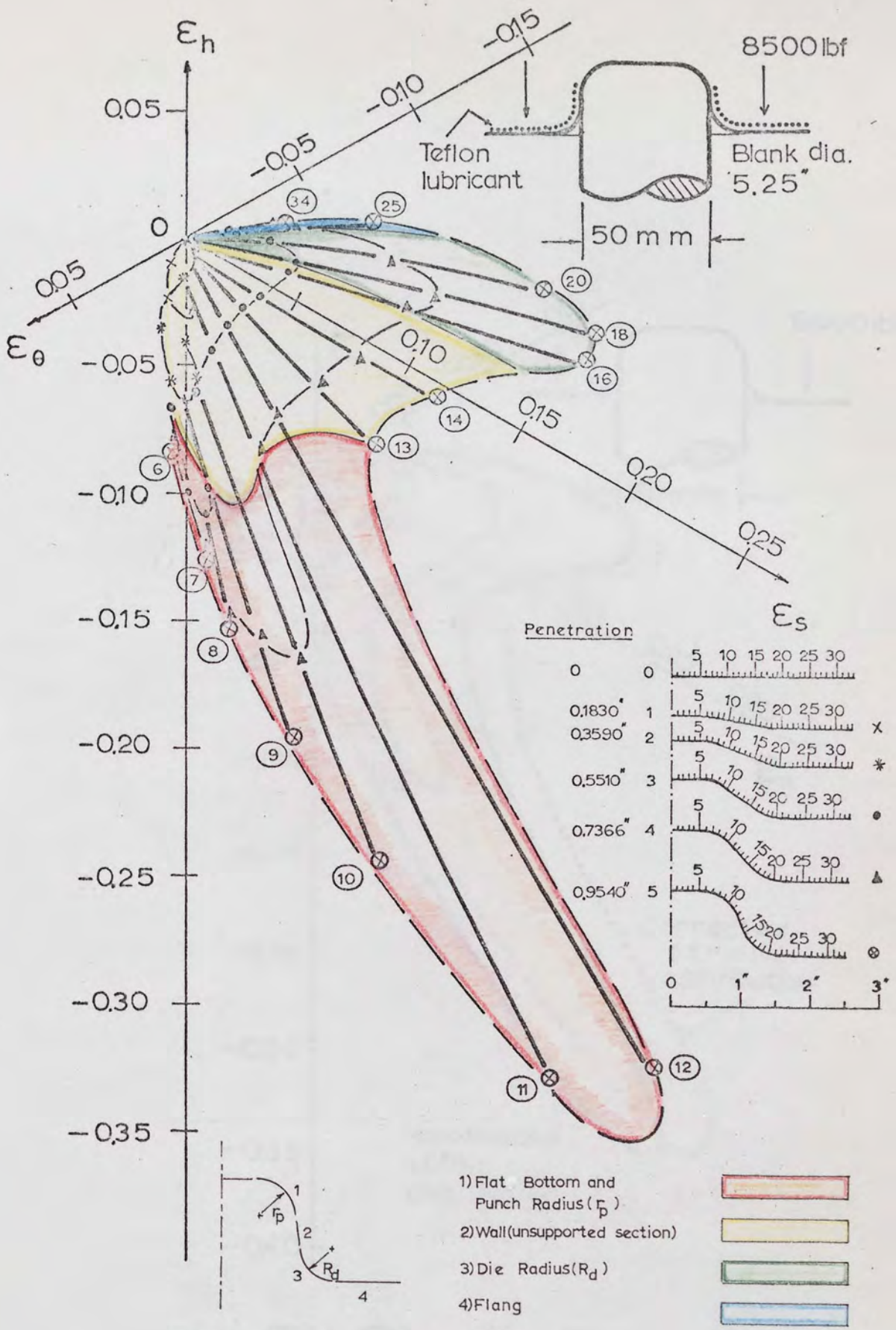
ε_h
ε_θ
ε_s
0.05
0
-0.05
-0.10
-0.15
-0.20
-0.25
-0.30
-0.35
0.05
0.10
0.15
0.20
0.25
-0.05
-0.10
-0.15
8500 lbf
Teflon lubricant
Blank dia. 5.25"
50 m m
Penetration
0
0.1830"
0.3590"
0.5510"
0.7366"
0.9540"
0 1" 2" 3"
1) Flat Bottom and Punch Radius (r_p)
2) Wall (unsupported section)
3) Die Radius (R_d)
4) Flang

FIG. 4 5.

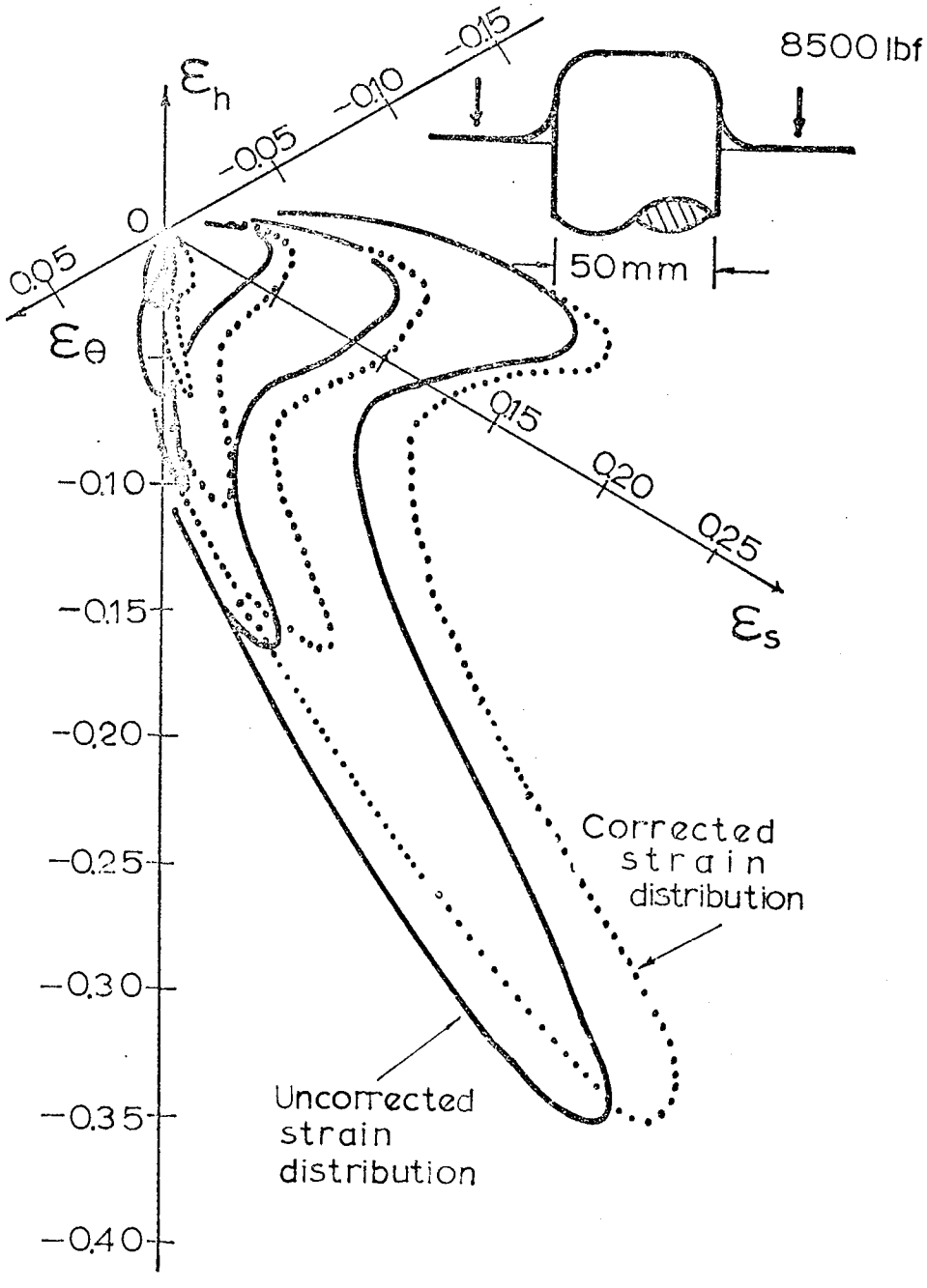
8500 lbf
50mm
ε_h
ε_θ
ε_s
-0.15
-0.10
-0.05
0
0.05
0.15
0.20
0.25
-0.10
-0.15
-0.20
-0.25
-0.30
-0.35
-0.40
Corrected strain distribution
Uncorrected strain distribution

FIG. 4.6.

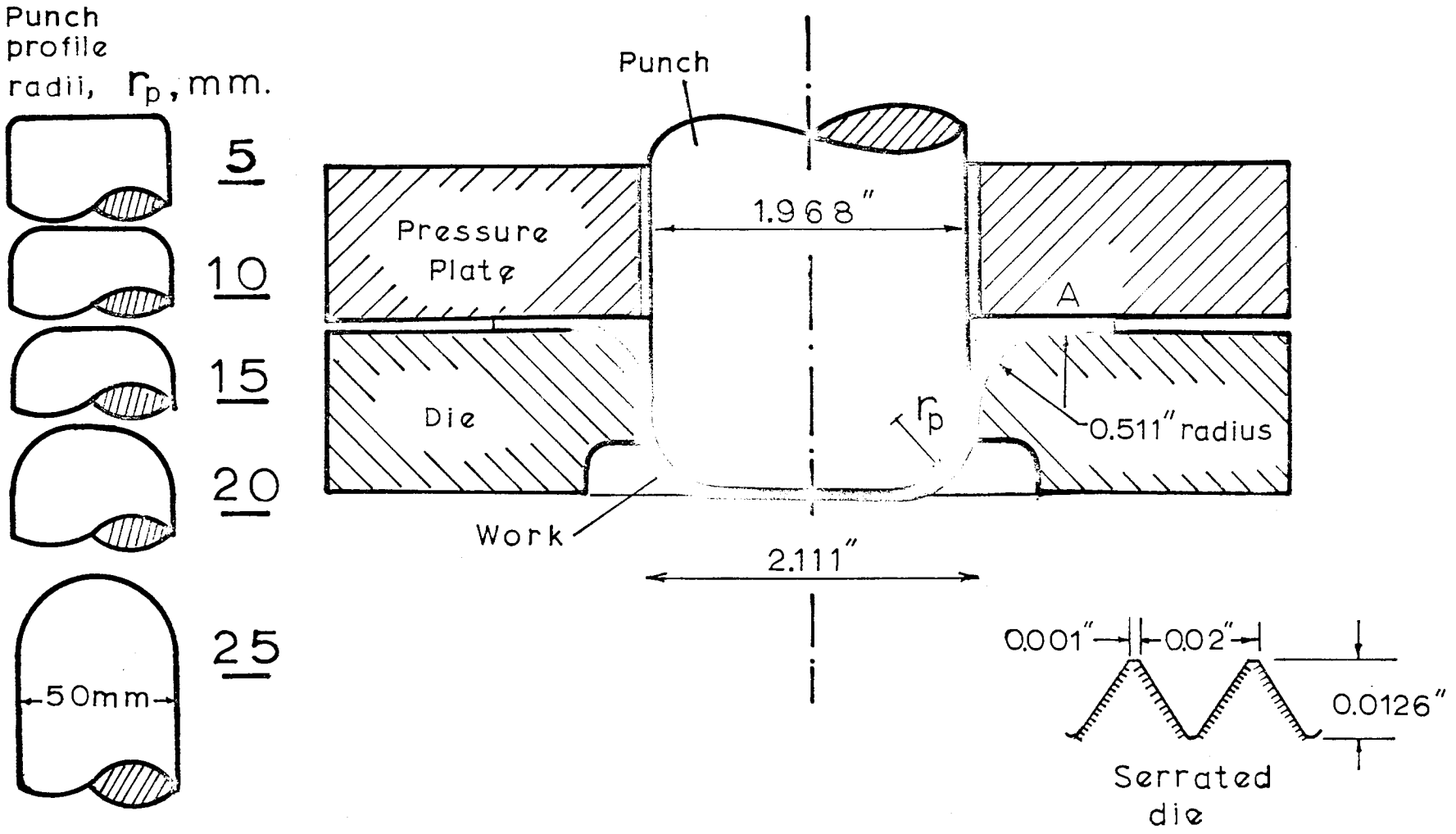
Punch profile radii, r_p, mm.
5
10
15
20
25
50mm
Punch
Pressure Plate
1.968"
A
Die
r_p
0.511" radius
Work
2.111"
0.001"
0.02"
0.0126"
Serrated die

FIG. 5.1.

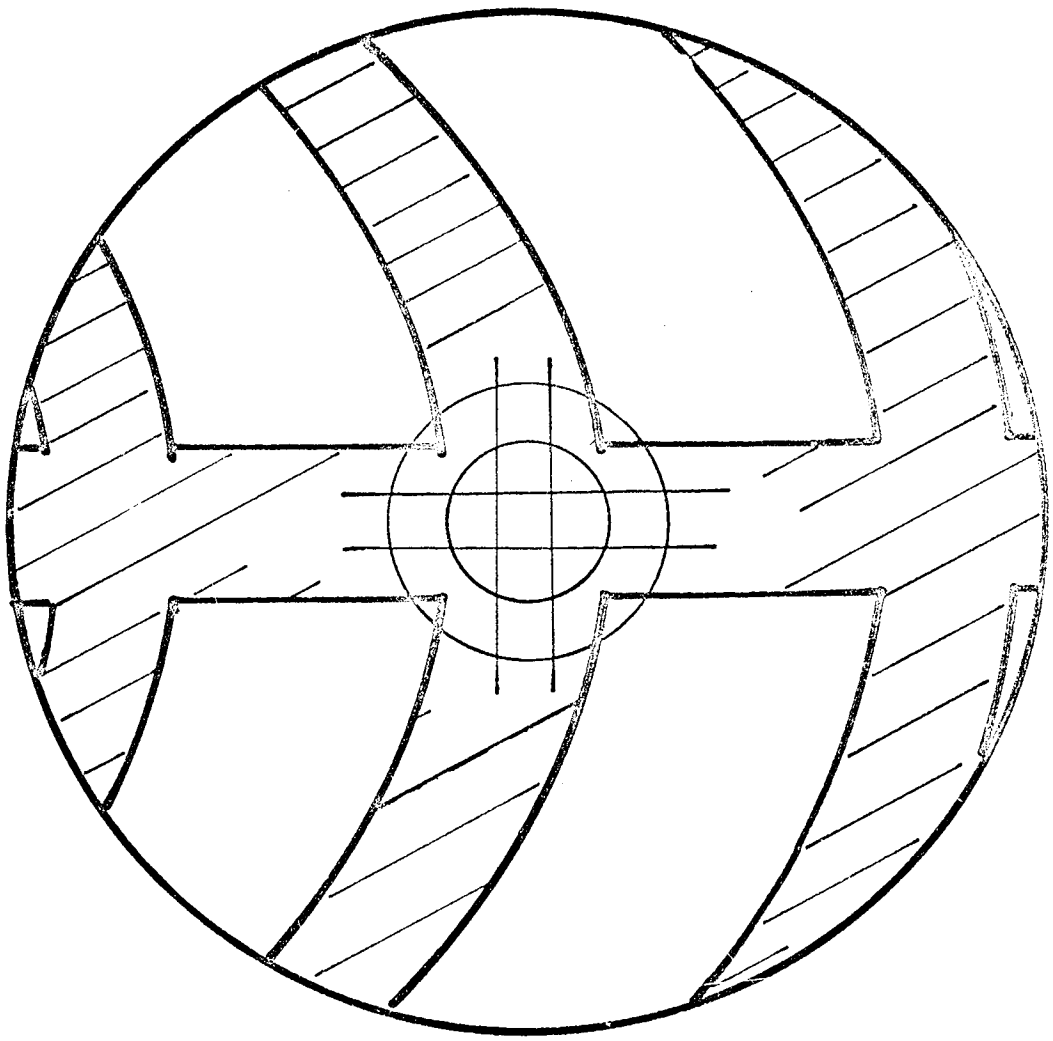

FIG. 5. 2.

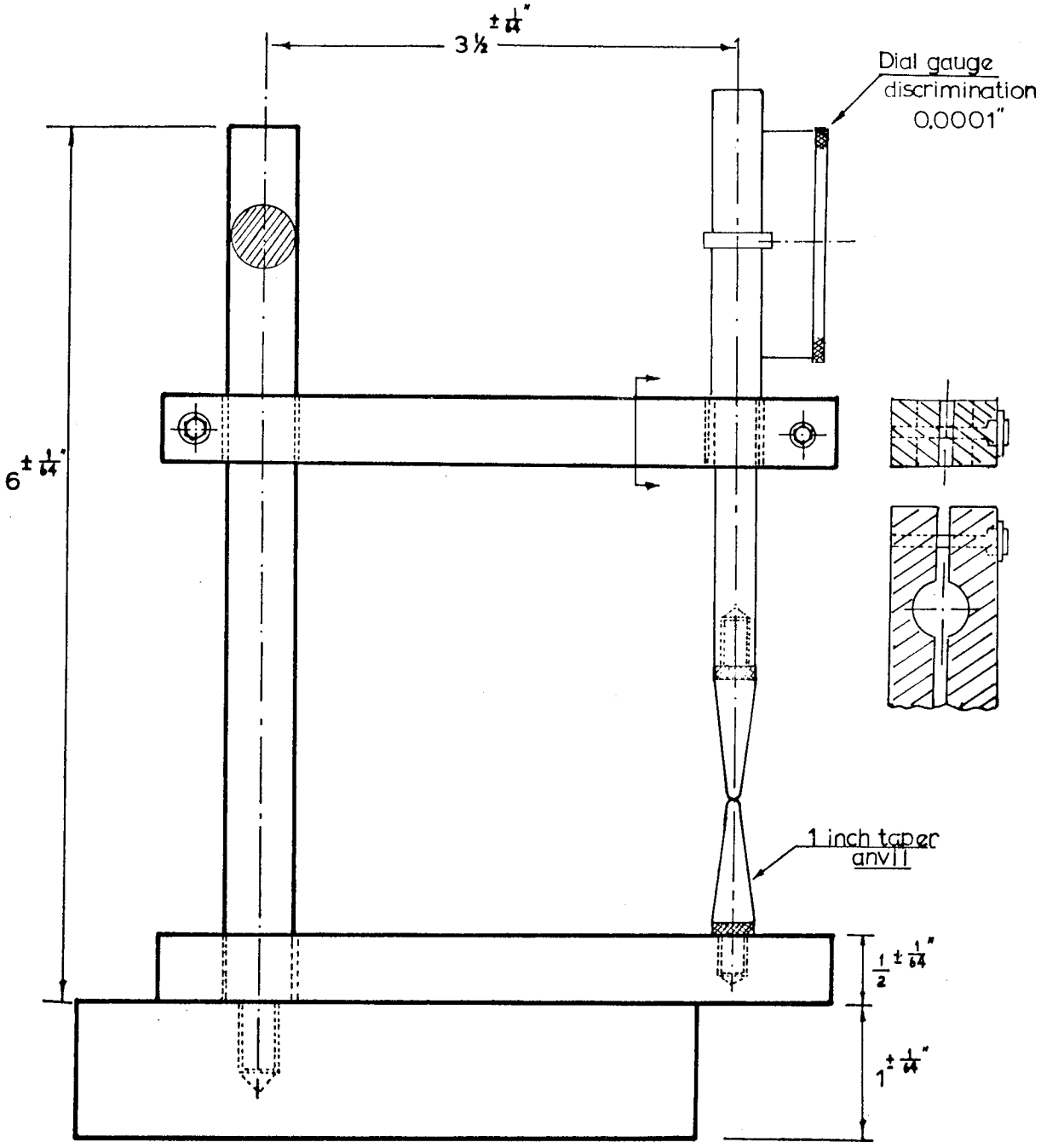
3½ ± 1/64"
Dial gauge
discrimination
0.0001"
6 ± 1/64"
1 inch taper
anvil
1/2 ± 1/64"
1 ± 1/64"

FIG. 5.3.

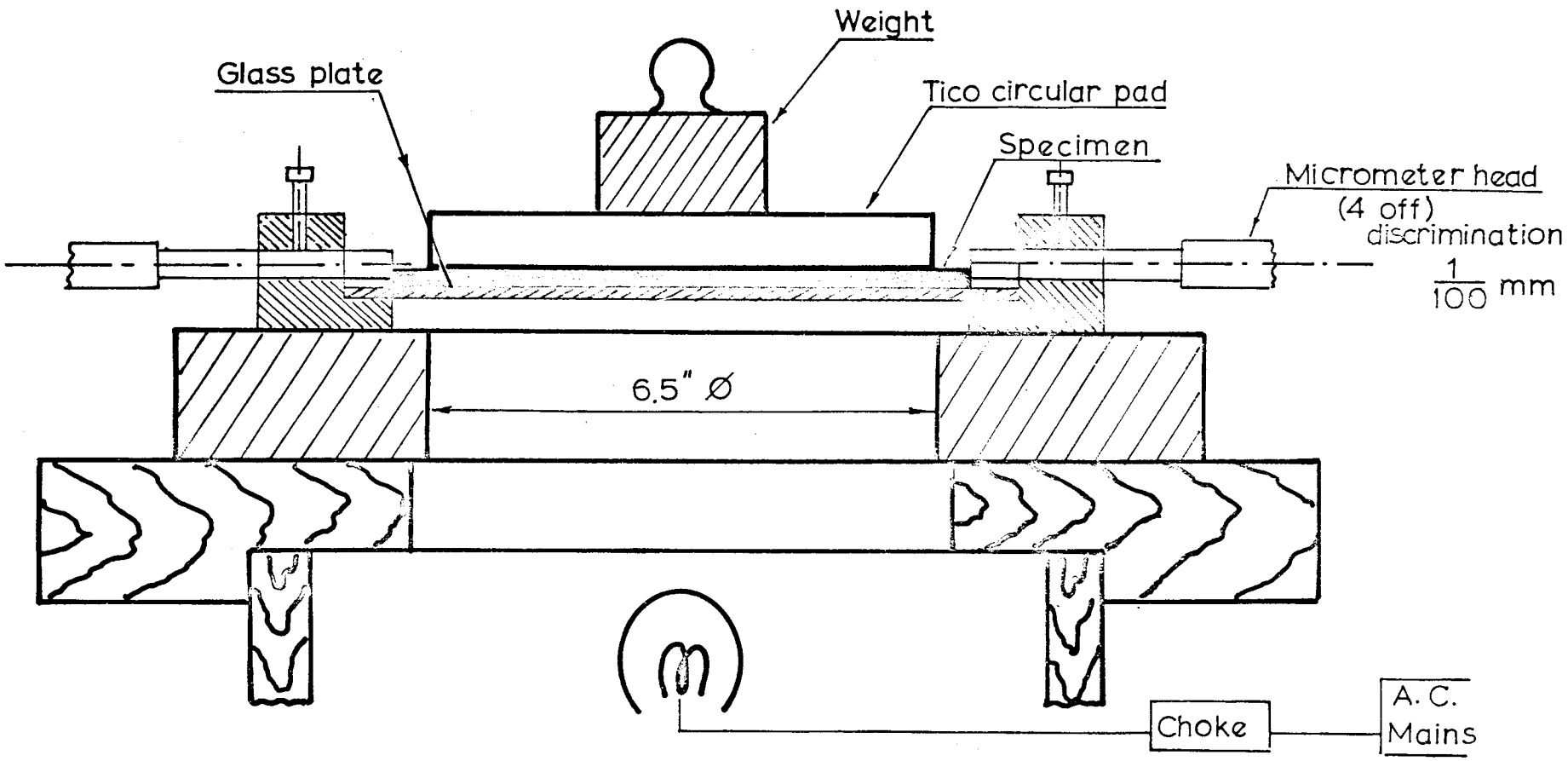
Weight
Glass plate
Tico circular pad
Specimen
Micrometer head
(4 off)
discrimination
1/100 mm
6.5" Ø
Choke
A. C.
Mains

FIG. 5.4.

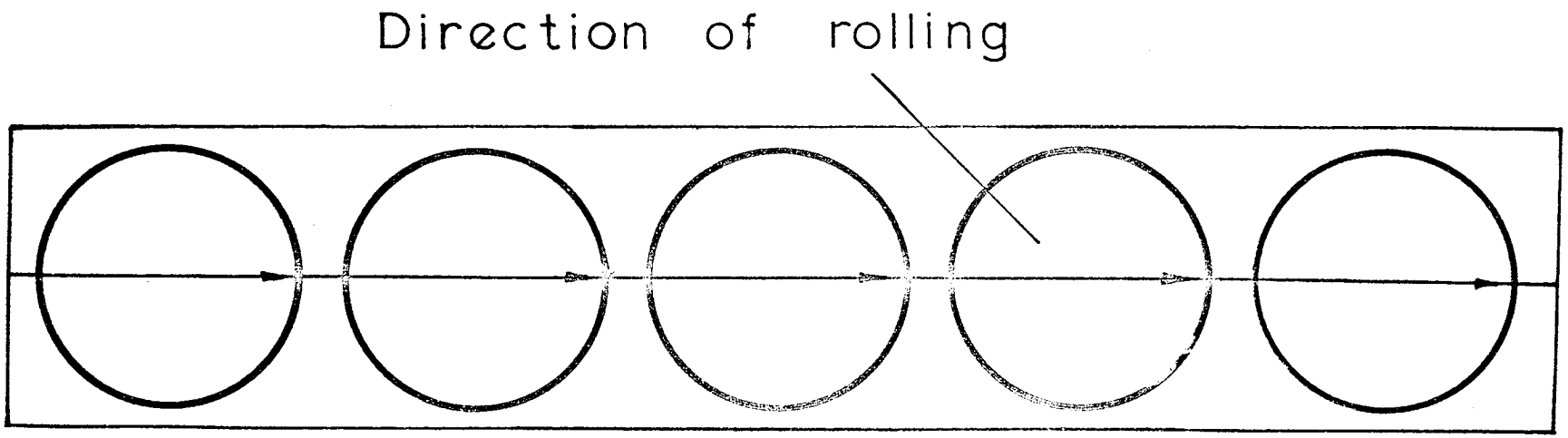

FIG. 5.5.

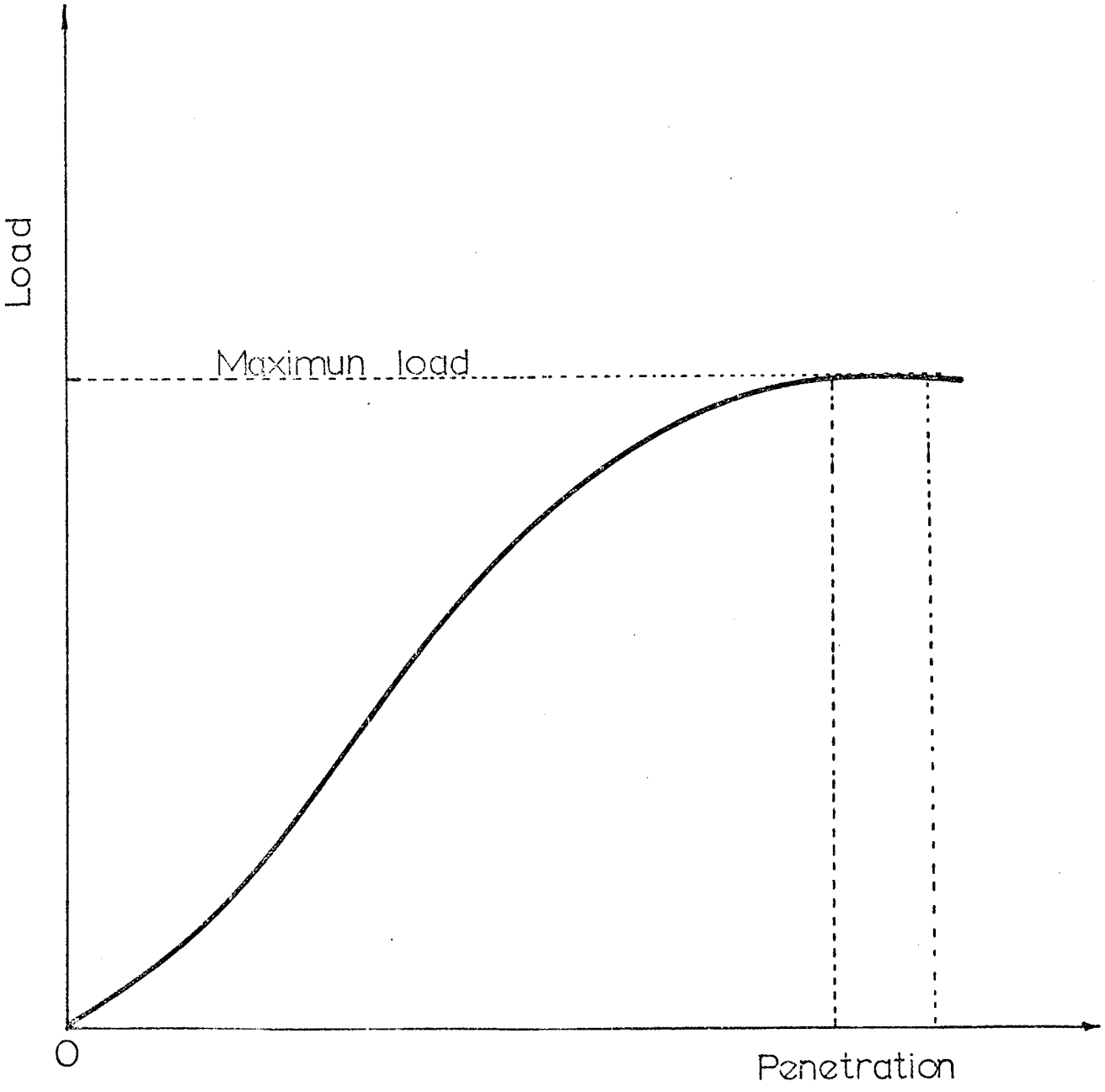

FIG. 6.1. after ref.(8)

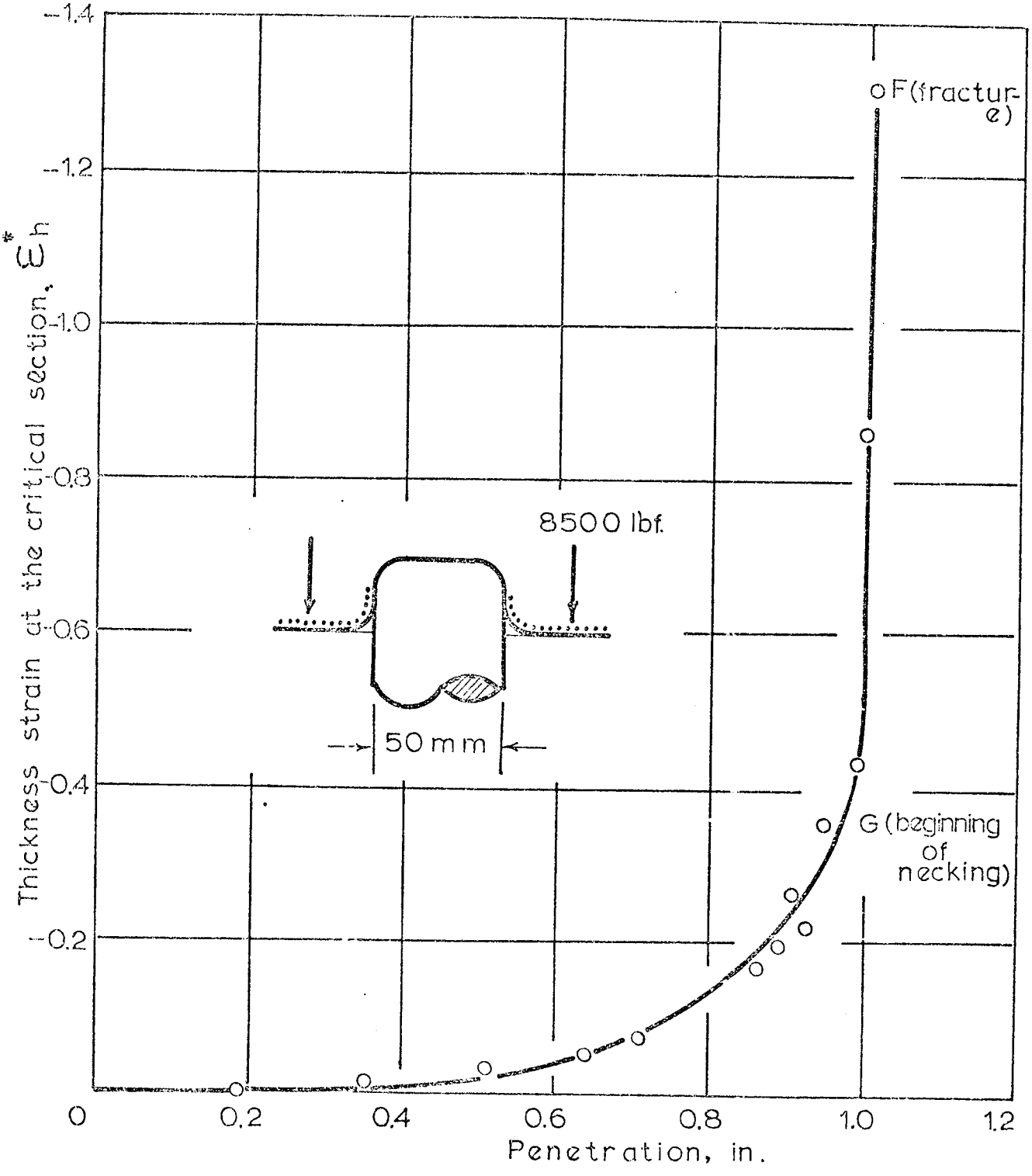
-1.4
-1.2
-1.0
-0.8
-0.6
-0.4
-0.2
0
0.2
0.4
0.6
0.8
1.0
1.2
Thickness strain at the critical section, ε_h^*
Penetration, in.
F (fracture)
G (beginning of necking)
8500 lbf.
50 mm

FIG. 6.2.

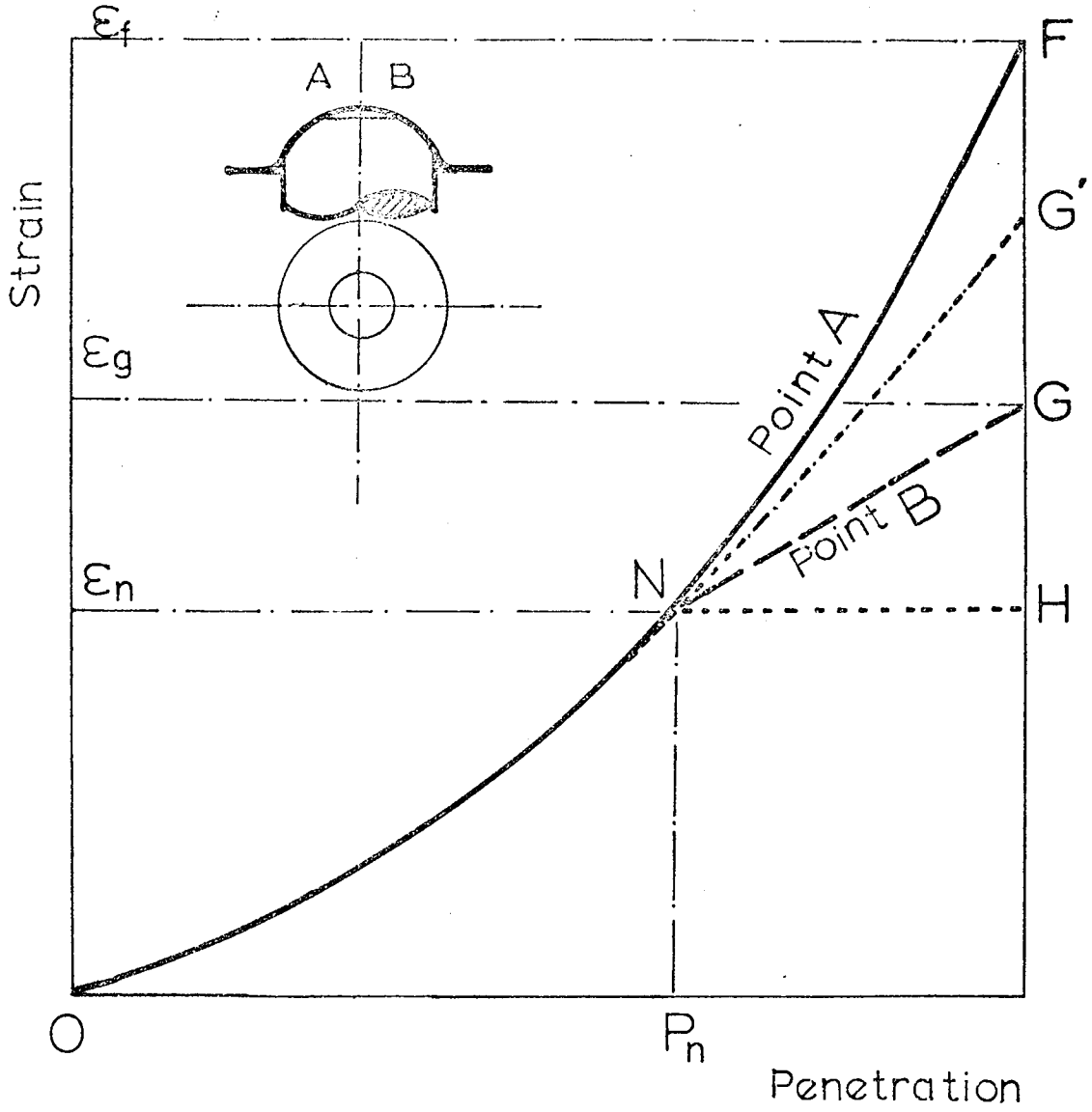
ε_f
F
A
B
Strain
G'
ε_g
Point A
G
Point B
ε_n
N
H
O
P_n
Penetration

FIG. 6.3.

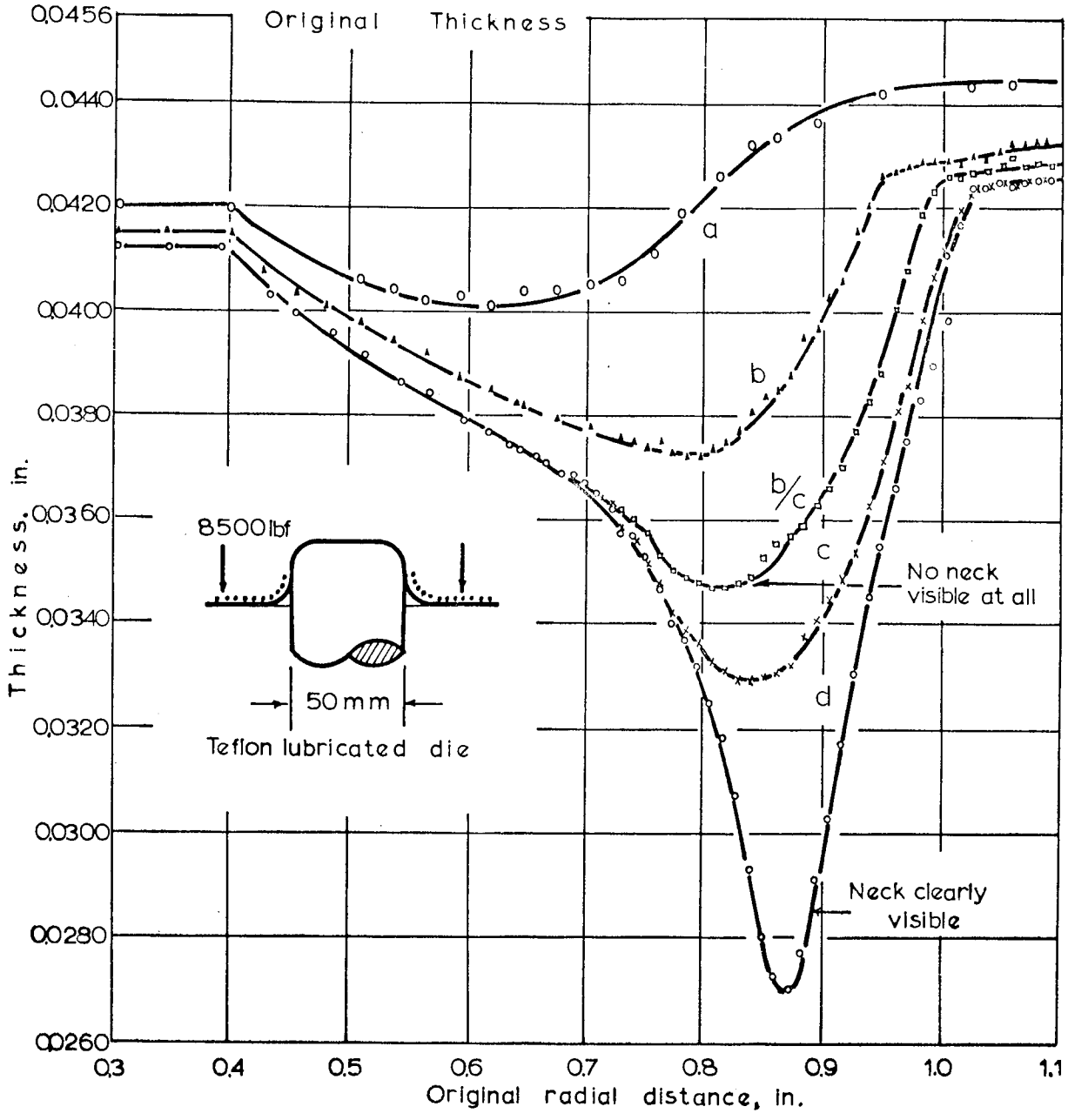
Original Thickness
0.0456
0.0440
0.0420
0.0400
0.0380
0.0360
0.0340
0.0320
0.0300
0.0280
0.0260
Thickness, in.
0.3
0.4
0.5
0.6
0.7
0.8
0.9
1.0
1.1
Original radial distance, in.
a
b
b/c
c
d
8500 lbf
50 mm
Teflon lubricated die
No neck visible at all
Neck clearly visible

FIG. 6. 4.

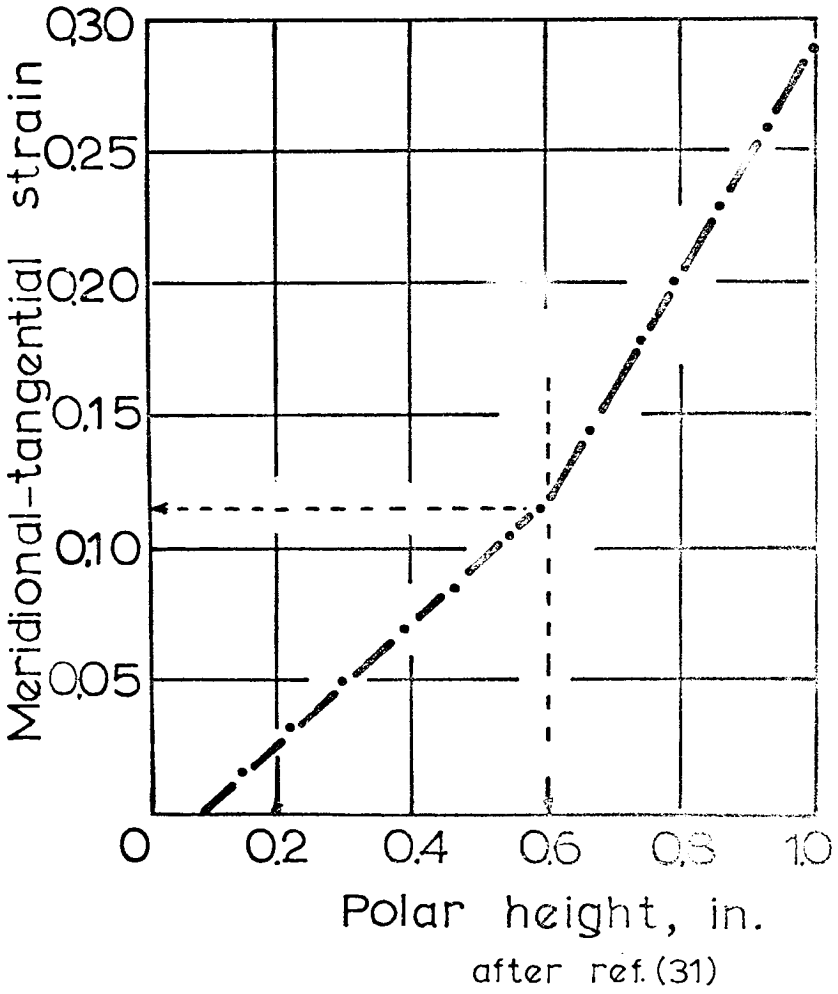

FIG. 6.5.A.

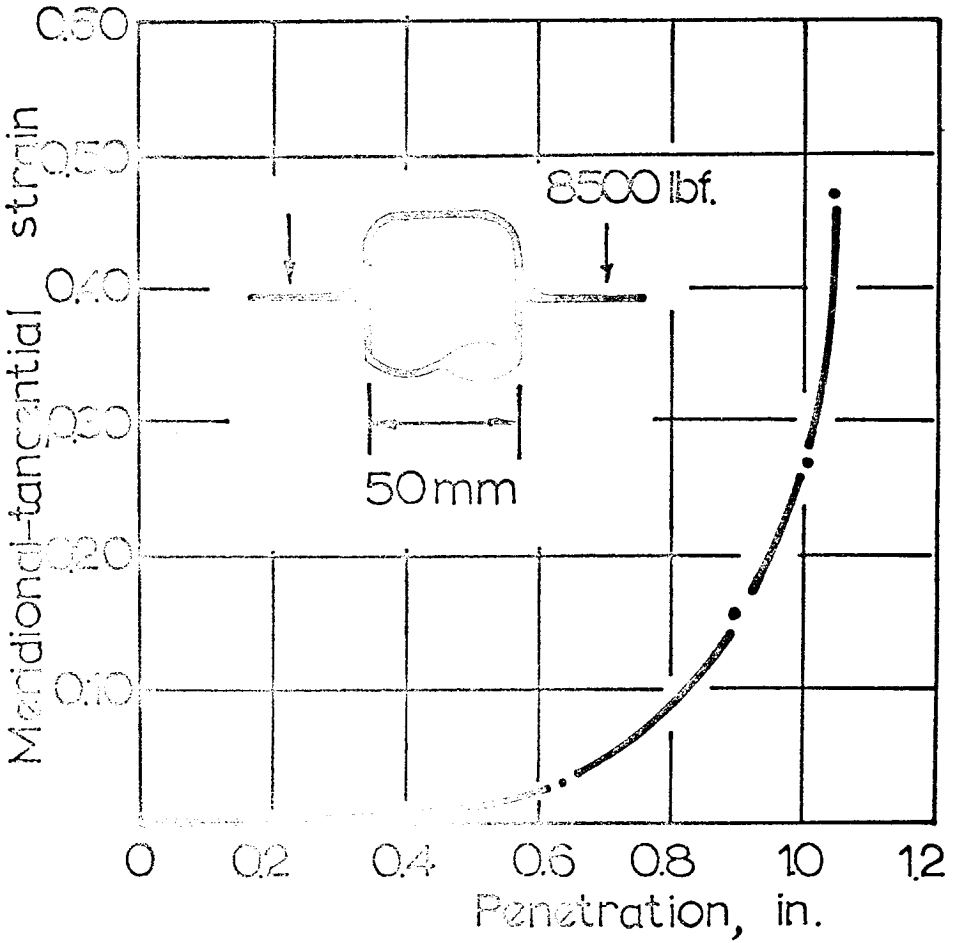

FIG. 6.5. B.

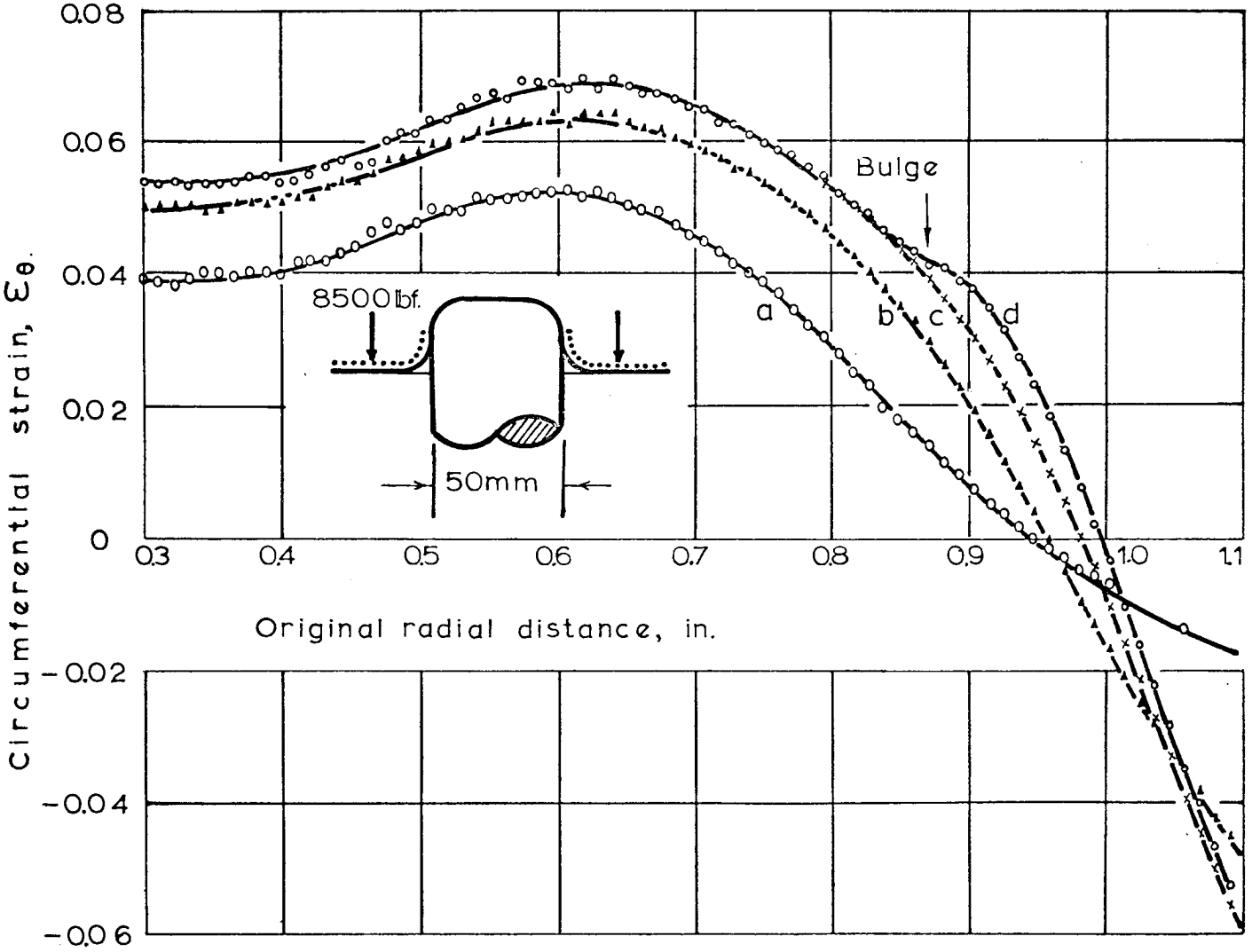
0.08
0.06
0.04
0.02
0
-0.02
-0.04
-0.06
Circumferential strain, ε_θ
0.3
0.4
0.5
0.6
0.7
0.8
0.9
1.0
1.1
Original radial distance, in.
Bulge
8500 lbf.
50mm
a
b
c
d

FIG. 6.6.

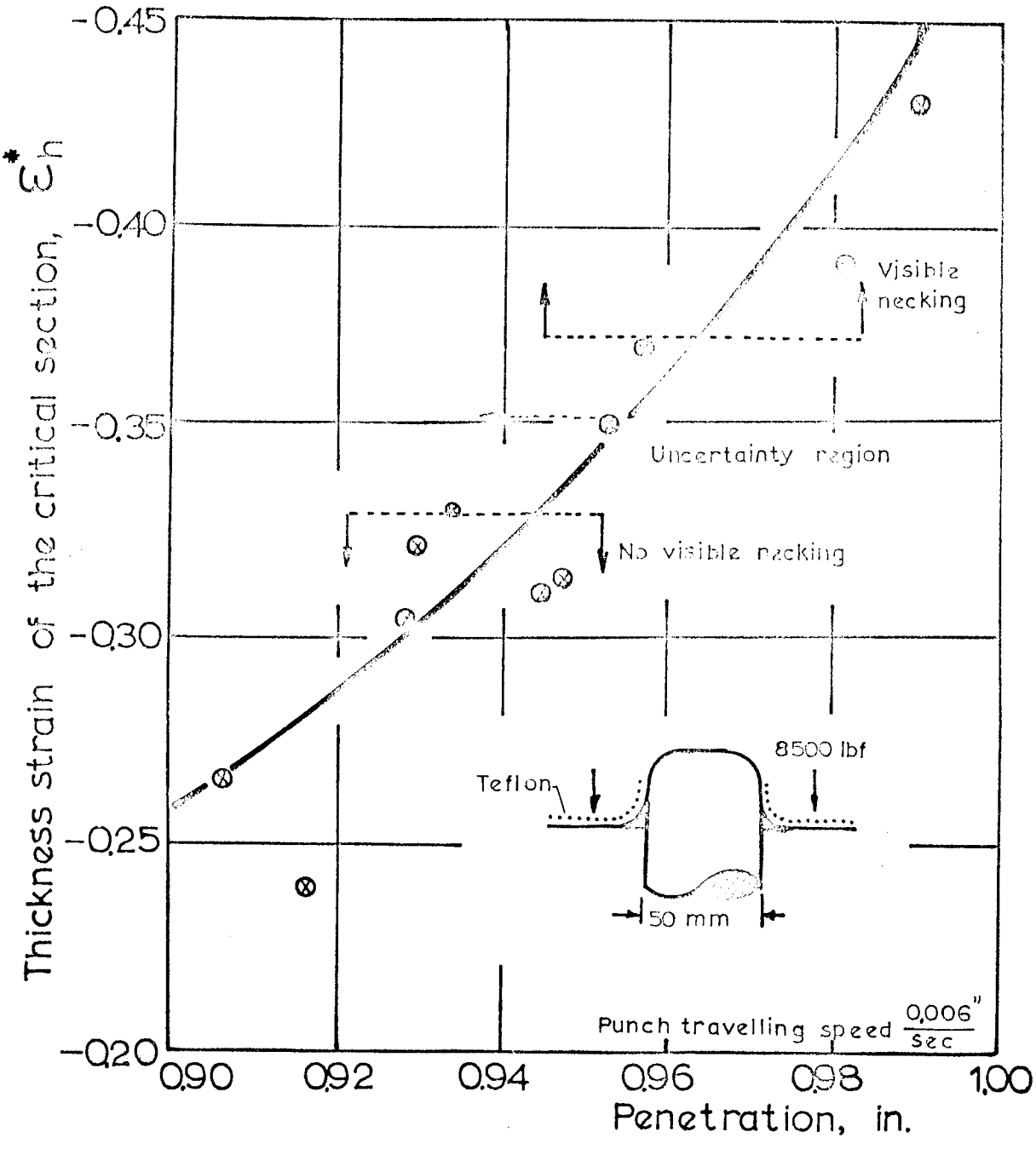
-0.45
-0.40
-0.35
-0.30
-0.25
-0.20
0.90
0.92
0.94
0.96
0.98
1.00
Penetration, in.
Thickness strain of the critical section, ε_h^*
Visible necking
Uncertainty region
No visible necking
8500 lbf
Teflon
50 mm
Punch travelling speed 0.006" / sec

FIG. 6. 7.

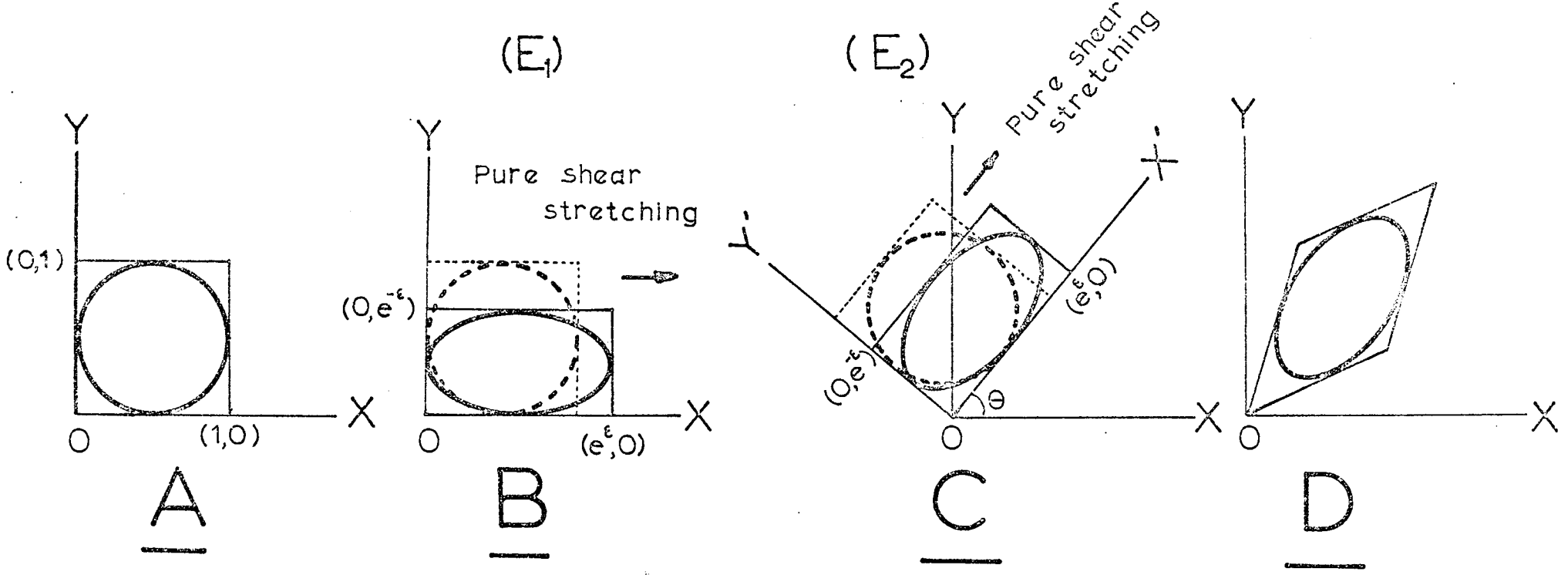
Step 1 + Step 2 = Resultant
(E1)
(E2)
Y
X
(0,1)
O
(1,0)
A
Pure shear
stretching
(0,e^-ε)
(e^ε,0)
B
Pure shear
stretching
Y'
X'
(0,e^-ε)
(e^ε,0)
θ
C
D

FIG. 7.1.

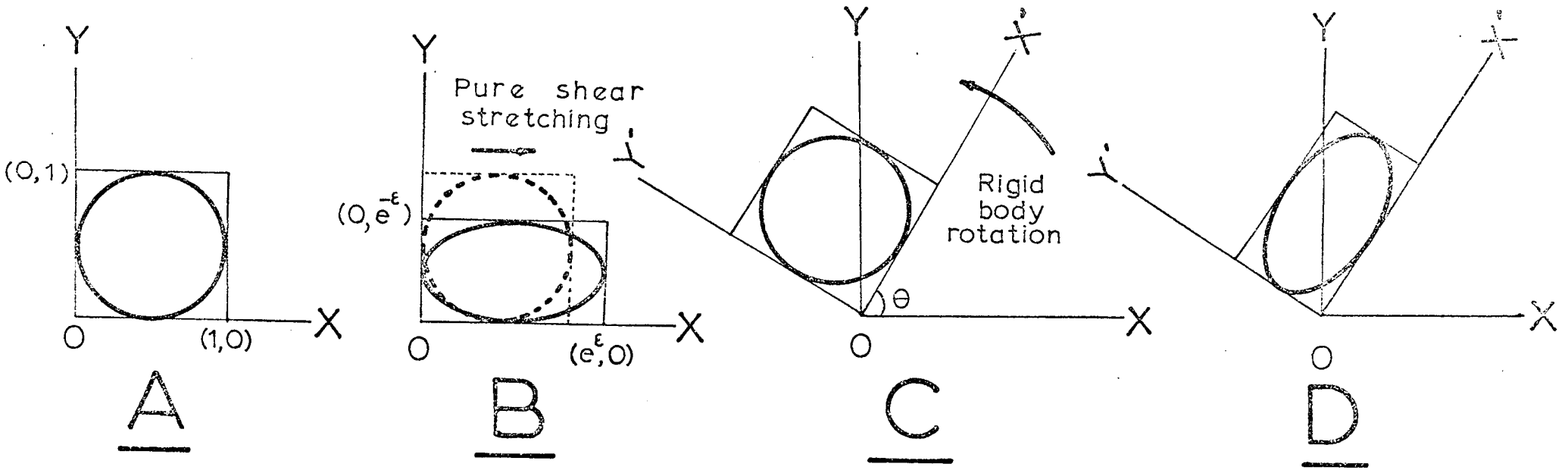
Step 1 + Step 2 = Resultant
(E1)
Y
(0,1)
O
(1,0)
X
A
Y
Pure shear
stretching
(0,e^-ε)
O
(e^ε,0)
X
B
Y
Y'
X'
Rigid
body
rotation
θ
O
X
C
Y
X'
Y'
O
X
D

FIG. 7.2.

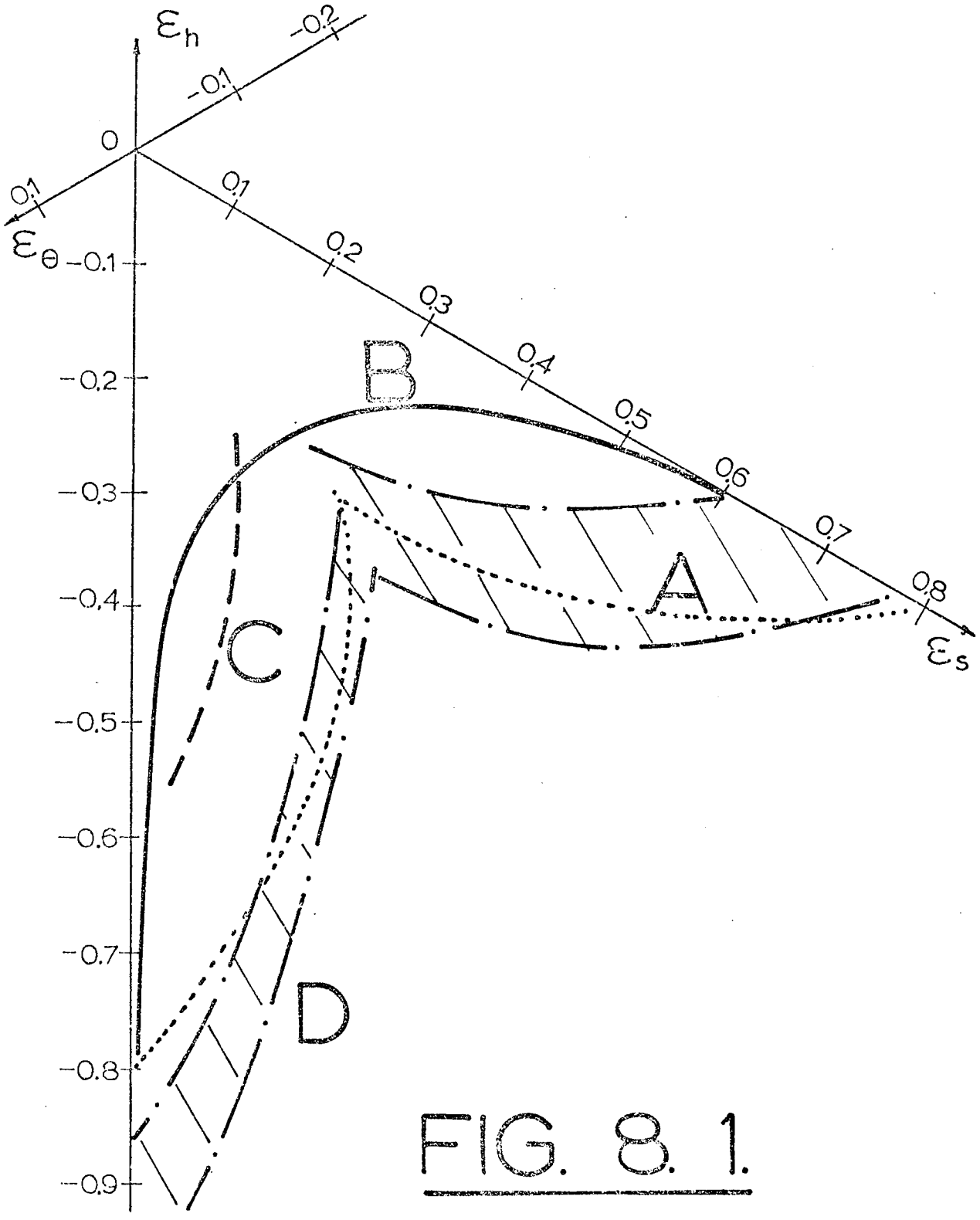
ε_h
-0.2
-0.1
0
0.1
ε_θ
0.1
0.2
0.3
0.4
0.5
0.6
0.7
0.8
ε_s
-0.1
-0.2
-0.3
-0.4
-0.5
-0.6
-0.7
-0.8
-0.9
A
B
C
D

FIG. 8. 1.

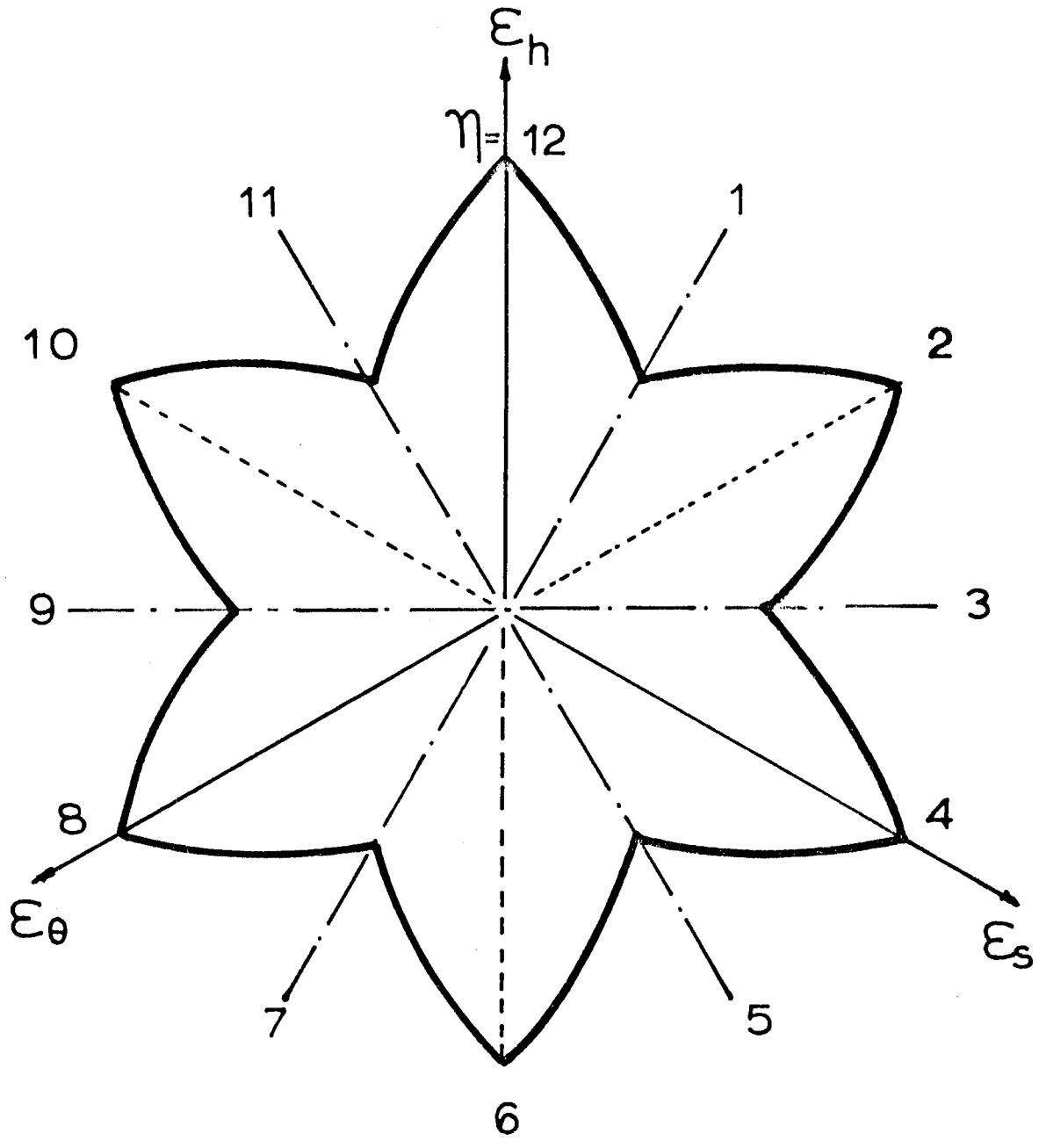
ε_h
η=
12
1
2
3
4
5
6
7
8
9
10
11
ε_θ
ε_s

FIG. 8.2.

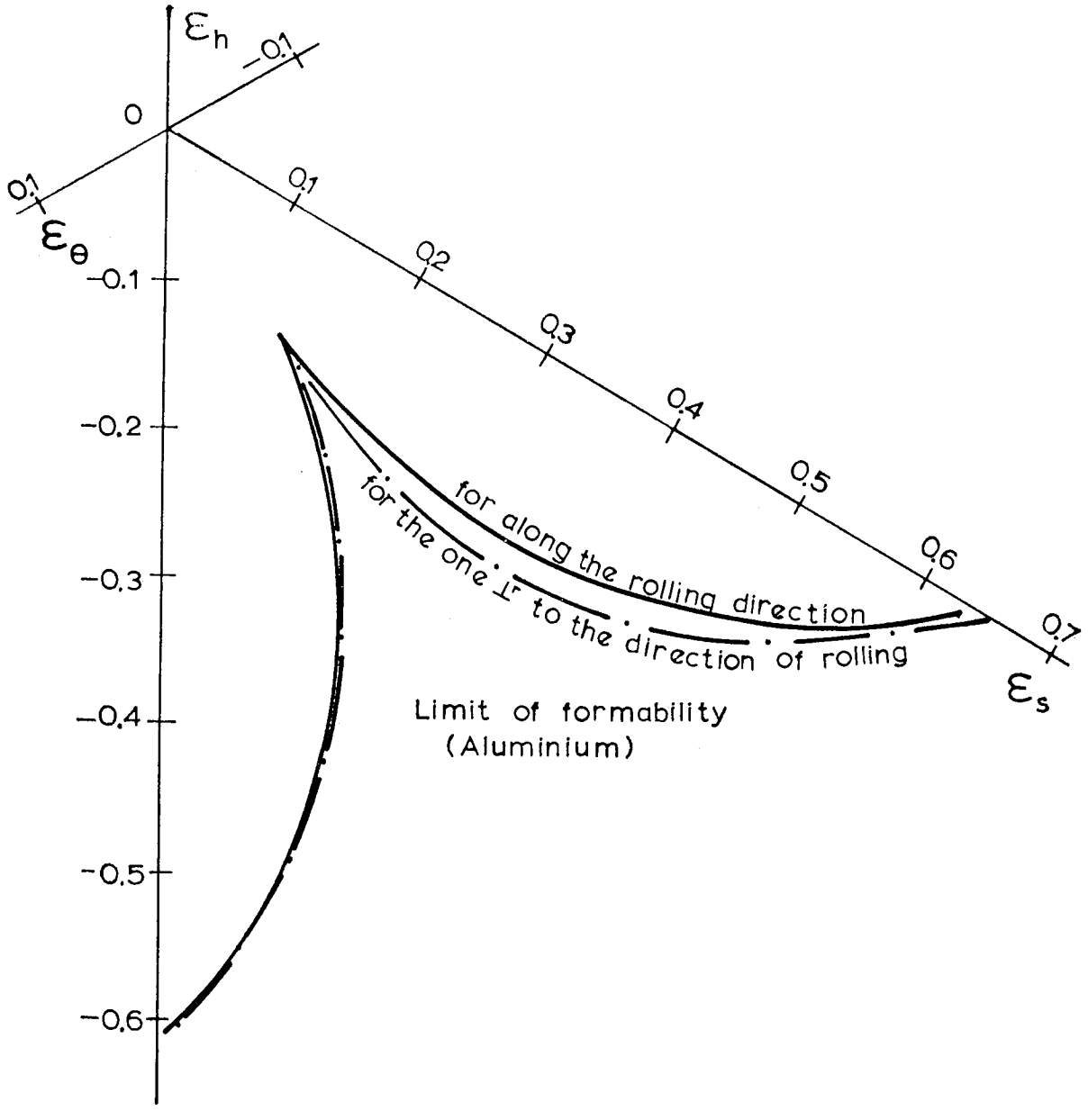

FIG. 8.3.

after ref.(46)

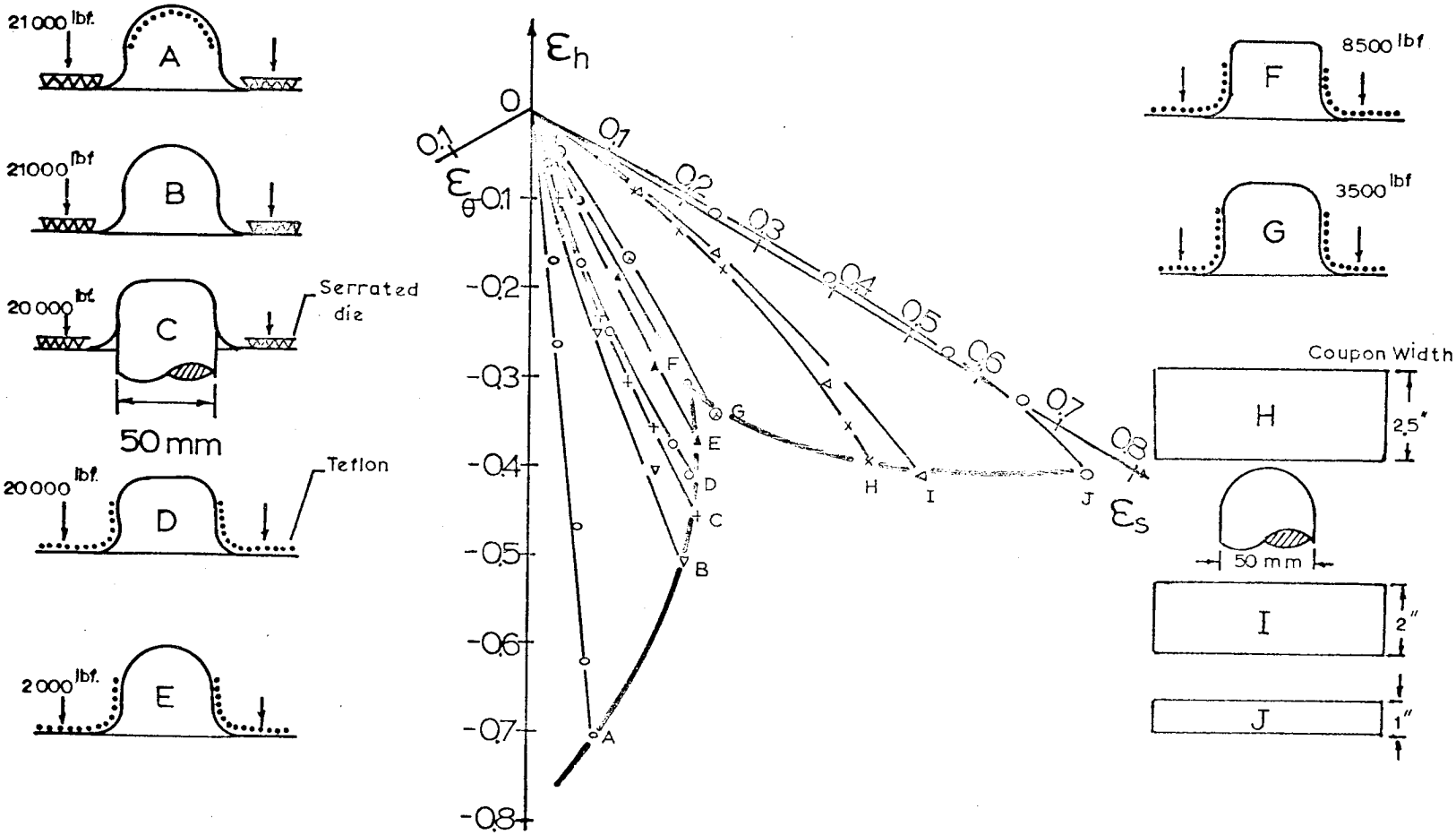
21000 lbf.
A
21000 lbf
B
20000 lbf.
C
Serrated die
50 mm
20000 lbf.
D
Teflon
2000 lbf.
E
εh
0
0.1
εθ
0.1
0.2
0.3
0.4
0.5
0.6
0.7
0.8
-0.1
-0.2
-0.3
-0.4
-0.5
-0.6
-0.7
-0.8
A
B
C
D
E
F
G
H
I
J
εs
8500 lbf
F
3500 lbf
G
Coupon Width
H
2.5"
50 mm
I
2"
J
1"

FIG. 8.4.

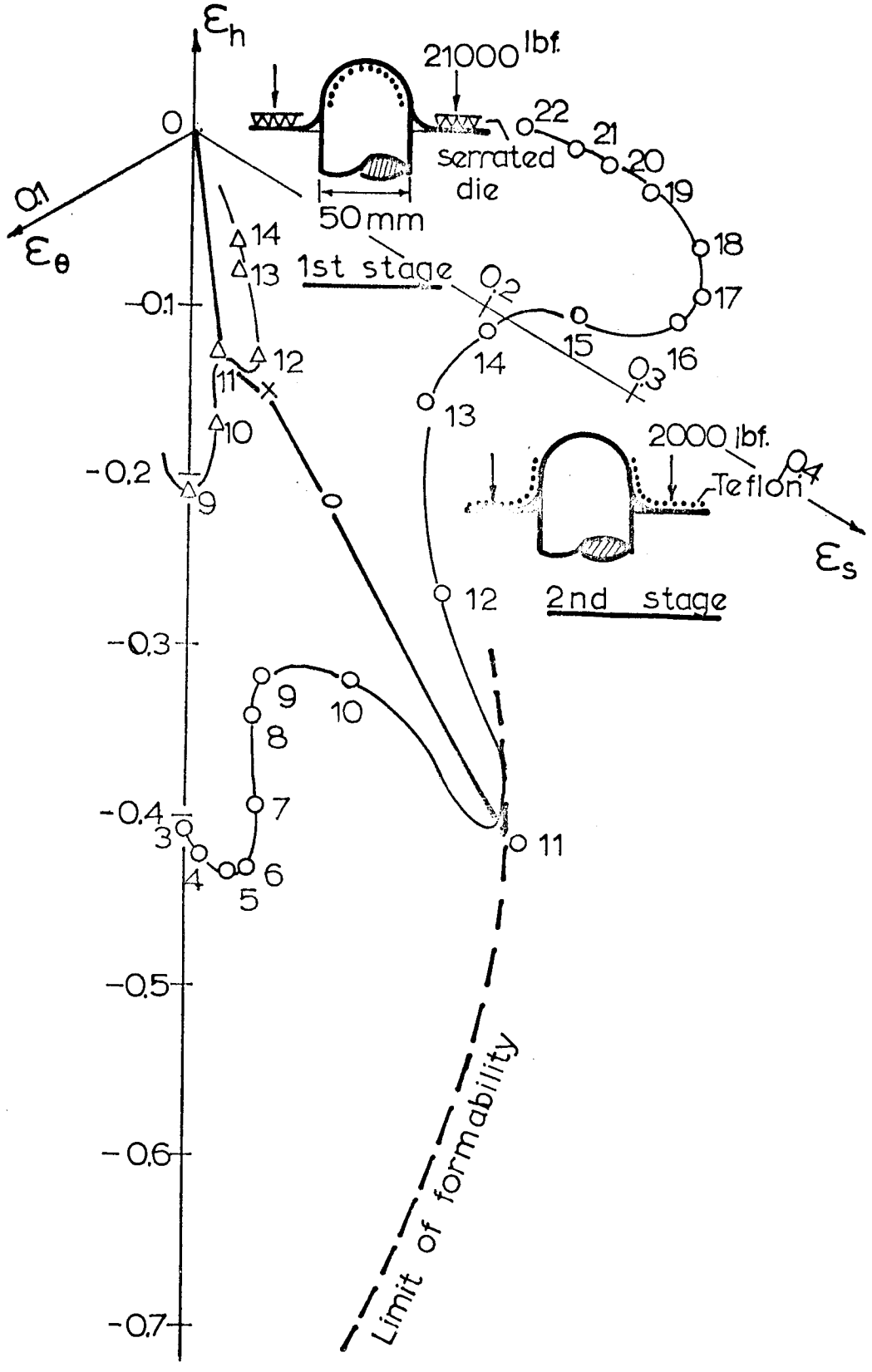
ε_h
ε_θ
0.1
0
-0.1
-0.2
-0.3
-0.4
-0.5
-0.6
-0.7
21000 lbf.
serrated die
50 mm
1st stage
2000 lbf.
Teflon
2nd stage
ε_s
Limit of formability
1
2
3
4
5
6
7
8
9
10
11
12
13
14
15
16
17
18
19
20
21
22

FIG. 8.5.

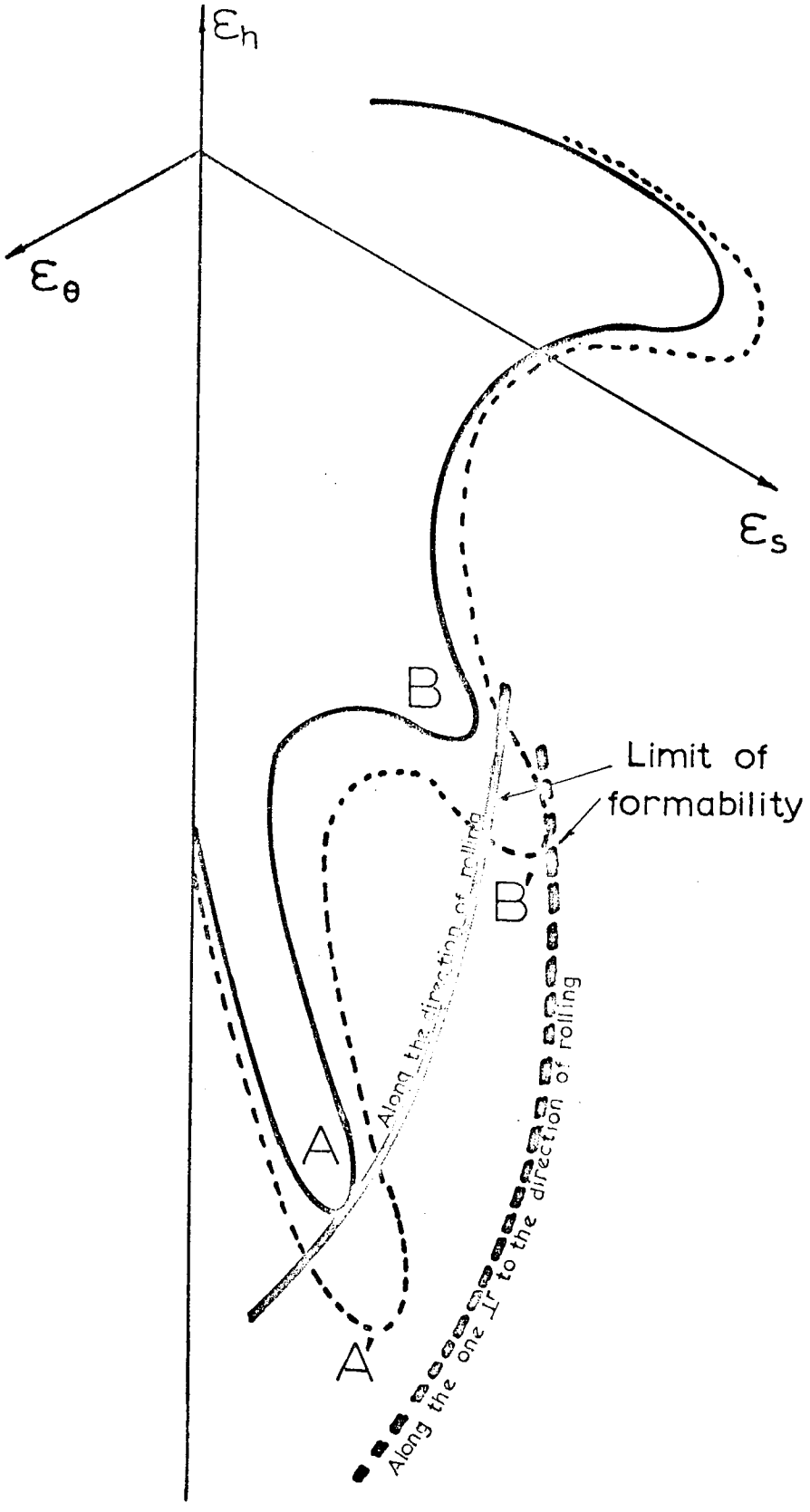
ε_h
ε_θ
ε_s
B
B'
Limit of formability
A
A'
Along the direction of rolling
Along the one ⊥r to the direction of rolling

FIG. 8.6.

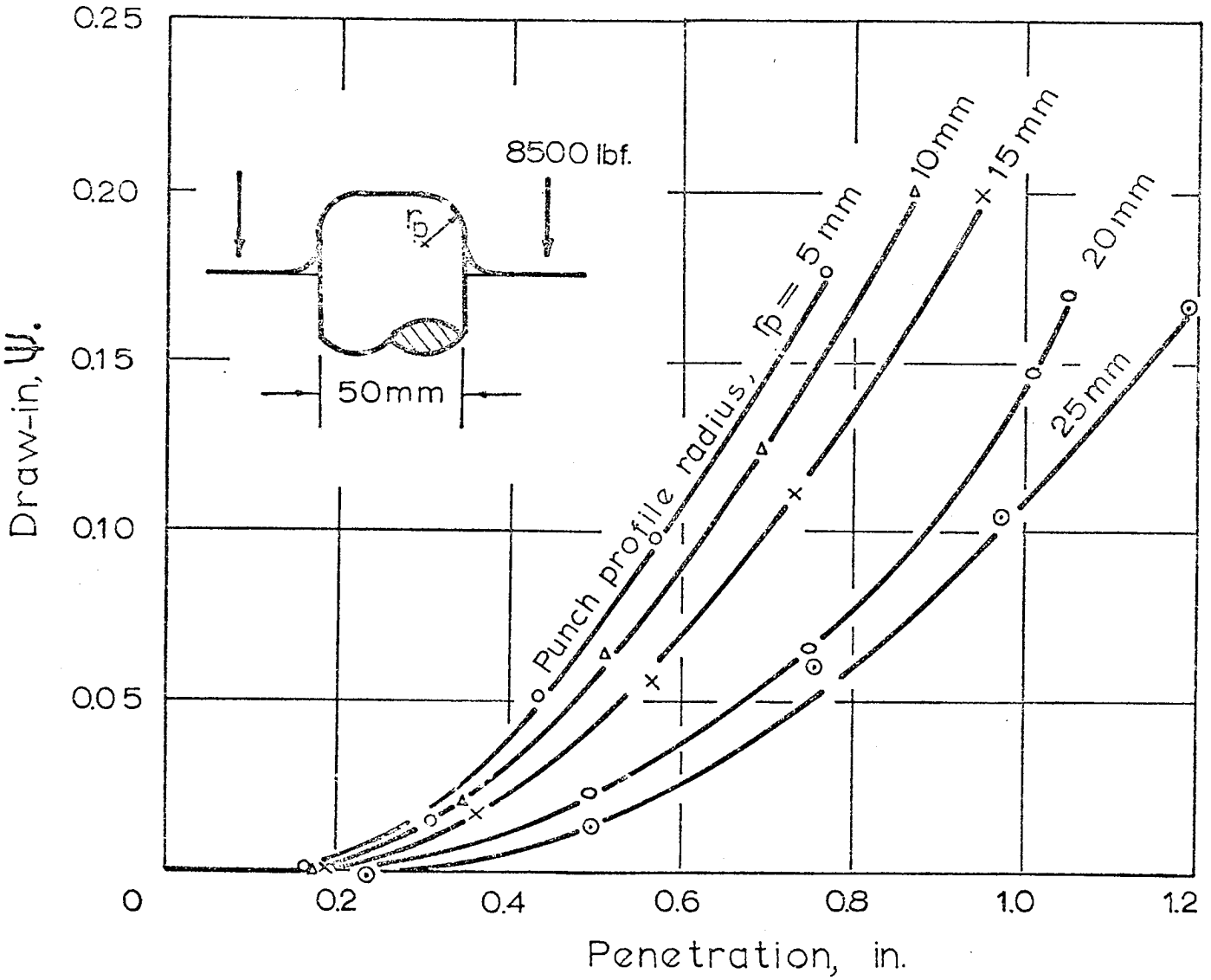
0.25
0.20
0.15
0.10
0.05
0
0.2
0.4
0.6
0.8
1.0
1.2
Draw-in, ψ.
Penetration, in.
8500 lbf.
50mm
r_p
Punch profile radius, r_p = 5 mm
10mm
15 mm
20mm
25mm

FIG. 9.1.

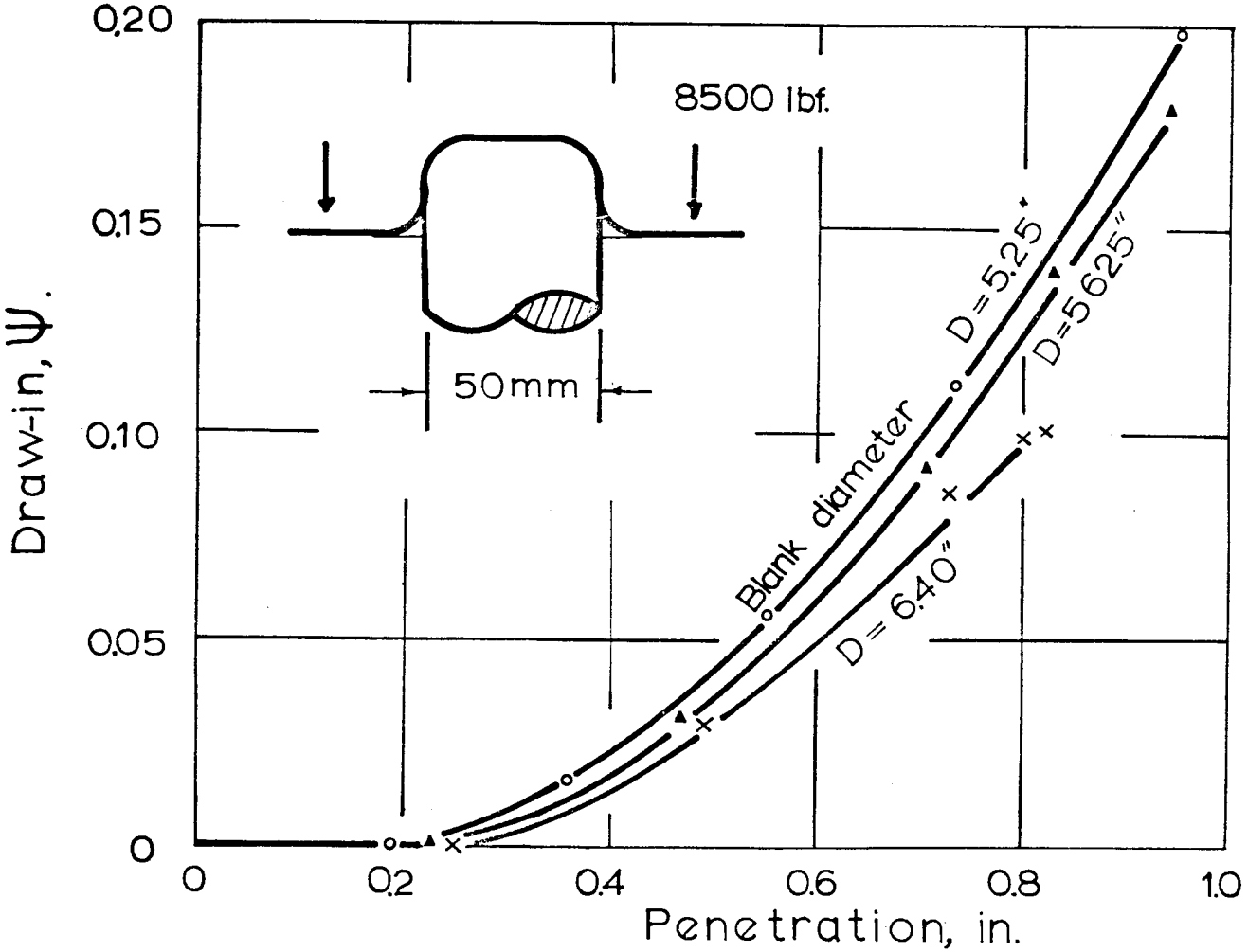
0.20
0.15
0.10
0.05
0
Draw-in, Ψ.
8500 lbf.
50mm
Blank diameter
D=5.25"
D=5625"
D=6.40"
0
0.2
0.4
0.6
0.8
1.0
Penetration, in.

FIG. 9. 2.

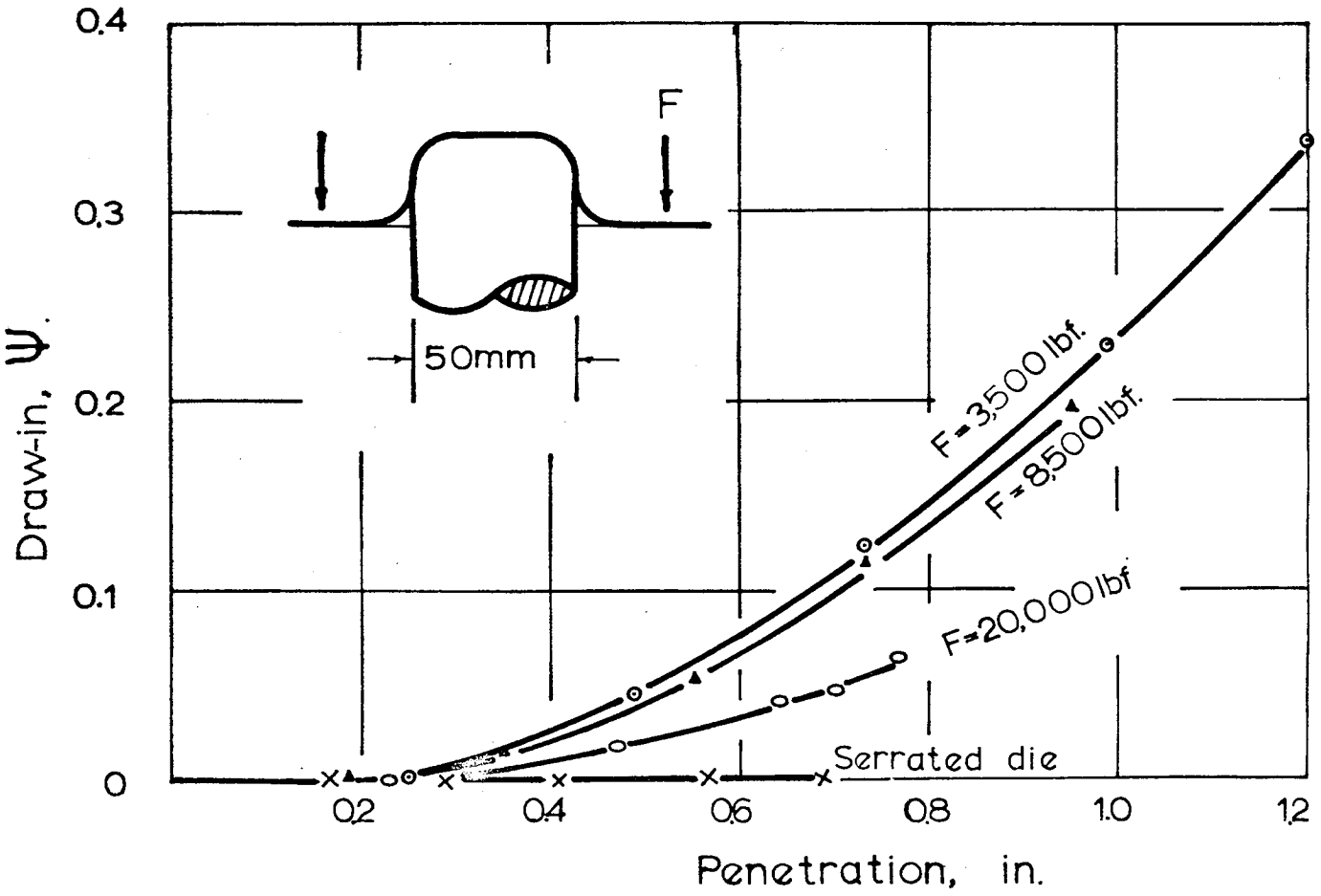
0.4
0.3
0.2
0.1
0
Draw-in, Ψ
F
50mm
F=3,500 lbf.
F=8,500 lbf.
F=20,000 lbf
Serrated die
0.2
0.4
0.6
0.8
1.0
1.2
Penetration, in.

FIG. 9.3.

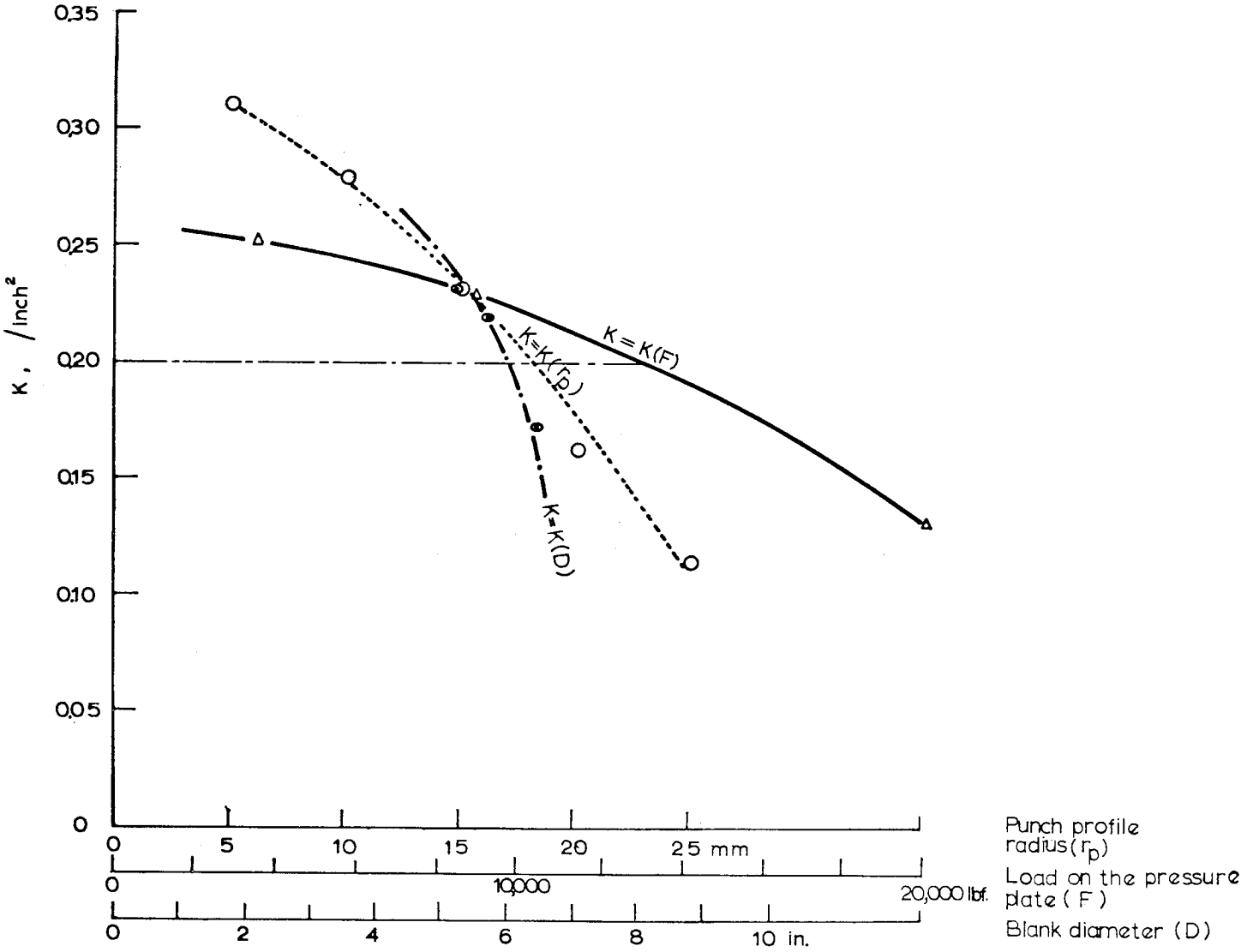
0.35
0.30
0.25
0.20
0.15
0.10
0.05
0
K , /inch²
K = K(F)
K = K(r_p)
K = K(D)
0
5
10
15
20
25 mm
Punch profile radius (r_p)
0
10,000
20,000 lbf.
Load on the pressure plate (F)
0
2
4
6
8
10 in.
Blank diameter (D)

FIG. 9. 4.

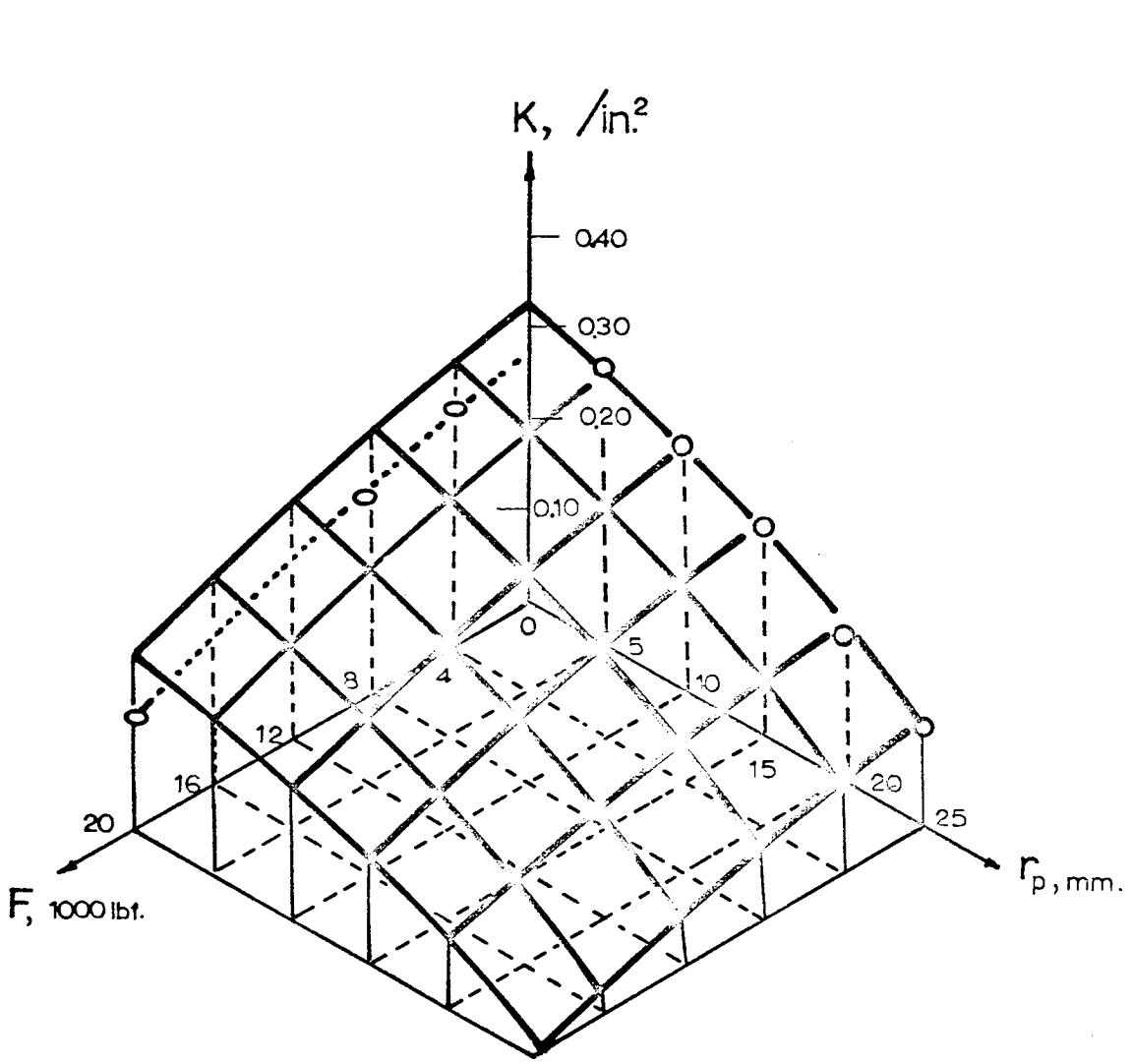
K, /in.²
0.40
0.30
0.20
0.10
0
4
8
12
16
20
5
10
15
20
25
F, 1000 lbf.
rp, mm.

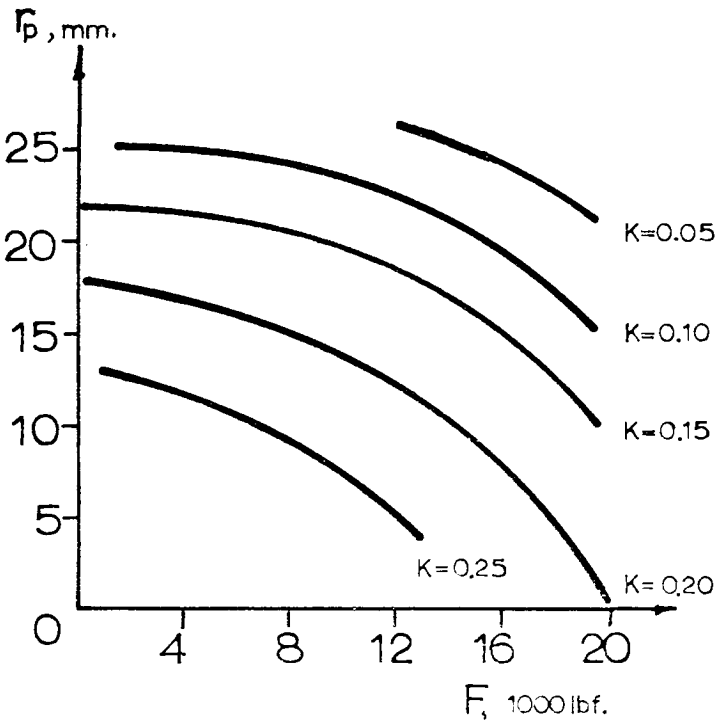
rp, mm.
25
20
15
10
5
0
4
8
12
16
20
F, 1000 lbf.
K=0.05
K=0.10
K=0.15
K=0.20
K=0.25

FIG. 9. 5.

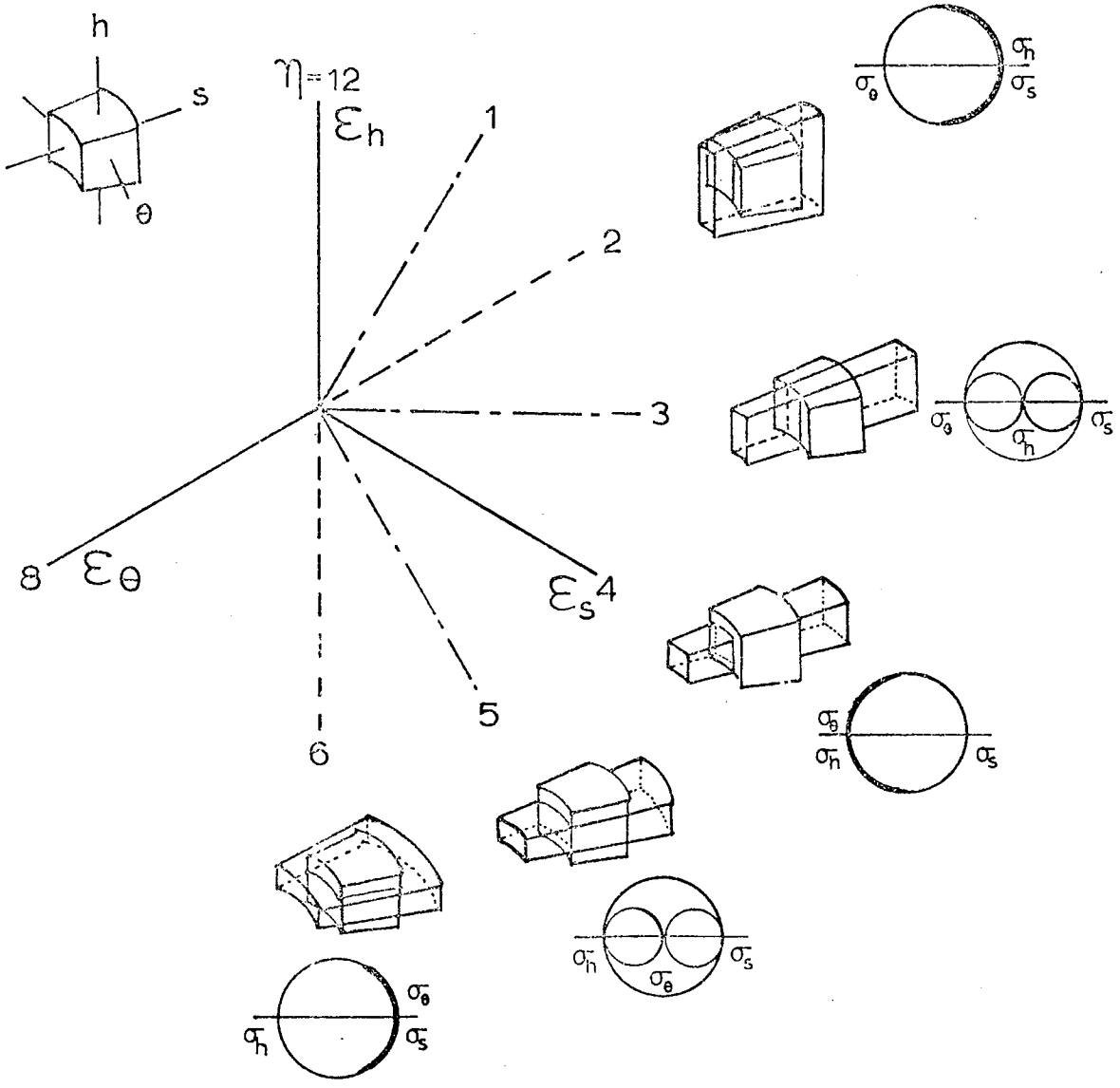

FIG. 10. 1.

FIG. 10. 2.

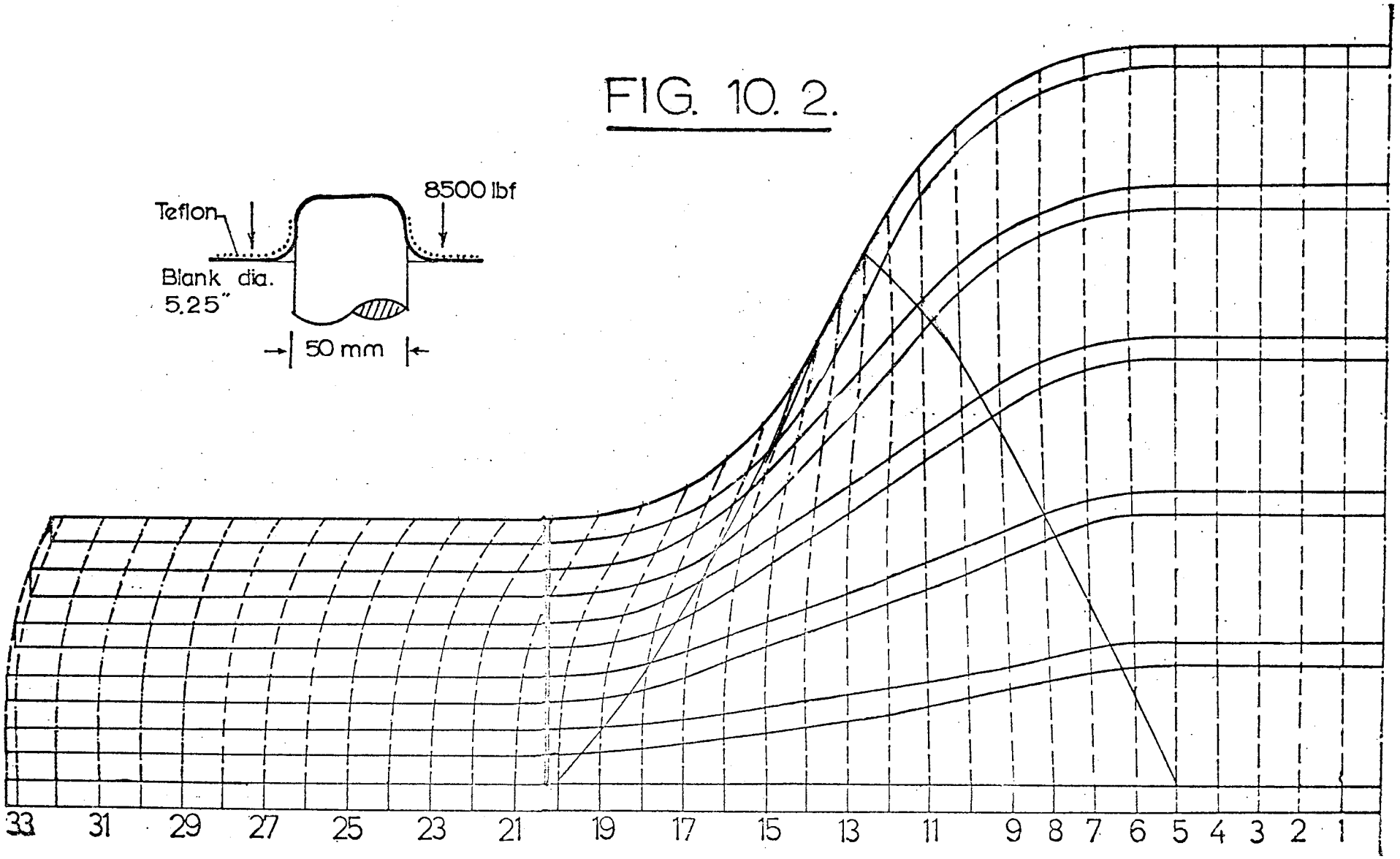
Teflon
8500 lbf
Blank dia.
5.25"
50 mm
33
31
29
27
25
23
21
19
17
15
13
11
9
8
7
6
5
4
3
2
1

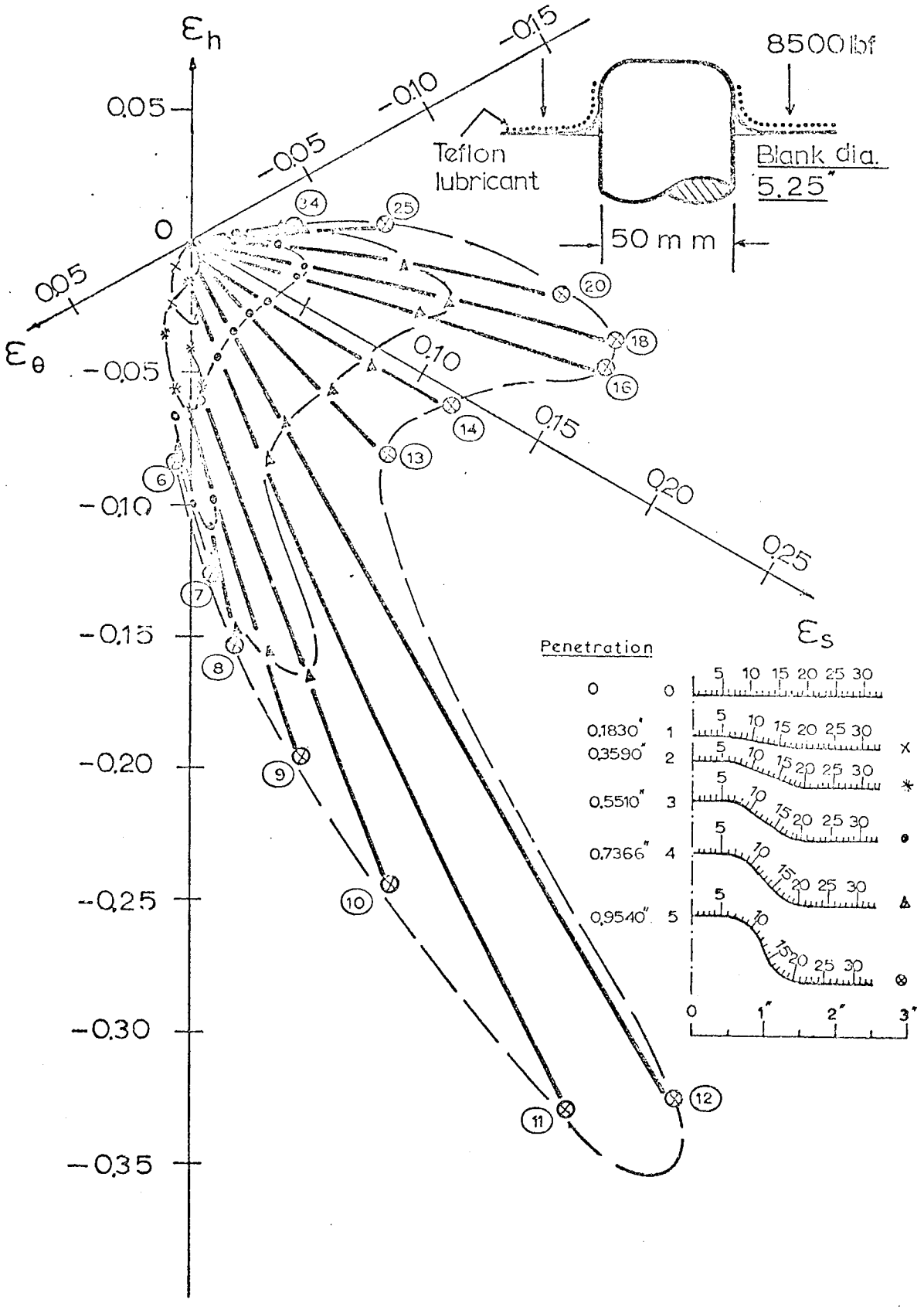
ε_h
ε_θ
ε_s
0.05
0
-0.05
-0.10
-0.15
-0.20
-0.25
-0.30
-0.35
0.05
0.10
0.15
0.20
0.25
8500 lbf
Teflon lubricant
Blank dia. 5.25"
50 mm
Penetration
0
0.1830"
0.3590"
0.5510"
0.7366"
0.9540"
0 1" 2" 3"

FIG. 10. 3.

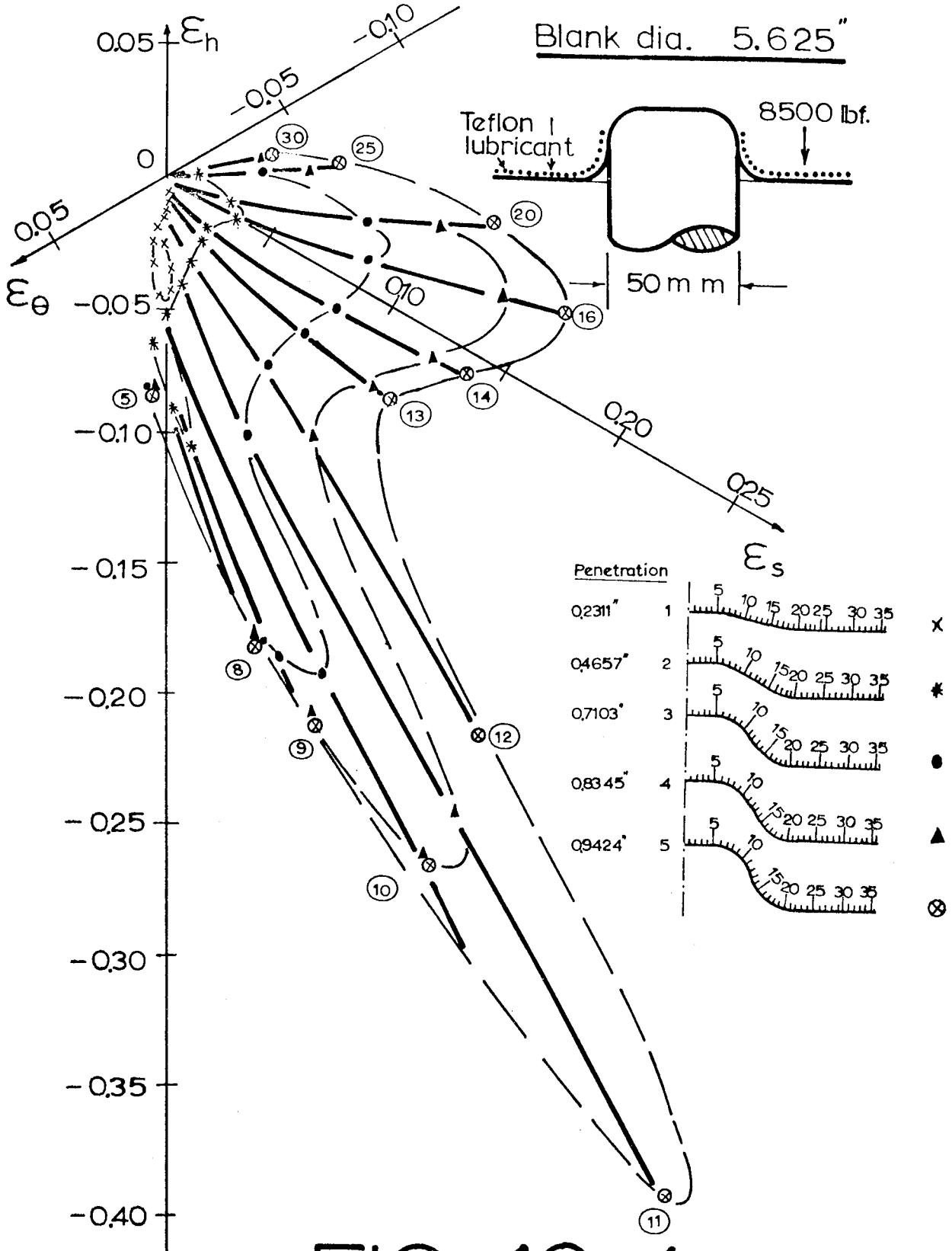
Blank dia. 5.625"
Teflon lubricant
8500 lbf.
50 m m
ε_h
ε_θ
ε_s
0.05
-0.05
-0.10
0
0.05
-0.05
-0.10
-0.15
-0.20
-0.25
-0.30
-0.35
-0.40
0.10
0.20
0.25
Penetration
0.2311" 1
0.4657" 2
0.7103" 3
0.8345" 4
0.9424" 5
5 10 15 20 25 30 35

FIG. 10.4.

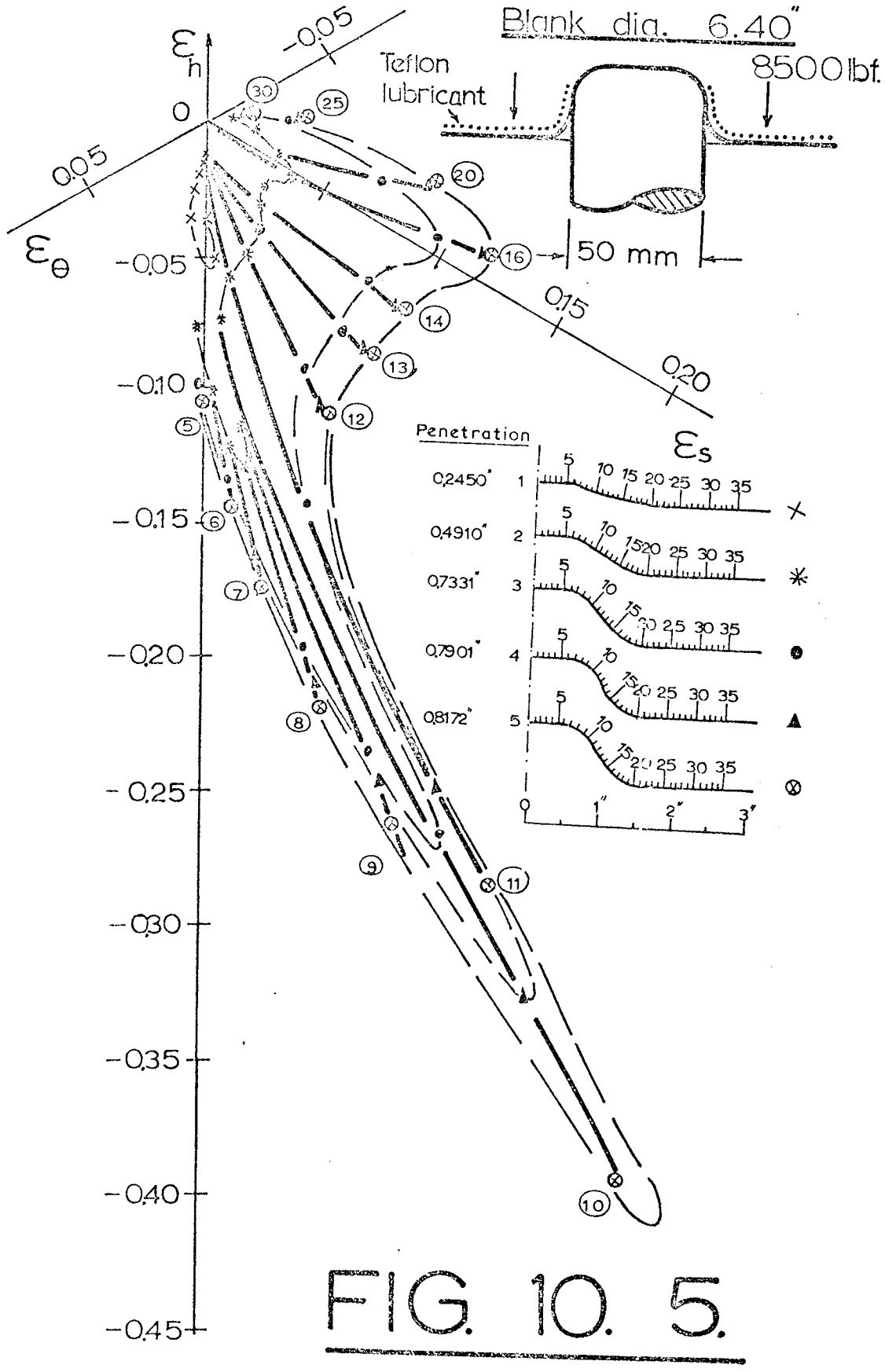
Blank dia. 6.40"
Teflon lubricant
8500 lbf.
50 mm
ε_h
ε_θ
ε_s
-0.05
0
0.05
0.15
0.20
-0.10
-0.15
-0.20
-0.25
-0.30
-0.35
-0.40
-0.45
Penetration
0.2450"
0.4910"
0.7331"
0.7901"
0.8172"
1
2
3
4
5
0
1"
2"
3"

FIG. 10. 5.

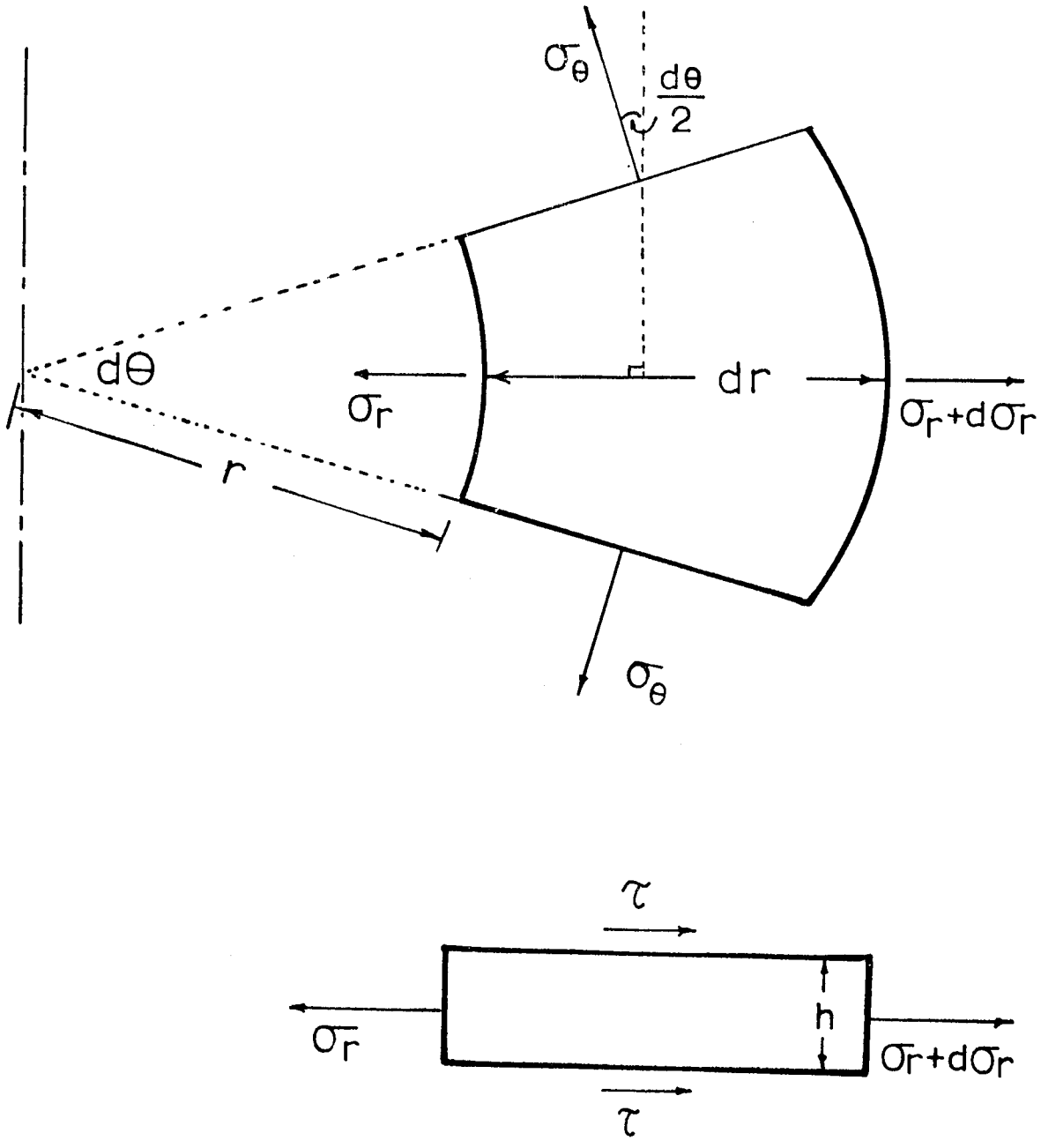
σ_θ
$\frac{d\theta}{2}$
$d\theta$
σ_r
dr
$\sigma_r+d\sigma_r$
r
σ_θ
τ
σ_r
h
$\sigma_r+d\sigma_r$
τ

FIG. 10. 6.

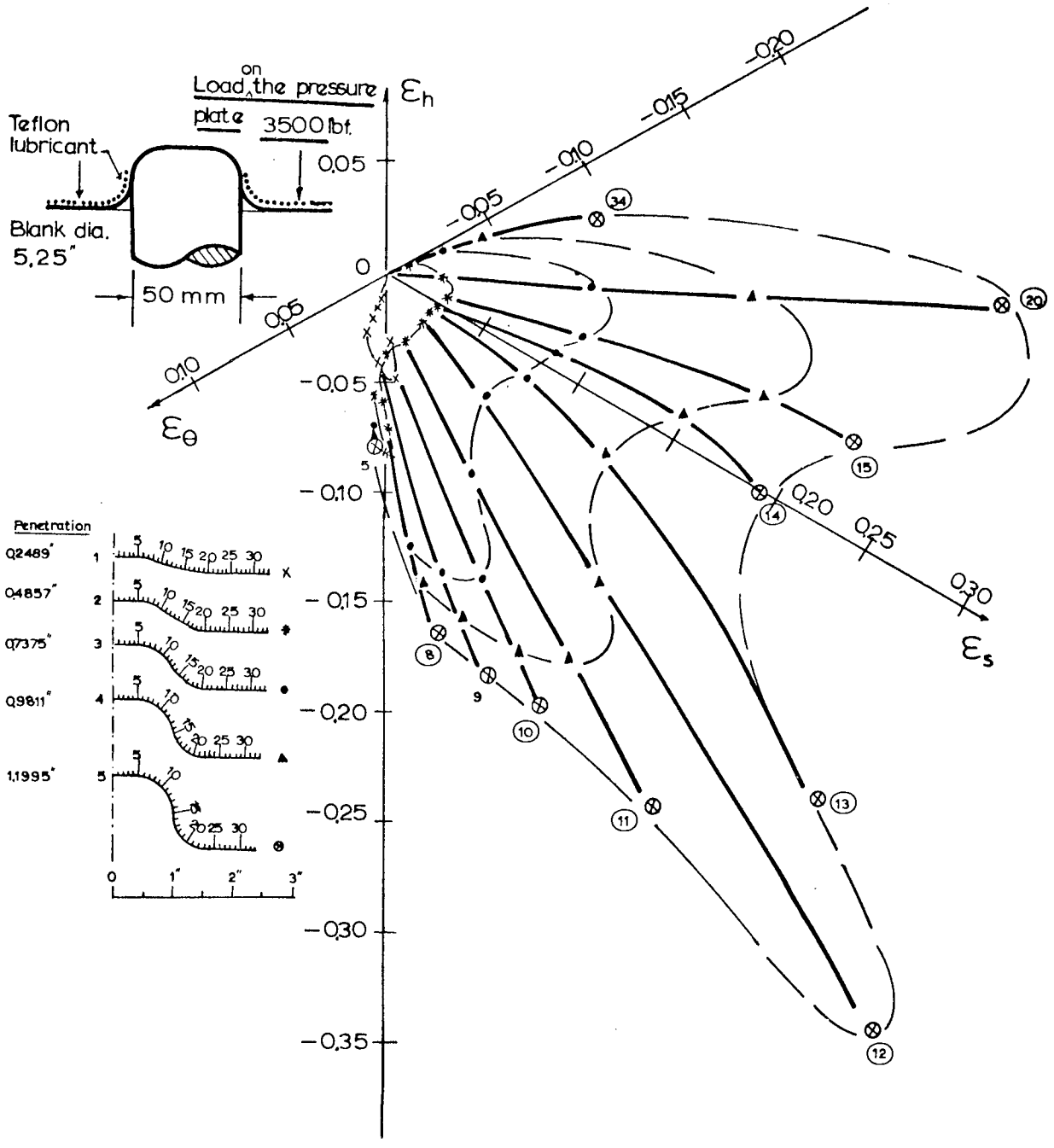
Load on the pressure plate 3500 lbf.
Teflon lubricant
Blank dia. 5.25"
50 mm
ε_h
ε_θ
ε_s
0.05
0
-0.05
-0.10
-0.15
-0.20
-0.25
-0.30
-0.35
0.05
0.10
0.20
0.25
0.30
Penetration
0.2489"
0.4857"
0.7375"
0.9811"
1.1995"
0
1"
2"
3"

FIG. 10. 7.

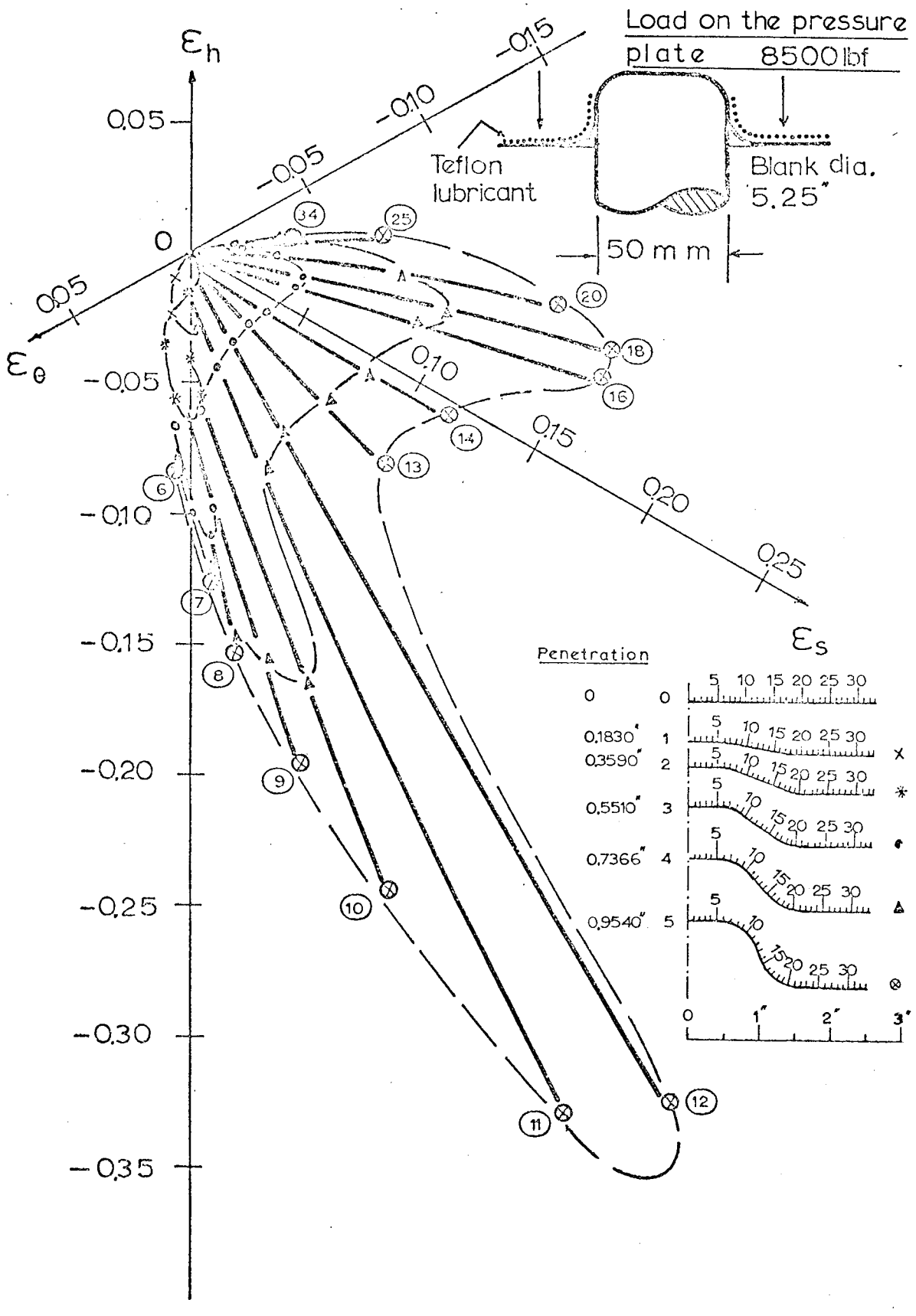
Load on the pressure plate 8500 lbf
Teflon lubricant
Blank dia. 5.25"
50 m m
ε_h
ε_θ
ε_s
0.05
-0.05
0
0.05
-0.10
0.10
-0.15
0.15
0.20
0.25
-0.05
-0.10
-0.15
-0.20
-0.25
-0.30
-0.35
Penetration
0
0.1830"
0.3590"
0.5510"
0.7366"
0.9540"
5 10 15 20 25 30
0 1" 2" 3"

FIG. 10.8.

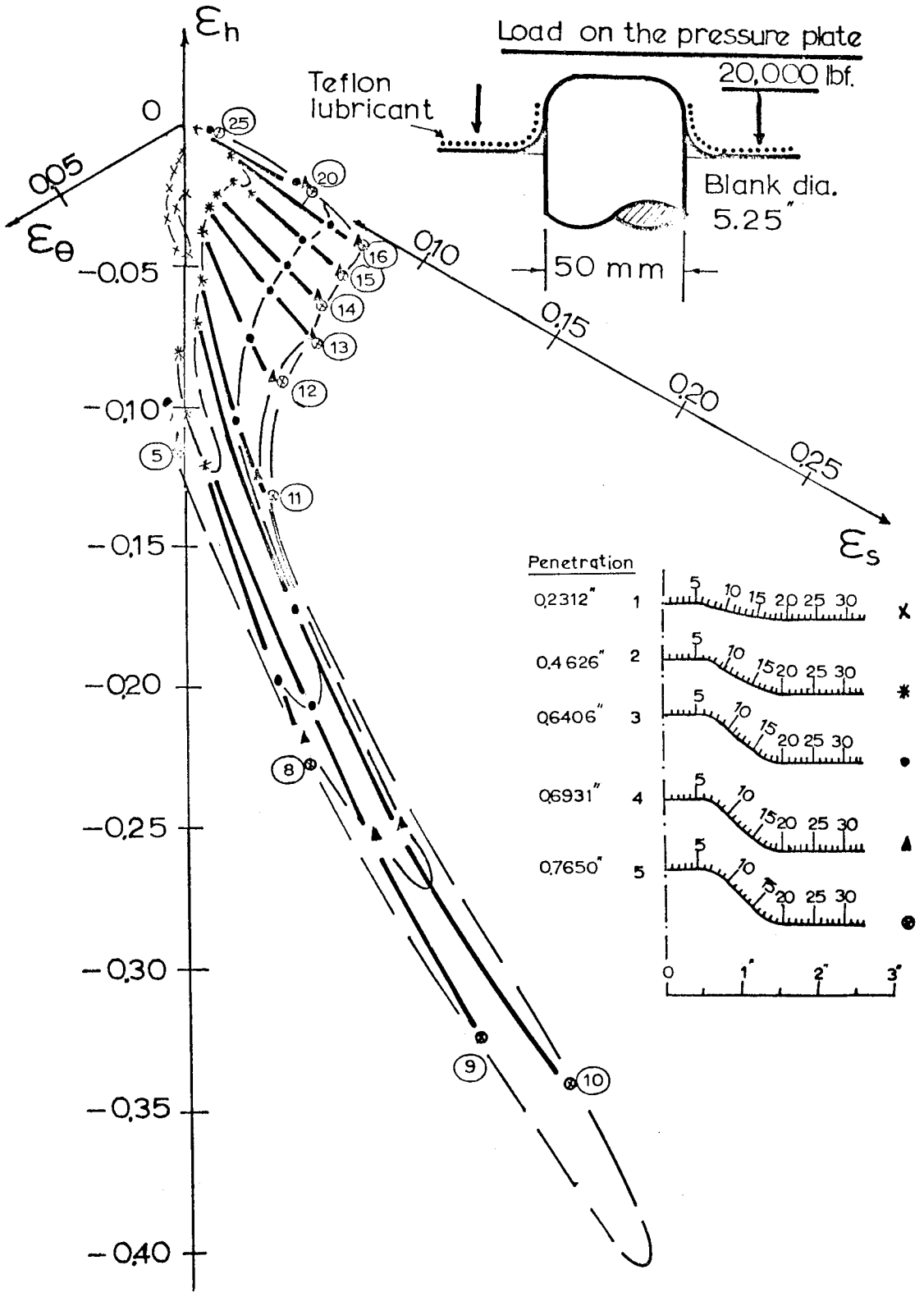
ε_h
ε_θ
ε_s
0
0.05
-0.05
0.10
-0.10
0.15
-0.15
0.20
-0.20
0.25
-0.25
-0.30
-0.35
-0.40
Load on the pressure plate
20,000 lbf.
Teflon lubricant
Blank dia. 5.25"
50 mm
Penetration
0.2312" 1
0.4626" 2
0.6406" 3
0.6931" 4
0.7650" 5
5 10 15 20 25 30
0 1" 2" 3"

FIG. 10.9.

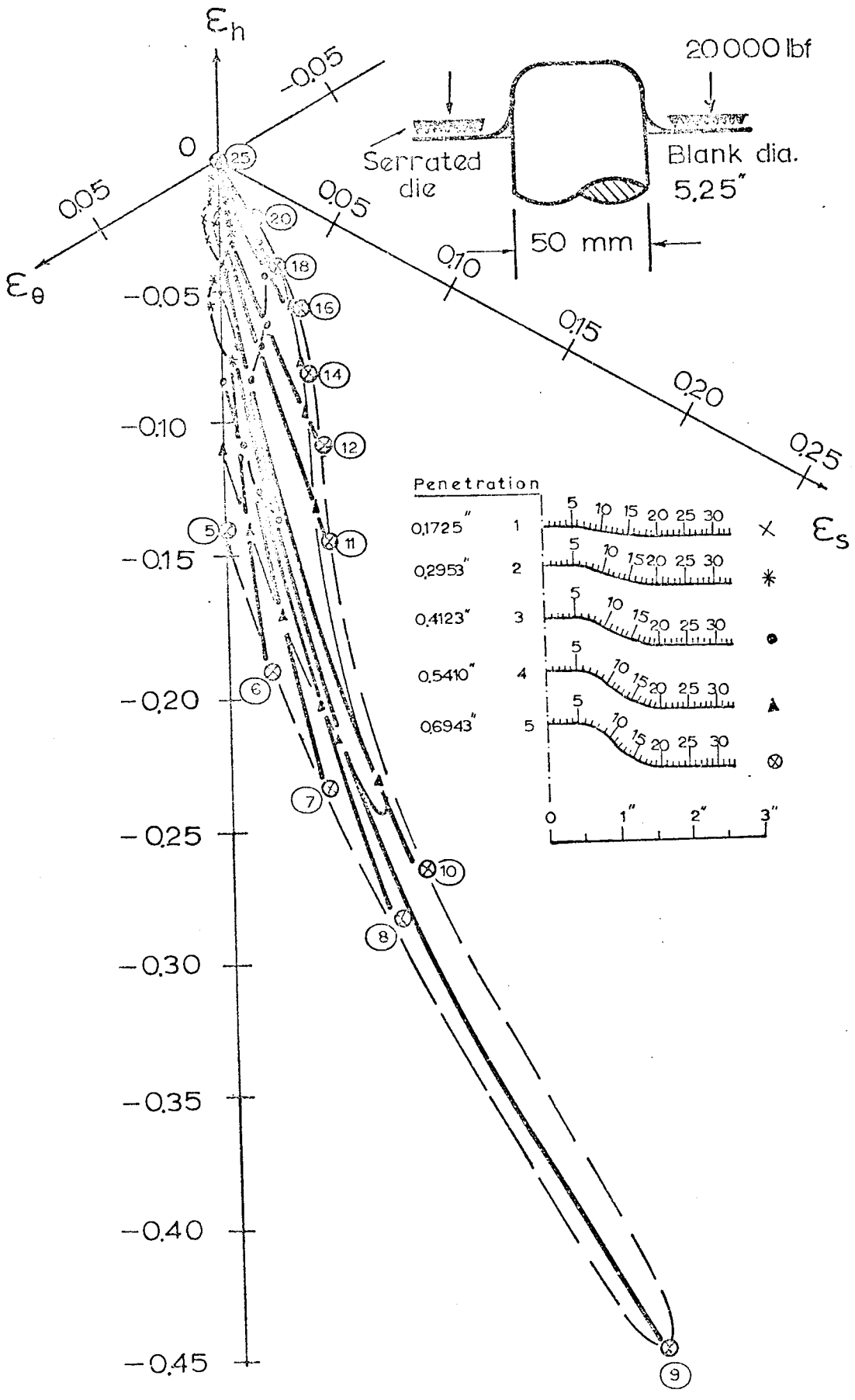
ε_h
ε_θ
ε_s
0
-0.05
0.05
0.10
0.15
0.20
0.25
-0.10
-0.15
-0.20
-0.25
-0.30
-0.35
-0.40
-0.45
20 000 lbf
Serrated die
Blank dia. 5.25"
50 mm
Penetration
0.1725" 1
0.2953" 2
0.4123" 3
0.5410" 4
0.6943" 5
0 1" 2" 3"

FIG. 10. 10.

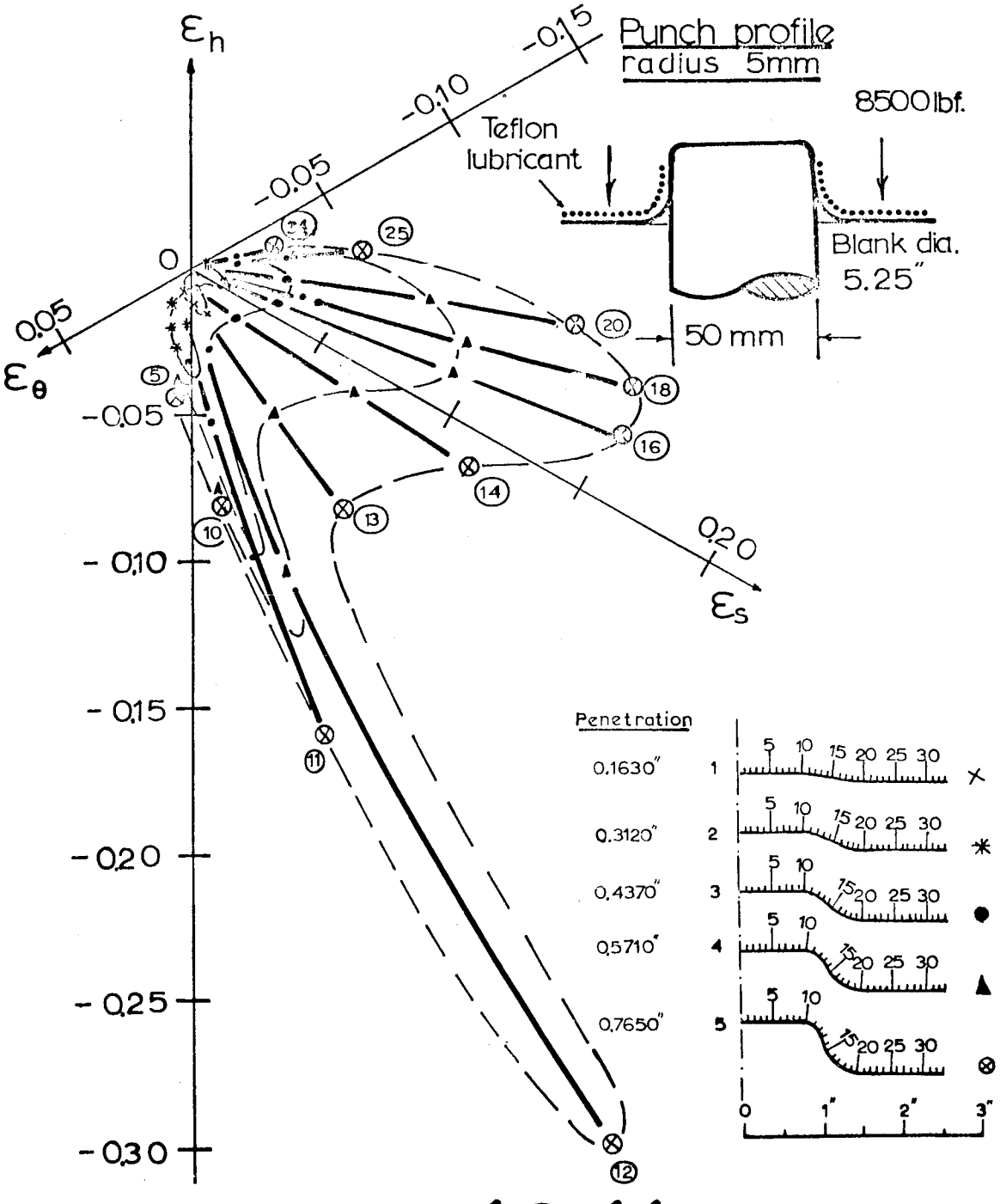
ε_h
ε_θ
ε_s
-0.15
-0.10
-0.05
0
0.05
0.20
-0.05
-0.10
-0.15
-0.20
-0.25
-0.30
Punch profile
radius 5mm
8500 lbf.
Teflon
lubricant
Blank dia.
5.25"
50 mm
Penetration
0.1630"
0.3120"
0.4370"
0.5710"
0.7650"
0
1"
2"
3"

FIG. 10.11.

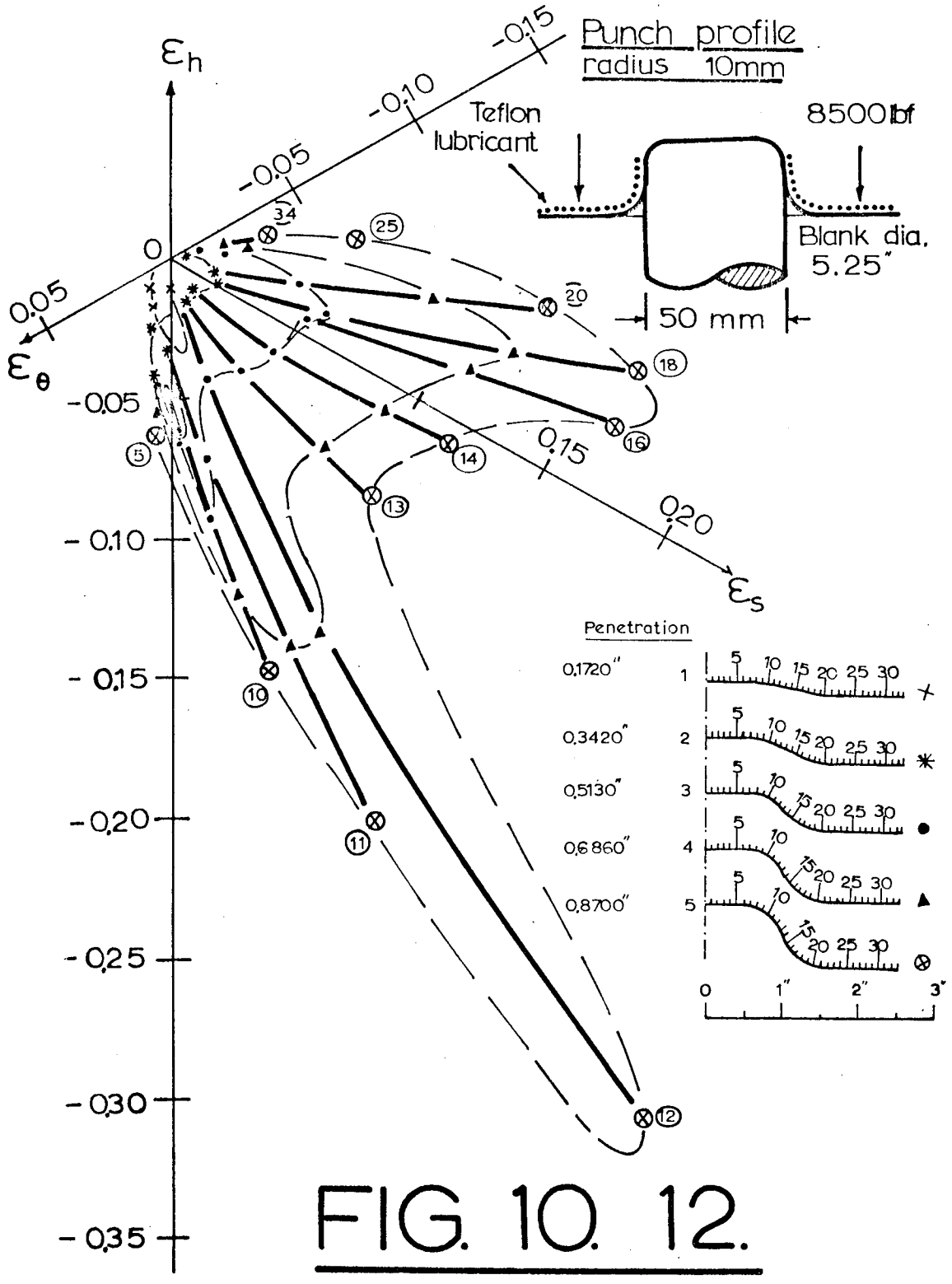
Punch profile
radius 10mm
Teflon
lubricant
8500 lbf
Blank dia.
5.25"
50 mm
ε_h
ε_θ
ε_s
-0.15
-0.10
-0.05
0
0.05
0.15
0.20
-0.05
-0.10
-0.15
-0.20
-0.25
-0.30
-0.35
Penetration
0.1720"
0.3420"
0.5130"
0.6860"
0.8700"
0
1"
2"
3"

FIG. 10. 12.

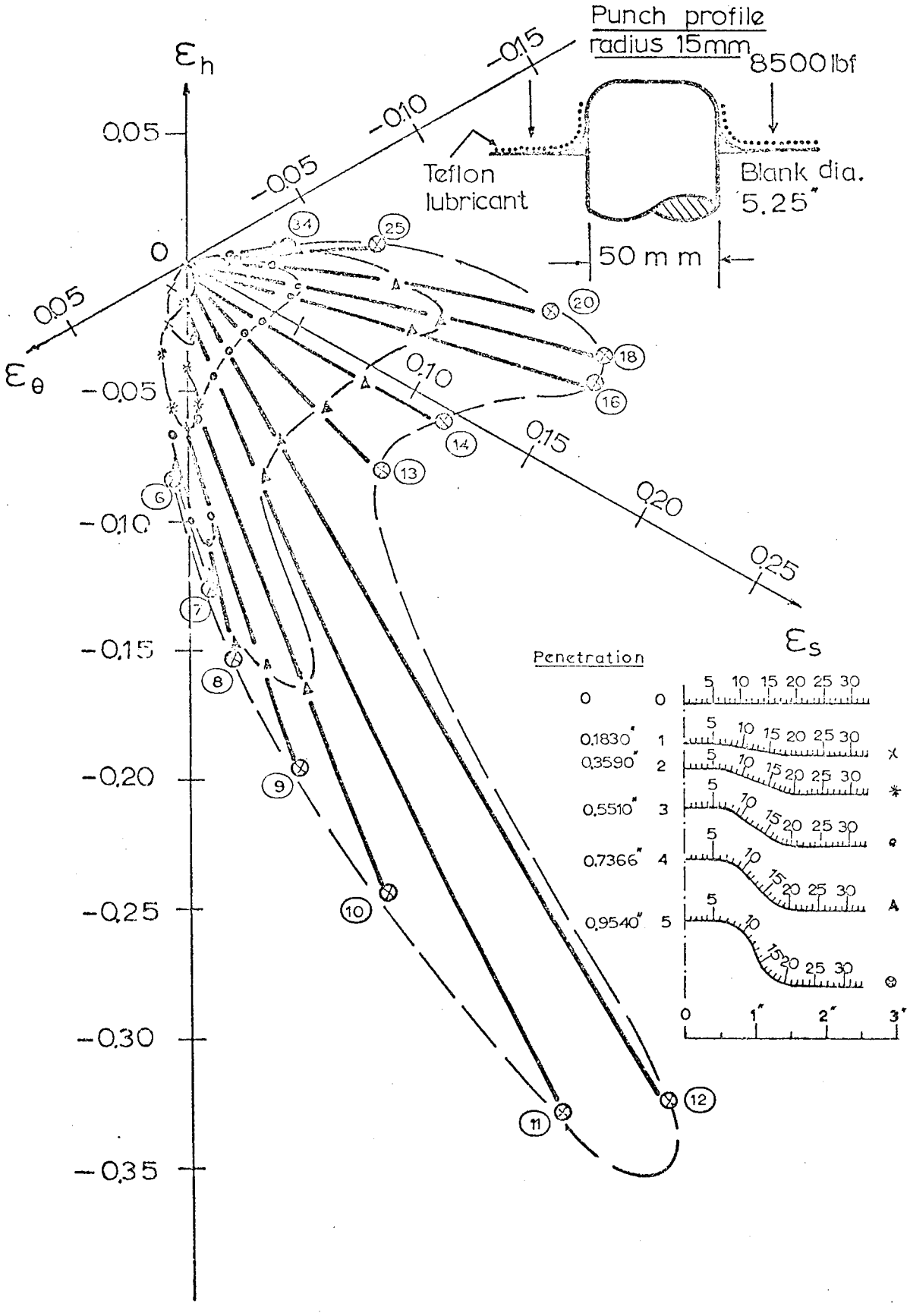
Punch profile
radius 15mm
8500 lbf
Teflon
lubricant
Blank dia.
5.25"
50 m m
ε_h
ε_θ
ε_s
0.05
0
-0.05
-0.10
-0.15
-0.20
-0.25
-0.30
-0.35
0.05
0.10
0.15
0.20
0.25
-0.15
-0.10
-0.05
Penetration
0 0
0.1830" 1
0.3590" 2
0.5510" 3
0.7366" 4
0.9540" 5
5 10 15 20 25 30
0 1" 2" 3"
6
7
8
9
10
11
12
13
14
16
18
20
25
34

FIG. 10. 13.

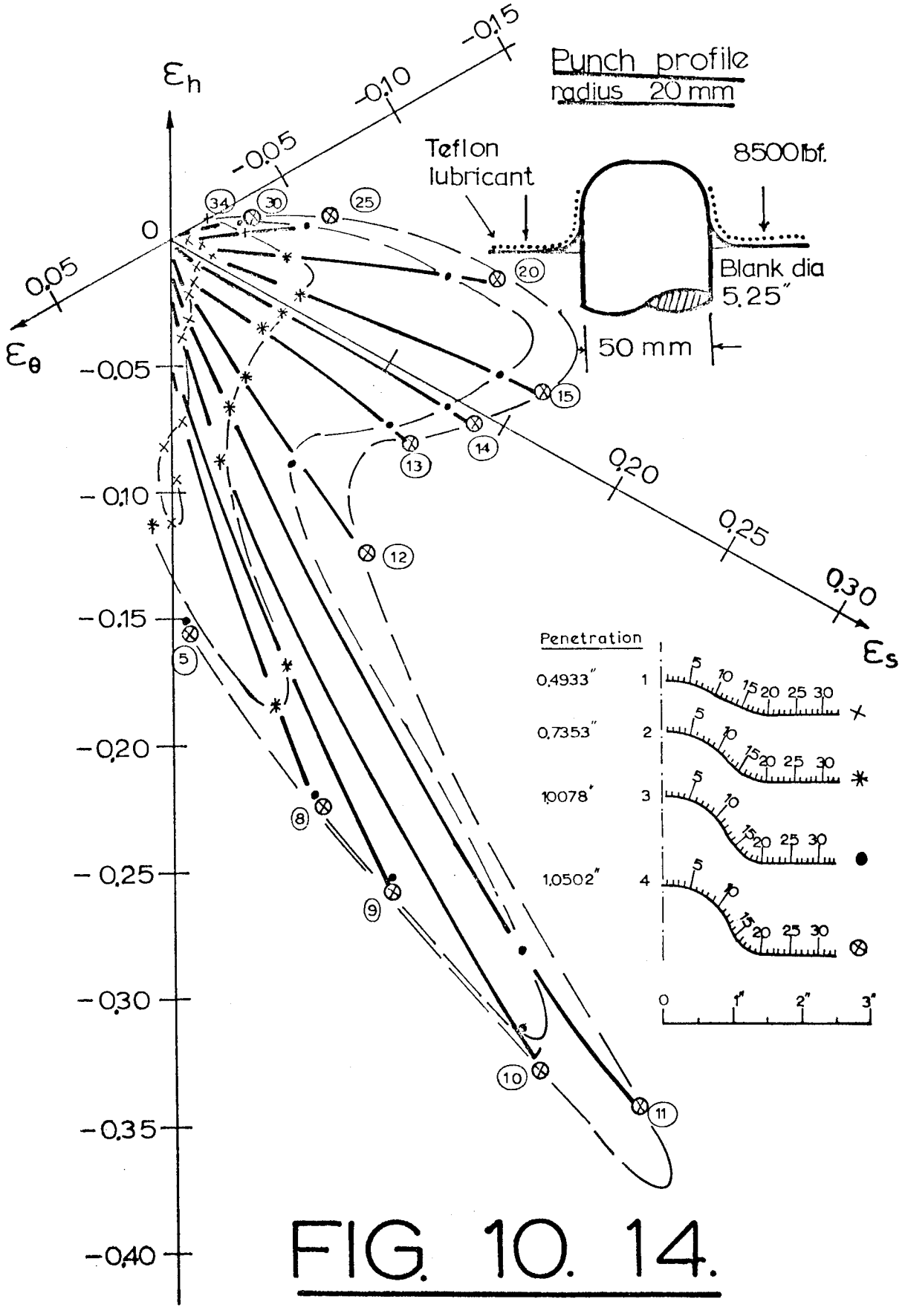
ε_h
ε_θ
ε_s
-0.15
-0.10
-0.05
0
0.05
-0.05
-0.10
-0.15
-0.20
-0.25
-0.30
-0.35
-0.40
0.20
0.25
0.30
Punch profile
radius 20 mm
Teflon
lubricant
8500lbf.
Blank dia
5.25"
50 mm
Penetration
0.4933"
0.7353"
1.0078"
1.0502"
1
2
3
4
5
10
15
20
25
30
0
1"
2"
3"
34
30
25
20
15
14
13
12
5
8
9
10
11

FIG. 10. 14.

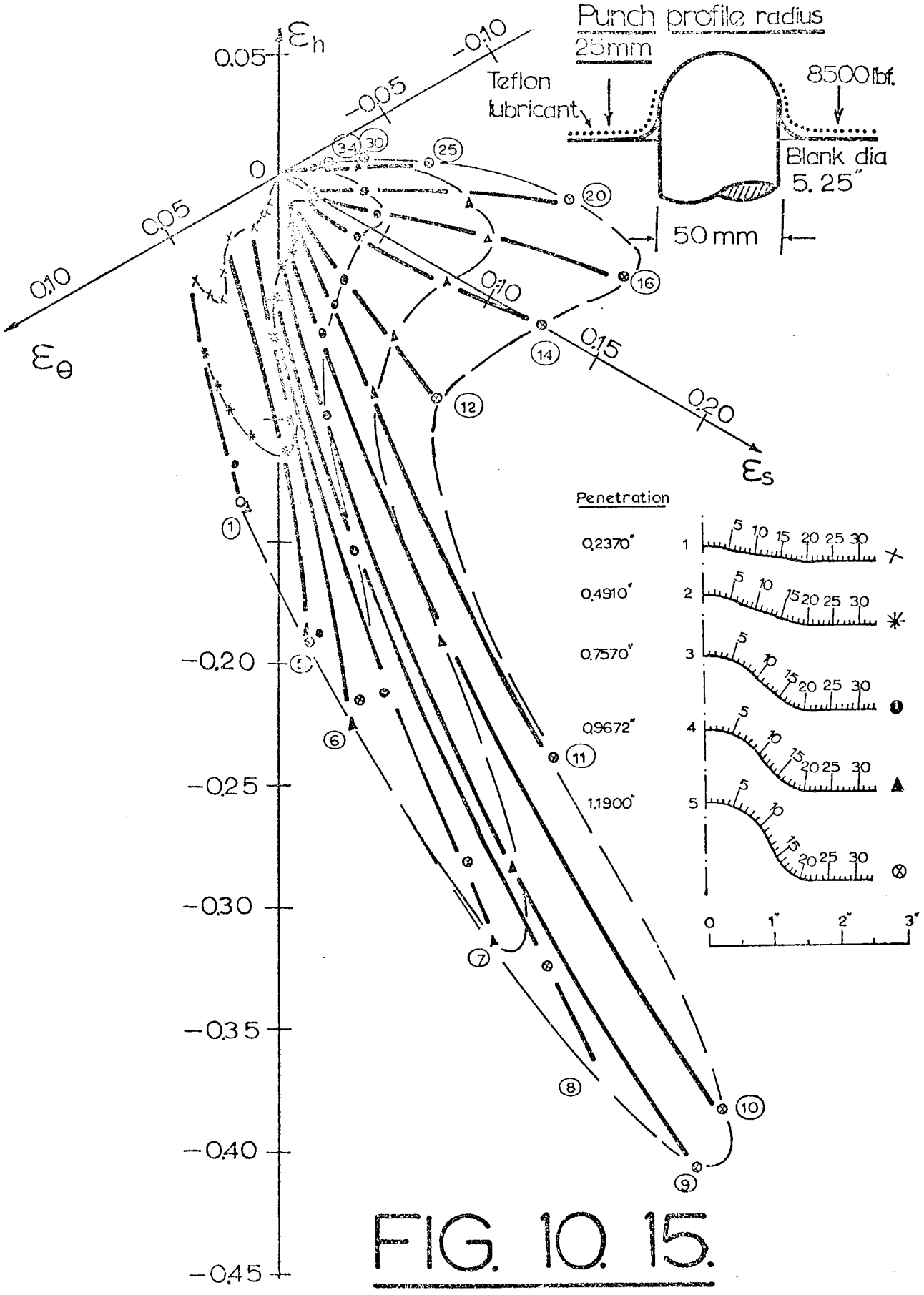
Punch profile radius
25mm
Teflon
lubricant
8500 lbf.
Blank dia
5.25"
50 mm
ε_h
ε_θ
ε_s
0.05
0
-0.10
-0.05
0.05
0.10
0.10
0.15
0.20
-0.20
-0.25
-0.30
-0.35
-0.40
-0.45
Penetration
0.2370"
0.4910"
0.7570"
0.9672"
1.1900"
0
1"
2"
3"

FIG. 10.15.

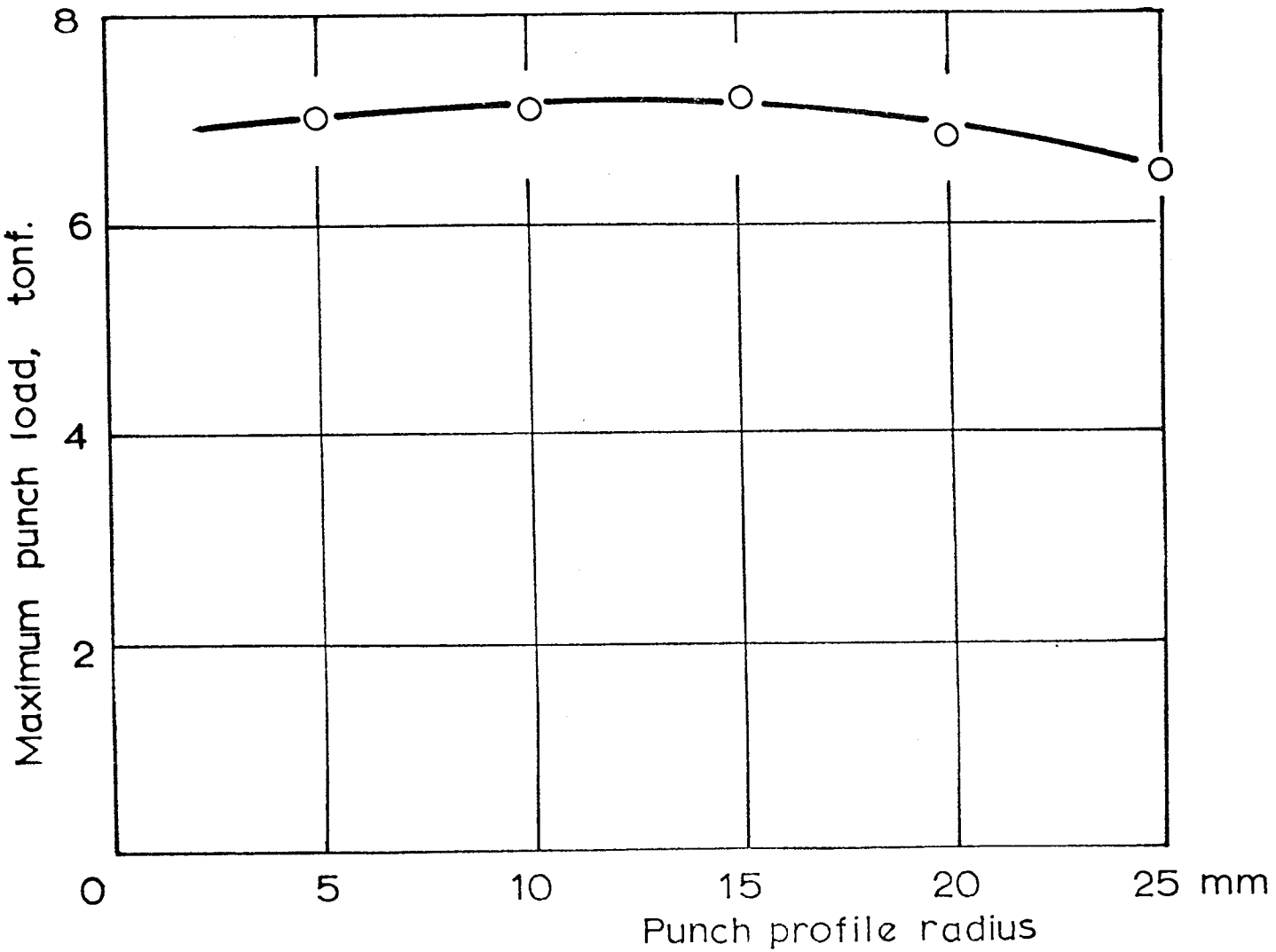
8
6
4
2
0
Maximum punch load, tonf.
5
10
15
20
25 mm
Punch profile radius

FIG. 10.16.

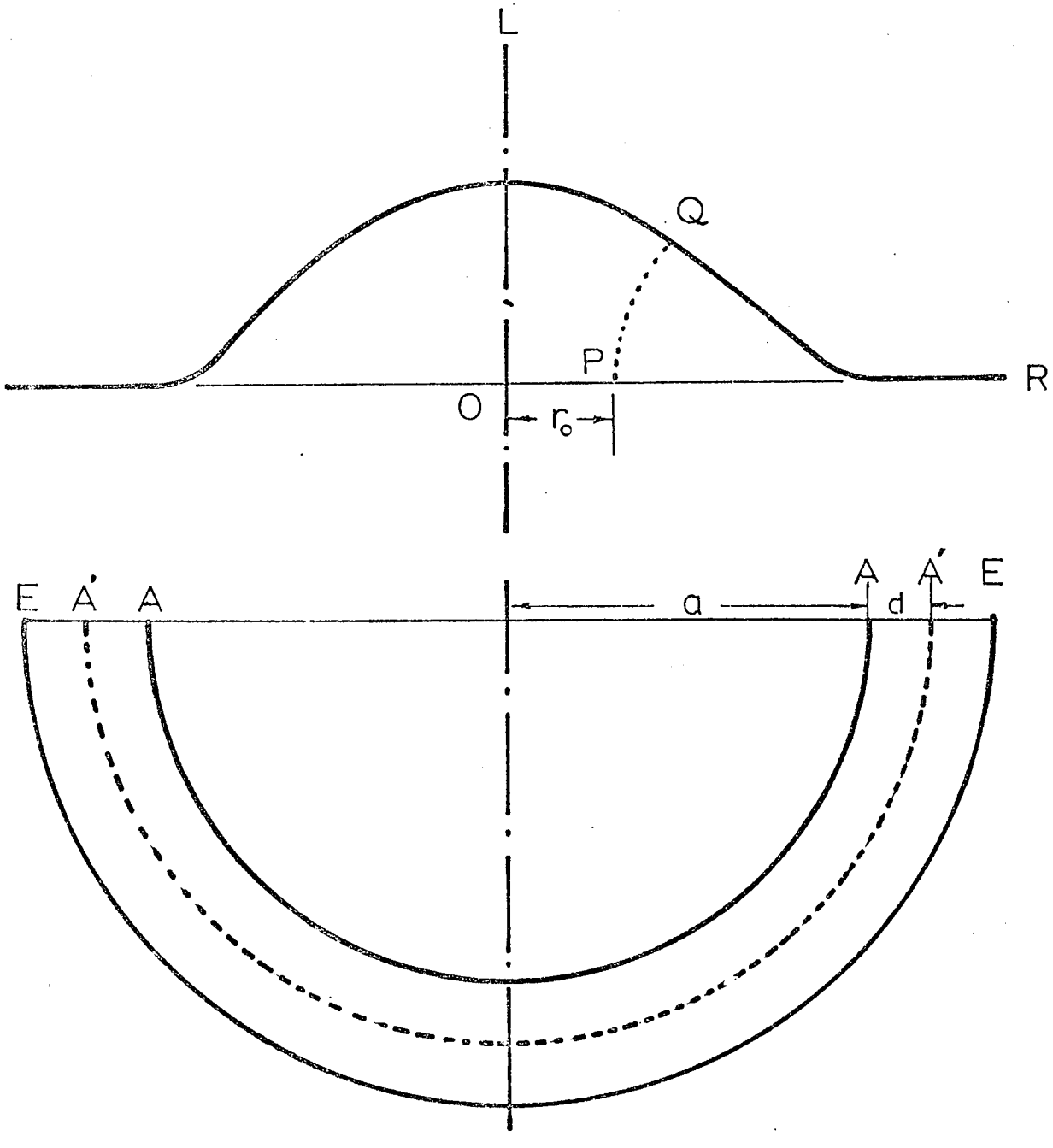

FIG. 11. 1.

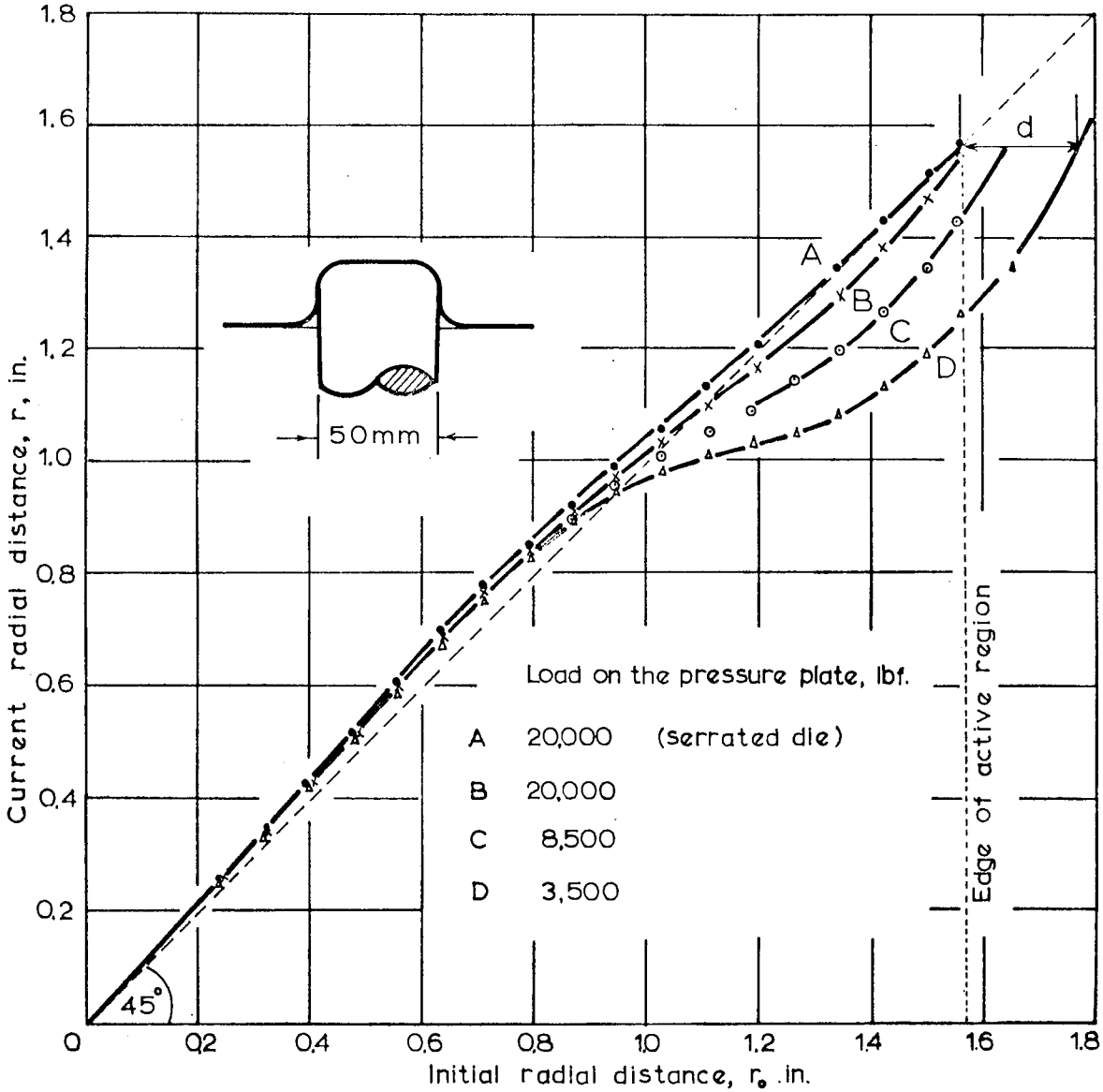
1.8
1.6
1.4
1.2
1.0
0.8
0.6
0.4
0.2
0
0.2
0.4
0.6
0.8
1.0
1.2
1.4
1.6
1.8
Current radial distance, r, in.
Initial radial distance, r_o, in.
d
A
B
C
D
50mm
45°
Load on the pressure plate, lbf.
A 20,000 (serrated die)
B 20,000
C 8,500
D 3,500
Edge of active region

FIG. 11. 2.

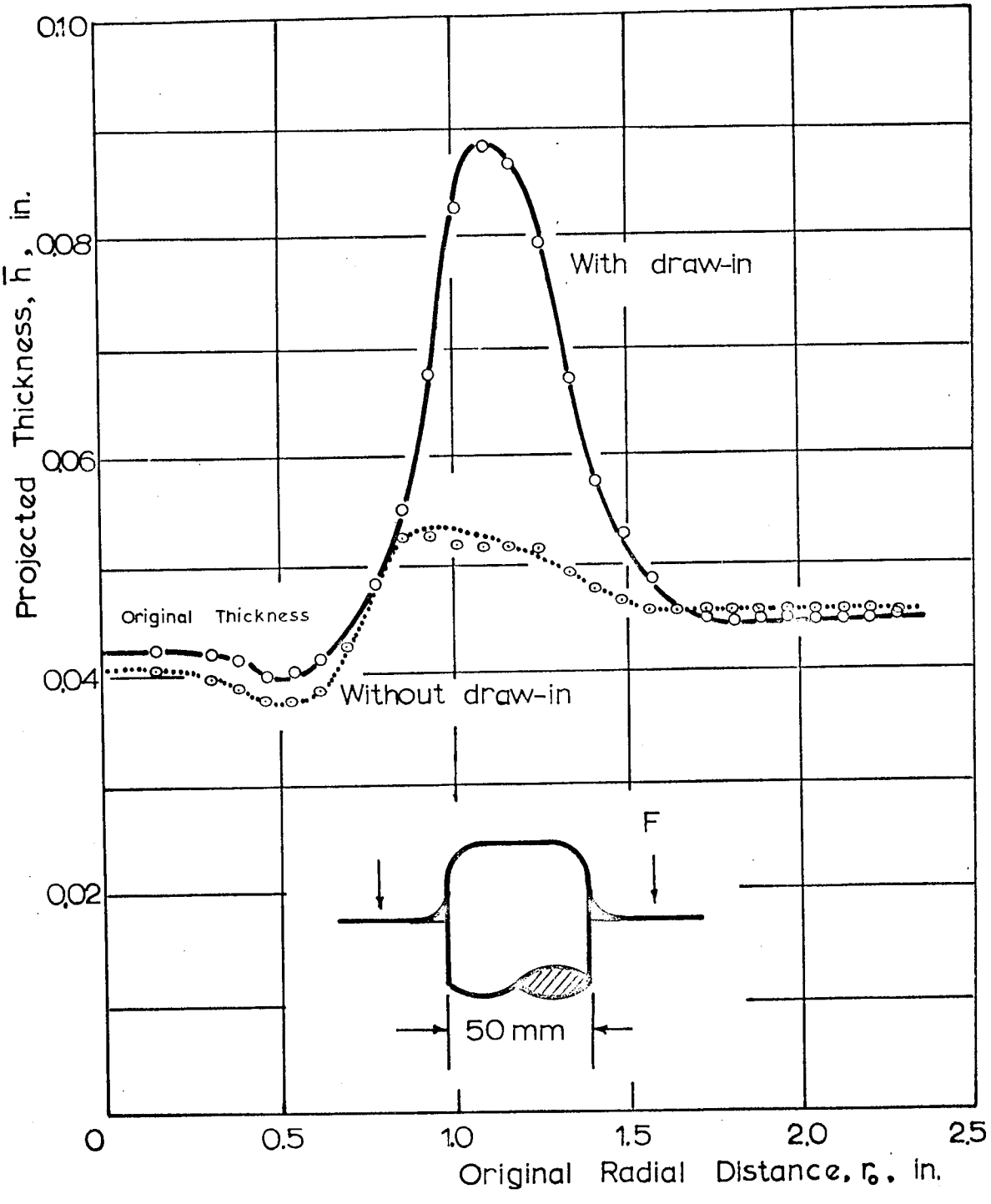
0.10
0.08
0.06
0.04
0.02
0
0.5
1.0
1.5
2.0
2.5
Projected Thickness, $\bar{h}$, in.
Original Radial Distance, r_o, in.
With draw-in
Without draw-in
Original Thickness
F
50 mm

FIG. 11. 3.

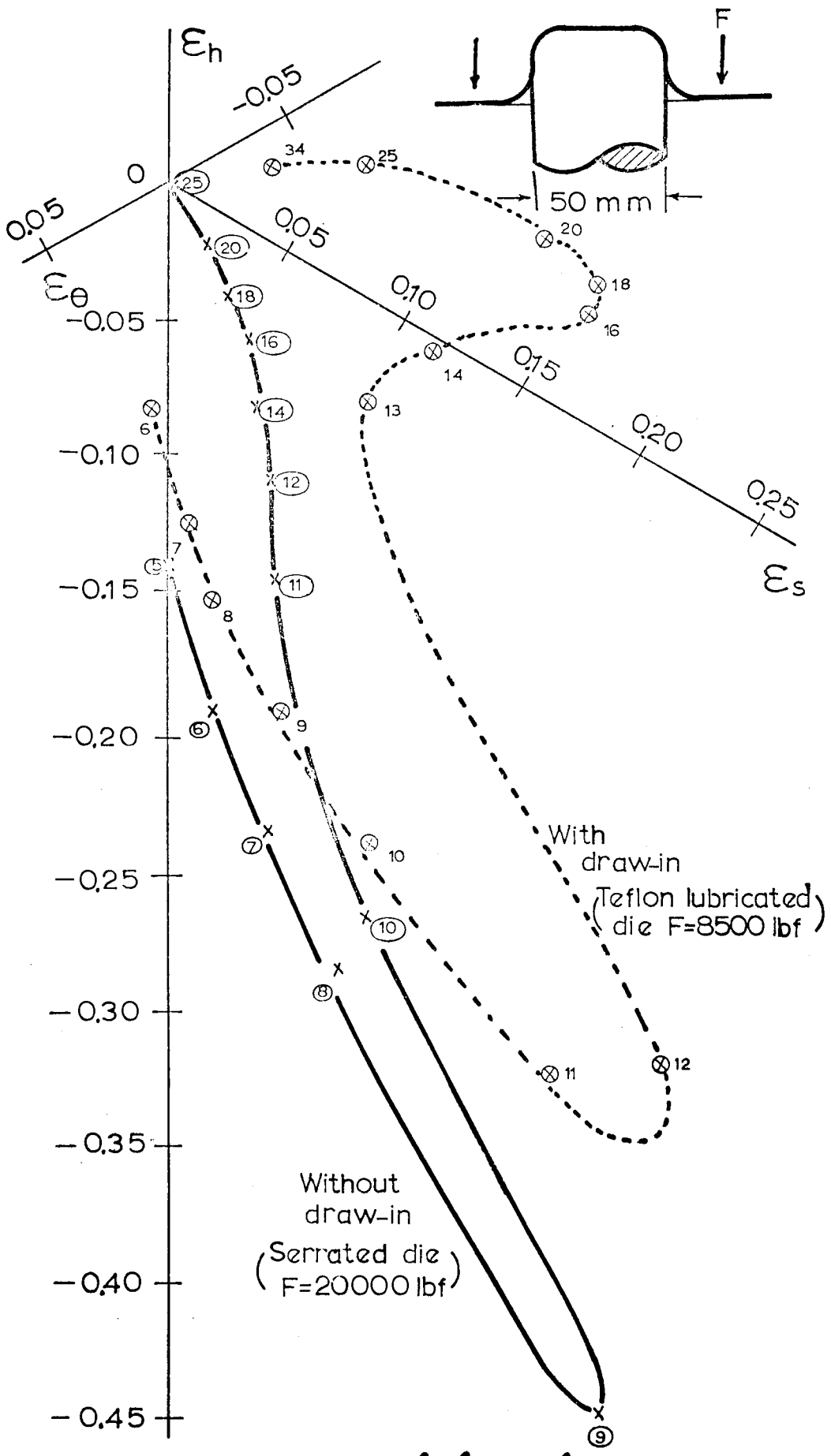
ε_h
ε_θ
ε_s
-0.05
0
0.05
0.05
0.10
0.15
0.20
0.25
-0.05
-0.10
-0.15
-0.20
-0.25
-0.30
-0.35
-0.40
-0.45
F
50 mm
With draw-in
(Teflon lubricated die F=8500 lbf)
Without draw-in
(Serrated die F=20000 lbf)

FIG. 11.4.

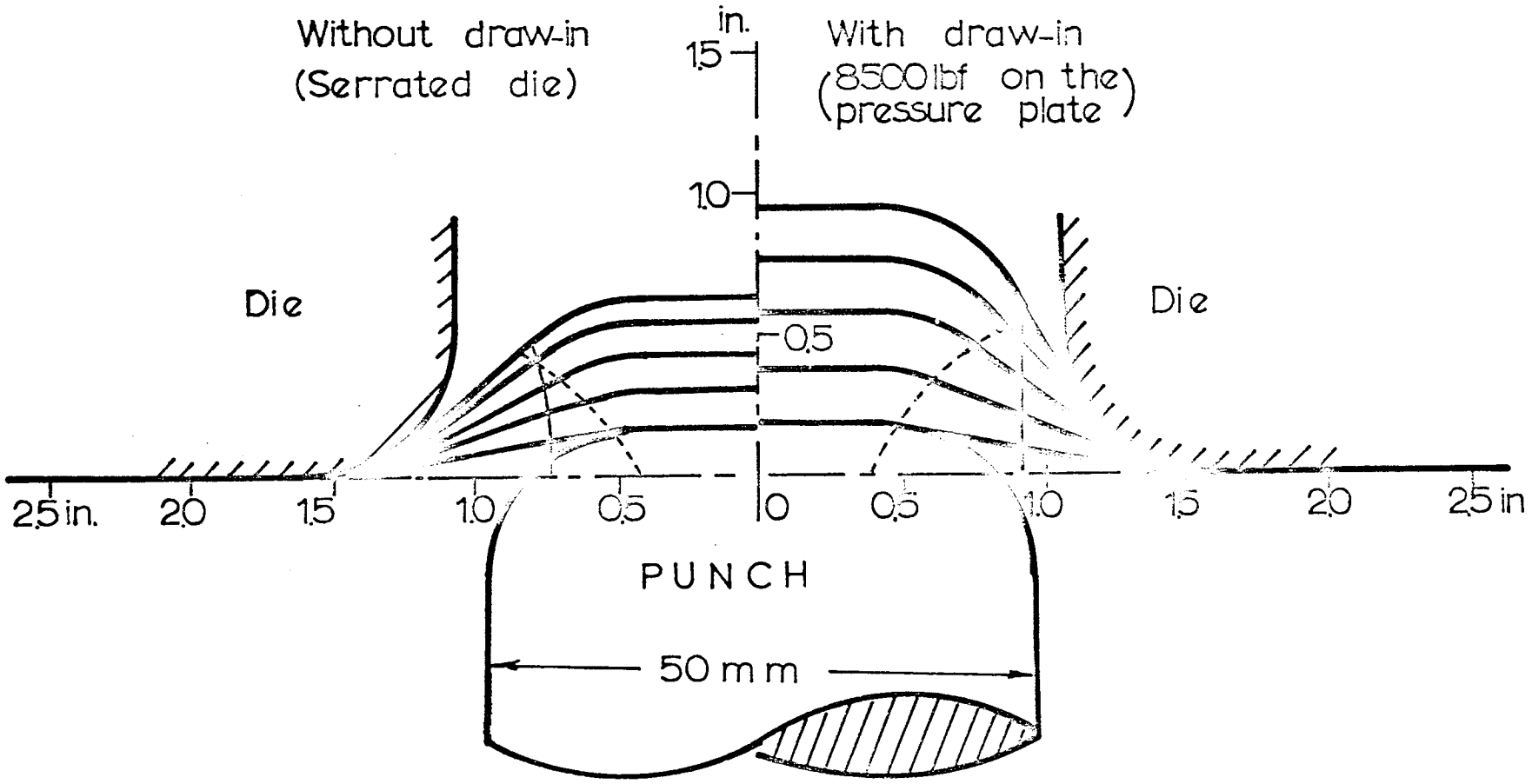
Without draw-in
(Serrated die)
in.
1.5
With draw-in
(8500 lbf on the
pressure plate)
1.0
Die
0.5
Die
2.5 in.
2.0
1.5
1.0
0.5
0
0.5
1.0
1.5
2.0
2.5 in
PUNCH
50 mm

FIG. 12. 1.

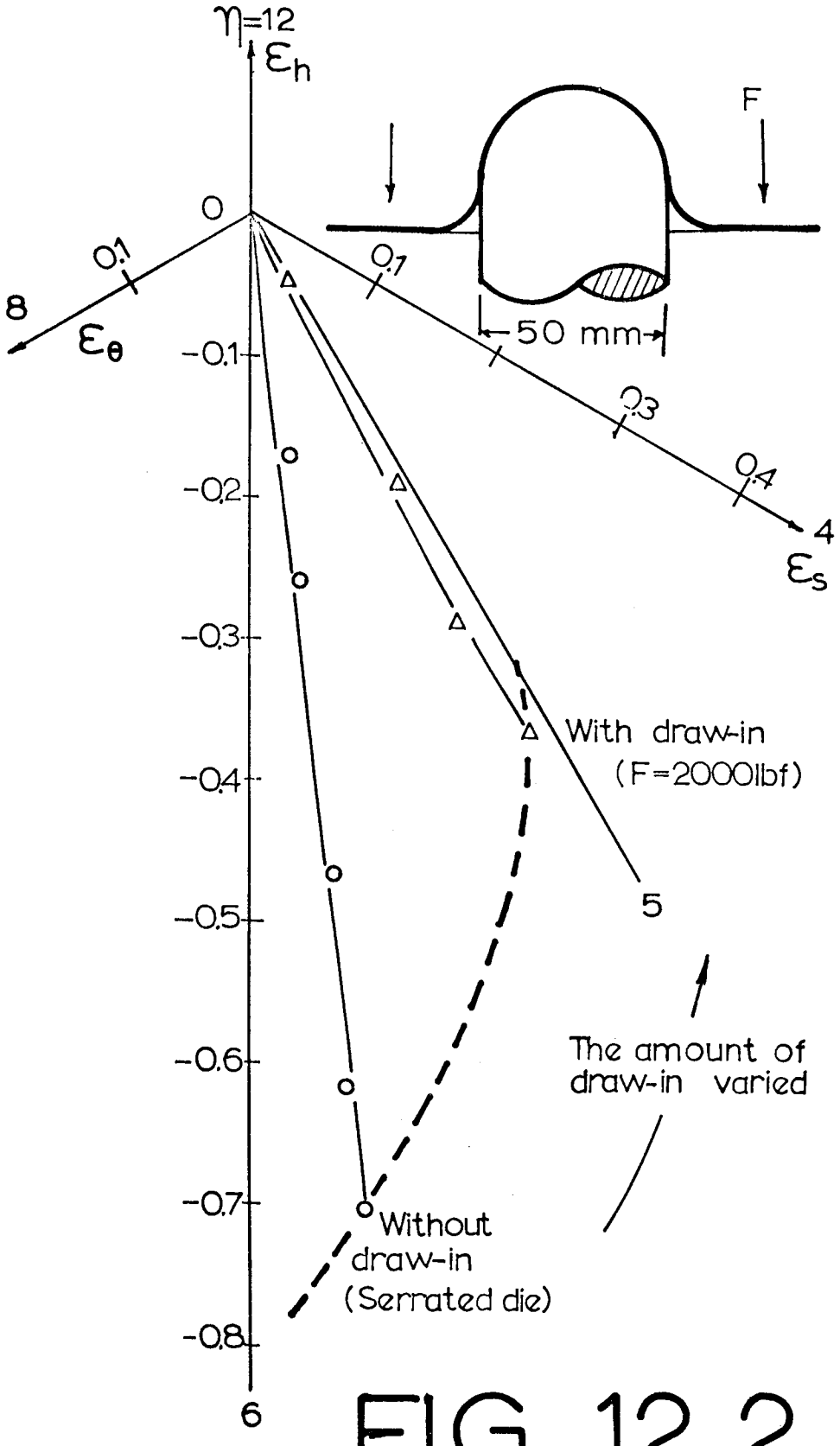
η=12
εh
F
0
0.1
0.7
8
εθ
50 mm
0.3
0.4
4
εs
-0.1
-0.2
-0.3
-0.4
-0.5
-0.6
-0.7
-0.8
With draw-in
(F=2000lbf)
5
The amount of
draw-in varied
Without
draw-in
(Serrated die)
6

FIG. 12.2.

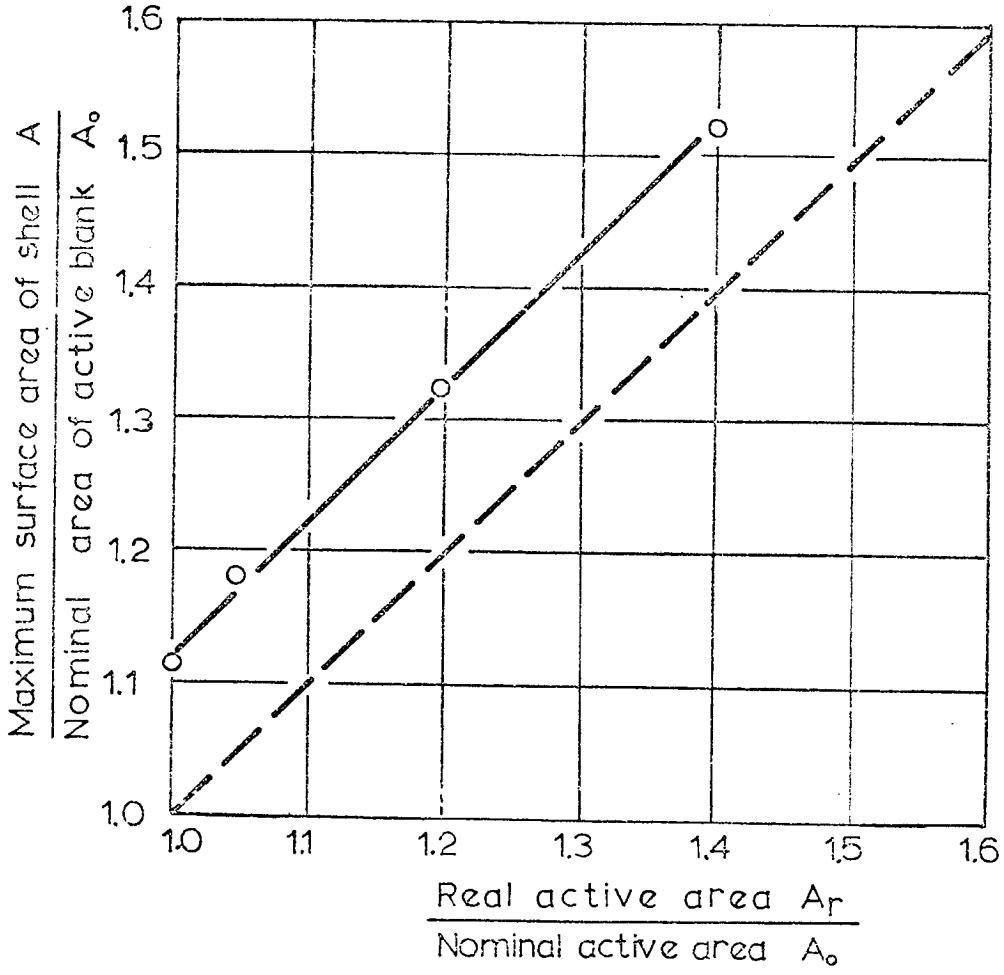
Maximum surface area of shell A / Nominal area of active blank A₀
1.6
1.5
1.4
1.3
1.2
1.1
1.0
1.0
1.1
1.2
1.3
1.4
1.5
1.6
Real active area Ar / Nominal active area A₀

FIG. 13. 1.

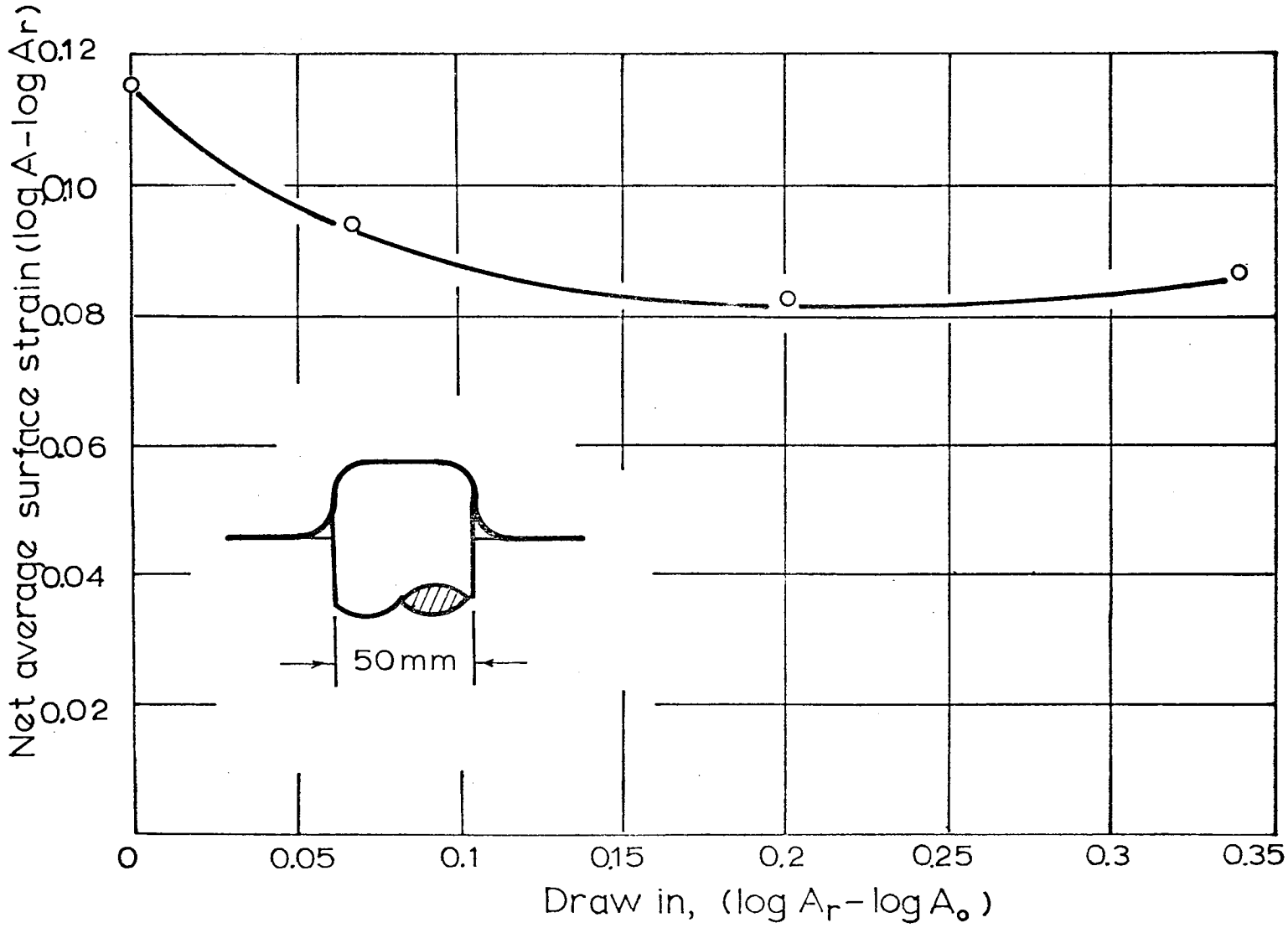
Net average surface strain (log A - log Ar)
0.12
0.10
0.08
0.06
0.04
0.02
0
0.05
0.1
0.15
0.2
0.25
0.3
0.35
Draw in, (log Ar - log Ao)
50mm

FIG. 13. 2.

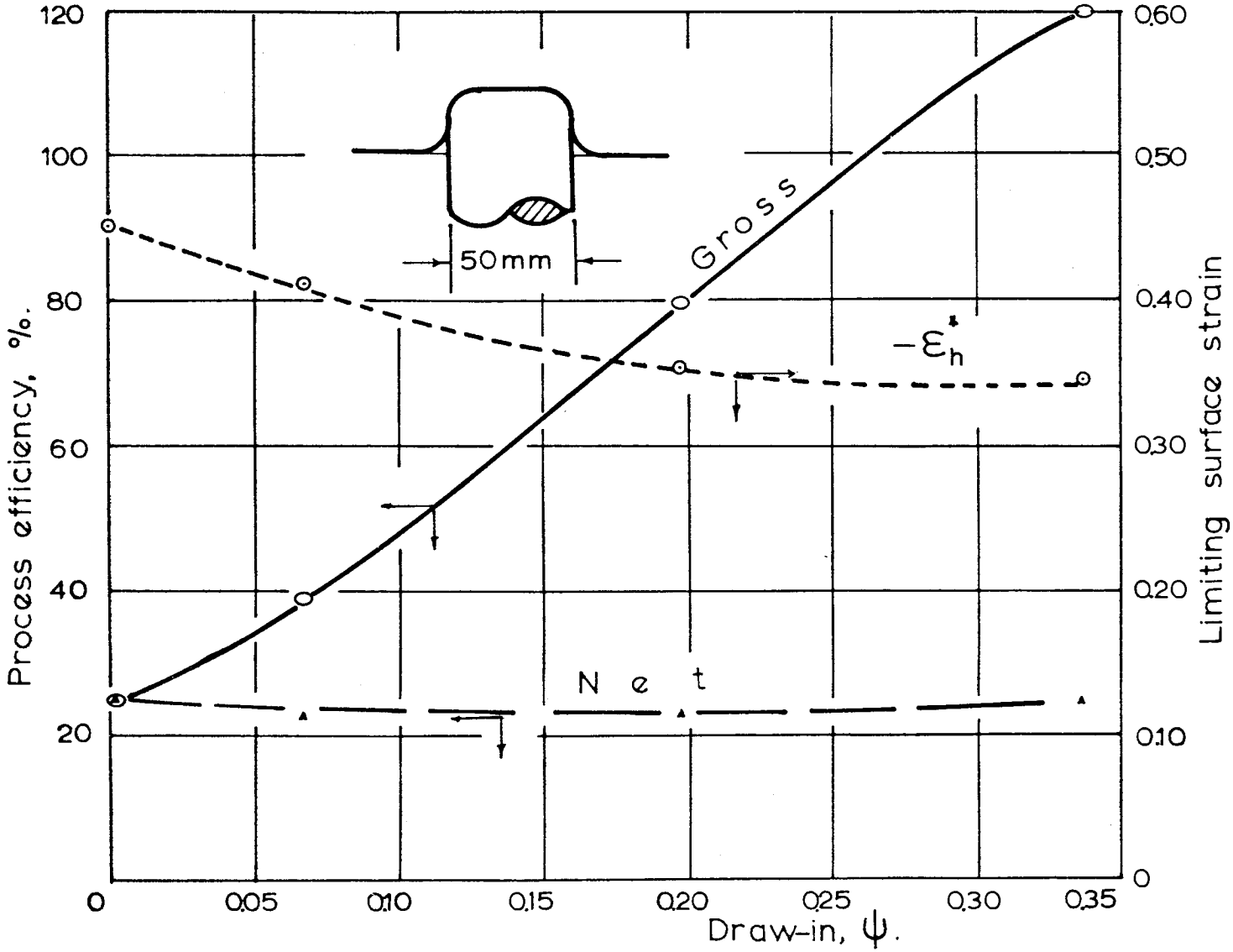
120
100
80
60
40
20
0
0.05
0.10
0.15
0.20
0.25
0.30
0.35
0.60
0.50
0.40
0.30
0.20
0.10
0
Process efficiency, %.
Limiting surface strain
Draw-in, ψ.
50mm
Gross
Net
$-\varepsilon_h^*$

FIG. 13. 3.

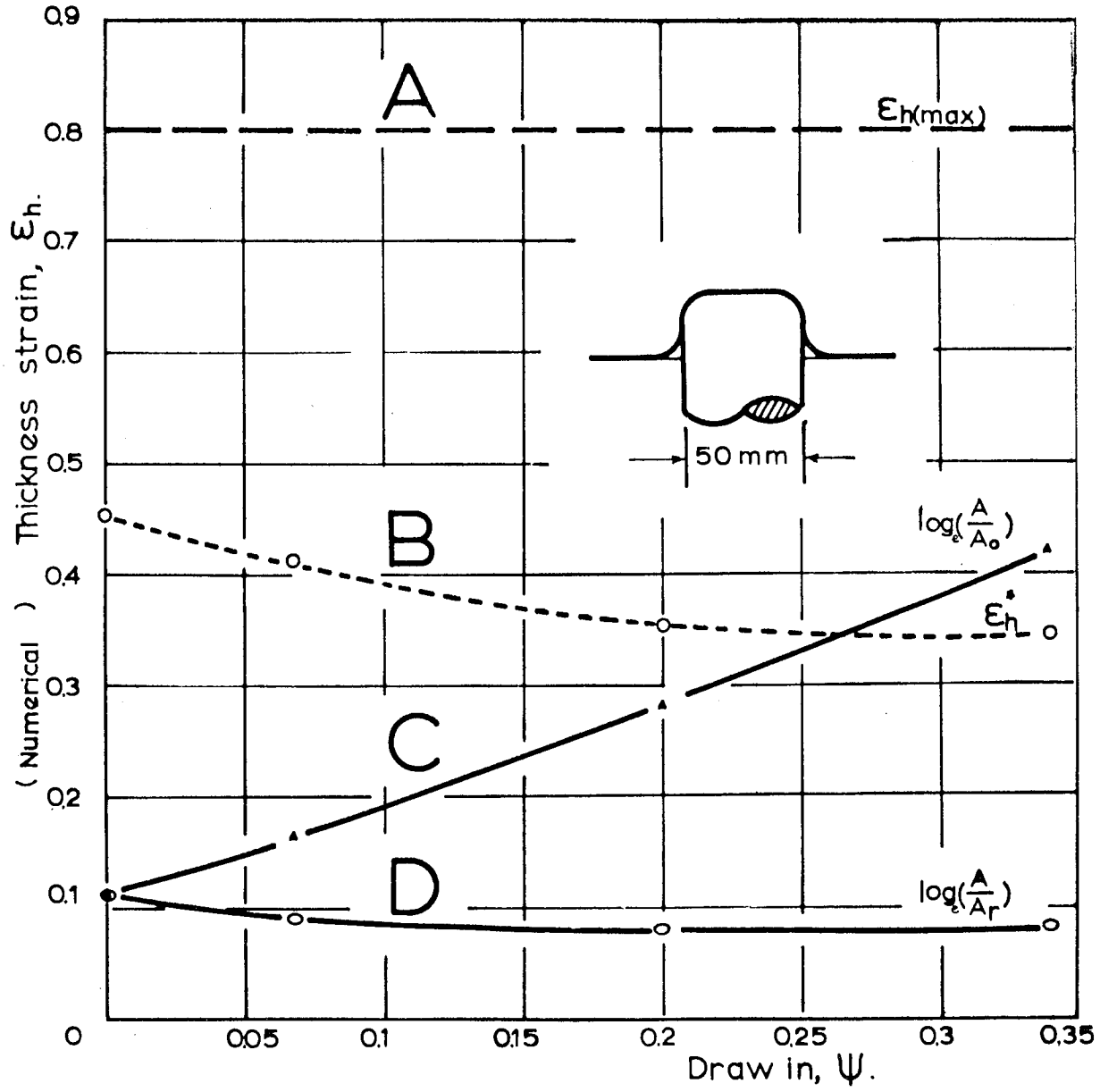
0.9
0.8
0.7
0.6
0.5
0.4
0.3
0.2
0.1
0
Thickness strain, ε_h.
(Numerical)
A
$\varepsilon_{h(max)}$
50 mm
B
$\log_e(\frac{A}{A_o})$
ε_h^*
C
D
$\log_e(\frac{A}{A_r})$
0.05
0.1
0.15
0.2
0.25
0.3
0.35
Draw in, ψ.

FIG. 13. 4.

Photo
5. 1.

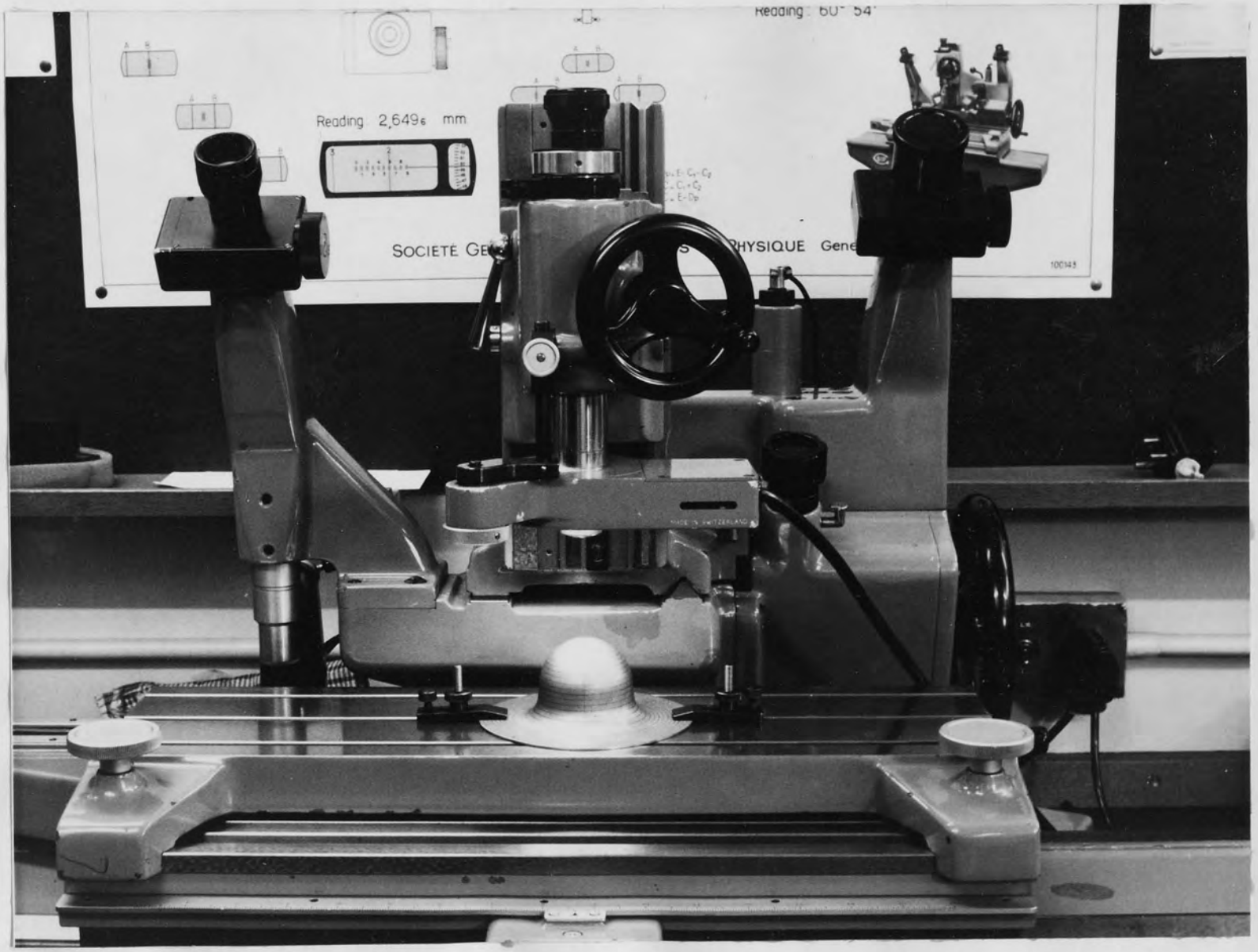

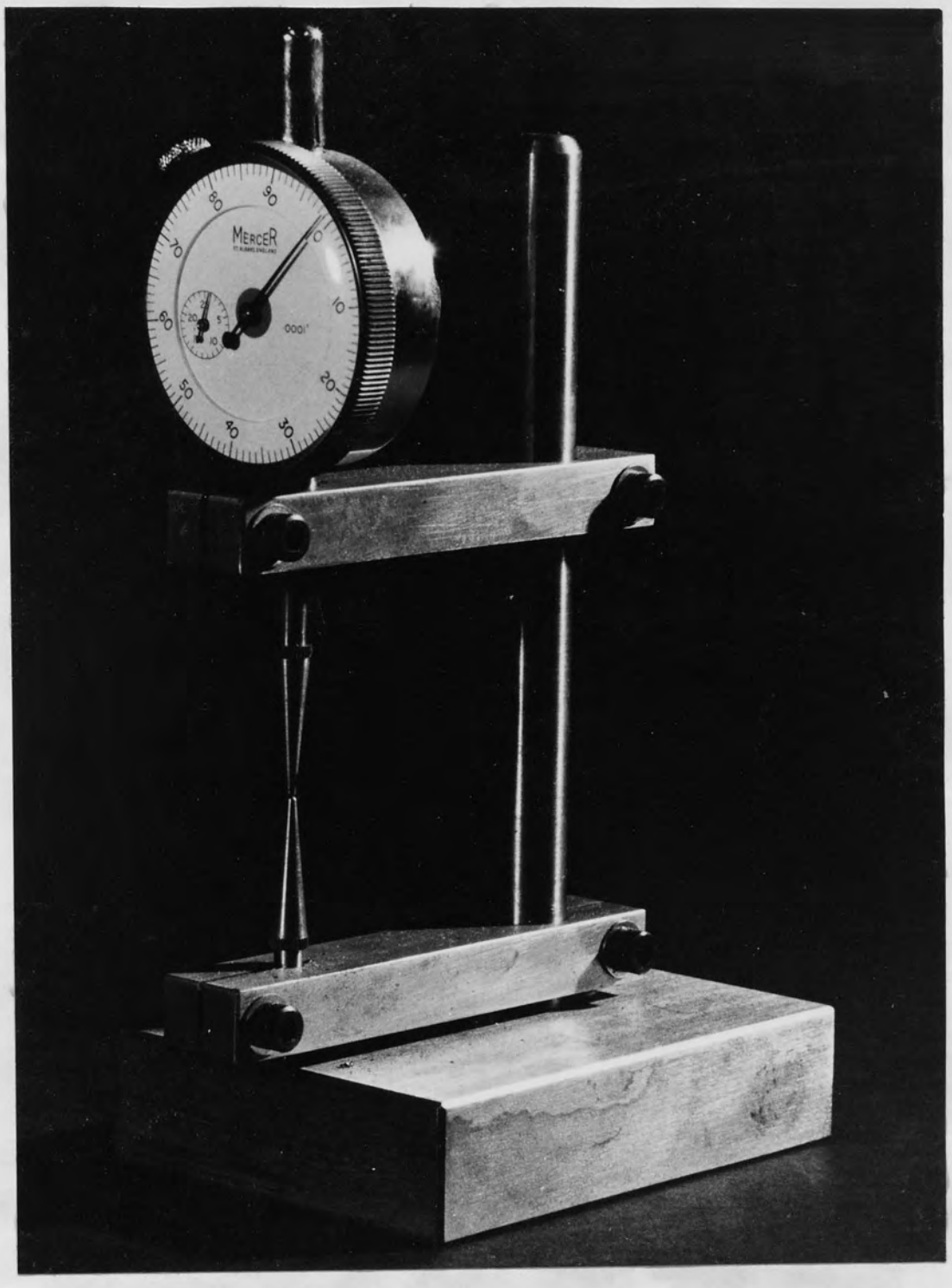

Photo 5. 2.

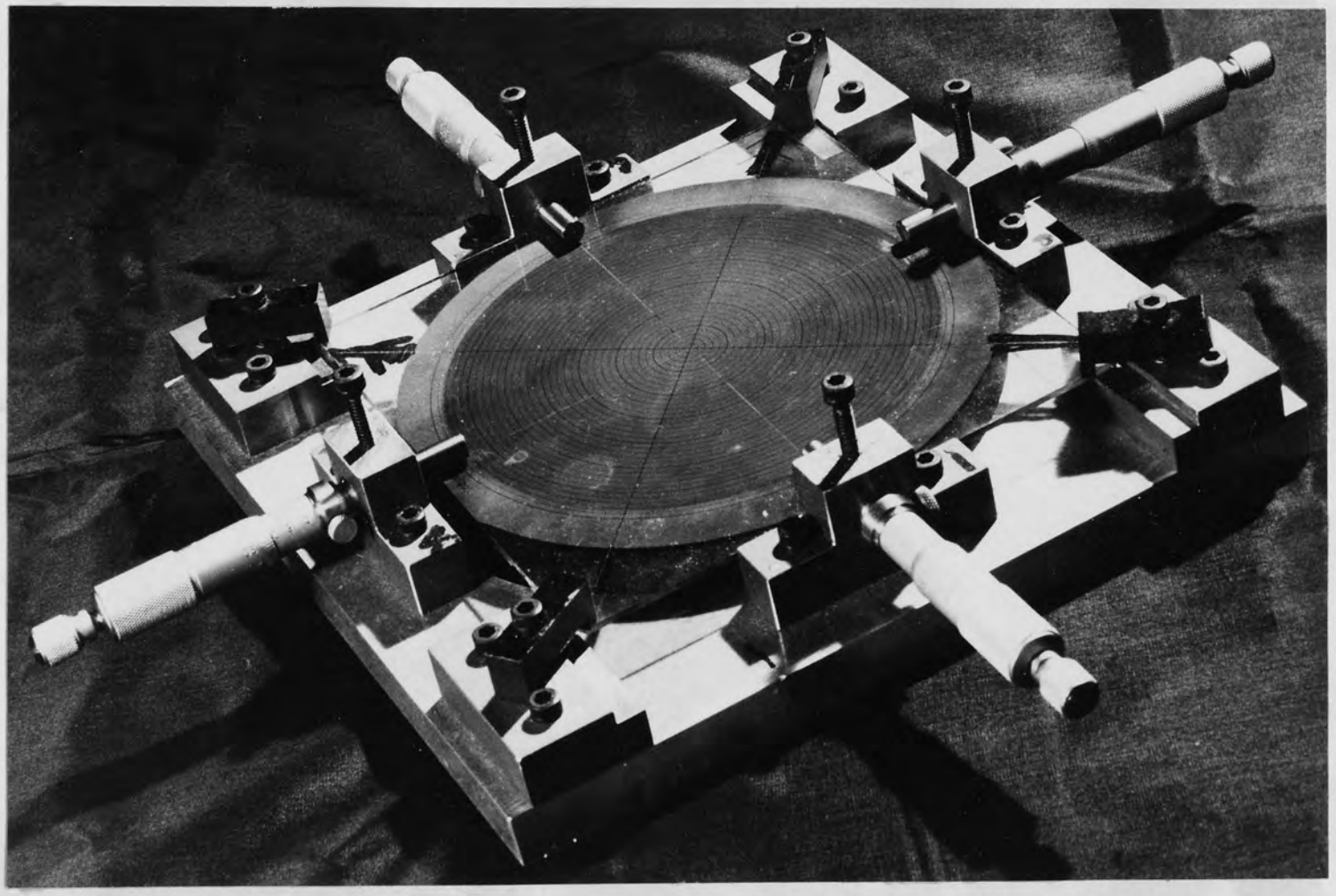

Photo 5. 3.

Photo
8. 1.